INTERACTION OF GRAVITATIONAL WAVES WITH NON-ABELIAN GAUGE FIELDS AND QUARK-GLUON PLASMA

NARASIMHA REDDY GOSALA
Master of Science, National Institute of Technology Rourkela, 2020

A thesis submitted
in partial fulfilment of
the requirements for the degree of

DOCTOR OF PHILOSOPHY

in

THEORETICAL AND COMPUTATIONAL SCIENCE

Department of Physics and Astronomy
University of Lethbridge
LETHBRIDGE, ALBERTA, CANADA

INTERACTION OF GRAVITATIONAL WAVES WITH NON-ABELIAN GAUGE FIELDS AND QUARK-GLUON PLASMA

NARASIMHA REDDY GOSALA

Date of Defence: December 5, 2024

Dr. Arundhati Dasgupta Thesis Supervisor	Associate Professor	Ph.D.
Dr. Mark Walton Thesis Examination Committee Member	Professor	Ph.D.
Dr. Steve Patitsas Thesis Examination Committee Member	Associate Professor	Ph.D.
Dr. Rainer Dick External Examiner University of Saskatchewan Saskatchewan, Canada	Professor	Ph.D.
Dr. Behnam Seyed-mahmoud Chair, Thesis Examination Committee	Associate Professor	Ph.D.

Dedication

I dedicate this work to my family for their unwavering support, love, and affection. .

Abstract

Gravitational waves (GWs), often referred to as ripples in spacetime, were first detected in 2015, revolutionizing our understanding of the universe. On the other hand, the quark-gluon plasma (QGP)—a state of matter believed to have existed microseconds after the Big Bang—provides insights into the fundamental forces of nature. My research bridges these two fascinating areas, exploring how gravitational waves interact with this exotic matter governed by non-abelian (Yang-Mills (YM)) gauge fields. We aim to investigate this in two ways: (i) Study the fundamental interactions of GW with YM fields, and (ii) Explore the thermodynamic aspects of QGP.

QGP is a liquid that behaves like an almost perfect fluid at temperatures observed in particle accelerators (around T_c, $T_c \sim 10^{12}$K) and like a gas of non-interacting particles at $T \gg T_c$. We explore the QGP under these approximations using two models: waves and condensates. We then investigate the effect of GWs on these configurations. We find that the GW changes the frequency and direction of YM waves. In case of condensates, GW induces the decay of condensate into waves. When we study the dynamics of fermions in the presence of condensate and GWs, we found that GWs induce flavour transitions which are relevant in explaining the strangeness enhancement of QGP as observed in colliders. We then discuss thermodynamic aspects, starting with a study of the effect of GWs on YM phase transition using classical nucleation theory and showing that GW increases nucleation rate, resulting in lesser transition time. Finally, we study the thermodynamic properties of QGP using finite temperature Quantum Field Theory. We show that the GWs play an important role in stabilizing the QGP condensates at finite temperatures, as without the GW, the QGP has negative energy and pressure.

Acknowledgments

I would like to express my heartfelt gratitude to all those who supported me throughout my research.

First and foremost, I would like to thank my supervisor, Dr. Arundhati Dasgupta for her invaluable guidance and support throughout my Ph.D. program. I was able to learn a lot of things from her and her constructive feedback immensely shaped the way I think about scientific research. She gave me opportunities to work in various fields and showed the ways to improve myself as a person. Her positive nature helps me during my hardest times in research. Above all, she was kind and always cared to look after my well-being. I am truly grateful to work with her and looking forward to work in the future.

I would like to thank my supervisory committee members, Dr. Steve Patitsas and Dr. Mark Walton, for their valuable comments and for dedicating time to evaluate and oversee my research.

I am grateful to my parents, Prahallada Reddy and Vijaya Lakshmi, for their love and support in letting me do the research despite the situations. I am also grateful to my brother, Mahendra, for his care and for introducing me to "relativity" which makes me love physics even more. Their love, affection, and understanding sustained me through the challenging phases of my program.

I would like to extend my heartfelt thanks to all my friends with whom I share this journey. First, I would like to thank my best friend, Vaishnavi who stood beside me during my hard times and cheered me up. I would like to thank other graduate students at the time of my Ph.D. program, specifically, Sean Nieuwenhuis, Michael Osei, Dr. Mitja Fridman, and Mustafa Amin, for their discussions, useful suggestions as well as pleasant breaks

in between the research. I would also like to thank my friends, specifically, Sivaji, Jinitha, Mahendra, Akash, Natassya, Naveen, Chandra, and Yash. Whether it is through fun outings and heartwarming conversations, helping me adjust to new things and making me feel at home right away, or providing encouragement throughout my career, I am truly grateful for their support. I cherish each one of you and look forward to more adventures together.

I would like to thank Overleaf for providing an exceptional platform for writing and collaborating on my thesis.

Finally, I would like to thank the University of Lethbridge for providing a research-friendly environment.

Contents

List of Tables

List of Figures

List of Abbreviations

ΛCDM Lambda Cold Dark Matter 157

BBN Big Bang Nucleosynthesis 4
BNL Brookhaven National Laboratory 5

CERN European Organization for Nuclear Research 5
CMB Cosmic Microwave Background 1
CNB Cosmic Neutrino Background 4

EFE Einstein's Field equations 14
EM Electromagnetic 7
EW Electroweak Phase Transition 37

FLRW Friedmann–Lemaître–Robertson–Walker 8

GR General Relativity 9
GW Gravitational Waves 3

KAGRA Kamioka Gravitational Wave Detector 3

LEP Large Electron-Positron Collider 46
LHC Large Hadron Collider 5
LIGO Laser Interferometer Gravitational-Wave Observatory 3
LISA Laser Interferometer Space Antenna 3

PGW Primordial Gravitational Waves 3
PTA Pulsar Timing Array 17

QCD Quantum Chromodynamics 4
QFT Quantum Field Theory 11
QGP Quark Gluon Plasma 4

RHIC Relativistic Heavy Ion Collider 5

SLC Stanford Linear Collider 46
SVT Scalar-Vector-Tensor 24

TT Transverse-Traceless 22

YM Yang-Mills 6

Chapter 1

Introduction

"Somewhere, something incredible is waiting to be known."

Carl Sagan

Understanding the universe has been the holy grail for human endeavor. The inhabitants of Earth observe the interplay of natural and human-made features which encompass the surface of the Earth. These include terrestrial characteristics such as sky-raising mountains, expansive plains, and rugged canyons, water masses consisting of vast oceans, intricate rivers, serene lakes, and dynamic glaciers, and vegetation varying from dried deserts to huge rainy forests.

At astronomical scales, we see more complex features filling the universe with magnificent displays of stars, stunning natural light shows (Auroras), vast systems of stars (galaxies), colorful gas and dust clouds serving as a birthplace for stars (Nebulae), the remnants of an exploded stars (Neutron Stars, White dwarfs, Black holes), and extremely violent supermassive black holes.

Compared to previous cases, the cosmological perspective/ view is much simpler. When we observe the universe at cosmological scales (means the greatest observable cosmic distances), the universe looks the same everywhere, with only minute deviations from homogeneity. This is well observed in Cosmic Microwave Background (CMB), which was discovered by Arno Penzias and Robert Wilson in 1965 [1]. The CMB is a relic radiation from the Big Bang, filling the universe almost uniformly. It is the afterglow of the hot, dense

state of the universe approximately 380,000 years after the Big Bang. It has a blackbody spectrum, indicating thermal radiation at an average temperature of about 2.7 K. While the CMB is remarkably uniform, there are very small temperature fluctuations that are related to the density fluctuations that led to the formation of galaxies and large-scale structures. In addition to supporting the Big Bang theory, the CMB also helps in understanding the universe's composition, including Dark matter and Dark energy.

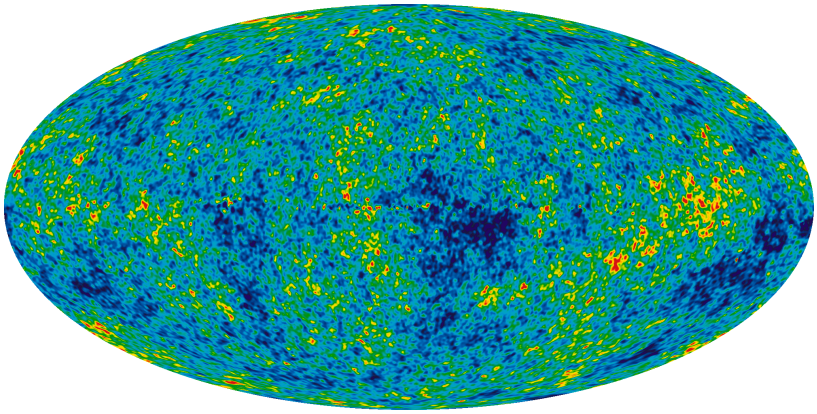

Figure 1.1: Cosmic Microwave Background Radiation [2]

The age of high-precision cosmology has become highly developed with ever more accurate measurements of the distribution of mass in the universe using galaxy surveys [3, 4] and measurements of temperature fluctuations and polarization in CMB [2, 5]. From these measurements, it indicates that the early universe was homogeneous to better than one part in 10,000. The major goal of any cosmological theory is to develop a physical model that accounts for the observed features of the universe. The majority of models have been ruled out due to their lack of consistency with the observed results. The standard cosmological model suggests that the primordial quantum perturbations (or density perturbations) are the source of these inhomogeneities [6] and these quantum perturbations are imprinted onto the early universe by a process of rapid exponential expansion known as inflation [7], which happened during 10^{-36} s to 10^{-32} s after the Big Bang.

The simplest form of inflationary model is single-field slow-roll inflation. The inflation is usually driven by a high energy density hypothetical field known as the inflaton field, that

causes the rapid expansion. As the inflaton field evolves, it can decay into particles, reheat the universe, and sets an initial stage for the standard Big Bang theory after the inflation. In addition to explaining the present cosmological data with high accuracy, this model also made several predictions which were subsequently verified with more precise cosmological data obtained over the past two decades. Although inflation rectifies many of the issues with the Big Bang model, it is still not void of its problems (for example: what sets inflation in motion?).

In addition to the predictions of density perturbations, inflation also predicts the generation of gravitational waves (GWs) [8]. As the inflaton field undergoes rapid changes, it can lead to the stretching and compressing of spacetime, creating GWs. As these GWs are generated during inflation, labeled as Primordial GWs (PGWs), they provide a unique way to study the conditions of the very early universe. These PGWs induce a specific gradient-free B-mode polarization pattern in the CMB [9]. Thus, detecting these PGWs provides an independent way of confirming the theory of inflation. There are already several current and upcoming observatories to detect these primordial GWs. GWs from distant and most energetic processes in the universe such as merging binary neutron stars or black holes have already been detected in these GW observatories [10]. Based on their location, there are two types of observatories: ground-based and space-based GW observatories. Some of the current ground-based observatories include Laser Interferometer Gravitational-wave Observatory (LIGO), Virgo, and Kansai Advanced Gravitational Wave Observatory (KAGRA). There is also a future space-based gravitational wave observatory, Laser Interferometer Space Antenna (LISA) which can detect the GWs from sources that are not accessible to ground-based observatories such as GWs from inflation and supermassive black holes.

The PGWs were being generated from each and every point of the universe which makes them stochastic in nature resulting in a PGW Background [11]. This PGW background encloses the entire universe. As the universe evolved from the inflationary era, it underwent several phase changes and processes leading to the universe as we see it today (Fig. 1.2).

After the inflation, the universe undergoes a process known as reheating, which heats the universe through the production of elementary particles from the inflaton field [12, 13]. Up until around the 10^{-5} sec after the Big Bang, the universe was still filled with a hot soup of elementary particles such as quarks, gluons, electrons, and others. This new state of matter consisting of quarks and gluons which existed deconfined until the first microseconds after the Big Bang is known as Quark-Gluon Plasma (QGP). As the universe cooled down due to expansion, the quarks and gluons combined into hadrons such as neutrons and protons in a process called Hadronization, which occurs via Quantum Chromodynamics (QCD) phase transition. Soon after the formation of hadrons, the neutrinos stopped interacting with baryonic matter and formed the Cosmic Neutrino Background (CNB). This stage of the universe is called neutrino decoupling. Later, as the universe cools down further, the protons and neutrons combine to form nuclei in a process called Big Bang Nucleosynthesis (BBN), which later combines with electrons to form the first atoms in a process called Recombination. At this time, the universe becomes transparent for the first time and photons propagate freely after this time creating the CMB [14, 15]. Apart from the PGW Background, the CMB and CNB are also used to study the state of the early universe. Unlike the PGW background, we cannot use either CMB or CNB to deduce the state of the very early universe before their generation periods. Thus, the Primordial GW background has an advantage over the CMB or CNB in studying the very early universe. Thus, detecting and studying the primordial GWs is crucial for our understanding of the very early universe.

All the phenomena described above happened in the PGW background which means that the PGWs influence these cosmological processes and that information might be imprinted in the present-day universe. In our work, we mainly focus on non-abelian gauge fields which describe QGP and QCD phase transition. As described before, QGP is an exotic state of matter formed at very high temperatures and densities when the composite particles like protons and neutrons, become deconfined and break into their constituent elementary particles such as quarks and gluons. QGP has also been created and studied in

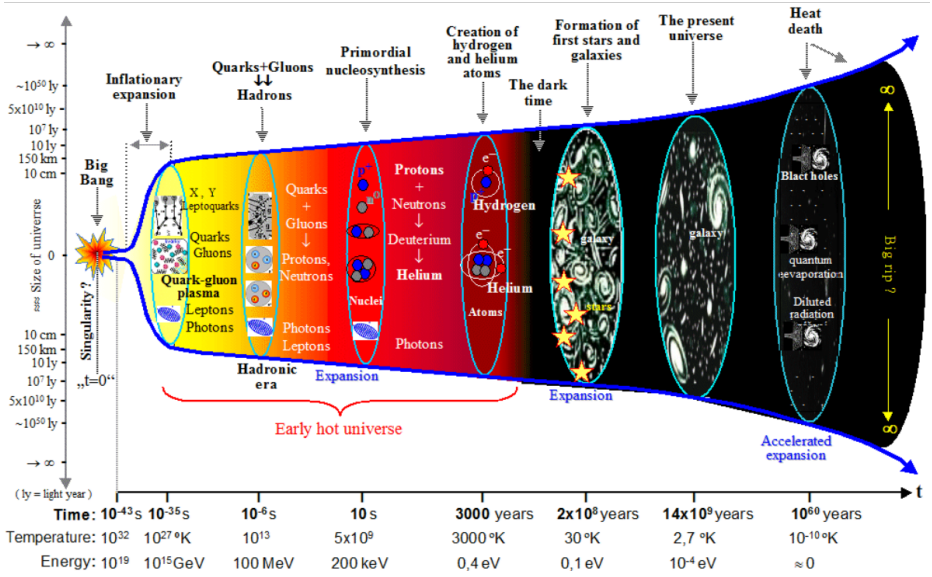

Figure 1.2: Stages of the evolution of universe [16]

heavy-ion colliders such as the Large Hadron Collider (LHC) at the European Organization for Nuclear Research (CERN), the Relativistic Heavy Ion Collider (RHIC) at Brookhaven National Laboratory (BNL), Nucleotron based Ion Collider Facility (NICA) in Russia and Facility for Antiproton and Ion Research (FAIR) in Germany. These particle accelerators first accelerate the heavy nuclei to very high speeds and make them collide with each other. Then, the heavy nuclei get broken down into quarks and gluons forming QGP. But, the QGP formed exists for only a very short amount of time (around 10^{-24} sec) before combining into hadrons again. By studying the resultant particles, physicists try to understand the properties of QGP. The dynamics of scattered/resultant particles might change with a passing GW from a distant event like merging black holes/neutron stars. Thus, the study of the influence of GWs on QGP is relevant for early universe cosmology as well as particle physics.

With the above motivations, we intend to investigate the effect of GWs on non-abelian gauge fields which ultimately leads to the effects on QGP. In the entirety of our work, we worked with the $SU(2)$ gauge group. As $SU(2)$ is a subgroup of $SU(3)$, we can generalize our results to $SU(3)$ (Sec: 5.4). We classify our work into two parts (Fig: 1.3): One is

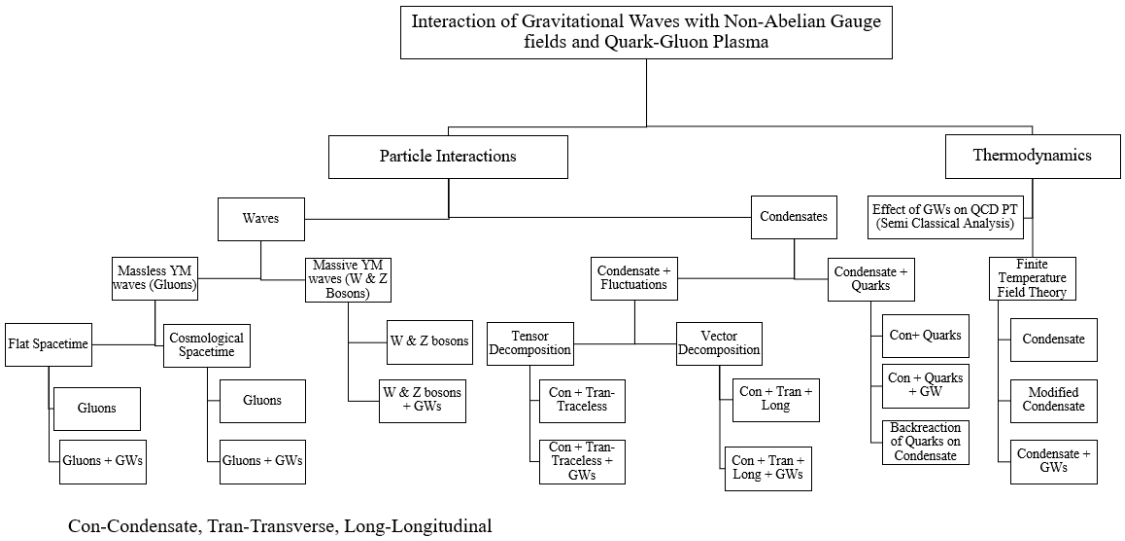

Figure 1.3: Classification of work done in this thesis

by studying the fundamental particle interactions of quarks and gluons, and the other by investigating the QGP as a thermodynamic system.

During half of the first part of the thesis, we explored the different ways to study the QGP, and during the later half, we will deal with its interactions with GWs. One cannot directly observe quarks and gluons outside the hadrons due to a property called Confinement (Sec: 3.1.1). In QGP, at such high temperatures and densities, the interaction between quarks and gluons becomes very weak due to asymptotic freedom (Sec: 3.1.1). It is a property that the effective coupling constant is strong at large distances or low energies while decreasing logarithmically at high energies or short distances. Thus, in these thermodynamic conditions, the QGP system as an ideal gas of non-interacting quarks and gluons is a good approximation. By the above reasoning, one can assume the gluons and quarks in QGP propagate as waves. For simplicity, we first consider gluons only. Gluons are the force carrier particles of the strong nuclear force. They are described using $SU(3)$ non-abelian gauge theory. Non-abelian gauge theories are also known as Yang-Mills (YM) theories. In most of our work, we will be dealing with $SU(2)$ YM theory. Since the $SU(2)$ is a subgroup of $SU(3)$, the solutions/ results obtained for $SU(2)$ are also valid for $SU(3)$ case. The YM

waves are the wave solutions of the YM equations of motion (simply, YM equations). Unlike electromagnetic (EM) waves, YM waves cannot be observed in nature in the current epoch (Sec: 3.1). One can only infer their impacts from other observables. There is only limited work on studying QGP using YM waves, most of it dates back to before the 2000s. Some of the work includes studies on non-linear excitations of QGP at high temperatures [17] and the recent works include quasi-particle models using massive gluon waves for the thermodynamic description of non-abelian interacting gluon plasma [18].

Similarly, there have been only a few studies on the interactions between GWs and YM waves. The recent studies include the phenomenon of parametric resonance of the waves in the presence of GWs [19]. Unlike the YM waves, there have been many studies devoted to the interaction of GWs with other kinds of matter such as EM waves, fermions, and scalar waves. Some of such noted studies in the case of EM waves include the resonant conversion between GWs and EM waves in the presence of a strong EM field [20], frequency splitting [21], deflection of rays [22–24], intensity fluctuations [21, 22], and resonant amplification of EM waves in the presence of GWs [25, 26]. With that, we begin the study of interactions of GWs with gluon waves in the background of Minkowski spacetime [27]. The behaviour of a plane-polarized monochromatic gluon wave is studied when it interacts with a weak linearized GW. We studied the resultant perturbations in gluon waves in the first order. We also explored different aspects like the relative direction of propagation of waves and different types of waves. We classified the YM waves into two types based on the nonlinear dependence in YM equations as introduced in [28]. Type I waves, identified with the absence of nonlinear terms in YM equations, are similar to EM waves because YM equations are reduced to Maxwell's equations without nonlinear terms. And, these solutions do not involve a YM coupling constant. We found a nonzero interaction between the type I YM waves and GWs in the background of flat spacetime. When a linearized GW with frequency ω_g interacts with a plane-polarized monochromatic YM wave with frequency ω_y, we found a new frequency mode $\sqrt{\omega_g^2+\omega_y^2}$ apart from the usual frequency modes. This is expected

because the type I waves are similar to EM waves. This kind of mode was already found in the case of scalar fields [29] and EM waves [26]. We find zero interaction when both waves are propagating in the same direction and a nonzero interaction when waves propagating in anti-parallel directions. We also found that the perturbed solutions follow a beat pattern.

To understand the full nature of non-linearity, we considered another type of waves, Type II waves, which involve YM coupling constant in their solutions. In this case, we found a nonzero interaction even when they are propagating in the same direction. Here also, we found the solutions also follow a beats pattern with the inner frequency being the sum of GW and YM wave frequencies and the outer frequency being the difference between GW and YM wave frequencies. The type II wave perturbations have a dependence on the YM coupling constant and the amplitude of waves is inversely proportional to the coupling constant.

In the next part of the work, we investigate the similar interaction of gluon waves with GWs in the background of the Friedmann-Lemaitre Robertson-Walker (FLRW) spacetime. The FLRW spacetime describes a homogeneous, isotropic, and expanding universe. In particular, we consider the de-Sitter spacetime. This part of the work is just an extension of the work in [26], where the authors studied the interactions of EM waves with GWs in different cosmological backgrounds. A similar kind of interaction is also seen in a cosmological background. Due to the complicated expression for the GW in the cosmological background, we found a nonzero interaction even when GW and type I YM waves are propagating in the same direction. The above analysis shows the effect of weak GW on YM fields in different cosmological backgrounds.

Unlike gluons, W and Z bosons which are the force carriers of weak nuclear force are observable in heavy-ion collider experiments. Thus, in relevance to particle physics experiments, we investigated the Electroweak YM fields coupled with Higgs. We found new solutions for the massive YM fields that might be relevant for nuclear physics and particle physics experiments. Later, we investigated the effect of GWs on these solutions in

the linear order. We found that the numerical solutions grow very rapidly out of the linear regime. These are classical solutions, but provide the support for studying the quantum mechanics of W and Z bosons in the presence of GWs.

As discussed before, QGP is expected to behave like a gas of non-interacting quarks and gluons [30]. But, this was supposed to happen at very high temperatures higher than the critical temperature ($T_c \sim 10^{12}$ K or 150 MeV). However, the experiments at heavy ion colliders, in the neighborhood of critical temperature, show that the QGP behaves like a strongly interacting liquid sharing the features of an almost perfect fluid such as having a very low shear viscosity-to-entropy density ratio [31]. Perfect fluids are fluids that are characterized by the absence of dissipation, viscosity, and heat of conduction. These are like the perfect fluids that are discussed regularly in general relativity (GR). One of the ways to characterize these perfect fluids is by condensates. Condensates are homogeneous and isotropic configurations having a diagonal stress-energy tensor.

There has been some considerable work regarding the non-abelian condensates. As soon as it was known that the $SU(2)$ gauge field admits a homogeneous and isotropic configuration characterized by a single scalar function, there has been so much activity in this field [32–35] as this configuration provides an alternative to a scalar field, inflaton which is being used to explain inflation [36, 37]. Regarding the usage of non-abelian fields in describing QGP, some of the important works are [38–43]. In [38], the authors consider a condensate + fluctuations model for $SU(2)$ gluon plasma in different limiting cases. The fluctuations are needed to account for the deviations from the perfect fluidity. Motivated by their work, we started with their model and tried to investigate the influence of GWs on $SU(2)$ gluon plasma [44]. We found that the transverse traceless modes can be induced from the interactions between condensate and GW even when transverse traceless modes were zero initially. Later, using their tensor decomposition of fluctuations, we found that GWs are not interacting with longitudinal modes. Thus, we introduce a different way of mode decomposition, vector decomposition, to clearly identify longitudinal and transverse

modes. Using this decomposition, we studied the effect of fluctuations (plasmons) on condensate (plasma). We found there is an energy exchange between condensate and fluctuations, but after a certain time, there is a net energy transfer from condensate to fluctuations. We further studied the condensate + fluctuations system in the presence of GWs. We found that the GW delays the condensate decay by stabilizing the condensate. We also found that the GW initiates the condensate decay into fluctuations.

As quarks are constituents of QGP, one must study the behaviour of quarks along with the gluons. There are some works that deal with the dynamics of fermions in the background of gauge fields [45–49]. The initial works date back to the 1980s when there was considerable interest in classical gauge theory. Most of the works in this direction is by considering the background gauge fields to be of instantons and solitons [50]. In our work, we studied the dynamics of quarks in the background of a condensate. As condensate is a good approximation of gluon plasma, the behaviour of quarks in the presence of condensate will give an idea of the nature of QGP. We found that the condensate mixes the quarks on different flavors while keeping their probability densities unmixed. As quarks are an integral part of QGP, there is a high chance that the quarks would backreact on the condensate and change its inherent isotropic and homogeneous configuration. Thus, we investigated the condensate configuration in the presence of a source that is being generated from the quark currents. We found that the condensate loses its homogeneous and isotropy nature due to the backreaction of quarks on condensate. It means one cannot use the simple condensate solution for the description of QGP. Since we will be using the Background Field Method [51] for the thermodynamic study of QGP, the modified condensate solution is a good approximation for the description of QGP. We will be analyzing the role of both condensate configurations in the thermodynamics of QGP. Later, we studied the dynamics of quarks in the presence of a condensate in a GW background. Even in this case, the fermions of two different flavors get mixed up due to interactions between GW, condensate, and fermions. As opposed to the previous case, we found the probability densities fluctuate in time ex-

hibiting flavor transitions due to GW. It means if we have two quarks of the same doublet, their probability densities flip at regular intervals. In our work, we show the enhancement of one flavor in the GW-induced interactions with a quark doublet. The same analysis will work for a lepton doublet too. This study of fermion/quark flip is relevant for QGP and might explain the strangeness of QGP.

In the second part of the thesis, we discuss the thermodynamics of QGP. Part I discusses the fundamental particle interactions between the gluons and GWs. However, QGP is a thermodynamic system and one has to resort to studying it as a many-particle system in thermodynamic equilibrium. Initially, we investigated the effect of GWs on QCD phase transition using semi-classical analysis. We found that the QCD phase transition happens sooner in the presence of GWs than without them.

Later, we did full quantum analysis using finite temperature Quantum field theory (QFT). As quarks and gluons are quantum particles existing at a finite temperature in QGP, finite temperature QFT is the best theory suited to handle the quantum nature of particles at finite temperatures and densities. We investigated the thermodynamic properties of the QGP in different background fields [52]. These background fields include the initial condensate field, the modified condensate field obtained with the introduction of quarks, and the condensate field in the presence of GWs. Using condensate as a classical background field, we found that the QGP model shows a negative pressure with negative energy density indicating a new equation of state. This shows the system does not exist alone with the condensate field at a finite temperature. With the introduction of GWs, we found that the pressure and energy density of QGP become positive getting back to the standard behaviour as observed in lattice gauge calculations. The GWs were introduced through the modified condensate solution which contains the GW in its transverse mode terms. Thus, for the condensate to be a model of QGP at finite temperature, it has to include the plasmons (fluctuations) along with it. We also found that the results are in agreement with the lattice gauge results within certain reasonable parameters.

We split the new work in the thesis into two parts: First part involves the particle interactions (including the chapters: 4, 5 and 6) and second part involves the thermodynamic aspects of QGP (Chapter 7). Before that, we give an introduction to GWs and non-abelian gauge theory.

The thesis is organized as follows: in the next chapter (Chapter2), we give an overview of the GWs and their interaction with different types of matter. We start with the definition of GWs in different scenarios and different spacetimes. Then, we move on to classifying the types of GWs and exploring the different types of sources that generate them. We also discuss the previous work in the area of interaction of GWs with different types of matter such as scalar fields, fermionic fields, and EM waves.

In Chapter 3, we give an overview of the non-abelian gauge theory. We discuss the classical non-abelian gauge theory and the solutions of the classical YM equations of motion. Later, we discuss the Electroweak theory, a broken gauge theory suited for the study of W and Z bosons.

In Chapter 4, we discuss the interaction of GWs with the $SU(2)$ YM waves. For this, we consider the GWs solutions discussed in Chapter 2 and the YM wave solutions discussed in Chapter 3. We first consider the interaction in Minkowski spacetime and then in cosmological spacetime. After that, we studied the interaction of W and Z bosons with GWs.

In Chapter 5, we start with a discussion of condensates and their uses in different fields of physics. We then discuss the condensate + fluctuations model in two ways. First, we identify the modes in the fluctuations using tensor decomposition introduced in [38]. We start with a linearized analysis and then follow by considering higher-order corrections. In both cases, we consider the analysis of their interaction with GWs. Second, we split the fluctuation modes using vector decomposition. This way of decomposition also results in the interactions of GWs with longitudinal modes which otherwise was absent in the first way. In this analysis, we consider the terms to all orders without any approximations.

In Chapter 6, we discuss the behaviour of quarks in the presence of condensate and GWs. We first describe the dynamics of fermions in the background of condensate and discuss the backreaction effect of fermions on the condensate. Then, we consider how the fermions behave in the presence of condensate in a GW background.

In Chapter 7, we start with a little history of the evolution of the universe, followed by a review of QGP and QCD Phase transition. In the review, we discuss the thermodynamic and transport properties of the QGP, along with the QCD phase diagram and its different types of phases. Then, we discuss the QCD Phase transition starting with the definitions of phase transitions and order parameters. We later discuss nucleation rate, the main parameter in the case of first-order phase transition. After that, we discuss the volume effect of the GWs on the QCD phase transition. Then, we come to the main part of the chapter, the thermodynamics of QGP. We start with an introduction to finite temperature QFT, followed by a review of the functional methods of QFT. Then, we calculated the thermodynamic potential using techniques of functional determinants. We use our different condensate solutions in evaluating the thermodynamic quantities such as pressure, energy density, entropy density, and speed of sound. We then compare our models with lattice gauge theory results.

Throughout the thesis, we used natural units: $\hbar = c = 1$ unless otherwise stated. We used Mathematica and Maple for numerical plots. The Mathematica codes used for this thesis are available on GitHub: `https://github.com/Conan9133/PhD-codes`

Chapter 2

Gravitational Waves

> "If I have seen farther than others, it is because I was standing on the shoulders of giants."
>
> *Isaac Newton*

General Relativity (GR) is one of the fundamental theories of physics, proposed by Albert Einstein in 1915. According to GR, gravity is a consequence of the bending of spacetime, a 4-dimensional manifold that combines 3-dimensional space and time, caused by the existence of mass and energy. The curvature of spacetime is perceived as gravity. The most fundamental object in GR is the line element which has the information about the curvature of spacetime encoded through metric tensor. Line element is the measure of the infinitesimal separation between two points in spacetime. It is given by

$$ds^2 = g_{\mu\nu}\, dx^\mu\, dx^\nu, \tag{2.1}$$

where $g_{\mu\nu}$ is the metric tensor ($\mu, \nu = 0, 1, 2, 3$ represents the four spacetime indices) and dx^μ are components of infinitesimal coordinate displacements. In the above, we used Einstein's summation convention, i.e. $\sum_{\mu=0}^{3} a^\mu b_\mu \equiv a^\mu b_\mu$ for any two same indices. The entire dynamics of the theory are governed by a set of ten coupled partial differential equations known as Einstein Field equations (EFEs). These were given by [53]

$$G_{\mu\nu} \equiv R_{\mu\nu} - \frac{1}{2} g_{\mu\nu}\, R + \Lambda g_{\mu\nu} = \kappa\, T_{\mu\nu}, \tag{2.2}$$

where $G_{\mu\nu}$ is the Einstein tensor, which is a combination of Ricci Tensor $R_{\mu\nu}$ and metric tensor $g_{\mu\nu}$, $R = g^{\mu\nu} R_{\mu\nu}$ is the Ricci Scalar, Λ is the cosmological constant, $T_{\mu\nu}$ is the energy-momentum tensor and $\kappa = 8\pi$, where we set Newton's constant (G) to 1. The Ricci tensor is related to the metric tensor as

$$R_{\mu\nu} = \partial_\rho \Gamma^\rho_{\mu\nu} - \partial_\mu \Gamma^\rho_{\nu\rho} + \Gamma^\rho_{\rho\sigma} \Gamma^\sigma_{\mu\nu} - \Gamma^\rho_{\mu\sigma} \Gamma^\sigma_{\rho\nu}, \tag{2.3}$$

where $\Gamma^\rho_{\mu\nu}$ are Christoffel Symbols in torsion-free spacetimes given by

$$\Gamma^\rho_{\mu\nu} = \frac{1}{2} g^{\rho\sigma} (\partial_\mu g_{\nu\sigma} + \partial_\nu g_{\mu\sigma} - \partial_\sigma g_{\mu\nu}).$$

The solutions of Einstein's equations are the metrics of spacetimes that satisfy EFEs. One can see that one needs the stress-energy tensor in order to solve the equations exactly. The information regarding the content of matter and energy is in the stress-energy tensor ($T_{\mu\nu}$) and the Einstein tensor ($G_{\mu\nu}$) describes the geometry of the spacetime having this amount of stress-energy tensor. One needs the equation of state to specify the stress-energy tensor but usually, one takes a simple approximation to replace the full set of stress-energy tensor components. Some of these approximations are (i) vacuum ($T_{\mu\nu} = 0$), (ii) perfect fluid ($T_{\mu\nu} = (\rho + p) u_\mu u_\nu + p g_{\mu\nu}$ where $u_\mu u^\mu = -1$, ρ is mass-energy density, u_μ is fluid's 4-velocity and p is the pressure), and (iii) non-interacting dust ($T_{\mu\nu} = \rho u_\mu u_\nu$).

In GR, the laws of physics do not depend on the choice of coordinates i.e. the equations are in covariant form. Because of this, one cannot determine the metric uniquely from the EFEs even if one knows the metric at initial times. To remove the vagueness, one has to choose a particular coordinate system. The choice of coordinate system can be represented in terms of coordinate conditions [54]. One of the practical coordinate conditions is the

harmonic coordinate condition ($\Gamma^{\alpha}_{\beta\gamma} g^{\beta\gamma} = 0$). This one is often used in working with GWs and numerical relativity [55]. Another useful coordinate condition is the synchronous coordinates, also known as Gaussian coordinates. These are mostly used in cosmology [56].

In principle, once the equation of state and coordinate system is fixed, one can solve the EFEs exactly. However, the EFEs were too hard to solve even in the simplest case. Then, one has to try the numerical solutions for EFEs or find the exact solutions imposing some symmetries or using perturbation methods.

In GR, there are mainly two ways of studying the EFEs

1. In the first method, one finds the solutions of EFEs while keeping the stress-energy tensor fixed. For example, as in Stellar models.

2. In the second method, one assumes the geometry of spacetime and then tries to find the matter/ energy source that is creating this kind of geometry. For example, in the case of Dark Energy, we assume the Universe's structure based on observations like the Universe is homogenous, isotropic, and accelerating, and try to find the nature of matter that gives rise to these observations.

Most of the well-known exact solutions [57] come under the first method. Some of them include vacuum solutions (Minkowski spacetime (flat spacetime), Kerr (Rotating black hole), Schwarzschild (Stationary black hole)), Electro-vacuum solutions (where the electromagnetic field is the only source), etc.

In this thesis, we focus on gravitational waves which we discuss next.

2.1 Gravitational Waves

GWs are the wave solutions of EFEs. They have a great ability to explore the mysteries of the cosmos. They were first discovered on Sept. 2015 by the LIGO/Virgo collaboration [10], almost a century after its prediction by Einstein and almost half a century of experimental efforts in detecting GWs. The discovery of GWs leads to a new branch of astronomy known as Gravitational-Wave Astronomy. GWs are useful in detecting new as-

tronomical objects like the existence of a typical binary system consisting of slightly higher-mass stellar-mass black holes. They have also proven useful in probing several aspects of nuclear and particle physics [58, 59]. The discovery of GWs from merging two neutron stars [60] provided a new way to understand cosmology via multi-band multi-messenger cosmology i.e. GW observations combined with EM observations across varied frequency bands. It means we observe the neutron star mergers using both GW observatories and EM observatories. This kind of association of these observations provides new insights into fundamental physics. Especially, in the case of GR, these observations were used to constrain the speed of GWs, investigate the violation of Lorentz invariance, and test the equivalence principle [61]. GWs also seem helpful in cosmology by providing the tests for the modified gravity theories [62–67], theories that try to explain Dark matter, Dark energy, and cosmic inflation. Since many modified gravity theories predict the speed of gravity is different from the speed of light, the discovery of near equivalence of the speed of gravity and light, discards those theories. These observations also provide a different way of measuring the Hubble rate today[68].

Due to the weakly interacting nature of GWs [69], they were separated from the rest of matter and radiation as soon as they were produced. They can propagate freely in the Early Universe carrying the information about the mechanisms by which GWs were generated. Thus, GWs provide a way to understand the very early universe which we never explored before [70]. Since the GWs were produced by processes based on Standard Model and Beyond Standard model theories, the discovery of GWs provides information about these theories. It means that the GWs provide another way of studying particle physics theories apart from the usual heavy ion colliders (LHC, RHIC).

As we see the importance of GWs in many scenarios, the detection of GWs will reveal answers to so many cosmological mysteries. There are many GW detectors based across the world. Depending on the design of the detector, they were classified into 4 types: 1) Resonant mass detectors, 2) Interferometers, 3) Pulsar Timing Array (PTA), and 4) Others.

Resonant mass detectors [71] are the first type of GW detectors. These detectors consist of a large, solid body of metal isolated from outside vibrations. It depends on the principle that the body resonates when a GW passes through it. So far, these detectors haven't detected any kind of GW signal.

Interferometers, particularly laser interferometers, are mostly used in today's GW detectors. This is mainly because of the capability of laser interferometers to detect GW-induced differential motion between the separated masses. There are two types of interferometers: ground-based and space-based interferometers. A schematic picture is each detector consists of two very long arms placed at 90-degree angles to each other. A laser beam is sent through the arms and gets reflected, creating an interference pattern. When a GW passes through, it will stretch one arm and shorten the other, thus creating a difference in the interference pattern. Presently, the system of ground-based interferometers [72] includes advanced LIGO (aLIGO) [73], advanced Virgo (aVirgo), and KAGRA [74], and LIGO India [75] (which will join in the future). These are all second-generation interferometers. There are also upcoming third-generation interferometers [76] including the Einstein Telescope [77] and Cosmic Explorer [78] (to be ready in the 2030s). At present, there are no space-based interferometers in operation. But there are a few space-based ones (LISA [79], Deci-hertz Interferometer Gravitational-wave Observatory (DECIGO) [80], TianQin [81]) which will be operational in the coming future.

PTA [82] is a collaboration of radio telescopes used to detect GWs by observing the deviations in the incoming signals from an array of millisecond pulsars. The International PTA is a multi-national multi-telescope collaboration consisting of the European PTA, NanoGrav, Parkes PTA, and India PTA. In June 2023, all the PTA collaborations discovered evidence for the stochastic background of nanohertz GWs [83] independently. PTA plays an important role in detecting PGW background.

There are also new detectors focusing on high GW frequencies. These new detectors were based on various ideas like atomic interferometry [84], superconductors, etc.

The following sections are based on the papers [11] and [85]. In this section, we review some of the basic concepts regarding GWs. We start with defining GWs using linearised gravity in vacuum (Sec: 2.1.1) and in the presence of sources (Sec: 2.1.2) using Scalar-Vector-Tensor decomposition. Next, we start with defining GWs in arbitrary spacetimes and then, focus on GWs in the FLRW universe (Sec: 2.1.3). Then, we focused on the types and sources of GWs in Sec: 2.1.4.

2.1.1 Linearized gravity in vacuum

We first consider a weak-field metric that corresponds to a spacetime that is only slightly curved. Under this assumption, there exists a coordinate system where one can write the metric as

$$g_{\mu\nu}(x) = \eta_{\mu\nu} + h_{\mu\nu}(x),\ |h_{\mu\nu}(x)| \ll 1. \tag{2.4}$$

The smallness of perturbation ($h_{\mu\nu}(x) \ll 1$) means that we can keep the terms linear only and discard higher-order terms. Also, because of this we can raise and lower indices of tensor with Minkowski metric ($\eta_{\mu\nu} \equiv \mathrm{diag}(-1,+1,+1,+1)$). Then, one can expand the EFEs in powers of $h_{\mu\nu}$. By keeping terms only linear in $h_{\mu\nu}$, one arrives at the linearized version of GR which we call linearized gravity. Using the above metric (Eq: 2.4), one can write the Christoffel symbols in linear order in $h_{\mu\nu}$ as

$$\Gamma^{\rho}_{\mu\nu} = \frac{1}{2}\left(\partial_\nu h^{\rho}_{\mu} + \partial_\mu h^{\rho}_{\nu} - \partial^{\rho} h_{\mu\nu}\right). \tag{2.5}$$

Using this, one can write the Ricci tensor and Ricci scalar, up to linear order, as follows

$$R_{\mu\nu} = \frac{1}{2}\left(\partial_\nu \partial^{\rho} h_{\rho\mu} + \partial_\mu \partial^{\rho} h_{\rho\nu} - \partial_\mu \partial_\nu h - \Box h_{\mu\nu}\right), \tag{2.6}$$

$$R = R^{\mu}_{\mu} = \partial^\mu \partial^\nu h_{\mu\nu} - \Box h, \tag{2.7}$$

where $\Box = \partial^\mu \partial_\mu$ is the d'Alembertian operator and $h \equiv h^\mu_\mu$ is the trace of metric perturbation. Using these expressions, we arrive at the Einstein tensor (with $\Lambda = 0$) as

$$G_{\mu\nu} = \frac{1}{2}\left(\partial_\nu \partial^\rho h_{\rho\mu} + \partial_\mu \partial^\rho h_{\rho\nu} - \partial_\mu \partial_\nu h - \Box h_{\mu\nu} - \eta_{\mu\nu}\partial^\rho \partial^\sigma h_{\rho\sigma} + \eta_{\mu\nu}\Box h\right). \tag{2.8}$$

The above expression can further be simplified using the definition of "trace-reverse" metric perturbation as

$$\overline{h}_{\mu\nu} \equiv h_{\mu\nu} - \frac{1}{2}\eta_{\mu\nu} h. \tag{2.9}$$

As we can see the trace of $\overline{h}_{\mu\nu}$ is the reverse of $h_{\mu\nu}$, $\overline{h} = -h$ thus the name trace-reversed. Using this, we rewrite the Einstein tensor as

$$G_{\mu\nu} = \frac{1}{2}\left(\partial_\nu \partial^\rho \overline{h}_{\rho\mu} + \partial_\mu \partial^\rho \overline{h}_{\rho\nu} - \Box \overline{h}_{\mu\nu} - \eta_{\mu\nu}\partial_\rho \partial^\sigma \overline{h}^\rho_\sigma\right). \tag{2.10}$$

As we know GR is invariant under general coordinate transformations $x^\nu \to x'^\nu(x)$. But for the linearized theory, symmetry is only for slowly varying infinitesimal coordinate transformations $x'^\nu = x^\nu + \xi^\nu$, where ξ^ν is an arbitrary infinitesimal vector field. This is further discussed in Appendix A.

By using the infinitesimal coordinate symmetry, we can further simplify the Einstein tensor by making a coordinate transformation such that the $\overline{h}_{\mu\nu}$ satisfies

$$\partial^\mu \overline{h}_{\mu\nu}(x) = 0. \tag{2.11}$$

This gauge choice is popularly known as the Lorenz gauge. Using this gauge means choosing the coordinate systems that satisfy Lorenz gauge condition, which leads the Einstein tensor to a simple expression as

$$G_{(L)\mu\nu} = -\frac{1}{2}\Box \overline{h}_{\mu\nu}, \tag{2.12}$$

where L represents the Lorenz gauge. Finally, in the Lorenz gauge, the linearized EFEs (Eq. 2.2) become

$$\Box\overline{h}_{\mu\nu} = -2\kappa T_{\mu\nu}. \tag{2.13}$$

This is just an inhomogeneous wave function i.e. wave equation with a source. In a vacuum, where $T_{\mu\nu} = 0$, we get a homogeneous wave equation

$$\Box\overline{h}_{\mu\nu} = 0. \tag{2.14}$$

The general solution for a homogeneous wave equation can be written as a superposition of plane waves, as

$$\overline{h}_{\mu\nu}(x) = \int d^3k \left(\overline{h}_{\mu\nu}(k)e^{ikx} + \overline{h}^*_{\mu\nu}(k)e^{-ikx}\right), \tag{2.15}$$

where $kx \equiv k^\mu x_\mu$ and $\overline{h}_{\mu\nu}(k)$ ($\overline{h}^*_{\mu\nu}(k)$) are the mode functions of positive (negative) frequency modes. Using the Lorenz gauge, one gets $k^\mu\overline{h}_{\mu\nu} = 0$. One can see now why we talk about gravitational waves in the view of Eqs. (2.14) & (2.15).

The Lorenz gauge represents 4 constraints on $\overline{h}_{\mu\nu}$, thus reducing the number of degrees of freedom from 10 to 6. But imposing the Lorenz gauge does not remove the gauge freedom completely, it just reduces it. Then, by restricting the residual gauge freedom, we finally left with only two independent degrees of freedom. The discussion regarding gauge freedom is further explored in Appendix A.

One can take advantage of residual gauge freedom in eliminating some components of $\overline{h}_{\mu\nu}$. From the gauge transformation (Eq. (A.6)) and using the fact that $\Box\overline{h}_{\mu\nu} = 0$, we can set some of the components such as the trace and spatio-temporal components of $\overline{h}_{\mu\nu}$ to zero, $\overline{h} = \overline{h}_{0i} = 0$. The traceless condition means that we do not need to differentiate between $h_{\mu\nu}$ and $\overline{h}_{\mu\nu}$ (see Eq. 2.9). Using these conditions in the Lorenz gauge (Eq. 2.11), we get $\partial_0 h^{00} = 0$ & $\partial_i h^{ij} = 0$. Since the GWs only deal with the time-dependent part of the metric,

we can set $h_{00} = 0$. Finally, we modified the gauge to

$$h_{\mu 0} = 0, \;\; h = 0, \;\; \partial_i h_{ij} = 0. \tag{2.16}$$

This specialized gauge is known as the Transverse- Traceless (TT) gauge. By this, we can say the only spatial part of the metric is nonzero. It is very easy to count the degrees of freedom in this gauge. Out of 10 degrees of freedom: (1) the $h_{\mu 0} = 0$ eliminates 4, (2) the transversality conditions ($\partial_i h^{ij} = 0$) remove 3 degrees of freedom, and (3) the traceless condition ($h = 0$) removes another degree of freedom. Hence, we obtain the final 2 physical/ radiative degrees of freedom. Thus, the TT gauge completely fixes the gauge freedom.

Consider a plane GW propagating in a direction in the z-direction. From the transversality condition ($\partial_i h^{ij} = 0$), we can see that the tensor components of metric perturbation are zero along the propagating direction i.e. ($h_{13} = h_{31} = h_{32} = h_{33} = 0$). From Eq. 2.16, we set $h_{0\mu} = 0$. The remaining nonzero components are $h_{11}, h_{12}, h_{21}, h_{22}$. We also require the metric to be symmetric which gives $h_{12} = h_{21}$. Finally, from the traceless condition ($h = 0$), we have $h_{11} = -h_{22}$. With all these, we finally have 2 independent components which are $h_+ \equiv h_{11} = -h_{22}$ and $h_\times \equiv h_{12} = h_{21}$. Let A_+ and $A_\times$ be amplitudes of h_+ and $h_\times$, respectively. The expressions for h_+ and $h_\times$ in flat spacetime are simply given as

$$h_+ = A_+ \cos(\omega_g z - \omega_g t), \tag{2.17}$$

$$h_\times = A_\times \cos(\omega_g z - \omega_g t + \delta), \tag{2.18}$$

where ω_g is the angular frequency of the GW and δ is the phase difference. The reasons for $+$ and $\times$ notation can be understood in this way. Consider a set of particles arranged in a circular ring as shown in Fig. (2.1). If we let pass the GW with only h_+, we find the particles oscillate back and forth in $+$ shape while considering later mode $h_\times$, one can find the particles move in a $\times$ shape fashion as shown in Fig. (2.1).

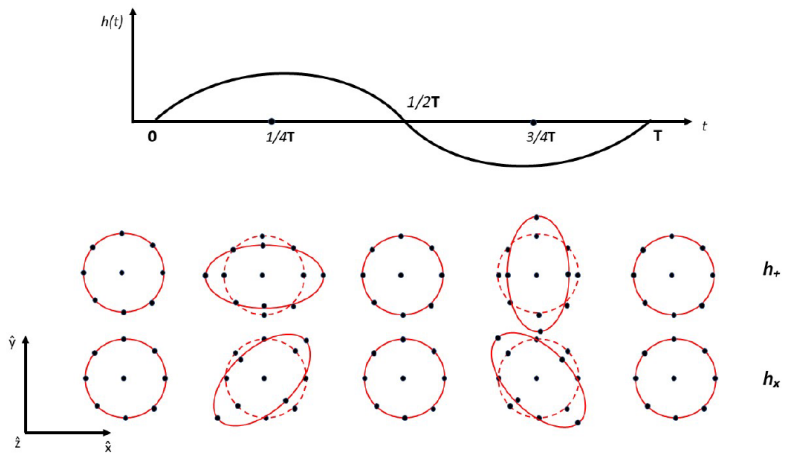

Figure 2.1: The $+$ and $\times$ polarisation modes of a GW. The dashed lines indicate the test particles in the absence of a GW.

One can also find the perturbed line element due to a GW as

$$ds^2 = -dt^2 + (1+h_+)dx^2 + (1-h_+)dy^2 + 2h_\times dxdy + dz^2. \tag{2.19}$$

This is the perturbed metric due to a GW propagating in the z-direction.

2.1.2 Linearized gravity in the presence of matter

In the previous section, we see that the GWs have only two radiative degrees of freedom by considering linearized gravity over a Minkowski background, in asymptotically flat ($h_{\mu\nu} \to 0$) and globally vacuum ($T_{\mu\nu} = 0$) spacetimes. Now we consider a more general case in which the stress-energy tensor is nonzero ($T_{\mu\nu} \neq 0$) while still keeping other assumptions. We follow the notations used in cosmological perturbation theory [86] by taking the background metric as $\overline{g}_{\mu\nu} = \eta_{\mu\nu}$ and the first order metric perturbation as $\delta g_{\mu\nu}$. Since the background is Minkowski, it means that the $\overline{T}_{\mu\nu} = 0$. In this case, the metric perturbation $\delta g_{\mu\nu}$ contains: 1) non-physical gauge degrees of freedom, 2) physical, non-radiative degrees of freedom, and 3) physical radiative degrees of freedom. To investigate the radiative degree of freedom, we start by decomposing the entire metric perturbation and stress-energy tensor into various terms corresponding to 1), 2), and 3) using scalar-vector-

tensor (SVT) decomposition [87–89]. The SVT decomposition is the decomposition of a tensor into components according to their transformations under spatial rotations. According to this, any second-rank tensor ($g_{\mu\nu}$ or $T_{\mu\nu}$) can be decomposed into four scalars, two divergence-free spatial vector fields, and a traceless, transverse, symmetric spatial tensor field. Using this and assuming the $\delta g_{\mu\nu} \to 0$ as $r \to \infty$, we write the metric perturbation as

$$\delta g_{00} = -2\phi, \tag{2.20}$$

$$\delta g_{oi} = \delta g_{i0} = \partial_i \psi + \Lambda_i, \tag{2.21}$$

$$\delta g_{ij} = \delta g_{ji} = -2\lambda\delta_{ij} + \left(\partial_i\partial_j - \frac{1}{3}\delta_{ij}\nabla^2\right)\sigma + \partial_i\chi_j + \partial_j\chi_i + h_{ij}, \tag{2.22}$$

where $\nabla^2 = \partial^i\partial_i$. The above functions are classified as scalars, vectors, and tensors depending on their transformation under a 3-dimensional Euclidean rotation group. For not overcounting degrees of freedom, the vector and tensor parts must also satisfy the following constraints:

$$\partial_i\Lambda_i = 0, \quad \partial_i\chi_i = 0, \tag{2.23}$$

$$\partial_i h_{ij} = 0, \quad h = h^i_i = 0. \tag{2.24}$$

We have introduced in total 16 functions: 4 scalars (1 for each scalar($\phi, \psi, \lambda, \sigma$)), 6 vector components (3 for each vector (Λ_i, χ_i)), 6 tensor components from symmetric tensor (h_{ij}). But, we also have 6 constraints (Eqs. 2.23 and 2.24), so the number of independent variables is 10, consistent for a 4×4 symmetric tensor.

All the above quantities are not gauge invariant and are related through the conservation of the Einstein tensor ($\partial^\mu G_{\mu\nu} = 0$), which gives an extra four constraints. To decrease the number of degrees of freedom from 10 to 6, we have to identify quantities that are actually coordinate invariant. As we see in the previous section, the linearized gravity is invariant under infinitesimal coordinate transformations. Now, we will see how the metric perturbation components change under arbitrary infinitesimal transformation $x_\mu \to x_\mu + \xi_\mu$.

For that, we parameterize the infinitesimal vector parameter as

$$\xi_\mu = (\xi_0, \xi_i) = (f_0, f_i + \partial_i f) \text{ with } \partial_i f_i = 0, \tag{2.25}$$

where f, f_0, f_i are general functions of spacetime coordinates. This is based on the usual Helmholtz decomposition [90] which states decomposing a vector field into an irrotational vector field and solenoidal vector field. As we saw before (see Appendix: A), the metric perturbation changes under infinitesimal transformation as $\delta g_{\mu\nu} \to \delta g_{\mu\nu} - \partial_\mu \xi_\nu - \partial_\nu \xi_\mu$, then one writes this in terms of irreducible parts as

$$\phi \to \phi + \dot{f}_0, \tag{2.26}$$

$$\psi \to \psi - f_0 - \dot{f}, \tag{2.27}$$

$$\lambda \to \lambda + \frac{1}{3}\nabla^2 f, \tag{2.28}$$

$$\sigma \to \sigma - 2f, \tag{2.29}$$

$$\Lambda_i \to \Lambda_i - \dot{f}_i, \tag{2.30}$$

$$\chi_i \to \chi_i - f_i, \tag{2.31}$$

$$h_{ij} \to h_{ij}, \tag{2.32}$$

where the dot represents the derivative with respect to time. As we see the 2 degrees of freedom in tensor h_{ij} are indeed gauge invariant. By combining and manipulating other terms, we can form other gauge invariant quantities as follows

$$\Phi \equiv \phi + \psi - \frac{1}{2}\ddot{\sigma}, \tag{2.33}$$

$$\Psi \equiv -2\lambda - \frac{1}{3}\nabla^2 \sigma, \tag{2.34}$$

$$\Omega_i \equiv \Lambda_i - \dot{\chi}_i, \ \partial_i \Omega_i = 0. \tag{2.35}$$

With these, the number of degrees of freedom comes down to 6. Now, we write the

Einstein tensor in terms of these gauge invariant quantities as

$$G_{00} = -\nabla^2\Psi, \tag{2.36}$$

$$G_{0i} = -\frac{1}{2}\nabla^2\Omega_i - \partial_i\partial_0\Psi, \tag{2.37}$$

$$G_{ij} = -\frac{1}{2}\Box h_{ij} - \partial_i\partial_0\Omega_j - \partial_j\partial_0\Omega_i - \frac{1}{2}\partial_i\partial_j(2\Phi+\Psi) + \delta_{ij}\Big(\frac{1}{2}\nabla^2(2\Phi+\Psi) - \ddot{\Psi}\Big). \tag{2.38}$$

Before writing EFEs, it is necessary to decompose the stress-energy tensor in a similar way as of metric as

$$\delta T_{00} = \rho, \tag{2.39}$$

$$\delta T_{0i} = \delta T_{i0} = \partial_i B + V_i, \tag{2.40}$$

$$\delta T_{ij} = \delta T_{ji} = P\delta_{ij} + \big(\partial_i\partial_j - \frac{1}{3}\delta_{ij}\nabla^2\big)S + \partial_i U_j + \partial_j U_i + \Pi_{ij}, \tag{2.41}$$

together with constraints

$$\partial_i V_i = 0, \quad \partial_i U_i = 0, \tag{2.42}$$

$$\partial_i \Pi_{ij} = 0, \quad \Pi_{ii} = 0. \tag{2.43}$$

Generally, all these quantities are not gauge invariant and are related by conservation equations ($\partial^\mu T_{\mu\nu} = 0$). To find the gauge invariant quantities, one can follow the procedure followed for metric perturbation. Alternatively, we can directly find them from the conservation equation. This is possible because of the stress-energy tensor being zero ($\overline{T}_{\mu\nu} = 0$) in the Minkowski background. The proof is as follows: Consider an infinitesimal transformation of perturbation of stress-energy tensor $T_{\mu\nu} = \overline{T}_{\mu\nu} + \delta T_{\mu\nu}$ which is $\delta T_{\mu\nu} \to \delta T_{\mu\nu} + L_\xi \overline{T}_{\mu\nu}$, where $L_\xi \overline{T}_{\mu\nu}$ is Lie-derivative of the background stress-energy tensor $\overline{T}_{\mu\nu}$ along the infinitesimal vector field ξ_μ. As we can see for a $\overline{T}_{\mu\nu} = 0$, the $T_{\mu\nu}$ is automatically gauge invariant. This is generalized in the well-known Stewart-Walker Lemma [91].

From the conservation of the stress-energy tensor ($\partial^\mu T_{\mu\nu} = 0$), one can get the following

4 constraints

$$\nabla^2 B = \dot{\rho}, \tag{2.44}$$

$$\nabla^2 S = \frac{3}{2}(\dot{B} - P), \tag{2.45}$$

$$\nabla^2 U_i = \dot{V}_i. \tag{2.46}$$

From equations, we can choose the 4 functions to be ρ, P, V_i and the remaining functions (B, S, U_i) can be found using constraints. Using the above constraints and combining with 2 independent functions in Π_{ij}, we can reduce the degrees of freedom from 10 to 6.

Finally, using the conservation equations, the EFEs can be written as

$$\nabla^2 \Theta = -\kappa \rho, \tag{2.47}$$

$$\nabla^2 \Omega_i = -2\,\kappa \Lambda_i, \tag{2.48}$$

$$\nabla^2 \Phi = \frac{1}{2}\,\kappa\,(\rho + 3P - 3\dot{B}), \tag{2.49}$$

$$\Box h_{ij} = -2\,\kappa\,\Pi_{ij}. \tag{2.50}$$

One can see that only the tensor part of metric (h_{ij}) obeys a wave equation. The other variables Θ, Φ and Ω_i, obey Poisson-type equations. In vacuum spacetimes ($T_{\mu\nu} = 0$), the above equations become four Laplace equations and a wave equation.

$$\nabla^2 \Theta = 0, \quad \nabla^2 \Phi = 0, \tag{2.51}$$

$$\nabla^2 \Omega_i = 0, \quad \Box h_{ij} = 0. \tag{2.52}$$

This shows that among the gauge invariant quantities, only tensor part h_{ij} represents the physical radiative degrees of freedom. As one can see the tensor part h_{ij} satisfied the TT gauge conditions (Eq. 2.16) discussed in the previous section, irrespective of gauge choice. In a vacuum, the TT gauge is supposed to be one in which the whole of metric perturbation

is reduced to only the physical radiative degrees of freedom. In the presence of matter, we have an extra 4 degrees of freedom (Θ, Φ and $\Omega_{\rm i}$) in addition to h_{ij}. From the analysis in this section, we find that only the tensor part of metric h_{ij} represents the gravitational radiation.

2.1.3 Propagation of Gravitational waves in the curved backgrounds

In Sec. 2.1.1, we have defined the GWs in the context of linearized gravity in Minkowski background, in asymptotically flat and globally vacuum spacetimes. In the previous Sec. 2.1.2, we defined the GWs by removing the global vacuum assumption. The next step is to move to a more general background than Minkowski. In GR, any source of energy and momentum can act as a source of gravity. By sticking to the Minkowski background, we removed the possibility of producing any form of curvature in the spacetime background. Also, our work deals with GWs produced in the Early Universe, so one needs to define the GWs over a curved background. Now, we want to generalize the theory to an arbitrary background $g^B_{\mu\nu}(x)$ as

$$g_{\mu\nu}(x) = g^B_{\mu\nu}(x) + \delta g_{\mu\nu}(x),\ |\delta g_{\mu\nu}| \ll |g^B_{\mu\nu}|. \tag{2.53}$$

Since both functions $(g^B_{\mu\nu}, \delta g_{\mu\nu})$ have a dependence on space and time, we need a way to define the GWs. GWs are defined in the context of separation of length scales/ frequencies: It means that for a GW of wavelength λ (frequency f), and for a background of length-scale L_B (frequency f_B), one can define the GWs on the background such that $L_B \gg \lambda$ ($f_B \ll f$).

Now, we will work out the same analysis as we did in the Sec. 2.1.1. We can still use most of the formulas by replacing $\eta_{\mu\nu}$ with $g^B_{\mu\nu}$ and ∂_μ with covariant derivative over the curved background,∇^B_μ. But, we will also find some more terms for some formulae because of having nonzero values for the Riemann tensor in the background. By defining generalized trace-reversed metric perturbation as $\overline{\delta g}_{\mu\nu} = \delta g_{\mu\nu} - \frac{1}{2} g^B_{\mu\nu} g^{B\alpha\beta} \delta g_{\alpha\beta}$, the EFEs at first order, in the case of curved background, are

$$-\frac{1}{2}\Box^B\overline{\delta g}_{\mu\nu}+R^B_{\lambda\mu\nu\rho}\,\overline{\delta g}_{\lambda\rho}+\nabla^B_{(\nu}\nabla^{B\sigma}\,\overline{\delta g}_{\mu)\sigma}-\frac{1}{2}g^B_{\mu\nu}\,\nabla^{B\alpha}\,\nabla^{B\beta}\,\overline{\delta g}_{\alpha\beta}+$$
$$R^{B\alpha\beta}\left[\frac{1}{2}g^B_{\mu\nu}\overline{\delta g}_{\alpha\beta}-\frac{1}{2}\overline{\delta g}_{\mu\nu}g^B_{\alpha\beta}+g^B_{\beta(\mu}\overline{\delta g}_{\nu)\alpha}\right]=\kappa\,\delta T_{\mu\nu}, \quad (2.54)$$

where $\Box^B, \nabla^B$, Riemann and Ricci tensors are defined on background ($g^B_{\mu\nu}$) and round parentheses in a subscript denote symmetrization. We also split the $T_{\mu\nu}$ into a background contribution and a first-order contribution $T_{\mu\nu}=\overline{T}_{\mu\nu}+\delta T_{\mu\nu}$, where the background stress-energy tensor ($\overline{T}_{\mu\nu}$) is sourcing the background metric ($\overline{g}_{\mu\nu}$).

As we discussed before, we need to study the GWs propagating in the Early Universe which is in the FLRW background. The GWs expressions in deSitter and Radiation-dominated universe are used in the coming chapters 4 and 7, respectively. The flat FLRW metric is given by

$$ds^2=-dt^2+a^2(t)(dx^2+dy^2+dz^2), \quad (2.55)$$

where $a(t)$ is the scale factor. The FLRW metric describes a homogeneous, isotropic, and expanding (contracting) universe. Because of these symmetries, the two-rank tensors can be irreducibly decomposed under spatial rotations and translations. It means one can perform the same analysis (SVT decomposition) as in the previous Sec. 2.1.2. In the view of cosmological perturbation theory, one can find that the only radiative modes are the two degrees of freedom of the spatial tensor perturbation h_{ij} and hence correspond to GWs. Similarly, as in Sec. 2.1.2, the scalar and vector modes are not radiative, and cannot propagate in the vacuum. Also, one can find that the h_{ij} is gauge invariant. If one works in Fourier modes, they also find that the scalar, vector, and tensor modes get decoupled from each other. It means we can study each mode separately. Then, the GWs can be represented as spatial tensor perturbations (h_{ij}) of FLRW metric as

$$ds^2=-dt^2+a^2(t)(\delta_{ij}+h_{ij})dx^idx^j, \text{ with } \partial_i h_{ij}=h_{ii}=0, \quad (2.56)$$

where h_{ij} is the symmetric, transverse, traceless spatial tensor, having only two physical

degrees of freedom. Using the metric (2.56) in the linearized EFEs (2.54) by keeping only the TT component h_{ij} of metric perturbation, we get

$$\ddot{h}_{ij}(t,\vec{x}) + 3H\dot{h}_{ij}(t,\vec{x}) - \frac{1}{a^2}\nabla^2 h_{ij}(t,\vec{x}) = 2\,\kappa\,\Pi_{ij}^{TT}, \tag{2.57}$$

where $H = \dot{a}/a$ is the Hubble rate, the dot represents derivative w.r.t comoving time (t), $\nabla^2 = \partial_i\partial_i$ is Laplacian in comoving coordinates x^i, Π_{ij}^{TT} is the transverse-traceless part of anisotropic stress. The anisotropic stress is given by $a^2\Pi_{ij} = T_{ij} - pg_{ij}$ where p is the pressure, T_{ij} denotes spatial components of stress tensor and g_{ij} is given by Eq. 2.56.

Most of the cosmological sources were present only for a short time and then, the GWs propagate freely in the FLRW spacetime. So, it is useful to study the propagation of free GWs in FLRW spacetime. For that, we start by working with conformal time (τ) instead of comoving time (t), $d\tau = dt/a(t)$, then the metric (Eq. 2.56) can be rewritten as

$$ds^2 = a^2(\tau)\big[-d\tau^2 + (\delta_{ij} + h_{ij})dx^i dx^j\big]. \tag{2.58}$$

The traceless and transverse perturbation h_{ij} can be decomposed into two polarization states $r = +, \times$ using Fourier transform, in terms of positive and negative frequency modes, as [92]

$$h_{ij}(\tau,\vec{x}) = \sum_{r=+,\times}\int \frac{d^3\vec{k}}{(2\pi)^3} h_r(\vec{k},\tau)e^{i\vec{k}\cdot\vec{x}}\varepsilon_{ij}^r(\hat{k}), \tag{2.59}$$

where the h_{ij} is taken to be real, $h_r^*(\vec{k},\tau) = h_r(-\vec{k},\tau)$ and $\varepsilon_{ij}^r(\hat{k})$ are the two polarisation tensors that are taken to be real and satisfy $\varepsilon_{ij}^r(-\vec{k}) = \varepsilon_{ij}^r(\vec{k})$. The two polarisation tensors are symmetric ($\varepsilon_{ij}^r = \varepsilon_{ji}^r$), transverse ($\hat{k}_i\varepsilon_{ij}^r = 0$) and traceless ($\varepsilon_{ii}^r = 0$). Then, writing the Eq. (2.57) with $\Pi_{ij}(\tau,\vec{x}) = 0$,in Fourier space as

$$h_r''(\vec{k},\tau) + 2\frac{a'}{a}h_r'(\vec{k},\tau) + k^2 h_r(\vec{k},\tau) = 0, \tag{2.60}$$

where prime denotes derivatives with respect to τ and $k = |\vec{k}|$. In order to solve the Eq.

(2.60), we need to specify the scale factor ($a(\tau)$). One can choose the scale factor to be of power law form: $a(\tau) = a_n \tau^n$, which covers the cases of radiation-dominated ($n = 1$), matter-dominated ($n = 2$) and also de Sitter phase ($n = -1$). The general solution of Eq. (2.60) can be found in terms of Bessel functions.

We consider a simple cosmological model consisting of three stages of the universe: Inflationary (I) phase for $\tau < \tau_1$, radiation-dominated (R) phase for $\tau_1 < \tau < \tau_2$, and matter-dominated (M) phase for $\tau_2 < \tau < \tau_0$, where τ_1 and τ_2 are the transition times from inflation to radiation-dominated and from radiation-dominated to matter-dominated, respectively. We assume the scale factor and its first derivative are continuous at transition times. The following derivation is based on [93]. The scale factor is given by

$$a^I(\tau) = -\frac{1}{H_{dS}\tau}, \ \tau < \tau_1, \tag{2.61}$$

$$a^R(\tau) = \frac{\tau - 2\tau_1}{H_{dS}\tau_1^2}, \ \tau_1 < \tau < \tau_2, \tag{2.62}$$

$$a^M(\tau) = \frac{(\tau - 4\tau_1 + \tau_2)^2}{4H_{dS}\tau_1^2(\tau_2 - 2\tau_1)}, \ \tau > \tau_2, \tag{2.63}$$

for the inflation, radiation-dominated, and matter-dominated stages, respectively. Also, τ_0 is the present conformal time and H_{dS} is the Hubble constant during the Inflationary stage. With these scale factors, one can easily solve the Eq. (2.60), and the modes solutions are given by

$$h_r^I(\vec{k},\tau) = \frac{1}{\sqrt{2k}}\frac{1}{a^I(\tau)}\left(1 - \frac{i}{k\tau}\right)e^{-ik\tau}, \tag{2.64}$$

$$h_r^R(\vec{k},\tau) = \frac{1}{\sqrt{2k}}\frac{1}{a^R(\tau)}e^{-ik(\tau-2\tau_1)}, \tag{2.65}$$

$$h_r^M(\vec{k},\tau) = \frac{1}{\sqrt{2k}}\frac{1}{a^M(\tau)}\left(1 - \frac{i}{k(\tau - 4\tau_1 + \tau_2)}\right)e^{-ik(\tau-4\tau_1+\tau_2)}, \tag{2.66}$$

at three stages in our model. For the inflationary phase, the solution is unique by requiring the vacuum state to have a minimized finite renormalized stress-energy tensor [94–98]. In

another way, if the Bunch-Davies vacuum [99] is chosen for the initial condition for the inflationary stage, one can write the mode solutions in any stage [100] as

$$\begin{aligned} h_r(\vec{k},\tau) &= h_r^I(\vec{k},\tau),\ \tau<\tau_1 && (2.67)\\ &= \alpha^{IR}h_r^R(\vec{k},\tau)+\beta^{IR}(h_r^R(\vec{k},\tau))^*,\ \tau_1<\tau<\tau_2 && (2.68)\\ &= \alpha^{IM}h_r^M(\vec{k},\tau)+\beta^{IM}(h_r^M(\vec{k},\tau))^*,\ \tau>\tau_2 && (2.69)\end{aligned}$$

where α and β are the Bogoliubov coefficients that can be found by imposing the continuity of $h_r(\vec{k},\tau)$ and its first derivative across each transition. The Bogoliubov transformation is a canonical transformation mapping one set of operators to another set of operators. Here, we deal with the GW modes in different stages of the universe's evolution. For a 3-stage cosmological model of the universe, the expression of GW in each stage will be a linear combination of modes obtained individually in different stages. The coefficients used in these transformations are called Bogoliubov coefficients. They are given by

$$\begin{aligned} \alpha^{IR} &= \left(-i-\frac{1}{k\tau_1}+\frac{i}{2k^2\tau_1^2}\right)e^{-2ik\tau_1}, && (2.70)\\ \beta^{IR} &= \frac{i}{2k^2\tau_1^2}, && (2.71)\\ \alpha^{RM} &= \left(-i+\frac{1}{2k(\tau_2-2\tau_1)}+\frac{i}{8k^2(\tau_2-2\tau_1)^2}\right)e^{ik(\tau_2-2\tau_1)}, && (2.72)\\ \beta^{RM} &= \frac{i}{8k^2(\tau_2-2\tau_1)^2}e^{-ik(\tau_2-2\tau_1)}, && (2.73)\\ \alpha^{IM} &= \alpha^{IR}\alpha^{RM}+\beta^{IR}(\beta^{RM})^*, && (2.74)\\ \beta^{IM} &= \alpha^{IR}\beta^{RM}+\beta^{IR}(\alpha^{RM})^*. && (2.75)\end{aligned}$$

With these, one can find the expression for GW propagating freely in any stage of the expanding universe.

2.1.4 Types and Sources of Gravitational waves

So far, we have explained how to define GWs in different scenarios. In this section, we explain the different types of GWs and the mechanisms that generate these types of GWs. From Eq. (2.57), we find that the GWs are generated by the anisotropic stress tensor. Using the compact object approximation, one can take the multipole expansion approximation, and show that the GWs can be generated by the quadrupole moments of matter density distribution [53]. One can find the analogy in the case of EM radiation, but the leading contribution of EM radiation comes from the dipole moment of the charge distribution rather than the quadrupole moment. This also tells us why gravitational radiation is much weaker than EM radiation since it is coming from the weaker quadrupole moments. As a consequence, a spherical star cannot radiate GWs as it does not generate any quadrupole moment. Based on the nature of GWs, they were classified into four types [101]: 1) Inspiral GWs, 2) Continuous GWs, 3) Burst GWs, and 4) Stochastic GWs.

Inspiral GWs are generated from the binary systems [10] during their end life. These binary systems generally consist of compact stars like white dwarfs, black holes, and neutron stars. During this process, the two objects in the system start spiraling toward each other until they merge to form a single object. This is an easy example of the application of a system where this is a nonzero quadrupole moment, thus generating GWs. Because GWs carry energy, when two objects revolve around one another, they lose energy, causing their orbital distances to decrease and their velocities to increase [102]. This causes the amplitude and frequency of GW to increase until the merger and then decrease, much like a chirp sound.

Continuous GWs are generated by objects or systems that have well-defined almost constant frequency. These systems correspond to binary star systems long before the merging. Another example is an asymmetric neutron star [103]. These neutron stars have bumps above the surface or other irregularity, thus making the object asymmetric and thus, having a nonzero quadrupole moment. These GWs are very weak compared to Inspiral GWs.

Burst GWs are generated from very short-duration and cataclysmic events. These GWs may be generated from supernovas when the explosion happens asymmetrically or in gamma-ray bursts. As these events can happen anytime, it is very hard to predict.

Stochastic GWs are the random background of GWs spreading across the universe. The signal may be produced by the superposition of a large number of independent astrophysical sources like supermassive black holes or maybe intrinsically random like the cosmological processes in the Early universe. The sources of GWs are broadly classified into two types based on their intrinsic nature (Table: 2.1): 1) Astrophysical sources, and 2) Cosmological sources.

Table 2.1: Different sources of GWs

Astrophysical Sources	Cosmological Sources
Binary compact stars	Inflation
Supermassive Black holes	Reheating
Rotating Supernovae, Neutron stars	Phase Transitions
Binary supermassive black holes	Cosmic Defects

An astrophysical GW background is generated from the combination of many unresolved, weak, independent astrophysical sources. These astrophysical sources vary from the supermassive binary black hole binaries to the stellar mass mergers at very large distances. On the other hand, the cosmological GW background is generated from the GWs generated by many cosmological processess happened in the very early universe [11]. These GWs from the early universe are called Primordial GWs (PGWs), as they are relic GWs. These are much like CMB, which is a remnant of the Big Bang. These PGWs carry information about the processes through which they are generated. The GWs produced from the cosmological processes are present across various frequencies of the spectrum, having different stochastic properties. Since our work deals with PGWs, we will go through a brief review of the cosmological sources of PGWs [11].

A. Inflation: Inflation is the most successful theory of the very early universe that resolves the problems that arise in the Big Bang theory. Inflation provides an explanation

for the formation of large-scale structures in the universe by linking to the origin of primordial density fluctuations [104, 105]. In addition to density perturbations, inflation also produces fluctuations in the gravitational field [106–108]. These quantum fluctuations later turn into a proper classical stochastic GW background. This GW background from inflation is expected to create a pattern of B-modes in the polarization of CMB [109, 110].

Although the scalar field's (inflaton) anisotropic stress tensor acts as a source term in the equation of motion for tensor modes, it is of second order in fluctuations. So, in linear order, there will be no source for the generation of GWs during inflation. However, the quantum fluctuations in metric are amplified by the exponential expansion of the universe. Consider the scalar and tensor modes of the metric fluctuations as perturbations over the homogeneous and isotropic inflationary background. Since the tensor modes of fluctuations (h_{ij}) are gauge invariant (Eq. 2.32), we can define the tensor power spectrum ($\mathcal{P}_h(k)$). The power spectrum describes how the power (or variance) of the gravitational wave perturbations is distributed over different wavelengths or scales. It is given by

$$\langle 0|\hat{h}_{ij}(x,\tau)\hat{h}_{ij}(x,\tau)|0\rangle = \int \frac{dk}{k}\mathcal{P}_h(k), \tag{2.76}$$

where $\mathcal{P}_h(k)$ is found to be

$$\mathcal{P}_h(k) \approx \frac{2}{\pi^2}\frac{H_k^2}{m_{pl}^2}, \tag{2.77}$$

where H_k is the Hubble rate at horizon crossing ($k = a_k H_k$) and $m_{pl} = 1/\sqrt{8\pi}$ is the reduced Planck mass.

Similarly, for the scalar modes of fluctuations, the scalar power spectrum is given by

$$\mathcal{P}_{\mathcal{R}}(k) \approx \frac{H_k^2}{8\pi^2\varepsilon m_{pl}^2}, \tag{2.78}$$

where ε is the slow roll parameter of the inflationary theory and $\mathcal{R}$ is the comoving curvature perturbation, which is a gauge invariant quantity in case of scalar fluctuations. The

observations related to the scalar fluctuations are obtained from the CMB measurements. From CMB measurements, it was found that the dimensionless scalar power spectrum is scale-invariant and Gaussian just as predicted by the inflation. Also, the B-modes in CMB are produced from the tensor mode fluctuations, thus the detection of B-mode in CMB verifies the inflationary theory.

The relative contribution of GW is usually indicated by the tensor-to-scalar ratio r, defined as

$$r = \frac{\mathcal{P}_h(k)}{\mathcal{P}_{\mathcal{R}}(k)} \approx 16\varepsilon. \tag{2.79}$$

With this, we get the so-called consistency relation for SFSR inflationary models,

$$r = -8n_T(k), \tag{2.80}$$

where the tensor spectral index ($n_T(k)$) is defined as $n_T(k) = \frac{d\log \mathcal{P}_h(k)}{d\log k} \approx -2\varepsilon$. The above relation is independent of the energy scale resulting in the scale-invariant spectrum. Surprisingly, the relation is independent of inherent details of the inflationary potential, it involves only the observable quantities.

There are also a couple of ways to generate GWs during the Inflation stage:

1) If additional fields are present during inflation, the coupling between the inflaton field and the other species also provides a way to generate GWs. One such way is particle production. In this, the other species such as a gauge field [111] is coupled with inflaton and the enhanced gauge fields act as a source for GWs.

2) If spectator fields (which do not influence inflation) were present, then spectator fields acquire perturbations that act as sources for GWs [112]. All these other ways provide a spectrum of GWs with large amplitude, occurring at certain frequencies. These new approaches provide very interesting targets for upcoming GW detectors.

B. Preheating: Hot Big Bang theory predicts the early universe is filled with all kinds of relativistic species in thermal equilibrium but after the inflation, the universe is left with

energy of inflation only. So, to reconcile with the Big Bang scenario, there must be a phase/stage of immense particle production, that happened after inflation. This stage is known as Preheating. This particle production happens by coupling the inflaton to other particle species, then the inflaton will decay into those species. This process is highly dependent on the model, which varies from perturbative decay [113] to nonperturbative effects like parametric resonance [114] or spinodal instabilities [115]. These nonperturbative effects in addition to creating particles, also produce large amounts of GWs at very high frequencies.

C. Phase Transitions: As the universe expands, the temperature also drops down which triggers many phase transitions in the early universe. These phase transitions are also known to produce the GWs from the non-zero component of anisotropic stress [116]. One of the prominent examples of phase transition that produces GWs is the Electro-weak (EW) Phase transition. Some of the things that trigger GWs are collisions of bubble walls [117], sound waves [118], and turbulence [119] in the fluid and primordial magnetic fields. These produce GWs in around the mHz frequency which might be detectable with future detectors like LISA.

D. Cosmic Defects: Cosmic defects are types of topological defects. Topological defects are irregularities that occur within continuous fields or ordered phases of matter [120, 121]. A Phase transition in the early universe is a process of changing from a symmetric phase to a symmetry-broken phase. EW phase transition is a spontaneous symmetry breaking of EW symmetry. Phase Transitions are usually driven by some scalar fields (like Higgs in the case of EW phase transition) acquiring a vacuum expectation value within the vacuum manifold. Depending on the nature of symmetry breaking (continuous or discrete), various topological defects are formed after the phase transitions according to the Kibble-Zurek mechanism [122]. The most popular topological defects are cosmic strings (1-dimensional), domain walls (2-dimensional), monopoles, Textures, etc. One can think of these defects as in the case of ferromagnetic materials having regions of magnetic align-

ment separated by domain walls. These cosmic defects while evolving generate GWs [123]. Since the processes generating cosmic defects mostly depend on beyond Standard model, detecting these types of GWs also tells us about beyond Standard model theories.

One can ask why the GWs from the cosmological processes in the very early universe are stochastic in nature? The reason for this depends on type of cosmological processes. The argument in case of inflation is as follows. It is due to its GW-generating process. As we discussed above, the source for the inflationary GW are quantum fluctuations in the metric tensor during inflation. Thus, the tensor modes of metric fluctuations are just random variables with random phases. As the universe expands, the occupation numbers of fluctuations become very large prompting a quantum-to-classical transition of the metric perturbation. This transition makes the metric perturbation which is inherently of quantum origin, behave similarly to a stochastic variable. Then, the metric perturbations re-enter the Hubble radius during the later stages like radiation and matter-dominated eras, generating a GW signal that is inherently stochastic.

The above way of argument for stochasticity does not work for other types of PGWs. For the remaining ones, one could think in this way [11]. Consider the cosmological horizon at time of GW generation is of order H_g^{-1}, where H_g is the Hubble parameter at the time of GW generation. Any GW source acting at that time cannot produce a signal correlated at length/ time scales larger than H_g^{-1}, i.e. $l_g \leq H_g^{-1}$ and $\Delta t_g \leq H_g^{-1}$, due to causality. Let the today's red-shifted length/time scale is l_g^0 / Δt_g^0 and the cosmological horizon is H_0^{-1}. At present time, we have access to much larger length/time scales than the l_g^0 or Δt_g^0. Even the correlation scale is very small, i.e. $l_g^0/H_0^{-1} \sim O(10^{-11})$. Thus, the GWs signal in the universe today is composed by a superposition of many signals uncorrelated in time and space.

2.2 Interaction of Gravitational Waves with Matter

We saw how the GWs are generated from different sources in Sec. 2.1.4. The different sources include scalar fields, fermionic fields, gauge fields and a variety of exotic fields. In order to interpret the measurements of GWs, we need to have information about how the GW is affected by its propagating medium. Now, let us consider that GWs were generated by other processes and investigate how the matter fields were affected in the presence of GWs. In this section, we will give a brief review of the work done on the influence of GWs on a scalar field (Sec. 2.2.1), fermions (Sec. 2.2.2), and electromagnetic field (Sec. 2.2.3) as these might provide further insights in detecting GWs.

2.2.1 Scalar fields in the background of Gravitational waves

Many people investigated the scalar fields in the background of GWs. This subsection is based on [29, 124–128]. The most important scalar fields relevant to the early universe are the Higgs field and the inflaton field. Since these fields were present in the early universe, they have a high chance of interacting with GWs. The Lagrangian density for a scalar field in a general curved spacetime is

$$\mathcal{L} = \sqrt{-g}\left[\frac{1}{2}g^{\mu\nu}\partial_\mu\phi\partial_\nu\phi - \frac{1}{2}(\mu^2+\xi R)\phi^2 - \frac{\lambda}{4}\phi^4\right], \tag{2.81}$$

where μ is the mass parameter of the scalar field (ϕ), λ is the self-coupling quartic coefficient of the scalar field, g is the determinant of the metric $g^{\mu\nu}$ and ξ is the coupling strength between the scalar field and Ricci scalar R. Using the above Lagrangian density, the vacuum expectation value of Higgs was found to be dependent on the curvature of the spacetime [124]. It was found to be true for a stationary gravitational field [125] and for a GW background [126]. For a scalar field in the presence of a GW, the dynamical equation is given by Klein Gordon equation in curved background as

$$\frac{1}{\sqrt{-g}}\partial_\mu\left(g^{\mu\nu}\sqrt{-g}\,\partial_\nu\,\phi\right) = 0. \tag{2.82}$$

Using this, it was shown that a massless scalar field acquires a non-zero expectation value when reacting with the GW background [127]. This is related to the above-discussed Higgs shifts. This case of study has consequences in the preheating stages of the early universe. There also has been considerable research along the quantum calculations regarding scalar fields in classical GW backgrounds. In [128], they constructed the massive scalar field propagator in GWs propagating in a flat background, which helps in understanding the scalar field's response to classical GW background from the quantum field theory picture. Recently in [29], the authors found a new scalar perturbation mode propagating in the direction of resultant of the initial scalar field and GW directions. They also found that the amplitude of perturbed waves depends on the GW frequency.

2.2.2 Fermionic fields in the background of Gravitational waves

The studies of fermions in the background of GWs date back to the 1980s. These studies are motivated by trying to understand the behaviour of electrons and neutrinos in different cosmological backgrounds and their behaviour in near black holes. The main equation in studying the dynamics of fermions is the Dirac equation in a general curved background,

$$i\bar{\gamma}^{\mu}(\partial_{\mu}+\Gamma_{\mu})\psi_{\alpha}=0, \tag{2.83}$$

where $\bar{\gamma}^{\mu}$ are the spacetime-dependent gamma matrices and Γ_{μ} is the spinor affine connection. The details regarding the terms in the Dirac equation are given in Appendix B. The first known studies of fermions in the background of plane GWs are given in [129], where authors find the exact solutions of the Dirac equation in the presence of an exact gravitational plane wave [130]. Recently in [29], authors found that the neutrino has a non-trivial interaction with GW. The perturbed neutrino density shows an oscillatory behaviour and has physical implications that it might induce corrections to the effective number of neutrino species for cosmic neutrino background. These perturbations might also influence the neutrino flux observations from neutron star collisions. They also found a new resonant

mode when neutrinos interact with cross-polarised GW and might be useful for GW detection experiments. There are some studies on the Dirac equation in the GW background using Quasi-normal modes. These are used to investigate perturbations of a black hole to determine its parameters (The frequencies of these modes contain two parts: the real part corresponds to oscillations and the imaginary part corresponds to damping effects). Particularly in [131], the authors investigated the massive and massless Dirac equation in a 2+1 GW background with and without magnetic fields. It is found that in the case of a massless Dirac field in the presence of a magnetic field, the magnetic field acts like an "effective mass". In the case of a massive Dirac field, it is found that the magnetic field has a negative effect on GW by increasing the imaginary part of the frequency of quasi-normal modes.

2.2.3 Electromagnetic waves in the background of Gravitational waves

As opposed to previous cases, there were so many studies trying to investigate EM waves in the GW background. As we know almost all the GW detectors are based on using EM radiation. It is very easy to manipulate and create EM radiation. By studying the properties of EM waves to a higher precision, we might be able to detect GWs. Here, we give a simple review of important results obtained in this field. The main equation to be studied in this case is Maxwell's equation in general spacetimes,

$$\frac{1}{\sqrt{-g}}\partial_\mu\left(\sqrt{-g}g^{\mu\alpha}g^{\nu\beta}F_{\alpha\beta}\right)=0, \tag{2.84}$$

where $F_{\mu\nu}=\partial_\mu A_\nu-\partial_\nu A_\mu$ is field strength tensor in terms of the photon field A_μ. Using this equation, the authors in [132] calculated the GW-induced phase changes in EM wave for arbitrary angles of GW incidence, and authors in [133, 134] studied the EM wave amplitude perturbations for some specific incidence angles of GW. In [135], authors combined the calculations in both cases: phase and amplitude perturbations of EM waves for arbitrary incidence angles of GWs.

A more recent and detailed analysis of the interaction of GWs with EM waves is found

in [26] where they also consider the different orientations in different spacetimes. When they studied the interaction of a GW propagating in the z-direction and an EM wave propagating in the x-direction, it was found to generate inhomogeneous terms in Maxwell's equations in the linearised approximation. The inhomogeneous terms which are proportional to the product of EM wave and GW terms provide a driving force for perturbations. They found that the perturbed solution contains terms that cause phase shifts and also indicate the presence of a new frequency mode. They predicted that the phase shift identified in perturbation can be identified in a GW observatory, LIGO. Also, the new mode can be observed if the frequency of an electromagnetic wave is of the order of the frequency of gravitational waves. They also find that there is no interaction when GW and EM waves propagate in the same direction.

The authors also studied the interaction in the de Sitter background. It was found that the GW produces a modulation over the shape of the unperturbed wave. The perturbed gauge potential grows as τ^2 in contrast to the unperturbed one which grows linearly with τ (here τ is conformal time). Since there are no external sources for EM fields as imposed on equations, the EM perturbations are generated spontaneously from the GWs and cosmological background. This phenomenon corresponds to a particle creation when quantized in the cosmological background.

Apart from the amplitude and phase shifts, there is another way of detecting GW which is by using the polarization angle of light. The angle of polarization of a light beam will be rotated as it passes through the non-zero curvature regions like GWs [136].

As the matter inside the stars, neutron stars, etc, is in the plasma state, it is really important to investigate the influence of GWs on plasma. In the same line of thought, it was found that the plasma waves are parametrically excited in the presence of GWs [137, 138]. This conversion of GW energy to plasma waves is relevant in the case of supernovae as discussed in [139].

2.3 Conclusion

In this chapter, we discussed how to define GWs in different scenarios, starting with linearized gravity in vacuum using the familiar transverse and traceless gauge in Sec. (2.1.1). We discussed the GWs in the presence of sources using SVT decomposition in Sec. (2.1.2) and found that the GWs are defined with only two degrees of freedom. After that, we discussed the GWs in more general backgrounds (Sec: 2.1.3) using the definition based on length scales and applied it to more familiar spacetime like the FLRW background. We then derive the expressions of GWs (Eqs. 2.67 - 2.69) propagating in different stages of the Early universe like de Sitter, radiation-dominated, and matter-dominated stages. After that, we gave a brief review of different types of GWs and their sources more focused on Early universe sources. We explained more about GW generation during inflation including the observational aspects complementing with CMB measurements. We also explained why the inflationary GWs are stochastic in nature. Finally, we discussed the effect of GWs on different matter fields like scalar particles, fermions, and EM fields. The study of GW's influence on matter is essential for the discovery of primordial GWs as well as understanding their physics in greater depth.

Chapter 3

Non-Abelian Gauge Theory

> ”Not only is the Universe stranger than we think, it is stranger than we can think.”
>
> *Werner Heisenberg*

Gauge theory provides a theoretical framework for describing the dynamics of fundamental forces and particles in the universe. It is crucial in explaining the three fundamental forces of nature: electromagnetic force, weak nuclear force, and strong nuclear force. It also plays an essential role in unifying the electromagnetic and weak nuclear force as an electro-weak force. It unifies the different types of forces under the principles of symmetry into one standard model of particle physics.

Any physical theory describing nature is given by Lagrangian that is invariant under some symmetry transformations. There are two types of symmetries: Global symmetry and Local symmetry. If the Lagrangian is invariant under a transformation that is performed identically at every spacetime point, then the theory is said to have global symmetry. While the local symmetry of a theory is such that the transformations are functions of spacetime points. Local symmetry, which is a stronger constraint than global symmetry, is the cornerstone of the gauge theories.

Gauge theory is a type of field theory in which the Lagrangian of the system remains invariant under certain local transformations. This type of local ‘symmetry’ in the system is called Gauge symmetry and the transformations are called gauge transformations. These

gauge transformations form a Lie group known as the Symmetry group or gauge group of the theory. For every Lie group, there is an associated Lie algebra of group generators. For each group generator, there is a corresponding affine connection called the gauge field. These gauge fields are responsible for making the Lagrangian invariant under local group transformations. They mediate the interactions between the particles. When this type of theory is quantized, the particles corresponding to gauge fields are called gauge bosons.

Depending on whether the gauge group is commutative, there are two types of theories: Abelian gauge theory, the gauge theory in which the gauge group is commutative, and Non-Abelian gauge theory is the one which the gauge group is non-commutative. Quantum Electrodynamics is an Abelian gauge theory with the symmetry gauge group $U(1)$. Since U(1) has one generator, it has one gauge field, the four-vector electromagnetic potential, and the photon is the gauge boson. Yang-Mills (YM) Theory or non-abelian gauge theory is the generalization of electromagnetic theory to include non-Abelian gauge groups. The YM theory is essential for describing the strong nuclear force (Quantum chromodynamics (QCD)) and electroweak force (unification of electromagnetic and weak nuclear force). QCD is the non-abelian gauge theory with the gauge group $SU(3)$ and has eight gauge bosons (gluons). The Standard model, which is a unification of three fundamental forces: electromagnetic, weak, and strong nuclear forces, is a non-abelian gauge theory with the symmetry group $SU(3) \times SU(2) \times U(1)$ and has twelve gauge bosons: a photon, three weak bosons, and eight gluons. Gauge theories are also important in studying gravitation, which is well-studied as the theory of general relativity with gauge group GL(4, R).

Excluding photon, the other gauge bosons were predicted in the 1970s based on their underlying gauge theory. The W and Z bosons were predicted as gauge bosons responsible for mediating weak nuclear force or weak interactions. The first experimental evidence for W and Z bosons was found in 1973 from the neutrino interaction observations which resulted in final states that can only be explained after one took consideration of heavy gauge bosons. More concrete evidence was found in 1983 at CERN while studying the

proton-antiproton collisions resulting in the observation of $W^- \to e^- + \nu_e$ as well as $Z \to e^+ + e^-$ or $Z \to \mu^+ + \mu^-$ [140]. Gluons were predicted as gauge bosons for the strong nuclear force, responsible for mediating strong interactions. It is the second gauge boson to have been discovered experimentally, the first one being the photon discovered more than 50 years earlier. The indirect evidence for the existence of gluons and quarks came from the high-energy deep inelastic scattering experiments at Stanford Linear Collider (SLC) and Fermilab. The first direct evidence of gluons came from the electron-positron collision experiments at the Large Electron-Positron Collider (LEP) at CERN and Fermilab Tevatron. These experiments show three-jet events which indicate the presence of gluons since the gluons are also expected to hadronize along with quarks [141]. This process is known as the gluon bremsstrahlung process where the collisions of electron and positron result in three-jet events coming each from quarks, antiquarks, and gluons [142]. The discovery of gauge bosons has profound implications for our understanding of the fundamental forces of nature. These discoveries confirmed the validity of the Standard model of particle physics [143].

In the next section, we will focus on some formulation aspects of non-abelian gauge theory, followed by exploring some of the classical solutions of non-abelian gauge theory. Later, we will study one of the experimentally verified examples of YM theories, the Electroweak gauge theory.

3.1 Classical Non-Abelian Gauge Theory

YM theory is the generalization of the EM theory to more complicated non-abelian groups. Classical electrodynamics has been studied very well in the literature because of its high application capability in daily life and owing to its easily manipulated nature. As for the classical YM theory, the story is rather different. Because the physical observables of the theory are somewhat difficult to attain in the laboratories, the only interest in the theory comes from the purely theoretical point of view. The main motivation is the YM theory

is an astoundingly rich and complex theory. Because of its highly nonlinear nature, the YM theory has a vast solution space including the monopoles, instability, etc., and closely resembles classical GR rather than Electrodynamics. By studying the classical aspects of YM theory, we can distinguish the genuine quantum effects from the classical background [144].

Another motivation is as follows: The standard perturbative QCD does not solve one of the fundamental problems of particle physics, quark confinement (Sec: 3.1.1). There exists a confining force between quarks and they are always found in bound states such as protons. This is proved by the experiments at colliders and also from the computer simulations of gauge fields on lattice, lattice gauge theory. By studying the classical YM theory in depth, we hope to understand quark confinement. There is a way to quantize the gauge theory around the classical solution of YM equations. The idea is that changing the QCD vacuum from the standard one can result in understanding the problems of theory [144, 145].

Heavy ion collision experiments such as in RHIC and LHC provide interesting insights into properties of strongly interacting matter at high energies. Studies show that there are three main stages in heavy ion collision experiments: pre-equilibrium, equilibrium, and freeze-out. The state beginning right after the collision is described by the pre-equilibrium stage until thermalization occurs. Then, the evolving matter will be in the equilibrium QGP stage until the freeze-out, a stage where quarks and gluons combine to form a hadron gas again. For an evolution of QGP, we need to know the entire description of the pre-equilibrium stage. One of the popular choices of the models for the pre-equilibrium stages is the colour glass condensate [146–148]. This colour glass condensate is an effective description of high-energy nuclei using gauge fields, whose dynamics are governed by the classical YM theory. The material that is formed by the collision of two nuclei is called Glasma [149–151] and it is a precursor of QGP and is governed by classical field theory. Also, some studies show that the QGP can be modeled using condensates. We will discuss the condensates regarding QGP in Chapter 5 along with their interaction with Gravitational

waves.

As discussed before, the non-abelian gauge theories are based on non-abelian Lie groups. The discussion on Lie groups and Lie algebras is given in Appendix C. The theory is constructed based on classical electrodynamics. A compact Lie group G has an associated vector space called Lie algebra $\mathfrak{g}$, with T^a being the generators of the group which satisfy [152]

$$[T^a, T^b] = if^{abc}T^c, \tag{3.1}$$

where $a, b, c = 1, .., \dim\ G$, f^{abc} are the totally anti-symmetric structure constants of Lie algebra associated with gauge group G and also we used Einstein summation convention for group indices, i.e. $\sum_{a=1}^{\dim\ G} A^a A^a \equiv A^a A^a$.

For each element of Lie algebra, we assign a corresponding gauge field, A^a_μ ($\mu = 0, 1, 2, 3$) and these are combined into a compact structured gauge potential $A_\mu = A^a_\mu T^a$. One can see the similarity between this gauge potential and one in electrodynamics. The difference is that gauge potential is rather in abstract Lie algebra space. This is also an abstract object just like the vector potential in electromagnetic theory. For any arbitrary group element $\Omega \in G$, the compactified gauge field transforms as [153]

$$A_\mu \to \Omega\, A_\mu\, \Omega^{-1} - \frac{1}{ig_{ym}} \Omega\, \partial_\mu\, \Omega^{-1}. \tag{3.2}$$

where g_{ym} is the YM coupling constant which determines the interaction strength between the gauge fields. The discussion on gauge symmetry and physical observables of the theory is given later. Here, we will give some relevant concepts regarding Lie algebra. The Lie algebra $\mathfrak{g}$ has many different representations R, accordingly, there are generators $T^a(R)$ for each representation. There are mainly two types of representations: Fundamental representation and Adjoint representation. These generators can be thought of as square matrices of

dimension dim R and can be taken as

$$T^a(R)^i_j,\ i,j=1,..,\ \dim R,\ a=1,..,\dim G. \tag{3.3}$$

We deal with fundamental representation when we are considering matter fields (fermions) in the system and adjoint representation when dealing with gauge fields. Since, the matter fields (fermions) present in fundamental representation R of gauge group $G=SU(N)$, which are given by an N-dimensional vector ψ. The interaction of matter fields with gauge fields is given by gauge covariant derivative which is

$$D_\mu\psi=\partial_\mu\psi-i\ g_{ym}\ A_\mu\psi, \tag{3.4}$$

and in component form,

$$D_\mu\psi^i=\partial_\mu\psi^i-i\ g_{ym}\ A^a_\mu T^a(R)^i_j\psi^j. \tag{3.5}$$

Each of the representations has a different way of packing gauge fields A^a_μ into compact lie-algebra valued objects A_μ. In the fundamental representation as above, the $A_\mu=A^a_\mu T^a$ represents a $N\times N$ Hermitian matrix. For example, consider $G=SU(2)$, then the $T^a=\sigma^a/2$, where $\sigma^a,\ a=1,2,3$ are the Pauli matrices, each are 2×2 matrices. Similarly, for $G=SU(3)$, the $T^a=\lambda^a/2$ where $\lambda^a,\ a=1,...,8$ are the Gell-mann matrices, each are of 3×3 matrices.

The adjoint representation is for which the dim $R=$ dim G and the representation matrices are given by structure constants $(T^a)_{bc}=f^{abc}$. Consider an adjoint valued matter field ϕ^a with $a=1,...,\dim G$, and the gauge covariant derivative is given by

$$D_\mu\phi=\partial_\mu\phi-i\ g_{ym}\ [A_\mu,\phi], \tag{3.6}$$

where we used the compact notation $\phi=\phi^aT^a$ and commutator definition $[A,\phi]=[A^a_\mu T^a,\phi^bT^b]=$

$if^{abc}A^a_\mu\phi^b T^c$. Then, the in-component form

$$(D_\mu\phi)^a = D^{ab}_\mu\phi^b = \delta^{ab}\partial_\mu\phi^b + g_{ym}\, f^{acb}A^c_\mu\phi^b. \tag{3.7}$$

To formulate a theory, one needs to define Lagrangian density from the dynamical part of gauge fields. For that, one needs to define the field strength tensor as a function of gauge fields:

$$F_{\mu\nu} = \partial_\mu A_\nu - \partial_\nu A_\mu - i\, g_{ym}\, [A_\mu, A_\nu], \tag{3.8}$$

such that the field strength tensor transforms covariantly under gauge transformations, $F_{\mu\nu} \to \Omega\, F_{\mu\nu}\, \Omega^{-1}$. In component form, the field strength tensor is given by

$$F_{\mu\nu} = F^a_{\mu\nu}T^a,\ F^a_{\mu\nu} = \partial_\mu A^a_\nu - \partial_\nu A^a_\mu + g_{ym}f^{abc}A^b_\mu A^c_\nu. \tag{3.9}$$

One can also construct the field strength tensor from the commutator of covariant derivatives as $[D_\mu, D_\nu] = -ig_{ym}\, F_{\mu\nu}$. Following the electrodynamics, we can construct the gauge invariant action as

$$S_{ym} = \int d^4x \mathcal{L}_{ym} = -\frac{1}{2}\int d^4x\ \mathrm{tr}\, F^{\mu\nu}F_{\mu\nu} = -\frac{1}{4}\int d^4x\, F^a_{\mu\nu}F^{a\mu\nu}. \tag{3.10}$$

In the presence of sources, the Lagrangian density is given by

$$\mathcal{L}_{ym} = -\frac{1}{4}F^a_{\mu\nu}F^{a\mu\nu} + J^{a\mu}A^a_\mu, \tag{3.11}$$

where J^μ_a are the color source charges. Here, the first term represents the kinetic energy of gauge fields and their respective self-interactions. The second term describes the interactions between the gauge fields and matter fields.

The classical equations of motion are derived by minimizing the action with respect to

each gauge field A^a_μ:

$$\partial_\mu F^{a\mu\nu} + g_{ym} f^{abc} A^b_\mu F^{c\mu\nu} = J^{a\nu}. \tag{3.12}$$

One can also write this in a compact notation as

$$D_\mu F^{\mu\nu} = J^\nu, \tag{3.13}$$

where D_μ is the gauge covariant derivative in the adjoint representation. In gauge theory, the Eqs. (3.12) or (3.13) are referred to as YM equations. Without the sources, one can also define dual field strength tensor as follows

$${}^*F^{\mu\nu} = \frac{1}{2}\varepsilon^{\mu\nu\rho\sigma} F_{\rho\sigma}, \tag{3.14}$$

where $\varepsilon^{\mu\nu\rho\sigma}$ is the four-dimensional Levi-Civita tensor. It satisfies the following identity,

$$D_\mu \, {}^*F^{\mu\nu} = 0. \tag{3.15}$$

The equations (3.13) and (3.15) are the non-abelian generalizations of Maxwell's equations. As we can see, the only difference is in the commutator terms present in the definition of $F_{\mu\nu}$ and inside D_μ. Even in classical theory, the equations of motion are highly non-linear which means they interact with themselves.

In Electromagnetism, Maxwell's equations can be given entirely in terms of electric and magnetic fields. We can also represent the YM equation in terms of electric and magnetic fields by defining

$$E^a_i = F^a_{i0} = \partial_i A^a_0 - \partial_0 A^a_i + g_{ym} f^{abc} A^b_i A^c_0, \tag{3.16}$$

$$B^a_i = -\frac{1}{2}\varepsilon^{ijk} F^a_{jk} = -\frac{1}{2}\varepsilon^{ijk}(\partial_j A^a_k - \partial_k A^a_{ij} + g_{ym} f^{abc} A^b_j A^c_k), \tag{3.17}$$

where $i, j, k = 1, 2, 3$. Using the above definitions, one can rewrite the equations (3.13) and

(3.15) as

$$\partial_i E_i^a + g_{ym} f^{abc} A_i^b E^{ci} - \rho^a = 0, \tag{3.18}$$

$$\partial_i B_i^a + \frac{1}{2} g_{ym} f^{abc} \varepsilon_{ijk} \partial_i (A^{bj} A^{ck}) = 0, \tag{3.19}$$

$$-\partial_0 E_i^a + \varepsilon_{ijk} \partial^j B^{ak} - g_{ym} f^{abc} A_0^b E_i^c - g_{ym} f^{abc} \varepsilon_{ijk} A^{bj} B^{ck} - J_i^a = 0, \tag{3.20}$$

$$\partial_0 B_i^a + \varepsilon_{ijk} \partial^j E^{ak} + \frac{1}{2} g_{ym} f^{abc} \varepsilon_{ijk} \partial_0 (A^{bj} A^{ck}) + g_{ym} f^{abc} \varepsilon_{ijk} \partial_j (A_0^b A^{ck}) = 0, \tag{3.21}$$

In contrast to Maxwell's theory, we cannot represent the YM equations just in terms of electric and magnetic fields and it includes the terms involving gauge fields. These are due to non-linear terms in the equation. Also, if we set the sources $J_\mu^a(\rho^a, J_i^a) = 0$ in the above equations, we still observe that there is a presence of sources that are of gauge field origin. It means that the gauge fields are color-charged and act as a magnetic field source at the same time. From Eq. (3.19), the divergence of the magnetic field is nonzero which suggests the existence of magnetic monopoles in contrast to classical electromagnetism [154].

Gauge Symmetry

As we discussed before, for any arbitrary group element $\Omega \in G$, the gauge field transforms as Eq. (3.2), and the field strength tensor transforms covariantly. The Yang-Mills action given in Eq. (3.10) is then invariant under any transformations.

Gauge symmetry is not an actual symmetry in the sense that it does relate from physical state to another physical state, but rather signifies a redundancy in the degrees of freedom of the system. We can see this classically in the sense that Eqs. (3.13) and (3.15) does not describe the evolution of gauge field uniquely, but only a class of solutions related by gauge transformation (3.2). Due to this redundancy, the main postulate of gauge theory states that all the physical observables or quantities must be gauge invariant, i.e. invariant under gauge transformations. These quantities do not depend on the choice of description. For comparison, in GR, these types of quantities are coordinate invariant.

Let us consider the familiar theory of electromagnetism. In this case $G = U(1)$, the above transformations reduce to familiar ones in electromagnetism. Taking $\Omega = e^{i\alpha(x)}$, the gauge field transforms as $A_\mu \to A_\mu + \partial_\mu \alpha(x)$. Then, the field strength tensor transforms as

$$F_{\mu\nu} \to F'^{\mu\nu} = \partial_\mu(A_\nu + \partial_\nu\alpha) - \partial_\nu(A_\mu + \partial_\mu\alpha) = F_{\mu\nu}. \tag{3.22}$$

It means the field strength tensor in electromagnetism is invariant, implying that the electric and magnetic fields are also invariant, thus they are physical observables. But, in the case of YM theory, the field strength tensor is not gauge invariant and correspondingly electric and magnetic fields are also not gauge invariant. For this reason, these fields along with the gauge fields do not have any physical meaning. If we want to construct gauge invariant quantities, we should work with traces of gauge fields like tr $F^{\mu\nu}\ F_{\mu\nu}$ or tr $\varepsilon^{\mu\nu\rho\sigma}\ F_{\mu\nu}\ F_{\rho\sigma}$ or Wilson lines/loops [155].

Wilson lines and Wilson loops

Wilson loops are gauge-invariant objects arising from the parallel transport of gauge variables around the closed loops [30]. Mathematically, the gauge theory is an example of a principal fibre bundle, and the gauge field A_μ acts as a connection. Here, the term connection is the same as in General Relativity like the Levi-Civita connection, which tells us how to parallel transport vectors around the manifold. Similarly, in the YM case, the A_μ is an affine connection but for an appropriate internal degree of freedom. This internal degree of freedom is labeled as a "charge". For example, for QCD, these charges refer to color degree of freedom and the particles having these charges are quarks and gluons.

Consider a fixed background YM field $A_\mu(x)$ and a particle (like quark) carrying a complex vector (like charge), w, of fixed length,$w_i,\ i = 1, ..., \dim R$ such that $w^\dagger w =$ constant. As the particle moves around the manifold, the connection A_μ tells the vector w_i how to rotate. This parallel transport phenomena in Maxwell's theory is nothing more than the Aharonov-Bohm effect [156]. For a particle moving with worldline $x^\mu(\tau)$, the complex

vector w_i satisfies the following differential equation

$$i\frac{dw}{d\tau} = \frac{dx^\mu}{d\tau}A_\mu(x)w. \tag{3.23}$$

The general solution for the above equation is given by

$$w(\tau_f) = U[x_i, x_f; C]w(\tau_i), \tag{3.24}$$

where

$$U[x_i, x_f; C] = \mathcal{P}\exp\left(i\int_{\tau_i}^{\tau_f} d\tau\frac{dx^\mu}{d\tau}A_\mu(x(\tau))\right) = \mathcal{P}\exp\left(i\int_{x_i}^{x_f} A\right), \tag{3.25}$$

where $\mathcal{P}$ stands for path ordering, $x_i^\mu = x_i^\mu(\tau_i)$ and $x_f^\mu = x_f^\mu(\tau_f)$ corresponds to initial and final positions along the curve C. The quantity $U[x_i, x_f; C]$ is known as Wilson Line and it transforms under gauge transformation $\Omega(x)$ as

$$U[x_i, x_f; C] \to \Omega(x_i)\, U[x_i, x_f; C]\, \Omega^\dagger(x_f). \tag{3.26}$$

If we consider a closed path C, then the Wilson line tells us how the vector differs from its initial value. Using this, we can form a gauge invariant object known as the Wilson loop,

$$W[C] = \mathrm{tr}\mathcal{P}\exp\left(i\oint A\right). \tag{3.27}$$

Wilson loops come under a broad class of loop operators. Some of the examples are the t'Hooft loops [157], which are magnetic duals to Wilson loops, and Polyakov loops [158], which are thermal analogs of Wilson loops. In pure gauge theory, the Polyakov loops act as an order parameter for confinement at nonzero temperatures.

3.1.1 Asymptotic freedom and Confinement

Asymptotic Freedom and Confinement are two fundamental concepts in QCD, the theory that describes the strong interaction between quarks and gluons. Asymptotic freedom refers to the phenomenon where the interaction strength between quarks decreases as they come closer or at higher energy scales. It means the quarks behaves almost like free particles at higher energies or short distances. The interaction strength of the strong nuclear force is determined by the coupling constant (g_{ym}). As the interaction strength between the quarks depends on energy scale, the coupling constant must also be a function of energy scale. The coupling constant which depends on energy scale of the system is called running coupling constant ($g_{ym} \equiv g$) and is related to bare coupling constant ($g_{0ym} \equiv g_0$) as

$$g^2(\Lambda) = \frac{g_0^2}{1 + \frac{g_0^2}{16\pi^2}\left(\frac{11}{3}N - \frac{2}{3}N_f\right)\ln(\Lambda^2/M^2)} = \frac{g_0^2}{1 + g_0^2\,\beta_0\,\ln(\Lambda^2/M^2)}, \tag{3.28}$$

where $\beta_0 = \frac{1}{16\pi^2}\left(\frac{11}{3}N - \frac{2}{3}N_f\right)$, N is related to gauge group $SU(N)$, N_f is the number of fermion species, Λ is the energy of the system and M is the renormalisation scale. The above expression is obtained by solving a differential equation involving the well-known beta function ($\beta(g_0)$) as

$$\Lambda\frac{\partial g}{\partial \Lambda} = \beta(g), \tag{3.29}$$

with $\beta(g) = -\frac{g^3}{16\pi^2}\left(\frac{11}{3}N - \frac{2}{3}N_f\right)$.

Thus, as long as $\left(\frac{11}{3}N - \frac{2}{3}N_f\right) > 0$, we see the coupling constant decreases with increasing Λ. This is a discovery with enormous significance. On one hand, it says that if at some energy scale, the coupling constant is perturbative, it will decrease its values at higher and higher energy scales, making the perturbation theory results more and more precise. One can also make the same argument with distance scales. On the other hand, at lower and lower energy scales, the coupling constant becomes bigger and bigger moving away from the perturbative regime.

In QCD, the gauge group is $SU(3)$ and quarks are in the fundamental representation.

Thus, we get $11 - \frac{2}{3}N_f$, so for $N_f \leq 16$, we have the beta function to be negative. It means the QCD is an asymptotically free theory. The gauge coupling gets weaker at higher energies and stronger at lower energies. The energy scale at which the interaction strength is infinity is known as the QCD energy scale (Λ_{QCD}). One can also find this QCD energy scale by setting the running coupling constant to infinity, i.e. $g^2(\Lambda_{QCD}) = 0$. This gives

$$1 + g_0^2\, \beta_0\, \ln(\Lambda_{QCD}^2/M^2) = 0 \implies \Lambda_{QCD} = M e^{-\frac{1}{2g_0^2\, \beta_0}} \tag{3.30}$$

By inserting this in Eq. (3.28), we can eliminate M and rewrite the running coupling constant as

$$g^2(\Lambda) = \frac{1}{\beta_0\, \ln(\Lambda/\Lambda_{QCD})}. \tag{3.31}$$

As we go to low-energy physics around Λ_{QCD} scale, the coupling constant (interaction strength) becomes infinity. As expected, in nature, we do not see isolated quarks and gluons. This leads to the Confinement hypothesis: In an asymptotically free theory, only singlets under the strong gauge force could serve as asymptotic states. As QCD is asymptotically free, the asymptotic states are not isolated quarks and gluons but rather composite states made up of quarks, gluons, and antiquarks which makes the color charge neutral.

Rescaling

In general, in quantum field theory, the coupling constants appear in the interaction terms in the Lagrangian, and in the terms of higher order in coupling constant reflected by the non-linear terms in equations of motion. However, in the YM action, all terms appear with fixed coefficients determined by the definition of field strength tensor. If we define the gauge field in such a way that the coupling constant is absorbed into the gauge field ($\tilde{A}_\mu = g_{ym}\, A_\mu$), then the field strength tensor scales as

$$F_{\mu\nu} = \frac{1}{g_{ym}} \tilde{F}_{\mu\nu}, \;\; \tilde{F}_{\mu\nu} = \partial_\mu \tilde{A}_\nu - \partial_\nu \tilde{A}_\mu - i[\tilde{A}_\mu, \tilde{A}_\nu]. \tag{3.32}$$

Then, the Yang-Mills action is

$$S_{ym} = -\frac{1}{4}\int d^4x F^{a\mu\nu}F^a_{\mu\nu} = -\frac{1}{4g^2_{ym}}\int d^4x \tilde{F}^{a\mu\nu}\tilde{F}^a_{\mu\nu}. \tag{3.33}$$

In the second version of the action, the coupling constant is taken outside of the action. This second version of action is more useful in dealing with the quantized version of this theory.

3.2 Classical Solutions of non-Abelian gauge theory

We already discussed the use of classical non-abelian gauge theory in investigating the physical content of quantum field theory. To continue, we discuss some of the classical solutions of Yang-Mills theory.

The first exact solution of the $SU(2)$ YM equation is the Coulomb solution embedded in a larger theory which was found by Ikeda and Miyachi [159]. These types of embedding solutions turn out to be found for any other higher groups [160] and, these are just approximate solutions. A true non-abelian YM solution was found by Wu and Yang [161], which is point-like, i.e. gauge potential behaves like $1/r$ everywhere. This type of solution describes a non-abelian magnetic monopole which suggests that the non-abelian theories provide a natural setting for magnetic monopole solutions.

Apart from these point-like solutions, YM theories have different complicated solutions. One of the solutions includes Dyons, a monopole solution with arbitrary electric charge. $SU(2)$ YM theory is also known to have a magnetic monopole solution with a Higgs triplet [162], which has the properties of being non-singular and has finite energy. Another important solution of classical YM theory is the wave solutions [28, 163]. In our thesis, we will discuss the non-abelian wave solutions.

To keep the discussion, we move on to the solutions in Euclidean Spacetime [164, 165] which have raised more interest than those in Minkowski spacetime. In quantum-

mechanical problems having classical analogs, tunnelling is bound to occur where there exist solutions to classical equations of motion in Euclidean spacetime. The existence of these Euclidean solutions indicates the presence of tunnelling effects in quantized field theory. There are three types of Euclidean solutions which are Instantons, Merons, and Elliptic solutions. The main differences between these solutions is they depend on certain topological properties of Euclidean theory. The instanton solution is characterized as non-singular, localized, self-dual, and by a topological charge $q = 1$. These instanton solutions are known to play a key role in understanding the problems related to quantum tunnelling. It was found that the massless fermions in the presence of an instanton field become massive indicating the role of instantons in mass generation and chiral symmetry breaking. Unlike instantons, merons are point-like concentrations having a one-half unit of topological charge. There have been studies considering the role of merons in tunneling between two different topological vacua in real-time.

In the next section, we focus on wave solutions of non-abelian gauge theory.

3.2.1 Wave solutions of Yang-Mills Theory

Yang-Mills wave solutions are not that physically relevant as compared to the wave solutions in electrodynamics which are extremely useful. Although being a nonlinear wave, the YM wave might not be directly observed due to confinement. We can still discuss the systems in scenarios in which the system is deconfined and the YM wave can propagate freely [17]. This is the scenario of QGP. Also, it was suggested that the wave solutions of YM theory may be relevant for understanding the structure of theories of quantum vacuum and asymptotic states [166]. With these motivations, a lot of work has been done on wave solutions of Yang-Mills equations [28, 167–177].

All the known wave solutions of YM equations fall into two categories which are different in nature. The below sections closely follow the work given in [28].

A. Type I waves

The first category of waves is characterized by the requirement that the solutions satisfy the following conditions [28]:

$$[A_\mu, A_\nu] = [A_\mu, F^{\mu\nu}] = 0, \;\; [A_\mu, F^{\nu\lambda}] \neq 0, \tag{3.34}$$

where A_μ and $F^{\mu\nu}$ correspond to gauge field potential and field strength tensor, respectively. The above conditions or constraints are inspired by the solutions that satisfy plane wave criteria: (1) the energy density is bounded throughout the spacetime, (2) the direction of the Poynting vector is constant, and (3) the magnitude of the Poynting vector is equal to the energy density. The non-abelian electric and magnetic fields and the wave propagating direction are mutually perpendicular to each other but the magnitude of field strengths vary over each wavefront. Such types of waves are referred to as guided waves. To construct the above type of solution, we choose the following ansatz [28]:

$$A^a_\mu = (\psi_{\overline{\alpha}} f^a_{\overline{\alpha}}(U) + h^a(U))\, \partial_\mu U, \tag{3.35}$$

where U and $\psi_{\overline{\alpha}}$ are functions of spacetime coordinates, and $f^a_{\overline{\alpha}}$ and h^a are functions of U and the repeated index $\overline{\alpha}$ means summation from 1 to 4 (the index $\overline{\alpha}$ has nothing to do with spacetime index). Also, there is no reason why the $\overline{\alpha}$ is summed from 1 to 4. The function $h^a(U)$ can be removed by making a gauge transformation. We can see there are a total of three sets of arbitrary functions, U, $\psi_{\overline{\alpha}}$ and $f^a_{\overline{\alpha}}$. With the above ansatz, one can write the field strength as

$$F^a_{\mu\nu} = (\partial_\nu U \partial_\mu \psi_{\overline{\alpha}} - \partial_\mu U \partial_\nu \psi_{\overline{\alpha}}) f^a_{\overline{\alpha}}(U). \tag{3.36}$$

After substituting the above expressions in YM equation (3.12), we get the equation of motion for U along with the conditions:

$$\partial^\mu U \partial_\mu U = 0, \tag{3.37a}$$

$$\partial^{\mu}U\partial_{\mu}\psi_{\overline{\alpha}}=0, \tag{3.37b}$$

$$\partial_{\nu}\partial_{\mu}U\partial^{\mu}\psi_{\overline{\alpha}}+\partial_{\nu}U\,\Box\psi_{\overline{\alpha}}-\Box U\partial_{\nu}\psi_{\overline{\alpha}}-\partial^{\mu}U\partial_{\nu}U\partial_{\mu}\psi_{\overline{\alpha}}=0, \tag{3.37c}$$

where $\Box=\partial^{\mu}\partial_{\mu}$ is d'Alembertian operator. As we can see the equations or conditions do not contain $f^{a}_{\overline{\alpha}}$, which signifies the arbitrary nature of function $f^{a}_{\overline{\alpha}}$. The conditions (Eqs. 3.37a & 3.37b) are required to remove the functional dependence of $f^{a}_{\overline{\alpha}}$ on equations of motion. Also, the conditions are to be fulfilled not just for solving YM equations rather they have physical interpretation which we can see below. From the above ansatz, the non-Abelian wave solutions are obtained for a set of U and $\psi_{\overline{\alpha}}$ satisfying the equations of motion and conditions. Before discussing the actual solutions, we will discuss some of the properties of the above particular ansatz.

Using the above ansatz (3.35) and equations (3.37), one can find the energy momentum tensor as

$$\begin{aligned}T_{\mu\nu}&=g^{\rho\sigma}F^{a}_{\mu\rho}F^{a}_{\nu\sigma}-\frac{1}{4}g_{\mu\nu}F^{a}_{\rho\sigma}F^{a\rho\sigma}\\&=\left(\partial_{\rho}\psi_{\overline{\alpha}}\,\partial^{\rho}\psi_{\overline{\beta}}\,f^{a}_{\overline{\alpha}}\,f^{a}_{\overline{\beta}}\right)\partial_{\mu}U\partial_{\nu}U,\end{aligned} \tag{3.38}$$

so that

$$T_{00}=\left(\partial_{\rho}\psi_{\overline{\alpha}}\,\partial^{\rho}\psi_{\overline{\beta}}\,f^{a}_{\overline{\alpha}}\,f^{a}_{\overline{\beta}}\right)\partial_{0}U\partial_{0}U,\;\;T_{0i}=\left(\partial_{\rho}\psi_{\overline{\alpha}}\,\partial^{\rho}\psi_{\overline{\beta}}\,f^{a}_{\overline{\alpha}}\,f^{a}_{\overline{\beta}}\right)\partial_{0}U\partial_{i}U. \tag{3.39}$$

Now using the condition (3.37a), one can find the energy and momentum densities are equal in magnitude which was discussed as one of the criteria for being a type I wave. Using the definitions of non-abelian electric and magnetic fields, we write the

$$E^{a}_{i}=\left(\partial_{i}U\partial_{0}\psi_{\overline{\alpha}}-\partial_{0}U\partial_{i}\psi_{\overline{\alpha}}\right)f^{a}_{\overline{\alpha}}, \tag{3.40}$$

$$B^{a}_{i}=\varepsilon_{ijk}\partial_{k}U\partial_{j}\psi_{\overline{\alpha}}f^{a}_{\overline{\alpha}}. \tag{3.41}$$

From these, one can find that the electric, magnetic fields and wave propagation direction

are mutually perpendicular to each other:

$$E_i^a B_i^a = E_i^a T_{0i} = B_i^a T_{0i} = 0. \tag{3.42}$$

Using the equations (3.37), one can also prove that the conditions: $[A_\mu, A_\nu] = [A_\mu, F^{\mu\nu}] = 0$, but $[A_\mu, F^{\nu\lambda}] \neq 0$ which implies the above solution is definitely non-abelian. Now we will discuss some of the particular examples of non-abelian waves of Type I. As we discussed before, by choosing different $\psi_{\overline{\alpha}}$, we get different solutions for U which implies different types of waves. Based on that, we discuss some important wave solutions.

I. Type Ia waves

By choosing the $\psi_1 = x$, $\psi_{\overline{\alpha}} = 0$, $\overline{\alpha} = 2,3,4$, we get the equation of motion for U as

$$\Box U = 0, \tag{3.43}$$

along with the conditions: $\partial_x U = 0$, $\partial^\mu U \partial_\mu U = 0$. With the condition ($\partial_x U = 0$), we can see that U cannot be a function of x. The solution can be found by choosing the remaining dependence of U. One of the solutions is

$$U(t,z) = U_0 \cos(\omega_y (t+z)), \tag{3.44}$$

by choosing the wave propagating in the z-direction, where U_0 is the initial value of U and ω_y is the frequency of the YM wave.

II. Type Ib waves

As the choice of $\psi_{\overline{\alpha}}$ is arbitrary, we can use a more general choice based on the condition: $\partial^\mu \partial_\mu \psi_{\overline{\alpha}} = 0 \implies \psi_{\overline{\alpha}} = A_{\overline{\alpha}} e^{i\mathbf{q}\cdot\mathbf{x}}$, where q_μ is the real four-vector. With this choice, we get

$$\Box U = 0, \tag{3.45}$$

with conditions $q_\mu \partial^\mu U = 0$, $\partial^\mu U \partial_\mu U = 0$. By choosing the same functional dependence

as before the case, we find the solution to be $U(t,z) = U_0 \cos(\omega_y(t+z))$. From condition ($q_\mu \partial^\mu U = 0$), we get $q_0 = q_3$.

III. Coleman waves

The non-abelian waves discovered by Sidney Coleman [167] are a special case of type I waves. The Coleman waves are characterized by the following particular choice:

$$U = t \pm z,\ \psi_1 = x,\ \psi_2 = y,\ \psi_3 = \psi_4 = 0. \tag{3.46}$$

With the above choice, the gauge field found to be

$$A_0^a = \pm A_z^a = x f_1^a(t \pm z) + y f_2^a(t \pm z),\ A_x^a = A_y^a = 0. \tag{3.47}$$

The solution describes the waves travelling in $\pm z$-direction. One can easily find that the electric and magnetic fields depend on arbitrary functions only and are perpendicular to each other and also to the propagating direction.

IV. Plane-Fronted waves

Another choice of plane waves can be found by choosing

$$U = z \pm t,\ \psi_1 = x,\ \psi_2 = y,\ \psi_3 = \ln\rho,\ \psi_4 = \phi, \tag{3.48}$$

where $\rho^2 = x^2 + y^2$. The solution describes the waves travelling along the z-direction with plane fronts. It was found that the magnitude of electric and magnetic field strengths varies across each wavefront and hence, the waves are called plane-fronted non-Abelian waves [28, 177]. The energy-momentum tensor is given by

$$T_{\mu\nu} = \big[\rho^2(f_1^a f_1^a + f_2^a f_2^a) + f_3^a f_3^a + f_4^a f_4^a + 2\rho\cos\phi(f_1^a f_3^a + f_2^a f_4^a) + 2\rho\sin\phi(f_2^a f_3^a - f_1^a f_4^a)\big]\frac{1}{\rho^2}\partial_\mu U \partial_\nu U. \tag{3.49}$$

As we can see the Poynting vector is along the z-direction, thus this represents a wave travelling in z-direction. Choosing $U = z - t$, one can also find the electric and magnetic fields as

$$E^a_z = 0,\, E^a_\rho = -(\cos\phi f^a_1 + \sin\phi f^a_2 + \frac{f^a_3}{\rho}),\, E^a_\phi = -(-\rho\sin\phi f^a_1 + \rho\cos\phi f^a_2 + f^a_4),$$
$$B^a_z = 0,\, B^a_\rho = -\sin\phi f^a_1 + \cos\phi f^a_2 + \frac{f^a_4}{\rho},\, B^a_\phi = -(\rho\cos\phi f^a_1 + \rho\sin\phi f^a_2 + f^a_3).$$

From this also, one can see that the wave travels in z-direction as the electric and magnetic fields have only ρ and ϕ components. As the amplitude of fields across the plane wavefront varies, this is not a simple plane wave but rather a plane-fronted wave.

V. Spherical-fronted waves

Apart from plane wave choice, one can also choose the functions in the following way:

$$U = r \pm t,\, \psi_1 = \phi,\, \psi_2 = \ln\tan(\theta/2),\, \psi_3 = \psi_4 = 0, \tag{3.50}$$

where r,θ and ϕ are the spherical coordinates. This choice gives the spherical-fronted waves [28, 168, 177] where the waves propagate radially and magnitudes of electric and magnetic fields keep on varying over each wavefront. In this case, the energy-momentum tensor is

$$T_{\mu\nu} = \frac{f^a_1 f^a_1 + f^a_2 f^a_2}{(r\sin\theta)^2}\partial_\mu U \partial_\nu U. \tag{3.51}$$

It is clear that the wave propagates in the radial direction, but the Poynting vector does not have a spherical symmetry due to the factor $(r\sin(\theta))^{-2}$. Similarly, we found the field strengths as

$$E^a_r = 0,\, E^a_\theta = -\frac{f^a_2}{\sin\theta},\, E^a_\phi = -f^a_1;$$
$$B^a_r = 0,\, B^a_\theta = \frac{f^a_1}{\sin\theta},\, B^a_\phi = -f^a_2.$$

Similarly, here, the fields have only θ and ϕ components indicating that the wave propagates radially. As opposed to the spherical wave, the amplitudes of fields vary over each wavefront implying they are spherical-fronted waves.

VI. Other Solutions

Many other solutions can be constructed by choosing U and $\psi_{\overline{\alpha}}$ that satisfy the conditions (3.37). However, those solutions are of less significance due to having less physical resemblance. Some of the examples are the following choices [28]:

$$U = \ln R - \sinh^{-1}(t/R),\ R^2 = r^2 - t^2, r = x^2 + y^2 + z^2,$$

$$\psi_1 = \phi,\ \psi_2 = \ln\tan(\theta_2/2); \theta_2 = \cos^{-1}(z/r),\ \psi_3 = \psi_4 = 0.$$

and

$$U = \ln\overline{\rho} + \tanh^{-1}(t/z),\ \overline{\rho}^2 = z^2 - t^2,$$

$$\psi_1 = x,\ \psi_2 = y,\ \psi_3 = \ln\rho,\ \psi_4 = \phi.$$

B. Type II waves

To capture the full strength of the nonlinear structure of YM equations, we consider the second type of waves. These Type II waves are characterized by making non-linear terms in the YM equations nonzero:

$$[A_\mu, A_\nu] \neq 0,\ [A_\mu, F^{\mu\nu}] \neq 0,\ \ [A_\mu, F^{\nu\lambda}] \neq 0, \tag{3.54}$$

Type II waves are also characterized as the energy and momentum densities are not equal in magnitude, still, the waves propagate in the fixed direction.

Constructing a different ansatz with the above properties, we choose the ansatz given in [28] as

$$A^a_\mu = \delta^a_1\ \Phi(u)\ k_\mu + \delta^a_3\ \Psi(u)\ l_\mu, \tag{3.55}$$

where $u = p_\mu x^\mu + e; e$ is an arbitrary constant and k_μ,l_μ, p_μ are three constant vectors orthogonal to each other. By substituting the above ansatz in YM equation (3.12), we get the following coupled nonlinear partial differential equations:

$$\partial_\mu \partial^\mu \Phi - g_{ym}^2 \, l^2 \, \Phi \Psi^2 = 0, \tag{3.56}$$

$$\partial_\mu \partial^\mu \Psi - g_{ym}^2 \, k^2 \, \Psi \Phi^2 = 0, \tag{3.57}$$

where g_{ym} is the YM coupling constant, $l^2 = l_\mu l^\mu$ and $k^2 = k_\mu k^\mu$. Since Φ and Ψ are functions of a single variable (u), we can rewrite the equations as

$$\Phi''(u) - \frac{g_{ym}^2 \, l^2}{p^2} \, \Phi(u) \Psi(u)^2 = 0, \tag{3.58}$$

$$\Psi''(u) - \frac{g_{ym}^2 \, k^2}{p^2} \, \Psi(u) \Phi(u)^2 = 0. \tag{3.59}$$

These are two coupled nonlinear differential equations and the solutions can be expressed in terms of the Jacobi elliptic functions as

$$\Phi(u) = \pm \frac{1}{\sqrt{\beta}} \mathrm{cn}(u, \frac{1}{2}), \tag{3.60}$$

$$\Psi(u) = \pm \frac{1}{\sqrt{\alpha}} \mathrm{cn}(u, \frac{1}{2}), \tag{3.61}$$

where $\alpha = -\frac{g_{ym}^2 l^2}{p^2}$, $\beta = -\frac{g_{ym}^2 k^2}{p^2}$ and $\mathrm{cn}(u, \lambda^2)$ is the cosine Jacobi elliptic function with elliptic modulus λ. The properties of Jacobi elliptic functions are given in Appendix D.1. The solutions correspond to wave solutions only if p_μ must be a time-like vector while l_μ and k_μ must be space-like vectors. The plots are given in Fig. (3.1).

The energy-momentum tensor for the above ansatz is given by

$$T_{\mu\nu} = k^2 \partial_\mu \Phi \partial_\nu \Phi + k_\mu k_\nu \partial_\sigma \Phi \partial^\sigma \Phi + l^2 \partial_\mu \Psi \partial_\nu \Psi + l_\mu l_\nu \partial_\sigma \Psi \partial^\sigma \Psi + g_{ym}^2 (l^2 k_\mu k_\nu + k^2 l_\mu l_\nu) \Phi^2 \Psi^2 - \frac{1}{2} \eta_{\mu\nu} \left(k^2 \partial_\sigma \Phi \partial^\sigma \Phi + l^2 \partial_\sigma \Psi \partial^\sigma \Psi + g_{ym}^2 l^2 k^2 \Phi^2 \Psi^2 \right). \tag{3.62}$$

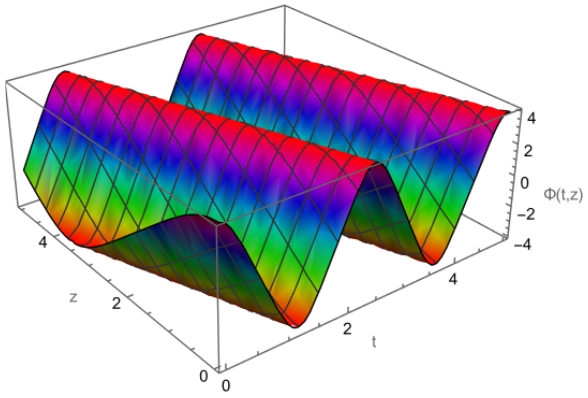

Figure 3.1: The plot of Φ as a function of t and z. As the Ψ differs from Φ only in magnitude, Ψ also has the same functional behaviour. Here, we choose $k_\mu = (0,0,1,0)$, $l_\mu = (0,1,0,0)$, $p_\mu = (3,0,0,1)$ and $g_{ym} = 0.5$.

Using the above solutions, the stress tensor is reduced to

$$T_{\mu\nu} = \frac{1}{\alpha\beta}\left[\beta(l^2 p_\mu p_\nu + l_\mu l_\nu p^2) + \alpha(k^2 p_\mu p_\nu + k_\mu k_\nu p^2) - \frac{1}{2}\eta_{\mu\nu}(\alpha k^2 + \beta l^2)p^2\right] \mathrm{sn}^2(u,\tfrac{1}{2})\mathrm{dn}^2(u,\tfrac{1}{2}) + \frac{1}{\alpha\beta}\left[l^2 k_\mu k_\nu + k^2 l_\mu l_\nu - \frac{1}{2}\eta_{\mu\nu} l^2 k^2\right] \mathrm{cn}^4(u,\tfrac{1}{2}). \quad (3.63)$$

The above expression is no longer a constant but a periodic function in Jacobi elliptic functions (here, sn and dn are other Jacobi elliptic functions, please refer to Appendix D.1). To get a clear interpretation, we choose the vectors to be $k_\mu = (0,0,1,0)$, $l_\mu = (0,1,0,0)$, $p_\mu = (p_0,0,0,1)$, $|p_0| > 1$ owing to orthogonality conditions. Then, the energy density and momentum density becomes

$$T_{00} = \frac{1}{\alpha\beta}(\alpha+\beta)\left(p_0^2 + \frac{1}{2}p^2\right)\mathrm{sn}^2(u,\tfrac{1}{2})\mathrm{dn}^2(u,\tfrac{1}{2}) + \frac{1}{2\alpha\beta}\mathrm{cn}^4(u,\tfrac{1}{2}),$$
$$T_{03} = \frac{\alpha+\beta}{\alpha\beta}\mathrm{sn}^2(u,\tfrac{1}{2})\mathrm{dn}^2(u,\tfrac{1}{2})p_0,$$

where $u = p_0\, t + z$. From the expression of momentum density (T_{0i}), it is found that the direction of T_{0i} is constant, here along $i = 3$ direction only. The energy density is also found to be bounded throughout spacetime (Fig. 3.2). With these, the solutions (3.60 & 3.61) can be interpreted as non-abelian plane waves propagating along a fixed direction.

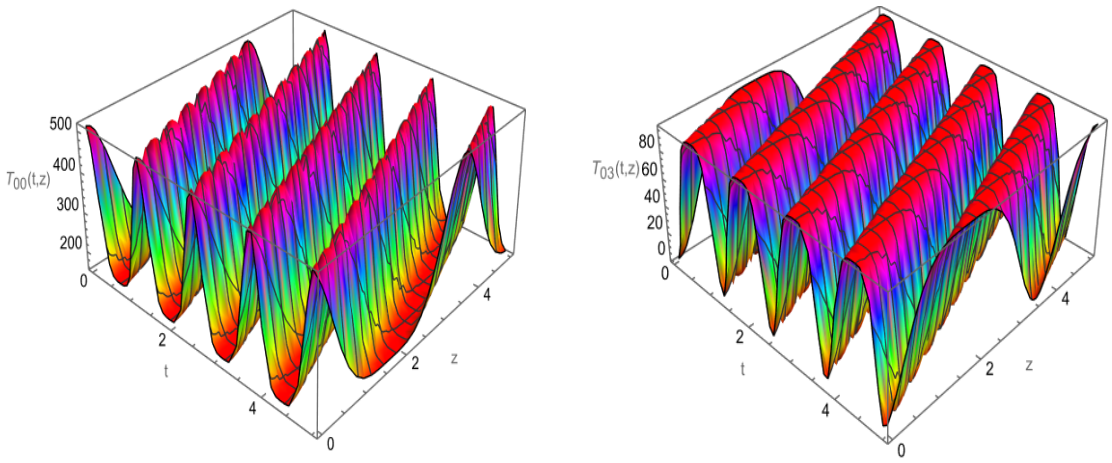

Figure 3.2: Plots of energy density T_{00} and Poynting vector T_{03} as a function of t and z. We choose $p_0 = 3$ and $g_{ym} = 0.5$.

Similarly, by finding the electric and magnetic fields for the above solutions, we get

$$E_i^a = -\delta_1^a \delta_i^2 \frac{p_0}{\sqrt{\beta}} \mathrm{sn}(u, \frac{1}{2}) \mathrm{dn}(u, \frac{1}{2}) - \delta_3^a \delta_i^1 \frac{p_0}{\sqrt{\alpha}} \mathrm{sn}(u, \frac{1}{2}) \mathrm{dn}(u, \frac{1}{2}),$$
$$B_i^a = \delta_1^a \delta_i^1 \frac{1}{\sqrt{\beta}} \mathrm{sn}(u, \frac{1}{2}) \mathrm{dn}(u, \frac{1}{2}) - \delta_3^a \delta_i^2 \frac{1}{\sqrt{\alpha}} \mathrm{sn}(u, \frac{1}{2}) \mathrm{dn}(u, \frac{1}{2}) + \delta_2^a \delta_i^3 \frac{g_{ym}}{\sqrt{\alpha\beta}} \mathrm{cn}^2(u, \frac{1}{2}).$$

The electric and magnetic fields are real and regular throughout spacetime. The magnetic fields are nonlinear in YM gauge fields and are not perpendicular to the propagating direction. The electric fields are linear in YM gauge fields and are perpendicular to the propagating direction. This suggests a possibility that the nonlinear terms presented in the YM equations can be regarded as arising from the medium.

3.3 Electroweak theory

Apart from the single gauge theories like QCD (based on $SU(3)$), some theories are based on bigger groups of form $SU(n_1) \times SU(n_2)$ or $SU(n_1) \times U(n_2)$. Most of the physical theories are of this form. For example, the Electroweak theory (based on $SU(2) \times U(1)$) which unifies Electromagnetic theory and weak nuclear theory. Another example is the famous Standard Model of Particle Physics (based on $SU(3) \times SU(2) \times U(1)$) which unifies

the three fundamental forces: electromagnetic, weak nuclear, and strong nuclear forces. The Electroweak theory is famous for unifying two fundamental forces. This theory is based on a phenomenon called Spontaneous Symmetry Breaking, which explains the origin of the masses for W and Z bosons by introducing a scalar-field doublet called Higgs. The electroweak theory is an example of partial breaking of gauge symmetry: $SU(2) \times U(1)$ breaks into $U(1)_{e.m.}$.

In this section, we will discuss the solutions of YM equations in Electroweak theory. We will start with an introduction to Electroweak theory. For simplicity, we do not include the fermions fields in our analysis.

Let the $A^a_\mu,\ a = 1,2,3$ be the gauge field of $SU(2)$ and the field B_μ be the gauge field of $U(1)$. The model includes one scalar-field doublet φ (with respect to $SU(2)$). Each gauge group has its own coupling constant, g_{ym} for $SU(2)$ and g_y for $U(1)$. The $U(1)$ charge is called weak hypercharge Y and the Higgs doublet has $Y = \frac{1}{2}$. With these fields and having a fourth-order polynomial function for Higgs potential, one can write the Lagrangian for Electroweak theory [50, 178] as

$$\mathcal{L}_{EW} = -\frac{1}{4}F^a_{\mu\nu}F^{a\mu\nu} - \frac{1}{4}B_{\mu\nu}B^{\mu\nu} + (D_\mu\varphi)^\dagger(D^\mu\varphi) + V(|\varphi|^2), \tag{3.64}$$

where

$$F^a_{\mu\nu} = \partial_\mu A^a_\nu - \partial_\nu A^a_\mu + g_{ym}\varepsilon^{abc}A^b_\mu A^c_\nu, \tag{3.65}$$

$$B_{\mu\nu} = \partial_\mu B_\nu - \partial_\nu B_\mu, \tag{3.66}$$

where ε^{abc} is the Levi-Civita tensor and the covariant derivative of field φ is given by

$$D_\mu\varphi = \partial_\mu\varphi - \frac{i}{2}\, g_{ym}\tau^a A^a_\mu\varphi - \frac{i}{2}\, g_y\, B_\mu\, \varphi, \tag{3.67}$$

where $\tau^a = \sigma^a/2,\ \sigma^a =$ Pauli matrices, are the generators of $SU(2)$ and the Higgs field φ is

a two-column vector, $\varphi = \binom{\varphi_1}{\varphi_2}$ and the potential $V(|\varphi|^2)$ is a quartic potential in field φ.

Due to the form of Higgs potential, Higgs acquires a non-zero value (v) at the ground state. Let the ground state be $\varphi = \binom{0}{v/\sqrt{2}}$, $A^a_\mu = 0$, $B_\mu = 0$. Now, consider small fluctuations around the vacuum. For the scalar field, it becomes

$$\varphi = \begin{pmatrix} 0 \\ \frac{1}{\sqrt{2}}(v+\chi) \end{pmatrix}, \tag{3.68}$$

where χ is the real scalar field. The mass term is generated for gauge fields from the term $(D_\mu\varphi)^\dagger(D_\mu\varphi)$. This can be calculated explicitly as follows:

$$D_\mu\varphi = \begin{pmatrix} -\frac{ig_{ym}}{2\sqrt{2}}(A^1_\mu - iA^2_\mu)(v+\chi) \\ -\frac{i}{2\sqrt{2}}(g_y B_\mu - g_{ym}A^3_\mu)(v+\chi) + \frac{1}{\sqrt{2}}\partial_\mu\chi \end{pmatrix}. \tag{3.69}$$

Now we will introduce the complex fields,

$$W^\pm_\mu = \frac{1}{\sqrt{2}}(A^1_\mu \mp iA^2_\mu), \tag{3.70}$$

and two real fields,

$$Z_\mu = \frac{1}{\sqrt{g^2_{ym} + g^2_y}}(g_{ym}A^3_\mu - g_y B_\mu), \tag{3.71}$$

$$A_\mu = \frac{1}{\sqrt{g^2_{ym} + g^2_y}}(g_{ym}B_\mu + g_y A^3_\mu), \tag{3.72}$$

where $W^\pm_\mu$, Z_μ corresponds to W^+, W^- and Z bosons, respectively, mediating weak-nuclear force. A_μ is identified with the familiar electromagnetic field. We can also introduce the weak mixing angle θ_W such that

$$\cos\theta_W = \frac{g_{ym}}{\sqrt{g^2_{ym} + g^2_y}}, \ \sin\theta_W = \frac{g_y}{\sqrt{g^2_{ym} + g^2_y}}.$$

With these, we can rewrite

$$Z_\mu = \cos\theta_W A^3_\mu - \sin\theta_W B_\mu, \tag{3.73}$$

$$A_\mu = \cos\theta_W B_\mu + \sin\theta_W A^3_\mu, \tag{3.74}$$

and

$$D_\mu\varphi = \begin{pmatrix} -i\frac{g_{ym}}{2}W^+_\mu(v+\chi) \\ \frac{1}{\sqrt{2}}\partial_\mu\chi + i\frac{\sqrt{g^2_{ym}+g^2_y}}{2\sqrt{2}}Z_\mu(v+\chi) \end{pmatrix}. \tag{3.75}$$

Then, the covariant derivative part becomes

$$(D_\mu\varphi)^\dagger(D_\mu\varphi) = \frac{1}{2}(\partial_\mu\chi)^2 + \frac{g^2_{ym}v^2}{4}W^+_\mu W^-_\mu + \frac{1}{2}\left(\frac{(g^2_{ym}+g^2_y)v^2}{4}\right)Z^2_\mu. \tag{3.76}$$

Introducing a notation: $m_W = g_{ym}v/2$ and $m_Z = \sqrt{g^2_{ym}+g^2_y}\,v/2$, we get

$$(D_\mu\varphi)^\dagger(D_\mu\varphi) = \frac{1}{2}(\partial_\mu\chi)^2 + m^2_W W^+_\mu W^-_\mu + \frac{1}{2}m^2_Z Z^2_\mu. \tag{3.77}$$

From the above equation, we can identify the mass term for complex vector field W^+_μ with mass m_W (W-boson field) and mass term for a real vector field Z_μ with mass m_Z (Z-boson field). This is the mechanism by which the particles acquire mass through spontaneous symmetry breaking.

Now, we will come to our analysis which is finding the solutions for the gauge fields in the Electroweak theory. For this, we consider the Type II ansatz of Oh-Teh paper [27, 28] described in Sec: 3.2.1:

$$W^\pm_\mu = \frac{1}{\sqrt{2}}k_\mu\Phi,\ Z_\mu = l_\mu\Psi,\ A_\mu = 0,\ \chi = 0. \tag{3.78}$$

We can rewrite everything in terms of original gauge fields,

$$A^1_\mu = k_\mu \Phi,\ A^2_\mu = 0,\ A^3_\mu = l_\mu \cos\theta_W \Psi,\ B_\mu = -l_\mu \sin\theta_W \Psi. \tag{3.79}$$

Now, substituting the above gauge fields in the Electroweak Lagrangian, we get

$$\mathcal{L}_{EW} = -\frac{1}{2}\left[k^2(\partial_\mu\Psi)^2 + l^2(\partial_\mu\Phi)^2 - (k\cdot\partial\Psi)^2 - (l\cdot\partial\Phi)^2\right] - \frac{g^2_{ym}}{2}\cos^2\theta_W l^2 k^2 \Phi^2\Psi^2 + \frac{1}{8}g^2_{ym}k^2v^2\Phi^2 + \frac{1}{8}(g^2_{ym}+g^2_y)l^2v^2\Psi^2. \tag{3.80}$$

By varying the above Lagrangian, one gets the equations of motion as follows

$$l^2\Box\Psi - l^\mu\partial_\mu\Psi - g^2_{ym}\ k^2\ l^2\ \Psi\ \Phi^2\cos^2\theta_W + \frac{1}{2}m^2_Z\ l^2\Psi = 0, \tag{3.81}$$

$$k^2\Box\Phi - k^\mu\partial_\mu\Phi - g^2_{ym}\ k^2\ l^2\ \Psi^2\ \Phi\ \cos^2\theta_W + m^2_W\ k^2\Phi = 0. \tag{3.82}$$

We use the same conditions as before $l_\mu\partial^\mu\Psi = 0,\ k_\mu\partial^\mu\Phi = 0$ as discussed in Sec: 3.2.1. To obtain an analytical solution, we set $\Phi = \Psi$ and $l^2 = k^2$. This means that the approximation of setting two fields as equal can be taken as zeroeth order in g_y coupling constant and also equating masses of W and Z bosons. With this, the equation becomes

$$\Box\Phi - g^2_{ym}l^2\cos^2\theta_W\Phi^3 + \frac{v^2g^2_{ym}}{4}\Phi = 0. \tag{3.83}$$

The solution found to be

$$\Phi(t,z) = \Psi(t,z) = \pm\frac{v}{2|l|\cos\theta_W}\tanh\left(Az \pm \frac{1}{2}\sqrt{4A^2 - \frac{g^2_{ym}v^2}{2}}t + B\right), \tag{3.84}$$

where A and B are arbitrary constants. The behaviour of the solutions depends on constants and boundary conditions. In particular, the solutions show hyperbolic functional behaviour (Fig: 3.3(a)) when $4A^2 - g^2_{ym}v^2/2 > 0$ and the solutions show oscillatory behaviour (Fig:

3.3(b)) when $4A^2 - g_{ym}^2 v^2/2 < 0$.

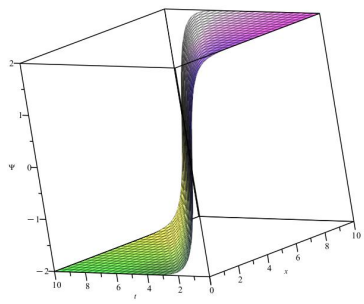

((a)) The YM gauge field with mass showing hyperbolic behaviour.

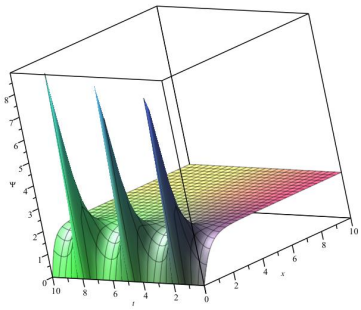

((b)) The YM gauge field with mass showing oscillatory behaviour.

Figure 3.3: Figures showing $\Psi = \Phi$ as a function of t and z with two different choices for constants.

3.4 Conclusion

In this chapter, we discuss the importance of gauge theory, especially the non-abelian gauge theory, in explaining the interactions of fundamental forces with matter fields. We started with the introduction to non-abelian gauge theory, discussing Lie groups, Lie algebra, and gauge symmetry in Sec: (3.1). Then, we discussed some of the important classical solutions for non-abelian gauge theory, both in Minkowski and Euclidean spacetimes (Sec: 3.2). The Euclidean YM solutions are useful in studying phenomena like tunneling in the quantum version of the theory. The QGP, a deconfined phase consisting of quarks and gluons, existed in the Early universe and is being created in heavy ion colliders like LHC, and RHIC. Since the quarks and gluons are deconfined and due to asymptotic freedom, they are weakly interacting and can propagate as waves. Thus, we focused on discussing the different types of wave solutions for YM equations in Sec: 3.2.1. We discussed two types of waves based on their dependence on the coupling constant (g_{ym}): Type I waves and Type II waves. All the known wave-type solutions fall under these two categories. So far, we considered the massless YM waves. To discuss the massive YM waves, we considered

one of the well-known theories, the Electroweak theory in Sec: 3.3. In Electroweak theory, the gauge fields acquire mass through spontaneous symmetry breaking and the Higgs effect. We found the solutions for YM equations in Electroweak theory turn out to show hyperbolic or oscillatory functional behaviour depending on the argument of the hyperbolic function. In the next chapter, we will study the interaction of GWs, studied in Chapter: 2, with YM waves, studied in this chapter: 3.

Part I

Particle Interactions

Chapter 4

Interaction of Gravitational waves with SU(2) Yang-Mills Fields

"The Universe is under no obligation to make sense to you."

Neil deGrasse Tyson

Since the discovery of GWs, it has been the birth of a new field in astronomy, GW astronomy. As the GWs have a weakly interacting nature, they can be used to probe the earliest times of the universe farther than the CMB. We discussed the importance and scope of GWs in understanding the early universe in Chapter 2. QGP, a deconfined mixture of quarks and gluons, generated from the breakdown of hadrons (nuclei) at very high temperatures (above temperature 10^{12} K or $\sim$ 150 MeV). As we will discuss in Chapter 7, the QGP phase existed in the very early universe around $\sim \mu s$ after the Big Bang and is also created and studied in the heavy ion colliders. At temperatures higher than this critical temperature, the interaction between quarks and gluons is very weak due to asymptotic freedom. At this stage, the gluons and quarks are expected to propagate as waves. There have been studies on the combined topics of GWs and non-abelian gauge fields. So far, the studies on these topics have gone in the following way: The non-abelian gauge fields will generate a non-zero anisotropic tensor and act as a source for the GWs. In our thesis, we took a different approach and studied the influence of GWs on the non-abelian gauge fields. We have already discussed the relevance of the interaction of GWs with the matter in Sec.

2.2, particularly with scalar fields (Sec: 2.2.1), fermions (Sec: 2.2.2) and EM waves (Sec: 2.2.3). In this chapter, we take it further and study the interaction of GWs with non-abelian waves.

The study of non-abelian gauge fields in the presence of GWs is relevant for (i) Early Universe Cosmology, (ii) Heavy ion colliders, (iii) Neutron stars, and (iv) new ways of GW detection in the following ways:

- In our work, we considered the YM wave interaction with GWs in Minkowski and de-Sitter backgrounds. Our results can be extended to other cosmological backgrounds by changing the scale factor.

- During heavy ion collisions, the gluons and quarks become deconfined for a short duration of time. If any GW passes through the collisions at this time, it might change the trajectory of the massive YM waves. The quantum version of this interaction can be interpreted as changes in the flux of particles, and hence cross-section, which is observable. This will also provide another way for GW detection.

- Recently, through neutron star studies [179], it was found that there has been a connection between the GWs generation and the phase transition of hadrons to quarks and gluons. The work we did is thus relevant to the study of neutron stars as well.

This chapter closely follows the work we did in the paper [27]. In this chapter, we will discuss the interaction of GWs with YM waves in different cosmological backgrounds. We start with the YM equation in a general background (Sec: 4.1). We start with the interaction of GWs with YM progressive waves in the Minkowski Background in Sec. 4.2, followed by a cosmological background, especially in de Sitter spacetime, in Sec. 4.3. Later, we discussed the Electroweak symmetry broken phase which is experimentally accessible in Sec. 4.4.

4.1 Yang Mills equations in general spacetime

In a general background with metric $g_{\mu\nu}$, the YM equation is given by

$$\nabla_\mu F^{a\mu\nu} + g_{ym} f^{abc} A^b_\mu F^{c\mu\nu} = 0, \tag{4.1}$$

where $F^a_{\mu\nu} = \partial_\mu A^a_\nu - \partial_\nu A^a_\mu + g_{ym} f^{abc} A^b_\mu A^c_\nu$ is the field strength tensor, f^{abc} are structure constants and ∇_μ is the covariant derivative with respect to the curved background, which is given by

$$\nabla_\mu F^{a\rho\nu} = \partial_\mu F^{a\rho\nu} + \Gamma^\rho_{\mu\sigma} F^{a\sigma\nu} + \Gamma^\nu_{\mu\sigma} F^{a\rho\sigma}, \tag{4.2}$$

where $\Gamma^\rho_{\mu\nu}$ is the Christoffel symbol given in chapter 2. Since the first term in the YM equation (4.1) is the divergence of $F^{a\mu\nu}$, we can also rewrite the YM eq. (4.1) as follows

$$\frac{1}{\sqrt{-g}} \partial_\mu (\sqrt{-g}\, F^{a\mu\nu}) + g_{ym}\, f^{abc}\, A^b_\mu\, F^{c\mu\nu} = 0, \tag{4.3}$$

where g is the determinant of the metric $g_{\mu\nu}$. By expanding the above equation, we get

$$\frac{1}{\sqrt{-g}} \partial_\mu (\sqrt{-g}\, g^{\mu\rho}\, g^{\nu\sigma} F^a_{\rho\sigma}) + g_{ym} f^{abc}\, A^b_\mu\, g^{\mu\rho}\, g^{\nu\sigma} F^c_{\rho\sigma} = 0. \tag{4.4}$$

This is the main equation of this chapter. We will mainly focus on $SU(2)$ Lie group, then the structure constants are simply given by Levi-Civita tensor with values

$$\begin{aligned} f_{abc} = \varepsilon_{abc} &= +1 \text{ if } (a,b,c) \text{ is even permutation, } (1,2,3),\ (2,3,1),\ (3,1,2) \\ &= -1 \text{ if } (a,b,c) \text{ is odd permutation, } (3,2,1),\ (1,3,2),\ (2,1,3) \\ &= 0 \text{ if any index is repeated, i.e. remaining terms.} \end{aligned}$$

4.2 In Minkowski spacetime

In this section, we discuss the interaction of GWs with YM waves in the Minkowski (flat) background. We consider a GW with only plus (+) polarisation propagating in the z-direction. The flat spacetime metric with a GW can be written as (Eq: 2.19)

$$ds^2 = -dt^2 + (1+h_+(t,z))dx^2 + (1-h_+(t,z))dy^2 + dz^2, \tag{4.5}$$

where $h_+(t,z) = A_+\cos(\omega_g(t-z))$, A_+ is the amplitude of the GW and ω_g is the GW frequency. In the metric component form, it is given by

$$\eta_{\mu\nu} = \begin{pmatrix} -1 & 0 & 0 & 0 \\ 0 & 1 & 0 & 0 \\ 0 & 0 & 1 & 0 \\ 0 & 0 & 0 & 1 \end{pmatrix}, \text{ and } h_{\mu\nu} = \begin{pmatrix} 0 & 0 & 0 & 0 \\ 0 & h_+ & 0 & 0 \\ 0 & 0 & -h_+ & 0 \\ 0 & 0 & 0 & 0 \end{pmatrix}.$$

We consider the gauge field to be of the following form:

$$A^a_\mu = \overline{A}^a_\mu + \tilde{A}^a_\mu, \tag{4.6}$$

where $\overline{A}^a_\mu$ is the gauge field in the flat background given in Sec: 3.2.1 and $\tilde{A}^a_\mu$ is the perturbed gauge field due to the interaction of the unperturbed gauge field and GW. Using the inverse metric as $g^{\mu\nu} = \eta^{\mu\nu} + h^{\mu\nu}$, we expand the YM equation (4.4) in the first order of h_+ and $\tilde{A}_\mu$ as follows:

$$\begin{aligned}\eta^{\mu\rho}\eta^{\nu\lambda}\partial_\mu\tilde{F}^a_{\rho\lambda} + g_{ym}\varepsilon^{abc}\left(\eta^{\mu\rho}\eta^{\nu\lambda}\tilde{A}^b_\mu\overline{F}^c_{\rho\lambda} + \eta^{\mu\rho}\eta^{\nu\lambda}\overline{A}^b_\mu\tilde{F}^c_{\rho\lambda}\right) = -\Big(\eta^{\mu\rho}\partial_\mu\left(h^{\nu\lambda}\overline{F}^a_{\rho\lambda}\right) \\ + \eta^{\nu\lambda}\partial_\mu\left(h^{\mu\rho}\overline{F}^a_{\rho\lambda}\right) + \tilde{\Gamma}^\mu_{\mu\rho}\eta^{\rho\lambda}\eta^{\nu\sigma}\overline{F}^a_{\lambda\sigma} + \tilde{\Gamma}^\nu_{\mu\rho}\eta^{\mu\lambda}\eta^{\rho\sigma}\overline{F}^a_{\lambda\sigma} + g_{ym}\varepsilon^{abc}\big(h^{\mu\rho}\eta^{\nu\lambda}\overline{A}^b_\mu\overline{F}^c_{\rho\lambda} \\ + \eta^{\mu\rho}h^{\nu\lambda}\overline{A}^b_\mu\overline{F}^c_{\rho\lambda}\big)\Big),\end{aligned} \tag{4.7}$$

where the terms with $\bar{}$ denotes the unperturbed functions and terms with $\tilde{}$ denotes the perturbed functions.

Now we will solve the above equation for different gauge field ansatzs as described in Sec. (3.2.1).

4.2.1 Type I waves

We consider the ansatz of type I waves described in Sec. (3.2.1) which is of form [28]

$$A^a_\mu = \psi_{\overline{\alpha}} f^a_{\overline{\alpha}}(U)\partial_\mu U, \tag{4.8}$$

where U and $\psi_{\overline{\alpha}}$ are functions of x_μ, $f^a_{\overline{\alpha}}$ depend on U only and the index $\overline{\alpha} = 1..4$. The functions $\psi_{\overline{\alpha}}$ represent degrees of freedom which is an arbitrariness in the form of the ansatz.

We then assume the perturbation due to the GW only modifies the function U as $U = \overline{U} + \tilde{U}$. Then, the function $f^a_{\overline{\alpha}}$ becomes $f_{\overline{\alpha}}(\overline{U}+\tilde{U}) = f_{\overline{\alpha}}(\overline{U}) + f'_{\overline{\alpha}}(U)\tilde{U}$. Even though the $f^a_{\overline{\alpha}}$ function contains zero and first-order terms, only zero-order terms contribute to the first-order in the perturbations. With these assumptions, we write the total ansatz as

$$A^a_\mu = \overline{A}^a_\mu + \tilde{A}^a_\mu = \psi_{\overline{\alpha}}\, f^a_{\overline{\alpha}}(\overline{U})\, \partial_\mu \overline{U} + \psi_{\overline{\alpha}}\, f^a_{\overline{\alpha}}(U)\, \partial_\mu \tilde{U}. \tag{4.9}$$

The form $\psi_{\overline{\alpha}}\ f^a_{\overline{\alpha}}$ is motivated by the gauge internal group structure, which we expect the GW does not have the influence to break. The mixing of indices a and $\overline{\alpha}$ in the function $f^a_{\overline{\alpha}}$ is needed in order for the ansatz to be in non-abelian form. Therefore, we used the same form as in the original ansatz, even in GW perturbed form. Using the above ansatz (4.9) in YM equation (4.4), we get the following inhomogeneous differential equations

$$\partial^\mu\partial^\nu\tilde{U}\partial_\mu\psi_{\overline{\alpha}} + \partial^\nu\tilde{U}\Box\psi_{\overline{\alpha}} - \partial^\lambda\partial^\nu\psi_{\overline{\alpha}}\partial_\lambda\tilde{U} - \partial^\nu\psi_{\overline{\alpha}}\Box\tilde{U} = \partial^\mu\overline{U}\partial_\mu(h^{\nu\sigma}\partial_\sigma\psi_{\overline{\alpha}}) + h^{\mu\rho}\partial_\rho\overline{U}\partial_\mu\partial^\nu\psi_{\overline{\alpha}}$$
$$+ h^{\nu\sigma}\partial_\sigma\psi_{\overline{\alpha}}\eta^{\mu\rho}\partial_\mu\partial_\rho\overline{U} + \partial^\nu\psi_{\overline{\alpha}}\partial_\mu(h^{\mu\rho}\partial_\rho\overline{U}) - \eta^{\mu\rho}\partial_\mu\partial_\rho\psi_{\overline{\alpha}}h^{\nu\sigma}\partial_\sigma\overline{U}$$

$$-\partial^{\nu}\overline{U}\partial_{\mu}(h^{\mu\rho}\partial_{\rho}\psi_{\overline{\alpha}})-\eta^{\mu\rho}\partial_{\rho}\psi_{\overline{\alpha}}\partial_{\mu}(h^{\nu\sigma}\partial_{\sigma}\overline{U})-h^{\mu\rho}\partial_{\rho}\psi_{\overline{\alpha}}\partial_{\mu}\partial^{\nu}\overline{U}, \quad (4.10)$$

with conditions

$$\eta^{\mu\nu}\partial_{\mu}\tilde{U}\partial_{\nu}\psi_{\overline{\alpha}}+h^{\mu\nu}\partial_{\mu}\overline{U}\partial_{\nu}\psi_{\overline{\alpha}}=0, \quad (4.11)$$

$$2\eta^{\mu\nu}\partial_{\mu}\tilde{U}\partial_{\nu}\overline{U}+h^{\mu\nu}\partial_{\mu}\overline{U}\partial_{\nu}\overline{U}=0. \quad (4.12)$$

These conditions are the same as in unperturbed section (Sec:3.2.1) but are implemented to first-order in perturbations. As we discussed earlier, when choosing the different $\psi_{\overline{\alpha}}$, we get different solutions for $\tilde{U}$.

A. Type Ia waves

Using the same assumption as in the Type Ia waves section of Sec. (3.2.1), we choose $\psi_1 = x$. From one of the above conditions (4.11), we find $\partial_x\tilde{U}=0$. Then we were left with only one equation

$$\Box\,\tilde{U}=\eta^{\mu\rho}\partial_{\rho}\overline{U}\partial_{\mu}h_{+}+h_{+}\eta^{\mu\rho}\partial_{\mu}\partial_{\rho}\overline{U}-h_{+}\partial_{2}\partial_{2}\overline{U}. \quad (4.13)$$

If we take the YM waves (choosing $\overline{U}=U_0\cos(\omega_y(t-z))$, U_0 is the initial value of U and ω_y is the YM wave frequency) and GW ($h_+ = A_+\cos(\omega_g(t-z))$) propagating in the same direction, we find the terms on the right side of the equation become zero, thus showing no interaction between them.

If we consider waves to be propagating in anti-parallel directions (choosing $\overline{U}=U_0\cos(\omega_y(t+z))$, ω_y is the YM wave frequency), then there will be nonzero terms on the right side of Eq. (4.13). To get a non-trivial solution and wanting the solution be in the form of Type Ia, we further assume the $f^a_{\overline{\alpha}}$ are arbitrary constants, $f^a_{\overline{\alpha}}(U)=C^a_{\overline{\alpha}}$, which are arbitrary constants. With this assumption, we are left with a single equation without any

further conditions on $\tilde{U}$,

$$\Box\,\tilde{U} = -2\,\partial_0\overline{U}\,\partial_0 h_+. \tag{4.14}$$

By solving the above equation, we get

$$\tilde{U}(t,z) = \frac{1}{2}A_+U_0\cos(\omega_g(t-z))\cos(\omega_y(t+z)), \tag{4.15}$$

and the gauge field is given by

$$\tilde{A}^a_0 = \frac{1}{2}x\,C^a_1A_+U_0\big(-\omega_g\sin(\omega_g(t-z))\cos(\omega_y(t+z)) - \omega_y\cos(\omega_g(t-z))\sin(\omega_y(t+z))\big), \tag{4.16}$$

$$\tilde{A}^a_1 = \tilde{A}^a_2 = 0, \tag{4.17}$$

$$\tilde{A}^a_3 = \frac{1}{2}x\,C^a_1A_+U_0\big(\omega_g\sin(\omega_g(t-z))\cos(\omega_y(t+z)) - \omega_y\cos(\omega_g(t-z))\sin(\omega_y(t+z))\big). \tag{4.18}$$

We further consider the different orientations. We consider the YM wave propagating in the perpendicular direction ($\overline{U} = U_0\cos(\omega_y(t+y))$). Then, the solution is found to be

$$\tilde{U}(t,y,z) = -\frac{1}{2}U_0A_+\frac{\omega_y}{\omega_g}\Big[\sin(\omega_g(t-z))\sin(\omega_y(t+y))\Big], \tag{4.19}$$

From the condition (4.11), we are restricting the propagating direction of YM waves.

B. Type Ib waves

We consider a different choice of $\psi_{\overline{\alpha}}$ which is discussed Type Ib waves section in Sec. (3.2.1). Choosing $\psi_{\overline{\alpha}} = A_{\overline{\alpha}}e^{i\mathbf{q}\cdot\mathbf{x}}$ such that it satisfies $\Box\psi_{\overline{\alpha}} = 0$, we get the following equation

$$q^\nu\Box\tilde{U} = \eta^{\nu\lambda}h^{\mu\rho}\partial_\mu\partial_\rho\overline{U}q_\lambda, \tag{4.20}$$

with some extra conditions $q_\rho\partial^\rho h^{\mu\nu} = 0$ and $q_\lambda h^{\nu\lambda} = 0$.

Using these extra conditions along with the form of GW ($h_{\mu\nu}$), we get the vector q has only two components $q_0 = -q_3 \neq 0$. To find the perturbative solutions, we used the same assumption as in the case of type Ia which is putting a relaxation on condition (4.12).

Similarly, in this case, we did not find any interaction when waves travelling in the same direction.

Then, by considering the waves propagating in perpendicular directions, we find the solutions to be

$$\tilde{U}(x,z,t) = -\frac{1}{2}A_+ U_0 \frac{\omega_y}{\omega_g}\Big[\sin(\omega_g(t-z))\sin(\omega_y(x+t))\Big]. \tag{4.21}$$

This is a particular solution of the inhomogeneous equation. Plot of $\tilde{U}$ as a function of t is given in Fig. (4.1).

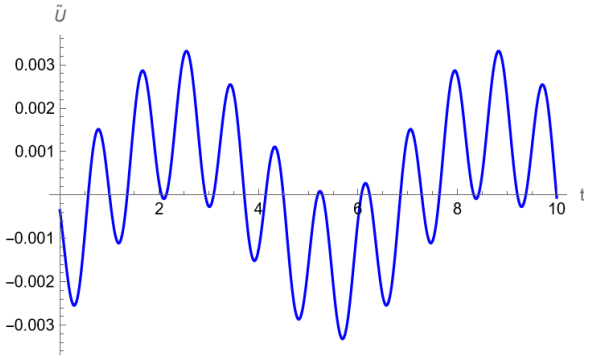

Figure 4.1: Plot of $\tilde{U}(1,1,t)$ as a function of t. We choose $A_+ = 0.01$, $U_0 = 0.5$, $\omega_g = 3$ and $\omega_y = 4$.

C. Coleman waves

This is a special case of type I waves with the choice $\psi_1 = x, \psi_2 = y$ & $U = t + z$ as described in the Coleman waves section of Sec. (3.2.1). To solve the perturbed YM equation, we use the same techniques of [167]. We write the metric in light-cone coordinates ($(x^{\pm} = t \pm z)$) as

$$ds^2 = -dx^- dx^+ + (1 + h_+(x^-))dx^2 + (1 - h_+(x^-))dy^2, \tag{4.22}$$

where $h_+(x^-) = A_+ \cos(\omega_g x^-)$. We assume the gauge field to be of the form $A^a_\mu = \overline{A}^a_\mu + \tilde{A}^a_\mu$ and the corresponding field strength tensors to be $F^a_{\mu\nu} = \overline{F}^a_{\mu\nu} + \tilde{F}^a_{\mu\nu}$ where the $\tilde{F}, \tilde{A}$ are the perturbed quantities proportional to the gravitational wave amplitude and $\overline{A}^a_\mu$ is the Coleman solution (Eq. (3.47)) in the lightcone coordinates which can be written as $\overline{A}^a_\mu = \delta^+_\mu \ (f^a(x^+)x + g^a(x^+)y)$, where f^a and g^a are arbitrary functions. With the above choice, we are considering the case where the YM wave propagates in -z-direction.

Using Coleman's gauge choice, we keep $\tilde{A}^a_x = \tilde{A}^a_y = 0$. By substituting the above ansatz in Eq. (4.7) for $\nu = +, 1, 2, -$, we get

$$\eta^{\mu\rho}\partial_\mu(\tilde{F}^a_{\rho-}) = 0, \tag{4.23}$$

$$\eta^{\mu\rho}\partial_\mu\left(\tilde{F}^a_{\rho 1}\right) + g_{ym}\varepsilon^{abc}\eta^{+-}\overline{A}^b_+\tilde{F}^c_{-1} + g_{ym}\varepsilon^{abc}\eta^{+-}\tilde{A}^b_-\overline{F}^c_{+1} = -\eta^{-+}\partial_-\left(h^{11}\overline{F}^a_{+1}\right), \tag{4.24}$$

$$\eta^{\mu\rho}\partial_\mu\left(\tilde{F}^a_{\rho 2}\right) + g_{ym}\varepsilon^{abc}\eta^{+-}\overline{A}^b_+\tilde{F}^c_{-2} + g_{ym}\varepsilon^{abc}\eta^{+-}\tilde{A}^b_-\overline{F}^c_{+2} = -\eta^{-+}\partial_-\left(h^{22}\overline{F}^a_{+2}\right), \tag{4.25}$$

$$\eta^{\mu\rho}\partial_\mu\left(\tilde{F}^a_{\rho+}\right) + g_{ym}\varepsilon^{abc}\eta^{+-}\eta^{-+}\overline{A}^b_+\tilde{F}^c_{-+} = 0. \tag{4.26}$$

To solve the above equations, we impose further restrictions which are (i) $F^a_{\mu\nu}$ are independent of x and y and (ii) the gauge fields are in the same direction in $SU(2)$ internal space. This choice makes the nonlinear terms zero because the terms involving ε^{abc} become zero. Then, the equations become

$$\partial_-(\tilde{F}^a_{+-}) = 0, \tag{4.27}$$

$$\partial_-(\tilde{F}^a_{+1}) + \partial_+(\tilde{F}^a_{-1}) = -(\partial_- h_+(x^-))f^a(x^+), \tag{4.28}$$

$$\partial_-(\tilde{F}^a_{+2}) + \partial_+(\tilde{F}^a_{-2}) = (\partial_- h_+(x^-))g^a(x^+), \tag{4.29}$$

$$\partial_+(\tilde{F}^a_{-+}) = 0. \tag{4.30}$$

From the first and last equations, it can be found that $\tilde{F}^a_{-+} = 0$ or $\partial_-\tilde{A}^a_+ = \partial_+\tilde{A}^a_-$. Using this relation in Eqs. (4.28 & 4.29), we can solve for $\tilde{A}^a_+$. Finally, using the relation ($\partial_-\tilde{A}^a_+ =$

$\partial_+\tilde{A}^a_-$), we can solve for $\tilde{A}^a_-$. The final solutions are given by

$$\tilde{A}^a_+ = \frac{1}{2}A_+\cos(\omega_g(x^-))\left[f^a(x^+)x - g^a(x^+)y\right], \tag{4.31}$$

$$\tilde{A}^a_- = -\frac{1}{2}A_+\omega_g\sin(\omega_g(x^-))\left[\left(\int f^a(x^+)dx^+\right)x - \left(\int g^a(x^+)dx^+\right)y\right], \tag{4.32}$$

$$\tilde{A}^a_x = 0, \tag{4.33}$$

$$\tilde{A}^a_y = 0. \tag{4.34}$$

To get a better understanding, we choose the arbitrary functions ($f^a(x^+)$ & $g^a(x^+)$) to be $f^a(x^+) = g^a(x^+) = \delta^a_1\sin(\omega_y x^+)$, where ω_y is the frequency of YM wave. We plot the non-zero functions in Fig. (4.2).

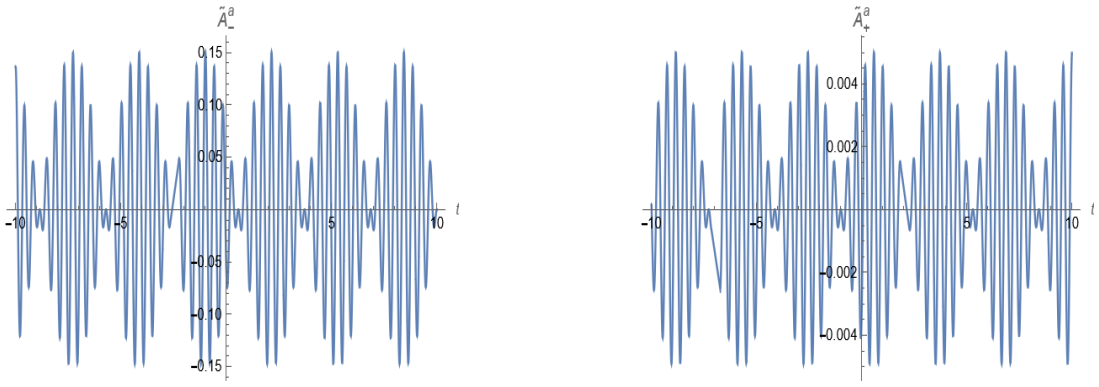

Figure 4.2: The plots of $\tilde{A}^a_-(z)$ and $\tilde{A}^a_+(z)$ as a function of z. We choose $x = 2,\ y = 1,\ \omega_g = 15,\ \omega_y = 1,\ A_+ = 0.01$ and $z = 1$.

We computed the non-abelian electric and magnetic fields by evaluating $E^a_i = F^a_{i0}$ and $B^a_i = \varepsilon_{ijk}F^{ajk}$. Now again converting into Cartesian coordinates, we can write the non-abelian electric and magnetic fields (up to first order) as

$$\tilde{E}^a_x = \delta^a_1\frac{1}{4\omega_y}\left[2A_+\omega_g\cos(\omega_y(t+z))\sin(\omega_g(t-z)) + \omega_y(2+A_+\cos(\omega_g(t-z)))\sin(\omega_y(t+z)\right], \tag{4.35}$$

$$\tilde{E}^a_y = \delta^a_1 \frac{1}{4\omega_y}\big[-2A_+\omega_g \cos(\omega_y(t+z))\sin(\omega_g(t-z)) + \omega_y(2-A_+\cos(\omega_g(t-z)))\sin(\omega_y(t+z)\big], \tag{4.36}$$

$$\tilde{E}^a_z = -\delta^a_1 \frac{1}{2} A_+(x-y)\omega_g \sin(\omega_g(t-z))\sin(\omega_y(t+z)), \tag{4.37}$$

$$\tilde{B}^a_x = \delta^a_1 \frac{1}{2\omega_y}\big[2A_+\omega_g \cos(\omega_y(t+z))\sin(\omega_g(t-z)) + \omega_y(2+A_+\cos(\omega_g(t-z)))\sin(\omega_y(t+z)\big], \tag{4.38}$$

$$\tilde{B}^a_y = \delta^a_1 \frac{1}{2\omega_y}\big[2A_+\omega_g \cos(\omega_y(t+z))\sin(\omega_g(t-z)) + \omega_y(-2+A_+\cos(\omega_g(t-z)))\sin(\omega_y(t+z)\big], \tag{4.39}$$

$$\tilde{B}^a_z = 0. \tag{4.40}$$

Unlike the EM case (abelian), the electric and magnetic fields are not observable. We calculated a gauge invariant quantity (observable), energy-momentum tensor which is given by

$$T_{\mu\nu} = g^{\rho\sigma}F^a_{\mu\rho}F^a_{\nu\sigma} - \frac{1}{4}g_{\mu\nu}F^a_{\rho\sigma}F^{a\rho\sigma}. \tag{4.41}$$

From this, one can calculate the Poynting vector as follows

$$S_x = S_y = \frac{1}{4\pi}T_{0x} = \frac{1}{16\pi}\, A_+\ (x-y)\ \omega_g\ \sin(\omega_g(t-z))\ \sin(\omega_y(t+z))^2, \tag{4.42}$$

$$S_z = \frac{1}{4\pi}T_{0z} = \frac{1}{8\pi}\ \sin(\omega_y(t+z))^2. \tag{4.43}$$

One can see that all the components of the Poynting vector are nonzero, signifying a deviation from the original -z-direction due to its interaction with the GW. From the expressions (Eqs. 4.42 & 4.43), it is clear that the wave is propagating along the -z - direction in the absence of a GW. The same behaviour is shown in Fig. (4.3) implying a slight deviation in the energy-momentum flow from the original direction.

We also investigate the interaction in different orientations. When the waves were propagating in the same direction i.e. choosing the gauge field of the form $\overline{A}^a_x = \overline{A}^a_y = \overline{A}^a_+ = 0$ and $\overline{A}^a_- = xf^a(x^-) + yg^a(x^-)$, then the source terms in Eq. (4.7) become zero signifying no interaction.

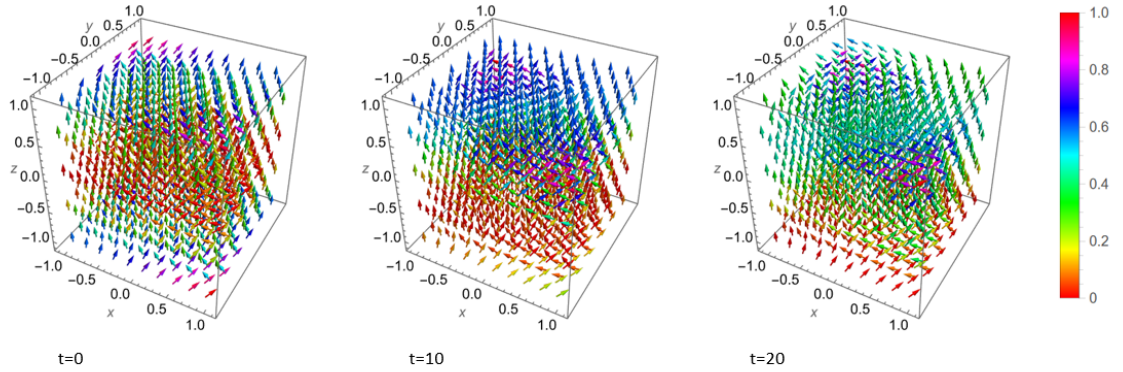

Figure 4.3: The graph showing the Poynting vector at different times. We choose $\omega_g = 15$, $\omega_y = 1$ and $A_+ = 0.1$.

Perpendicular directions

We also examined the case when the waves propagated in perpendicular directions. We consider a YM wave propagating in the $-x$-direction and GW propagating in the z-direction. In this case, the unperturbed gauge field can be written as $\overline{A}^a_\mu = \delta^+_\mu\ (f^a(x^+)y + g^a(x^+)z)$ where $x^+ = t + x$ and $x^- = t - x$. In these new light-cone coordinates, the metric becomes

$$ds^2 = \frac{1}{4}h_+(dx^+)^2 + \frac{1}{4}h_+(dx^-)^2 - \frac{1}{2}(2+h_+)dx^-dx^+ + (1-h_+(x^-))dy^2 + dz^2, \quad (4.44)$$

where $h_+ = A_+\cos(\frac{\omega_g}{2}((x^+ + x^-) - 2z))$. Using the same assumptions as before that the gauge fields pointing in the same direction in $SU(2)$ internal space and using Lorenz gauge ($\partial^\rho \tilde{A}^a_\rho = 0$), we can reduce the YM equations (4.7) to the following four inhomogeneous wave equations

$$\Box\tilde{A}^a_- = \frac{1}{2}g^a(x^+)\partial_z h_+, \quad (4.45)$$

$$\Box\tilde{A}^a_y = 2f^a(x^+)\partial_- h_+ + \partial_+(h_+ f^a(x^+)), \quad (4.46)$$

$$\Box\tilde{A}^a_z = -g^a(x^+)\partial_- h_+ + \partial_+(h_+ g^a(x^+)), \quad (4.47)$$

$$\Box\tilde{A}^a_+ = -\frac{1}{2}g^a(x^+)\partial_z h_+. \quad (4.48)$$

These are second-order inhomogeneous differential equations. These types of equations can be solved using Kirchoff's theorem and Duhamel's principle [29, 180]. The details of the technique used to solve inhomogeneous wave equations are given in Appendix D.2. Choosing the arbitrary functions as $f^a(x^+) = g^a(x^+) = \delta^a_1 e^{i\omega_y x^+}$, the final solutions for the above equations are given by

$$\tilde{A}^a_- = -\tilde{A}^a_+ = \delta^a_1 \frac{A_+}{4\omega_y}\Big(\cos(\omega_g(t-z))\sin(\omega_y(t+x)) - \cos(||\omega||t)\cos(\omega_g z)\sin(\omega_y x) + \frac{\sin(||\omega||t)}{||\omega||}\left(\omega_y\cos(\omega_y x)\cos(\omega_g z) - \omega_g\sin(\omega_y x)\sin(\omega_g z)\right)\Big), \quad (4.49)$$

$$\tilde{A}^a_y = \delta^a_1 \frac{A_+}{4\omega_y\omega_g}\Bigg(\frac{\sin(||\omega||t)}{||\omega||}\Big[5\omega_g\omega_y\cos(\omega_y x)\cos(\omega_g z) + (3\omega_g^2 + 2\omega_y^2)\sin(\omega_y x)\sin(\omega_g z)\Big] + \cos(||\omega||t)\Big[3\omega_g\sin(\omega_y x)\cos(\omega_g z) - 2\omega_y\cos(\omega_y x)\sin(\omega_g z)\Big] - 2\omega_y\sin(\omega_g(t-z))\cos(\omega_y(t+x)) - 3\omega_g\cos(\omega_g(t-z))\sin(\omega_y(t+x))\Bigg), \quad (4.50)$$

$$\tilde{A}^a_z = \delta^a_1 \frac{A_+}{2\omega_g}\Bigg(\frac{\sin(||\omega||t)}{||\omega||}\Big[\omega_g\cos(\omega_g z)\cos(\omega_y x) + \omega_y\sin(\omega_g z)\sin(\omega_y x)\Big] - \sin(\omega_g(t-z))\cos(\omega_y(t+x)) - \cos(||\omega||t)\cos(\omega_y x)\sin(\omega_g z)\Bigg), \quad (4.51)$$

where $||\omega|| = \sqrt{\omega_g^2 + \omega_y^2}$.

The solutions have an extra contribution from modes with frequency $\sqrt{\omega_g^2 + \omega_y^2}$ apart from the particular solution to inhomogeneous equations same as in [29]. We have used Green's function for solutions of massless inhomogeneous wave equations as described in [26, 29]. If we set the boundary condition such that the perturbations are zero at $t = 0$, then the solution gives the total perturbation of both particular and general solutions. This type

of boundary condition is also in agreement with the actual experiment as the perturbation of matter wave is zero before the arrival of GW. In types Ia and Ib, we did not use these boundary conditions because of the nature of the ansatz but obtained particular solutions to YM equations. Thus, one can use the Coleman ansatz with the boundary conditions considered in this case while studying the YM wave and GW interactions in a detector.

4.2.2 Type II waves

So far, the perturbed solutions did not involve the coupling constant (g_{ym}). To fully understand the nonlinear nature of YM fields, we have to take a different ansatz. This ansatz is already described in Sec. (3.2.1) and is given as follows

$$A^a_\mu = \delta^a_1\, \Phi(u)\, k_\mu + \delta^a_3\, \Psi(u)\, l_\mu, \tag{4.52}$$

where $u = p_\mu x^\mu + e; e$ is an arbitrary constant and the three vectors k_μ, l_μ, p_μ are orthogonal to each other.

Similarly, in this case, we assume the gauge fields of the form

$$A^a_\mu = \overline{A}^a_\mu + \tilde{A}^a_\mu \tag{4.53}$$

where $\overline{A}^a_\mu$ is the Type II YM wave solution in Minkowski background (Sec: 3.2.1) and $\tilde{A}^a_\mu$ is the perturbation function which we take as $\tilde{A}^a_\mu = \delta^a_1\, \tilde{\Phi}\, k_\mu + \delta^a_3\, \tilde{\Psi}\, l_\mu$. Now, we will restrict the propagation of the unperturbed YM solution by choosing p_μ vector to be $p_\mu = (p_0, 0, 0, p_3)$ such that p_μ is time-like. By choosing the p_0 and p_3, we can make the wave propagate in the z or $-z$ direction.

Here we have taken the perturbation to be of the same form as the unperturbed solution because the GW polarisations interact with YM polarisations in l_μ and k_μ directions only. The nature of solutions also depends on the choice of k_μ and l_μ vectors. To restrict the propagation of perturbed functions $(\tilde{\Phi}, \tilde{\Psi})$ along k_μ and l_μ vectors, we impose the following

conditions: $k_\mu \partial^\mu \Phi = l_\mu \partial^\mu \Phi = k_\mu \partial^\mu \Psi = l_\mu \partial^\mu \Psi = 0$. If we impose the perturbed functions to have t and z dependence, we can choose the k_μ and l_μ vectors as $k_\mu = (0,0,1,0)$ and $l_\mu = (0,1,0,0)$. By substituting the metric (4.5), unperturbed, and perturbed ansatz in YM Eq. (4.4), we will get the following equations for perturbation functions:

$$\Box\tilde{\Phi} - 2g_{ym}^2\, l^2\, \overline{\Psi}\, \overline{\Phi}\, \tilde{\Psi} - g_{ym}^2 l^2\, \overline{\Psi}^2\, \tilde{\Phi} = -\partial_\mu h_+(t,z)\, \partial^\mu \overline{\Phi} - h_+(t,z)(g_{ym}^2 l^2\, \overline{\Phi}\, \overline{\Psi}^2), \quad (4.54)$$

$$\Box\tilde{\Psi} - 2g_{ym}^2 k^2 \overline{\Psi}\, \overline{\Phi}\, \tilde{\Phi} - g_{ym}^2 k^2\, \overline{\Phi}^2\, \tilde{\Psi} = \partial_\mu h_+(t,z)\, \partial^\mu \overline{\Psi} + h_+(t,z)(g_{ym}^2 k^2\, \overline{\Psi}\, \overline{\Phi}^2), \quad (4.55)$$

where $\overline{\Phi}$ and $\overline{\Psi}$ are the unperturbed YM wave solutions (3.60 & 3.61). We solved the above coupled partial differential equations numerically and 3D plots were given in Fig. (4.4) and the perturbation plots as a function of time in Fig. (4.5). For this, we choose the YM wave propagating in -z-direction by choosing $p_0 = 3$ and $p_3 = 1$. We studied the influence of the coupling constant (g_{ym}) on the perturbation functions. We find that the coupling constant is inversely proportional to the magnitude of the perturbed functions while leaving the functional behaviour unchanged. This is shown in Fig. (4.6). This can be understood in this way: The unperturbed solutions are inversely proportional to the coupling constant. In the above differential equations, the terms on the left side involving the square of the coupling constant are always accompanied by the product of two unperturbed solutions which diminishes its influence on functional behaviour. The terms on the right side are left with an extra unperturbed function which causes the dependence of coupling constant on solutions.

We also analysed the solutions' spectrum ($\tilde{\Phi}(1,t)$ & $\tilde{\Psi}(1,t)$) to find the oscillation frequencies. As expected, the solutions follow a beat pattern with the inner frequency being equal to the sum of GW and YM wave frequencies and the outer frequency being equal to the difference of GW and YM wave frequencies. The plots of $\tilde{\Phi}(1,t)$ and $\tilde{\Psi}(1,t)$ are shown in Fig. (4.5), and the corresponding power spectrum and spectrogram of $\tilde{\Phi}(1,t)$ in Fig. (4.7). The spectrogram plot reveals that there is more to story than usual beat frequencies.

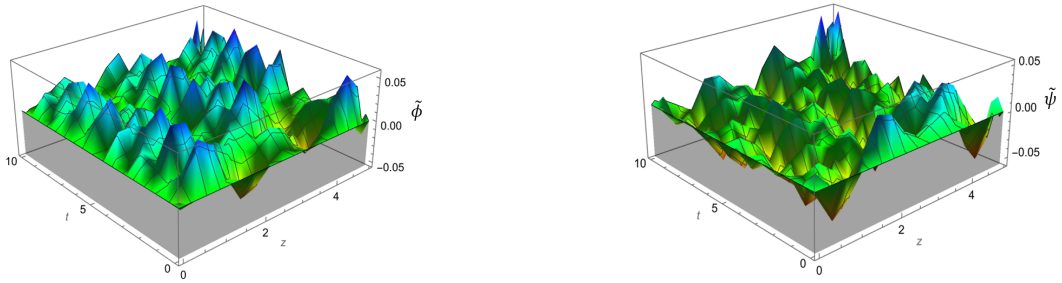

((a)) $\tilde{\Phi}$ ((b)) $\tilde{\Psi}$

Figure 4.4: Figures showing $\tilde{\Phi}$ and $\tilde{\Psi}$ as a function of t and z. We choose $l_1 = 1$, $k_2 = 1$, $A_+ = 0.01$, $g_{ym} = 0.5$ and $\omega_g = 20$.

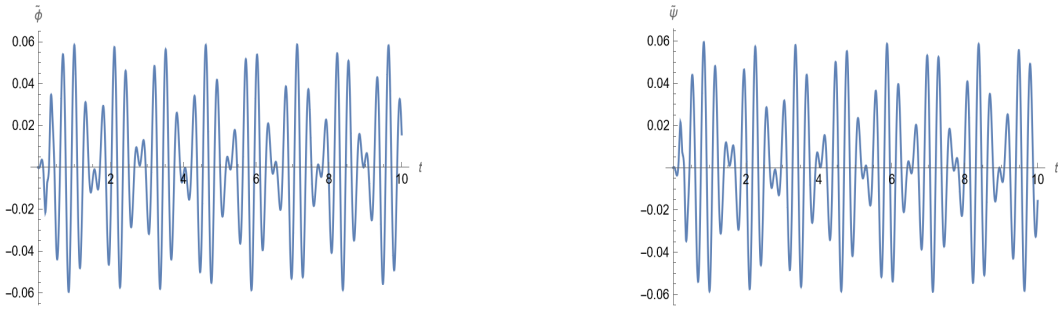

((a)) $\tilde{\Phi}(1,t)$ ((b)) $\tilde{\Psi}(1,t)$

Figure 4.5: Figures showing $\tilde{\Phi}$ and $\tilde{\Psi}$ as a function of t. We choose $z = 1$, $l_1 = 1$, $k_2 = 1$, $A_+ = 0.01$, $g_{ym} = 0.5$ and $\omega_g = 20$.

We can see that there are multiple peaks in the power spectrum. One can understand this as the cosine Jacobi elliptic function is not a single sine or cosine function, but a series of sine and cosine functions (Fig. 4.8). These multiple frequencies combine with a single GW frequency to produce these multiple peaks in the power spectrum.

The Poynting vector is given by

$$S_i = \frac{1}{4\pi} T_{0i} = \delta_i^3 \frac{1}{4\pi} \Big[k_2^2 \partial_0 \overline{\Phi}\, \partial_3 \overline{\Phi} (1 + A_+ \cos(\omega_g (t-z))) + l_1^2 \partial_0 \overline{\Psi}\, \partial_3 \overline{\Psi} \\ (1 - A_+ \cos(\omega_g (t-z))) + k_2^2 (\partial_0 \overline{\Phi}\, \partial_3 \tilde{\Phi} + \partial_0 \tilde{\Phi}\, \partial_3 \overline{\Phi}) + l_1^2 (\partial_0 \overline{\Psi}\, \partial_3 \tilde{\Psi} + \partial_0 \tilde{\Psi}\, \partial_3 \overline{\Psi}) \Big]. \quad (4.56)$$

and the energy density as

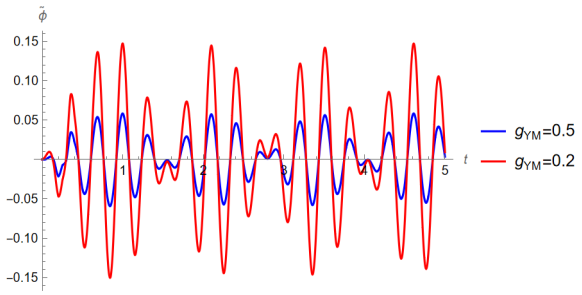

Figure 4.6: Figure showing $\tilde{\Phi}(1,t)$ for two different values of g_{ym}.

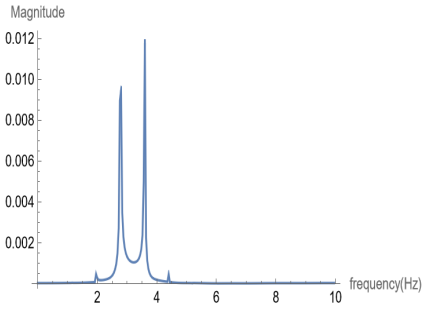

((a)) Power Spectrum

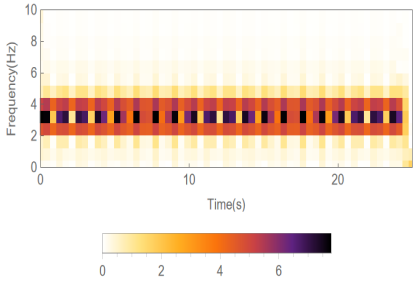

((b)) Spectrogram

Figure 4.7: Figures showing Power spectrum and spectrogram of $\tilde{\Phi}(1,t)$.

$$T_{00} = (1+A_+\cos(\omega_g(t-z)))(\partial_0\overline{\Phi}k_2+\partial_0\tilde{\Phi}k_2)^2+(1-A_+\cos(\omega_g(t-z)))(\partial_0\overline{\Psi}l_1+\partial_0\tilde{\Psi}l_1)^2-$$
$$\frac{1}{2}(1+A_+\cos(\omega_g(t-z)))[(\partial_0\overline{\Phi}k_2+\partial_0\tilde{\Phi}k_2)^2-(\partial_3\overline{\Phi}k_2+\partial_3\tilde{\Phi}k_2)^2]-g_{ym}^2\,(1+A_+\cos(\omega_g(t-z)))$$
$$(1-A_+\cos(\omega_g(t-z)))(\overline{\Phi}k_2+\tilde{\Phi}k_2)^2(\overline{\Psi}l_1+\tilde{\Psi}l_1)^2+(1-A_+\cos(\omega_g(t-z)))$$
$$[(\partial_0\overline{\Psi}l_1+\partial_0\tilde{\Psi}l_1)^2-(\partial_3\overline{\Psi}l_1+\partial_3\tilde{\Psi}l_1)^2]. \quad (4.57)$$

The expressions consist of Jacobi elliptic functions, that are real and oscillating, which shows that the energy density is bounded throughout space-time and the direction of the Poynting vector is fixed, which makes us interpret the solutions as non-abelian plane waves propagating in a fixed direction. We also found the expressions for non-abelian electric and magnetic fields as

$$\tilde{E}_i^a = -\left[\delta_1^a\delta_i^2(\partial_0\tilde{\Phi}k_2)+\delta_3^a\delta_i^1(\partial_0\tilde{\Psi}l_1)\right], \quad (4.58)$$

$$\tilde{B}_i^a = \delta_1^a\delta_i^1\left[-\partial_3\tilde{\Phi}\,k_2-A_+\,\cos(\omega_g(t-z))\partial_3\overline{\Phi}\,k_2\right]+\delta_2^a\delta_i^3 g_{ym}\left[\overline{\Phi}k_2\;\tilde{\Psi}l_1\right.$$

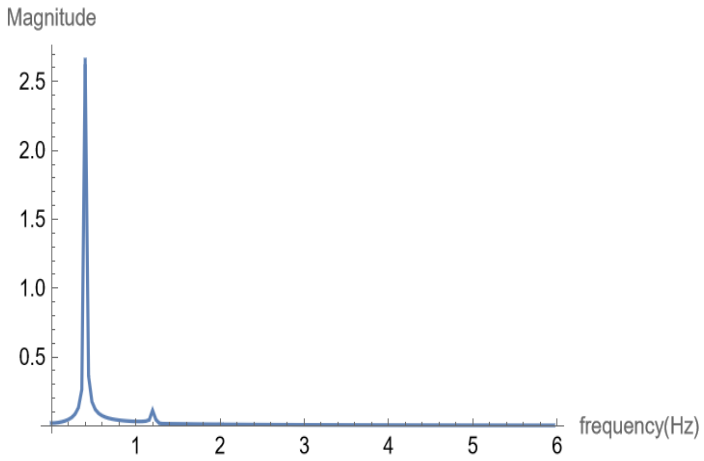

Figure 4.8: Power Spectrum of $\mathrm{cn}(3t+1,1/2)$.

$$+\tilde{\Phi}k_2\overline{\Psi}l_1 - A_+^2\cos(\omega_g(t-z))^2\overline{\Phi}\,\overline{\Psi}k_2l_1\big] + \delta_3^a\delta_i^2\big[-\partial_3\tilde{\Psi}l_1\big]. \quad (4.59)$$

We find that the electric fields are linear in YM solutions and also transverse to the propagating direction. However, the magnetic fields are nonlinear in YM solutions and not perpendicular to the propagating direction. This suggests that the YM solutions behave as if they are propagating in a nonlinear media.

4.2.3 Summary

In this section, we have solved the solutions for the YM waves propagating in the presence of a GW in a flat background. Owing to its dependence on the coupling constant (g_{ym}), we classified wave solutions into two types: Type I, which does not depend on the coupling constant, and Type II, which depends on the coupling constant. Due to the nature of ansatz for type I waves, the commutator terms that contain coupling constant become zero. The type I waves show a beat pattern similar to type II waves and the Poynting vector plots of type I waves show directional change similar to the EM case in [26]. We also find there is no interaction between the GW and YM waves when they are propagating in the same or parallel direction similar to the EM case in [26]. This is not surprising because, without the commutator terms, the YM equations reduce to Maxwell's equations.

The YM equations with type II waves have nonzero commutator terms which causes its dependence on the coupling constant. Even in linearized approximation, the YM equations become complicated to solve analytically. Thus, we solved those equations numerically. The overall behaviour of solutions is the same as in the case of type I waves, but the amplitude of solutions depends on the coupling constant. Due to the non-linear nature of YM equations in the type II waves case, we find there is a nonzero interaction between the waves even propagating they are propagating in the same direction.

Along the same direction, there are some prospects for this research. Some of them include relaxing the approximations we used to obtain our results. For example, while discussing the results of interaction between GWs and type Ia, and Ib waves, we set the functions $f^a_{\overline{\alpha}}$ to constants. One can relax this assumption by taking as functions which might give a different interesting solutions. With even bigger colliders, we can reach even more energy. At very high energies, the approximation of the gluons propagating as waves in QGP can be realizable. Then, the possibility of testing the effect of GWs on gluons might be possible.

In the next section, we will study the influence of GW on YM waves in the cosmological background, particularly the de Sitter background.

4.3 In Cosmological Background

To study the influence of GWs in the early universe phenomena, we need to move away from the flat space-time approximation. It has already been discussed about the generation of GWs from many processes that happened in the early universe in Sec. (2.1.4). These GWs which are stochastic in nature, form a background of GWs. All the cosmological processes such as QCD Phase Transition, and BBN that happened in the early universe must have happened in this GW background. Thus, it is important to study the YM waves in the GW background in curved space-time. Even though we can only describe the PGWs stochastically, for simplicity, we consider the effect of single mode of GW on YM wave

propagation. For this, we consider the FLRW metric in conformal coordinates as

$$ds^2 = a^2(\tau)(-d\tau^2 + dx^2 + dy^2 + dz^2), \tag{4.60}$$

where x,y, and z are the Cartesian coordinates and $a(\tau)$ is the scale factor in conformal time coordinate (τ). The conformal time is related to comoving time (t) by relation $d\tau = dt/a(t)$. By changing the scale factor ($a(\tau) \propto \tau^n$), we can vary the background from de Sitter ($a(\tau) \propto 1/\tau$), radiation-dominated ($a(\tau) \propto \tau$) to matter-dominated ($a(\tau) \propto \tau^2$) universes.

The sourceless YM equations are conformally invariant. This can be confirmed easily as follows: Consider the YM equation (Eq. 5.2) for a general metric as

$$\frac{1}{\sqrt{-g}}\partial_\mu\left(\sqrt{-g}g^{\mu\lambda}g^{\nu\rho}F^a_{\lambda\rho}\right) + g_{ym}\varepsilon^{abc}A^b_\mu g^{\mu\rho}g^{\nu\lambda}F^c_{\lambda\rho} = 0. \tag{4.61}$$

If we consider the metric as $g^{\mu\nu} = \frac{1}{a^2(\tau)}\eta^{\mu\nu}$, then one can easily find that the above equation reduces to one that of a flat metric.

Since the YM equations are conformally invariant, the solutions for the YM equation in the case of a homogeneous and isotropic cosmological background (FLRW metric) are the same as in Minkowski's background with the comoving time (t) being replaced with conformal time (τ).

To consider the interaction with GW, we need to define the GWs in a cosmological background. The discussion on GWs in the cosmological background is given in Sec. (2.1.3). Let us consider a $+$-polarised GW propagating in z-direction in a cosmological background. Then, the metric becomes

$$ds^2 = a^2(\tau)\big(-d\tau^2 + (1+h_+(\tau,z))dx^2 + (1-h_+(\tau,z))dy^2 + dz^2\big). \tag{4.62}$$

The explicit expressions for h_+ for different backgrounds are given in Sec. (2.1.3). For de

Sitter background, the expression can be rewritten as

$$h_+(\tau,z) = A_+(\omega_g\tau - i)e^{-i\omega_g(\tau-z)}, \tag{4.63}$$

where A_+ is the amplitude and ω_g is the frequency of GW.

We use the same procedure of the previous section (Sec. 4.2) to find the solutions for the linearized YM equation in the GW background in de Sitter spacetime. The same analysis will also work for other cosmological backgrounds just by replacing the h_+ expression in their respective backgrounds.

4.3.1 Type I waves

We use the same procedure as in Sec. (4.2.1). We start by taking the ansatz of the form $A^a_\mu = \overline{A}^a_\mu + \tilde{A}^a_\mu = \psi_{\overline{\alpha}}\, f^a_{\overline{\alpha}}(\overline{U})\, \partial_\mu \overline{U} + \psi_{\overline{\alpha}}\, f^a_{\overline{\alpha}}(U)\, \partial_\mu \tilde{U}$ and assuming perturbation in function U only. Using the metric (Eq. 4.62) with the above ansatz, we end up with Eq.(4.10) as

$$\begin{aligned}\partial^\mu\partial^\nu\tilde{U}\partial_\mu\psi_{\overline{\alpha}} + \partial^\nu\tilde{U}\Box\psi_{\overline{\alpha}} - \partial^\lambda\partial^\nu\psi_{\overline{\alpha}}\partial_\lambda\tilde{U} - \partial^\nu\psi_{\overline{\alpha}}\Box\tilde{U} &= \partial^\mu\overline{U}\partial_\mu(h^{\nu\sigma}\partial_\sigma\psi_{\overline{\alpha}}) + h^{\mu\rho}\partial_\rho\overline{U}\partial_\mu\partial^\nu\psi_{\overline{\alpha}} \\ &+ h^{\nu\sigma}\partial_\sigma\psi_{\overline{\alpha}}\eta^{\mu\rho}\partial_\mu\partial_\rho\overline{U} + \partial^\nu\psi_{\overline{\alpha}}\partial_\mu(h^{\mu\rho}\partial_\rho\overline{U}) - \eta^{\mu\rho}\partial_\mu\partial_\rho\psi_{\overline{\alpha}}h^{\nu\sigma}\partial_\sigma\overline{U} \\ &- \partial^\nu\overline{U}\partial_\mu(h^{\mu\rho}\partial_\rho\psi_{\overline{\alpha}}) - \eta^{\mu\rho}\partial_\rho\psi_{\overline{\alpha}}\partial_\mu(h^{\nu\sigma}\partial_\sigma\overline{U}) - h^{\mu\rho}\partial_\rho\psi_{\overline{\alpha}}\partial_\mu\partial^\nu\overline{U},\end{aligned} \tag{4.64}$$

with conditions

$$\eta^{\mu\nu}\partial_\mu\tilde{U}\partial_\nu\psi_{\overline{\alpha}} + h^{\mu\nu}\partial_\mu\overline{U}\partial_\nu\psi_{\overline{\alpha}} = 0, \tag{4.65}$$

$$2\eta^{\mu\nu}\partial_\mu\tilde{U}\partial_\nu\overline{U} + h^{\mu\nu}\partial_\mu\overline{U}\partial_\nu\overline{U} = 0. \tag{4.66}$$

The only difference is that we have to replace comoving time (t) with conformal time (τ). By choosing different $\psi_{\overline{\alpha}}$, we get different solutions.

A. Type Ia waves

If we choose $\psi_1 = x, \psi_{2,3,4} = 0$, the YM equation reduces to a single second-order inhomogeneous differential equation

$$\Box\tilde{U} = \eta^{\mu\rho}\partial_\rho\overline{U}\partial_\mu h_+ + h_+\eta^{\mu\rho}\partial_\mu\partial_\rho\overline{U} - h_+\partial_2\partial_2\overline{U}, \tag{4.67}$$

where h_+ is given by Eq. (4.63). Here, h_+ is not simply a sinusoidal function, so we find there is a nonzero interaction even when the waves propagate in the same direction. To get the perturbative solutions, we consider the same assumption for conditions as in Minkowski spacetime. Considering YM wave also propagating in z-direction ($\overline{U} = U_0\cos(\omega_y(\tau - z))$) , then the differential equation to be solved becomes

$$\Box\tilde{U} = A_+\ U_0\ \omega_y\ \omega_g\ \cos(\omega_g(\tau - z))\ \sin(\omega_y(\tau - z)). \tag{4.68}$$

The solution for the above equation was found to be

$$\tilde{U}(\tau, z) = -\frac{1}{8}A_+\ U_0\ \omega_y\ \omega_g(\tau + z)\left(\frac{\cos((\omega_g - \omega_y)(\tau - z))}{\omega_g - \omega_y} - \frac{\cos((\omega_g + \omega_y)(\tau - z))}{\omega_g + \omega_y}\right) + c_1(\tau - z) + c_2. \tag{4.69}$$

where ω_y is YM wave frequency, U_0 is the amplitude of YM wave, c_1 and c_2 are integration constants. As one can see from the expression there are two modes with beat frequencies.

Now, let us consider the waves propagating in anti-parallel directions ($\overline{U} = U_0\cos(\omega_y(\tau + z))$). In this case, the differential equation becomes

$$\Box\tilde{U} = A_+\ U_0\ \omega_y\ \omega_g\ \sin(\omega_y(\tau + z))(2\tau\omega_g\sin(\omega_g(z - \tau)) - \cos(\omega_g(\tau - z))). \tag{4.70}$$

The solution for $\tilde{U}$ is given by

$$\tilde{U}(\tau,z) = -\frac{1}{4\omega_y}A_+U_0\Bigg((\omega_g+2\omega_y)\sin((\omega_y-\omega_g)z+(\omega_g+\omega_y)\tau)+(\omega_g-2\omega_y)$$
$$\sin((\omega_y-\omega_g)\tau+(\omega_y+\omega_g)z)-2\tau\omega_y\omega_g\Big[\cos((\omega_y+\omega_g)z+(\omega_y-\omega_g)\tau)$$
$$+\cos((\omega_y+\omega_g)\tau+(\omega_y-\omega_g)z)\Big]\Bigg). \quad (4.71)$$

B. Type Ib waves

If we choose $\Box\psi_{\overline{\alpha}}=0$, the YM equation reduces to

$$q^{\nu}\Box\tilde{U} = \eta^{\nu\lambda}h^{\mu\rho}\partial_\mu\partial_\rho U q_\lambda. \quad (4.72)$$

Similarly, by considering the same assumption on conditions and letting the YM wave propagate in the x-direction, i.e.$\overline{U}=U_0\cos(\omega_y(\tau-x))$, we solve for $\tilde{U}$ as

$$\tilde{U}(\tau,x,z) = \frac{A_+U_0}{2\omega_g}e^{-i\omega_g(\tau-z)}\Big(i\omega_g\cos(\omega_y(\tau-x))+(2+i\tau\omega_g)\omega_y\sin(\omega_y(\tau-x))\Big). \quad (4.73)$$

Same as in type Ia waves, we find that there is nonzero interaction between waves propagating in the same direction.

C. Coleman Waves

In this case, we follow the procedure of Sec. (4.2.1) where we started by considering the metric in light-cone coordinates ($x^{\pm}=\tau\pm z$) as follows

$$ds^2 = a^2(x^+,x^-)\left(-dx^-dx^+ + (1+h_+(x^+,x^-))dx^2 + (1-h_+(x^+,x^-))dy^2\right), \quad (4.74)$$

where $h_+(x^+,x^-)$ is given by Eq. (4.63) in these coordinates. Then, we consider the gauge field as $A^a_\mu=\overline{A}^a_\mu+\tilde{A}^a_\mu$. Choosing the same gauge, $\tilde{A}^a_1=\tilde{A}^a_2=0$. Also, using the same assumptions, (i) The field strength tensor is independent of x and y, and (ii) The gauge field components point in the same direction in $SU(2)$ internal space. With all these, we reduce

the YM equation to Eqs. (4.27-4.30). By solving these, one can get the following solutions

$$\tilde{A}^a_+ = \frac{1}{2}A_+\left[\frac{\omega_g}{2}(x^+ + x^-) - i\right]\left[f^a(x^+)x - g^a(x^+)y\right]e^{-i\omega_g x^-}, \tag{4.75}$$

$$\tilde{A}^a_- = -\frac{1}{4}A_+\omega_g\left[\left(\int[1 + i\omega_g(x^+ + x^-)]f^a(x^+)dx^+\right)x - \left(\int[1 + i\omega_g(x^+ + x^-)]g^a(x^+)dx^+\right)y\right]e^{-i\omega_g x^-}, \tag{4.76}$$

By letting the arbitrary functions be $f^a(x^+) = g^a(x^+) = \delta^a_1 \sin(\omega_y x^+)$, we see that the magnitude of the solutions decreases with increasing time which is shown in Fig. (4.9). This decreasing behaviour is identified with $1/\tau$ functional dependence.

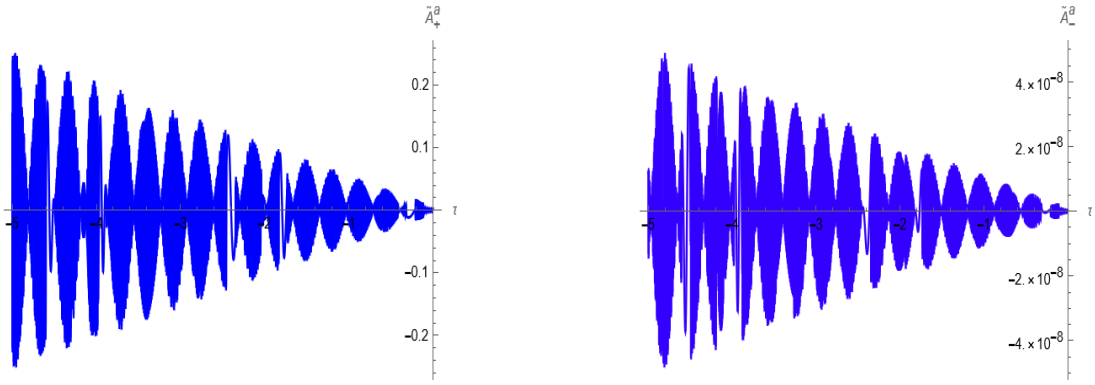

Figure 4.9: The perturbed gauge fields as a function of conformal time. We choose $x = 2$, $y = 1$, $\omega_g = 10$, $\omega_y = 10^8$, $A_+ = 0.01$ and $z = 1$.

4.3.2 Type II waves

To understand the influence of the coupling constant, we solve the YM equations for type II waves. We follow the same procedure as in Sec. (4.2.2). Considering the ansatz of the form

$$A^a_\mu = \overline{A}^a_\mu + \tilde{A}^a_\mu, \tag{4.77}$$

where $\overline{A}^a_\mu = \delta^a_1\,\overline{\Phi}\,k_\mu + \delta^a_3\,\overline{\Psi}\,l_\mu$ and $\tilde{A}^a_\mu = \delta^a_1\,\tilde{\Phi}\,k_\mu + \delta^a_3\,\tilde{\Psi}\,l_\mu$ and choosing the k_μ and l_μ vectors as $k_\mu = (0,0,k_2,0)$ and $l_\mu = (0,l_1,0,0)$, we get the following equations for $\tilde{\Phi}$ and $\tilde{\Psi}$:

$$\Box\tilde{\Phi} - 2g^2_{ym}l^2\,\overline{\Psi}\,\overline{\Phi}\,\tilde{\Psi} - g^2_{ym}l^2\,\overline{\Psi}^2\,\tilde{\Phi} = -\partial_\mu h_+(\tau,z)\partial^\mu\overline{\Phi} - h_+(\tau,z)(g^2_{ym}l^2\,\overline{\Phi}\,\overline{\Psi}^2), \quad (4.78)$$

$$\Box\tilde{\Psi} - 2g^2_{ym}k^2\overline{\Psi}\,\overline{\Phi}\,\tilde{\Phi} - g^2_{ym}k^2\,\overline{\Phi}^2\,\tilde{\Psi} = \partial_\mu h_+(\tau,z)\partial^\mu\overline{\Psi} + h_+(\tau,z)(g^2_{ym}k^2\,\overline{\Psi}\,\overline{\Phi}^2). \quad (4.79)$$

where $\overline{\Phi}$ and $\overline{\Psi}$ are YM solutions in the de Sitter background. We solve the above equations numerically using Mathematica and the plots are given in Figs. (4.10 & 4.11).

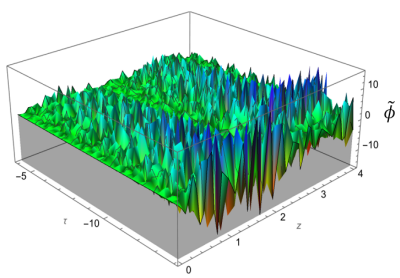

((a)) $\tilde{\Phi}$(z,τ)

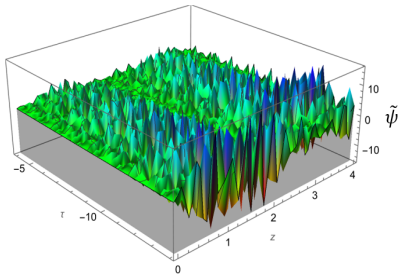

((b)) $\tilde{\Psi}$(z,τ)

Figure 4.10: Figures showing $\tilde{\Phi}$ and $\tilde{\Psi}$ as a function of τ and z. We choose $l_1 = 1$, $k_2 = 1$, $A_+ = 0.01$, $g_{ym} = 0.5$ and $\omega_g = 20$.

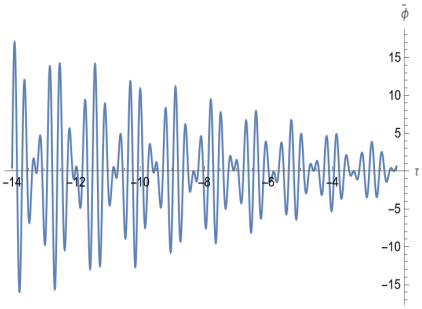

((a)) $\tilde{\Phi}(1,\tau)$

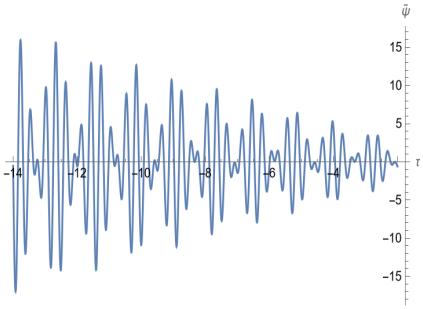

((b)) $\tilde{\Psi}(1,\tau)$

Figure 4.11: Figures showing $\tilde{\Phi}$ and $\tilde{\Psi}$ as a function of τ. We choose $z = 1$, $l_1 = 1$, $k_2 = 1$, $A_+ = 0.01$, $g_{ym} = 0.5$ and $\omega_g = 20$.

As we can see from the plots from this section and the previous one, the unperturbed solutions get attenuated due to the presence of GW. The amplitude of waves is a function of conformal time and the behaviour is similar to that in the EM case [26]. This attenuation

behaviour is the same for both type I and type II waves indicating the less influence of coupling constant on overall pattern.

4.3.3 Summary

In this section, we obtained the solutions for YM fields in the background of the GW-filled de-Sitter spacetime. For type I waves, we found analytical solutions, whereas for type II waves, we found numerical solutions. In both cases, it shows the same attenuation behaviour for solutions in the presence of GWs. This shows energy dissipation from YM waves to the medium of GW in de-Sitter space-time. Due to having a complicated expression for h_+, there is a nonzero interaction between YM waves and GWs even if they were propagating in the same or parallel direction for both type I and type II waves.

4.4 Electroweak Gauge Theory

So far, we have considered the interaction of GWs with pure Yang-Mills waves. Massless YM waves like gluons cannot exist freely as of now and could not be observed even in heavy ion colliders. But as for massive YM waves such as W and Z bosons do exist and be detected in heavy-ion colliders. To study these, one has to study the YM fields in the Electroweak symmetry broken phase. We already discussed the YM solutions in Electroweak gauge theory (Sec: 3.3). In this section, we will study the interaction of GWs with YM fields in the Electroweak symmetry broken phase.

For this, we will consider the Electroweak Lagrangian [50, 178] as

$$\mathcal{L}_{EW} = -\frac{1}{4}F^a_{\mu\nu}F^{a\mu\nu} - \frac{1}{4}B_{\mu\nu}B^{\mu\nu} + (D_\mu\varphi)^\dagger(D^\mu\varphi) + V(|\varphi|^2), \tag{4.80}$$

where

$$D_\mu\varphi = \left(\partial_\mu - i\frac{g_{ym}}{2}A_\mu - i\frac{g_y}{2}B_\mu\right)\varphi, \tag{4.81}$$

$$F^a_{\mu\nu} = \partial_\mu A^a_\nu - \partial_\nu A^a_\mu + g_{ym}\varepsilon^{abc}A^b_\mu A^c_\nu, \tag{4.82}$$

$$B_{\mu\nu} = \partial_\mu B_\nu - \partial_\nu, B_\mu, \tag{4.83}$$

where A^a_μ is the $SU(2)$ gauge field with coupling constant g_{ym}, B_μ is the $U(1)$ gauge field with coupling constant g_y, φ is the Higgs field with quartic potential $V(|\varphi|^2)$ and ε^{abc} is the Levi-Civita tensor. Under spontaneous symmetry breaking, Higgs field acquires a non-zero expectation value (v). Using the same transformations and definitions as in Sec: 3.3, we have

$$A_\mu = \sin\theta_W A^3_\mu + \cos\theta_W B_\mu, \tag{4.84}$$

$$Z_\mu = \cos\theta_W A^3_\mu - \sin\theta_W B_\mu, \tag{4.85}$$

$$W^\pm_\mu = \frac{1}{\sqrt{2}}(A^1_\mu \mp i A^2_\mu), \tag{4.86}$$

where θ_W is the electroweak mixing angle defined as

$$\cos\theta_W = \frac{g_{ym}}{\sqrt{g^2_{ym} + g^2_y}}, \ \sin\theta_W = \frac{g_y}{\sqrt{g^2_{ym} + g^2_y}}.$$

The A_μ field is identified with the Electromagnetic field of today, $W^\pm_\mu$ and Z_μ are the massive W and Z gauge bosons, respectively.

Now, consider a metric in the presence of a GW in a flat background as $g_{\mu\nu} = \eta_{\mu\nu} + h_{\mu\nu}$, where $h_{\mu\nu} = \text{diag}(0, h_+(t,z), -h_+(t,z), 0)$ considering only $+$-polarised GW wave. Using Oh-Teh ansatz [28],

$$W^\pm_\mu = \frac{1}{\sqrt{2}} k_\mu \Phi, \ Z_\mu = l_\mu \Psi, \ A_\mu = 0, \tag{4.87}$$

We can rewrite everything in terms of original gauge fields,

$$A^1_\mu = k_\mu \Phi, \ A^2_\mu = 0, \ A^3_\mu = l_\mu \cos\theta_W \Psi, \ B_\mu = -l_\mu \sin\theta_W \Psi. \tag{4.88}$$

Using this, one can find the Lagrangian in terms of functions Φ and Ψ. By varying the

Lagrangian, one gets the equations for Φ and Ψ as

$$k^2\Box\Phi - k^\mu\, k^\nu\partial_\mu\partial_\nu\Phi - g_{ym}^2\cos^2\theta_W\Psi^2\Phi l^2k^2 + \frac{v^2}{4}g_{ym}^2k^2\Phi = \partial_\mu(h^{\nu\rho})(k_\nu k_\rho\partial^\mu\Phi - k_\nu k^\mu\partial_\rho\Phi) + k^2h^{\mu\lambda}\partial_\mu\partial_\lambda\Phi - h^{\mu\lambda}k^\rho k_\lambda\partial_\mu\partial_\rho\Phi - h^{\nu\rho}k_\nu k_\rho\Box\Phi - k_\nu h^{\nu\rho}\partial_\rho k^\mu\partial_\mu\Phi, \quad (4.89)$$

$$l^2\Box\Psi - l^\mu l^\nu\partial_\mu\partial_\nu\Psi - g_{ym}^2\cos^2\theta_W\Phi^2\Psi l^2k^2 + \frac{v^2}{4}(g_{ym}^2+g_y^2)l^2\Phi = \partial_\mu(h^{\nu\rho})(l_\nu l_\rho\partial^\mu\Psi - l_\nu l^\mu\partial_\rho\Phi) + l^2h^{\mu\lambda}\partial_\mu\partial_\lambda\Psi - h^{\mu\lambda}l^\rho l_\lambda\partial_\mu\partial_\rho\Psi - h^{\nu\rho}l_\nu l_\rho\Box\Psi - l_\nu h^{\nu\rho}\partial_\rho l^\mu\partial_\mu\Psi, \quad (4.90)$$

In the linearized approximation, we take $\Phi = \overline{\Phi} + \tilde{\Phi}$ and $\Psi = \overline{\Psi} + \tilde{\Psi}$. By choosing the vector k_μ and l_μ to be $l_\mu = \delta_\mu^1$, and $k_\mu = \delta_\mu^2$, one gets the linearized equations for $\tilde{\Phi}$ and $\tilde{\Psi}$ as

$$\Box\tilde{\Phi} - 2g_{ym}^2\cos^2\theta_W\,\overline{\Psi}\,\overline{\Phi}\,\tilde{\Psi} - g_{ym}^2\cos^2\theta_W\overline{\Psi}^2\tilde{\Phi} + \frac{v^2}{4}g_{ym}^2\tilde{\Phi} = -\partial_\mu h_+\partial^\mu\overline{\Phi} - h_+\Box\overline{\Phi} - \frac{v^2}{4}g_{ym}^2h_+\overline{\Phi}, \quad (4.91)$$

$$\Box\tilde{\Psi} - 2g_{ym}^2\cos^2\theta_W\,\overline{\Psi}\,\overline{\Phi}\,\tilde{\Phi} - g_{ym}^2\cos^2\theta_W\overline{\Phi}^2\tilde{\Psi} + \frac{v^2}{4}(g_{ym}^2+g_y^2)\tilde{\Psi} = -\partial_\mu h_+\partial^\mu\overline{\Psi} - h_+\Box\overline{\Psi} - \frac{v^2}{4}(g_{ym}^2+g_y^2)h_+\overline{\Psi}. \quad (4.92)$$

For solving these equations, we set $\overline{\Psi} = \overline{\Phi}$ and $\tilde{\Phi} = \tilde{\Psi}$ and obtain numerical solutions. The constants were chosen such that the behaviour of the unperturbed massive gauge field is hyperbolic and not oscillatory. The perturbed solution obtained is oscillatory and the amplitude of perturbations increases with time and obtains a very high magnitude very quickly (Fig. (4.12)). As the GW amplitude is being multiplied by W and Z boson masses, this makes the perturbations acquire high magnitudes very quickly. Thus, the perturbation theory breaks down and one has to approach the nonperturbative methods to solve for an

exact solution. However, due to the mass term, W and Z bosons decay very quickly. Thus, we make a plot for an infinitesimal time ($0 < t < 10^{-6}$) in Fig. (4.13).

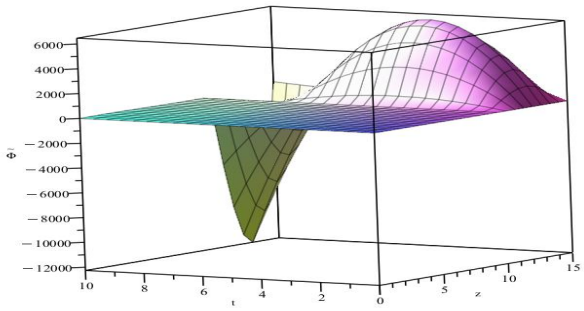

Figure 4.12: Figure shows the perturbed function ($\tilde{\Phi}$) in the presence of GW for large times. We choose $A = 4$, $B = 0$, $A_+ = 0.01$, $g_{ym}^2 \cos^2\theta_W = 0.1, v^2 g_{ym}^2 = 40$ and $\omega_g = 1$.

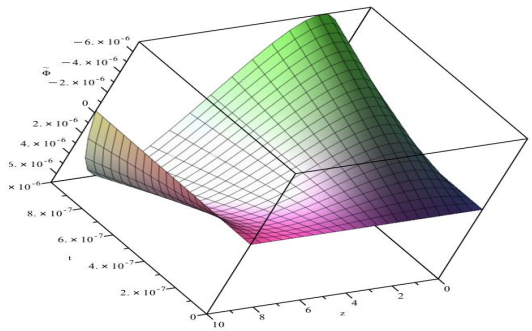

Figure 4.13: Figure shows the perturbed function ($\tilde{\Phi}$) in the presence of GW for short time $t < 10^{-6}$. In this short time, the perturbation is under control.

As GW is a solution to linearized Einstein equations, the linearised analysis is the correct approximation to study the above system. But to study the non-perturbative regime, one has to obtain the complete solution to the Einstein-Yang-Mills system. This work will be useful in predicting the behaviour of W and Z bosons in the presence of GWs in heavy ion collider experiments.

4.5 Conclusion

In this chapter, we studied the interaction of GWs with YM waves in different space-times. Our calculations are based on the following scenario: GWs are generated by various cosmological processes in the early universe and the gluons as YM waves were interacting with these GWs. We considered two types of YM waves based on their dependence on coupling constant as we labelled them as Type I and Type II. We found that both types of waves were perturbed and deviated from their original propagating direction due to GWs. The type I YM waves interacted with the GWs in the same way as EM waves. Particularly, for Coleman waves, we showed that the YM waves deviate from their original direction. We found that there is no interaction of GWs with YM waves when they are propagating in the same direction which was observed in the case of electromagnetic wave as well. This is because of the absence of commutator terms in the YM equations. To investigate the coupling constant dependence on solutions, we consider another type of waves, Type II waves, where the solutions depend on the coupling constant. We found that the coupling constant affects the amplitude of the waves rather than the functional behaviour. We found the coupling constant has an inverse effect on the perturbed solutions. This is the same as in the case of unperturbed YM solutions.

In relevance with particle physics experiments, we studied the interactions of massive YM waves with GWs in the Electroweak symmetry broken phase. In the short duration of W and Z bosons, we found that the GWs perturbed the YM fields, and the solutions were obtained numerically. As the perturbed YM solutions reach high magnitudes quickly, the perturbation theory is valid for only a very short amount of time. Thus, one has to deal with the system non-perturbatively to understand better. One can ask questions like whether the interaction with GWs can increase the 'mass' of W and Z bosons which might change its decay pattern. After the extension of our results to $SU(3)$, they can also be relevant for gluons which are being studied in particle accelerators. As these are extensions of the work [26] to non-abelian gauge fields, this work also provides ways to detect GWs. The

plan to discover GWs is as follows: There are experiments that produce and study massive gauge bosons (W and Z bosons). These particles can react to the GWs created by massive cataclysmic events and might change their decay pattern. The calculations we did were by solving the YM equations in the GW background. To make the predictions quantitative, one has to investigate the scattering amplitudes of GWs with electroweak gauge bosons.

Chapter 5

Yang-Mills Condensates and its interaction with Gravitational waves

> "What we observe is not nature itself, but nature exposed to our method of questioning."
>
> *Werner Heisenberg*

QGP is a deconfined mixture of quarks and gluons formed from the breakdown of the hadrons at very high temperatures. This kind of phase existed in the very early universe and is also being created and studied in heavy ion colliders such as LHC at CERN and RHIC at BNL. Due to asymptotic freedom, the coupling strength between quarks and gluons becomes weak at extremely high temperatures. At these thermodynamic conditions, the picture of QGP as an ideal gas of non-interacting quarks and gluons might be a good approximation. With that assumption, quarks and gluons are expected to propagate as waves. Along these lines, we investigated the QGP using YM waves in Chapter 3 and examined the interaction between GWs and YM waves in Chapter 4. However, the QGP created at heavy ion colliders like at CERN or RHIC is at temperatures around the critical temperature ($T_c \sim 150$ MeV or 10^{12}K), associated with the QCD phase transition from hadrons to QGP. At these temperatures, the interaction between quarks and gluons is strong and the QGP is far from the ideal gas scenario, and exhibits the features of an almost perfect fluid. Particularly, the shear viscosity-to-entropy density ratio of QGP is found to be very low, even lower than anything found on Earth [181]. The analysis we did in the previous chapter are

valid for extremely high temperatures higher than the critical temperatures. In this chapter, we consider a different model of QGP which captures the features of a perfect fluid. It is done by using condensates. These are the homogeneous and isotropic configurations of the gauge field, which show the properties of a perfect fluid with a diagonal stress-energy tensor. As the QGP is not an exact perfect fluid, we also consider the fluctuations around the condensate.

There were numerous theoretical studies on QGP in relevance with the early universe or heavy ion colliders [39–43, 149, 150, 182–186]. Most of the studies related to QGP were based on thermodynamic properties using effective field theories such as NJL or PNJL models [186]. There are some studies investigating the QGP using an ideal gas scenario which we described in detail in Chapter: 4. In this chapter, we are investigating the QGP using time-dependent condensate along with the fluctuations. The idea of using condensates in this area started with the discovery of the existence that the $SU(2)$ YM field can be parametrized by a single scalar function [32–35]. This kind of configuration is possible for the $SU(2)$ gauge group as there is a local isomorphism between the $SU(2)$ and spatial rotation group $SO(3)$. This configuration has a stress-energy tensor of a homogeneous and isotropic (perfect) fluid. Since then, there have been many applications to different problems of physics. The YM fields with condensate configuration have important applications in the Early Universe, particularly in the context of Dark Energy and gauge-flation. For those who are working on alternatives for familiar scalar field-driven inflation, the vector fields with condensate configuration served as an ideal choice. This idea was explored in [36, 37]. There were studies on explaining the origin of Dark energy within the Standard model, without requiring new fields [187, 188] based on the condensate field configurations. These studies revealed that the Dark Energy is related to the QCD Vacuum energy [189–191].

There are few studies on QGP using condensates and extensions thereof. One of those models is the condensate (plasma) + fluctuations (plasmons) model studied in the case of

$SU(2)$ in [38] and in the case of $SU(3)$ in [42]. In [38], authors studied the effect of fluctuations on $SU(2)$ YM condensate in different limiting cases and different spacetimes. In a semi-classical analysis [38], it was found that the plasmons are drawing energy from the plasma/condensate. In their work [38], they consider a spatially homogeneous and isotropic component of gauge field as a condensate and an inhomogeneous component as YM wave modes. It was shown that the interactions between large condensate and small YM modes set off a significant energy transfer from condensate to wave modes. They found that the longitudinal YM modes which are unphysical in degenerate YM theory become physical particles. They acquire frequency and dispersion, after quantization due to the interactions between condensate and the wave modes.

We found this model of the YM condensate to be most useful for studying the QGP as it captures the features of an almost perfect fluid. In this chapter, we wish to study the effect of GWs on the energy analysis found in [38]. When we consider their condensate + fluctuations model [38] in the presence of GWs, we found that the GWs do not interact with longitudinal modes. To include the longitudinal modes in the analysis, we consider a different type of decomposition for fluctuations modes using vector decomposition. With this decomposition, we can distinguish the longitudinal and transverse modes easily. In this model also, we investigate the energy swap effect from condensate to fluctuations. Later, we analyze the energy analysis in the presence of GWs using the alternate 'plasmons' decomposition.

This chapter closely follows the work we did in the paper [44]. We first consider the free condensate model for gluon plasma in Sec: 5.1. Then, we include the fluctuations around the condensate. We investigate it in two different ways: Using tensor decomposition (Sec. 5.2) and vector decomposition (Sec. 5.3). In both cases, we extended the study in the presence of GWs. In the end, we discussed the condensates in higher gauge groups in Sec: 5.4.

5.1 Free Condensate Model

We start with $SU(2)$ YM theory

$$\mathcal{L} = -\frac{1}{4} F^{a\mu\nu} F^{a}_{\mu\nu}, \tag{5.1}$$

and with the following equations of motion

$$\nabla_\mu F^{a\mu\nu} + g_{ym}\, \varepsilon^{abc}\, A^b_\mu\, F^{c\mu\nu} = 0, \tag{5.2}$$

where $F^a_{\mu\nu} = \partial_\mu A^a_\nu - \partial_\nu A^a_\mu + g_{ym}\varepsilon^{abc} A^b_\mu A^c_\nu$ being the field strength tensor of gauge field A^a_μ, ε^{abc} is the Levi-Civita tensor and ∇_μ is the covariant derivative.

In this section, we consider the free condensate model as a first approximation for Gluon Plasma. To zeroth order in wave modes, i.e. $|\tilde{A}_{ij}| \ll |U|$, we can rewrite the gauge field as

$$A^a_0 = 0, \;\; A^a_i = \delta^a_i U(t), \tag{5.3}$$

where $U(t)$ is the spatially homogeneous time-dependent scalar field representing YM condensate. Then, the YM equation (Eq. 5.2) becomes

$$\partial_0 \partial_0 U + 2 g^2_{ym} U^3 = 0, \tag{5.4}$$

and the solution for the above equation is given in terms of Jacobi elliptic functions as

$$U(t) = c_1\ \mathrm{sn}(g_{ym} c_1 (t + c_2), -1), \tag{5.5}$$

where $\mathrm{sn}(g_{ym} c_1 (t + c_2), -1)$ is the sine Jacobi elliptic functions, c_1 and c_2 are the integration constants.

The gauge field with this type of configuration behaves like a perfect fluid. A perfect fluid is a fluid with zero shear stresses, viscosity, or heat conduction. These are usually iden-

tified with a diagonal energy-momentum tensor. For condensate configuration, we found the equation of state to be

$$P = \frac{\varepsilon}{3} = \frac{1}{2}\left(\dot{U}^2 + g_{ym}^2 U^4\right), \tag{5.6}$$

where $\dot{U} = dU/dt$, P is the pressure and ε is the energy density of the system. It was found that the energy density of the system is constant (Fig: 5.1) and consequently pressure as well.

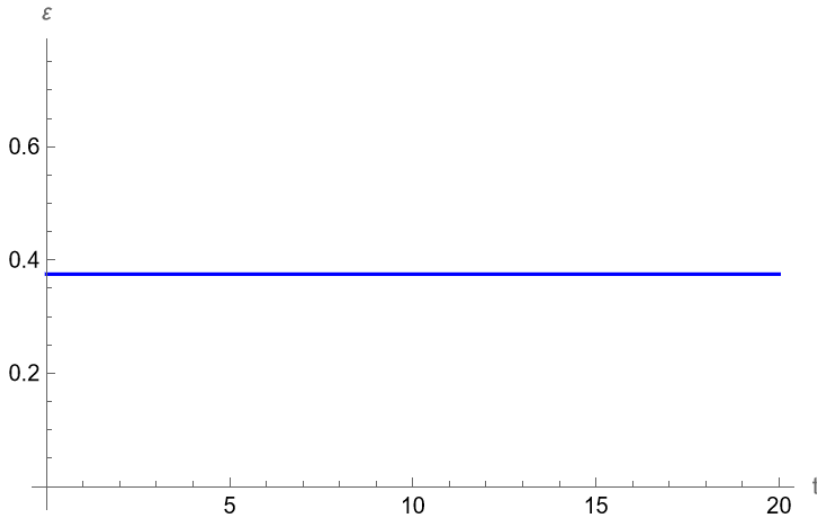

Figure 5.1: Condensate's energy density as a function of t. We choose $c_1 = 1$, $c_2 = 0$ and $g_{ym} = 0.5$

Out of two integration constants, c_1 regulates the magnitude of the condensate while c_2 regulates the phase difference of the condensate. That is shown in the Figs: (5.2) & (5.3).

5.2 Condensate + Fluctuations model (Tensor Decomposition)

In this section, we study the interaction of $SU(2)$ YM condensate with the fluctuations. In the first part of the section, we study the effect of YM gauge field fluctuations on the YM condensate. Later, we do the same analysis in the presence of GWs. We followed the tensor decomposition of fluctuations around the condensate as considered in [38]. Then, we write

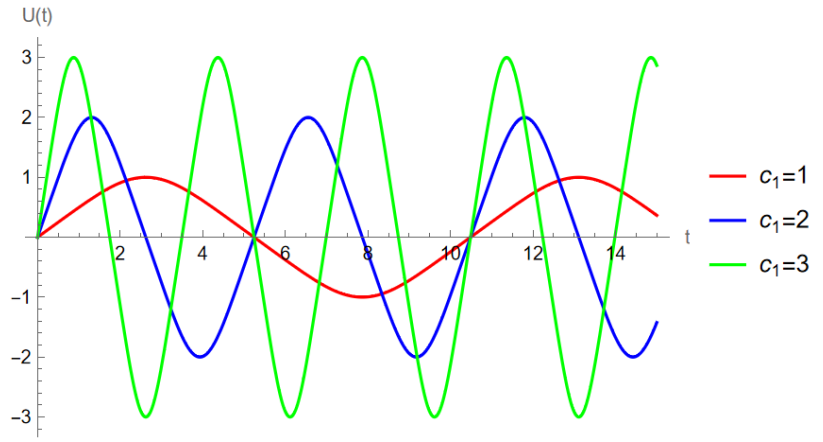

Figure 5.2: Condensate as a function of t for different c_1. We choose $c_2 = 0$ and $g_{ym} = 0.5$

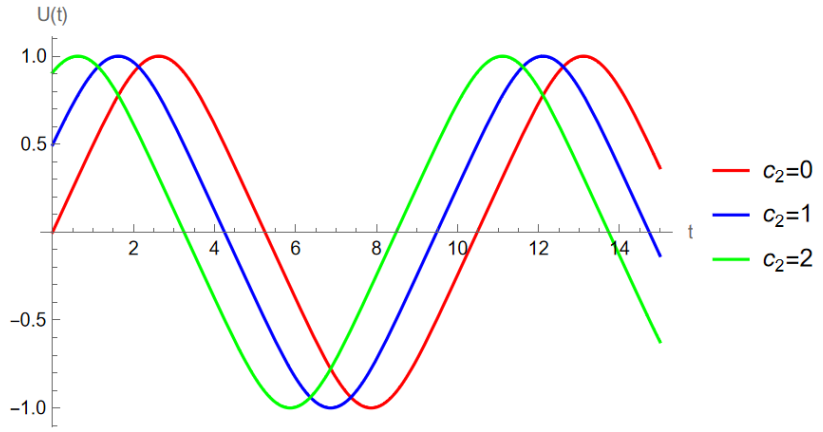

Figure 5.3: Condensate as a function of t for different c_2. We choose $c_1 = 1$ and $g_{ym} = 0.5$

the ansatz for the gauge field in Hamilton's gauge as follows

$$A_0^a = 0, \;\; A_i^a = U(t)\delta_i^a + \delta^{aj}\tilde{A}_{ji}(t,\vec{x}), \tag{5.7}$$

where $U(t)$ is the spatially homogeneous time-dependent scalar field representing YM condensate and the $\tilde{A}_{ji}$ is the spatially inhomogeneous fluctuations component.

Now, we consider the equations in linear order approximation in which only the interaction between condensate and the fluctuations are considered while neglecting the interaction between fluctuations. Physically, this approximation corresponds to a system during initial times with very few modes available with negligible interactions among them compared

with the condensate's interactions. Using the ansatz in Eq. 5.7, the YM equation (Eq. 5.2) becomes as

$$\Box\tilde{A}_{ij} - \partial_k\partial_j\tilde{A}_{ik} + g_{ym}U\left(2\varepsilon_{ikc}\partial_k\tilde{A}_{cj} + \varepsilon_{ibj}\partial_k\tilde{A}_{bk} + \varepsilon_{ibc}\partial_j\tilde{A}_{bc}\right) + g_{ym}^2U^2\left(\tilde{A}_{ji} - \tilde{A}_{ij} - 2\tilde{A}_{kk}\delta_{ij}\right) = 0. \quad (5.8)$$

where the d'Alembertian operator is defined as $\Box = \partial_\mu\partial^\mu$. The Gauss law obtained from the $\nu = 0$ component in the YM equation (5.2), acts as a constraint. In the linearized form, it is given by

$$\partial_k\partial_0\tilde{A}_{ik} + g_{ym}\varepsilon_{ijk}\partial_0 U\tilde{A}_{jk} + g_{ym}\varepsilon_{ikj}U\partial_0\tilde{A}_{jk} = 0. \quad (5.9)$$

To study the different modes of fluctuations clearly, the authors in [38] did the entire analysis in Fourier space in spatial coordinates. According to [38], the fluctuations ($\tilde{A}_{ik}$) component in Fourier modes can be decomposed as follows

$$\tilde{A}_{ik} = \Phi_{ik} + \varepsilon_{ikl}\,\chi_l, \quad (5.10)$$

where the antisymmetric part is given by $\chi_l = s_l^\sigma\eta_\sigma + n_l\lambda$ and the symmetric part is given by $\Phi_{ik} = \Psi_\lambda Q_{ik}^\lambda + \varphi_\sigma(n_i s_k^\sigma + n_k s_i^\sigma) + (\delta_{ik} - n_i n_k)\phi + n_i n_k\Lambda$ with $Q_{ik}^\lambda = Q_{ki}^\lambda,\ Q_{ii}^\lambda = 0,\ p_i Q_{ik}^\lambda = 0, p_k s_k = 0$, where the 3-vectors n_i and s_i are the longitudinal and transverse unit vectors, respectively and $\vec{p}$ is the corresponding Fourier 3-momentum.

We found that the other modes do not interact with GWs except for transverse traceless modes. So, we consider only those modes for our work. As for the energy analysis including the other modes, the reader can refer to [38]. Coming back to our case, the fluctuations can be rewritten as

$$\tilde{A}_{ij} = Q_{ij}^\alpha\Psi_\alpha, \quad (5.11)$$

where the coefficient (Q_{ij}^α) satisfies the following conditions: $Q_{ij}^\alpha = Q_{ji}^\alpha,\ Q_{ii}^\alpha = 0, \alpha = 1,2$. If we take the YM fluctuation to be propagating in the z-direction, then the non-zero com-

ponents of Q^{α}_{ij} are $Q^{1}_{11} = -Q^{1}_{22} = 1, Q^{2}_{12} = Q^{2}_{21} = 1$. With this choice, Gauss's constraint is automatically satisfied and the equations for the modes Ψ_{α} becomes

$$\Box\Psi_1 - 2g_{ym}U\partial_z\Psi_2 = 0, \tag{5.12}$$

$$\Box\Psi_2 + 2g_{ym}U\partial_z\Psi_1 = 0. \tag{5.13}$$

These equations were solved in Fourier space in spatial coordinates in [38] and were also analyzed in terms of generalized Mathieu equations in the view of parametric resonance in [192–194]. We numerically solved these equations in the configuration space using the Method of Lines, a numerical technique to solve partial differential equations (see Appendix D.3). The numerical solutions for Ψ_{α} are given in Figs. (5.4(a) & 5.4(b)).

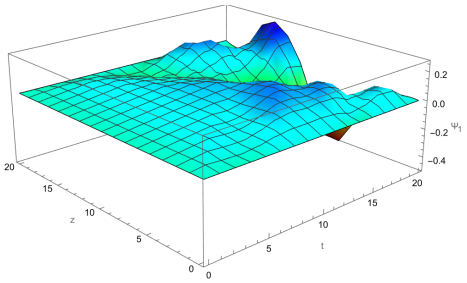

((a)) $\Psi_1(t,z)$

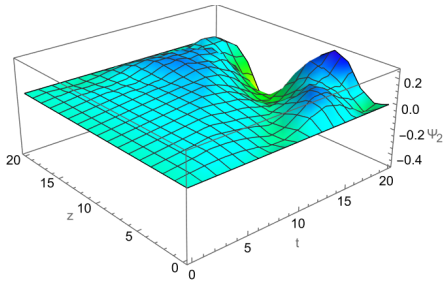

((b)) $\Psi_2(t,z)$

Figure 5.4: Figures showing $\Psi_1(t,z)$ and $\Psi_2(t,z)$ in the presence of a condensate. We choose $g_{ym} = 0.5$, $c_1 = c_2 = 1$, $\Psi_1(0,z) = \Psi_1(t,0) = \Psi_1(t,20) = 0.001$ and $\Psi_2(0,z) = \Psi_2(t,0) = \Psi_2(t,20) = 0.001$.

Initially, both functions show almost similar behaviour. As time increases, the $\Psi_1(t,z)$ behaves differently than $\Psi_2(t,z)$. It shows that transverse traceless modes show non-zero interaction with the condensate. In Fourier space, it is shown that the transverse modes draw energy from the condensate [38]. However, the transverse traceless modes have to be nonzero at $t = 0$ for them to evolve and absorb energy from condensate. What we are interested in is whether the GWs can generate fluctuations which then couple with condensate to evolve.

5.2.1 In the presence of Gravitational Waves

In this subsection, we will study the condensate + transverse traceless modes model in the presence of GWs. For studying the system in curved background, we start with writing the YM equation in general spacetime as follows [27]

$$\frac{1}{\sqrt{-g}}\partial_\mu\left(\sqrt{-g}g^{\mu\lambda}g^{\nu\rho}F^a_{\lambda\rho}\right)+g_{ym}\varepsilon^{abc}A^b_\mu F^{\mu\nu c}=0. \tag{5.14}$$

In the linearized approximation, we consider the metric to be $g_{\mu\nu}=\eta_{\mu\nu}+h_{\mu\nu}$ where $h_{\mu\nu}$ is the gravitational wave metric described in the previous chapters (Sec: 2.1.1). Using this metric, we expand the above equation by keeping GW-dependent terms on one side as follows

$$\begin{aligned}\eta^{\mu\lambda}\eta^{\nu\rho}\partial_\mu F^a_{\lambda\rho}+g_{ym}\varepsilon^{abc}A^b_\mu F^{\mu\nu c}=g_{ym}\varepsilon^{abc}A^b_\mu h^{\mu\lambda}\eta^{\nu\rho}F^c_{\lambda\rho}+g_{ym}\varepsilon^{abc}A^b_\mu h^{\nu\rho}\eta^{\mu\lambda}F^c_{\lambda\rho}\\ +\eta^{\nu\rho}\partial_\mu F^a_{\lambda\rho}h^{\mu\lambda}+\eta^{\mu\lambda}\partial_\mu(h^{\nu\rho}F^a_{\lambda\rho}).\end{aligned} \tag{5.15}$$

Using the same form of ansatz as in the previous section, the gauge field is given as

$$A^a_i=U(t)\delta^a_i+\delta^{aj}\tilde{A'}_{ji}, \tag{5.16}$$

where $\tilde{A'}_{ji}$ is the perturbation function due to the interaction of condensate and GW which is different from $\tilde{A}_{ji}$ in Eq. (5.7). In the linear-order approximation of both GW and fluctuations, the YM equation can be rewritten as

$$\begin{aligned}\Box\tilde{A'}_{ij}-\partial_k\partial_j\tilde{A}'_{ik}+g_{ym}U\left(2\varepsilon_{ikc}\partial_k\tilde{A'}_{cj}+\varepsilon_{ibj}\partial_k\tilde{A'}_{bk}+\varepsilon_{ibc}\partial_j\tilde{A'}_{bc}\right)\\ +g^2_{ym}U^2\left(\tilde{A'}_{ji}-\tilde{A'}_{ij}-2\tilde{A'}_{kk}\delta_{ij}\right)=-\partial_0(Uh_{ji})+g_{ym}U^2\varepsilon_{ikl}\partial_k h_{jl}-g^2_{ym}U^3h_{ji}.\end{aligned} \tag{5.17}$$

As we discussed before, only the symmetric transverse-traceless modes interact with GW. So, considering only those modes and + polarized GW propagating in the z-direction i.e.

$h_{ij} = e^{+}_{ij} h_{+}$, where e^{+}_{ij} is the polarisation vector of the GW with two non-zero values, $e^{+}_{11} = -e^{+}_{22} = 1$ and $h_{+}(t,z) = A_{+}\cos(\omega_g(t-z))$, the YM equation can be written as

$$\Box\Psi'_1 - 2g_{ym}U\partial_z\Psi'_2 = A_{+}(g^2_{ym}U^3\cos(\omega_g(t-z)) + \partial_0 U\, A_{+}\omega_g \sin(\omega_g(t-z)), \quad (5.18)$$

$$\Box\Psi'_2 + 2g_{ym}U\partial_z\Psi'_1 = -A_{+}g_{ym}\omega_g U^2 \sin(\omega_g(t-z)). \quad (5.19)$$

We solved these equations numerically using the same technique as in the previous section and the numerical solutions are shown in Figs. (5.5(a) & 5.5(b)).

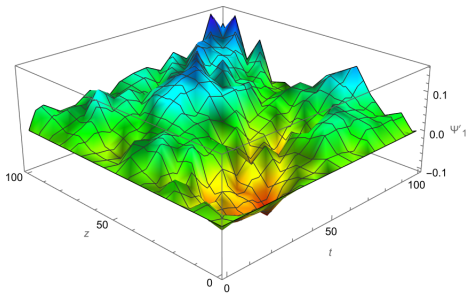

((a)) $\Psi'_1(t,z)$

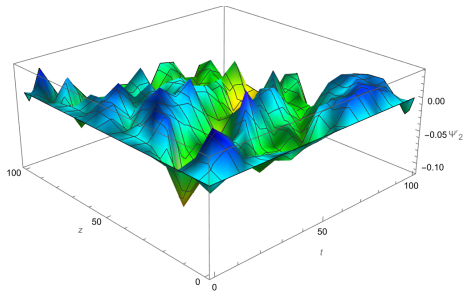

((b)) $\Psi'_2(t,z)$

Figure 5.5: Figures showing $\Psi'_1(t,z)$ and $\Psi'_2(t,z)$ in the presence of a gravitational wave. We choose $g_{ym} = 0.5$, $c_1 = c_2 = 1$, $A_{+} = 0.0001$, $\omega_g = 100$, $\Psi'_1(0,z) = \Psi'_1(t,0) = \Psi'_2(0,z) = \Psi'_2(t,0) = 0$ and $\partial_z\Psi'_1(t,0) = \partial_z\Psi'_2(t,0) = 0$.

Analytical solution

Apart from the numerical solutions, we also found the analytical solution for the perturbation function in terms of fluctuations in the absence of GWs. For this, we use the triad formalism introduced in [38] and rewrite the gauge field as

$$A^a_i = U(t)e^a_i + e^{aj}\tilde{A}_{ji}, \quad (5.20)$$

where e^a_i are soldering forms that connect the space-time metric to $SU(2)$ group manifold with following conditions:

$$e^a_i e_{aj} = g_{ij}; \qquad e^a_i e^i_b = \delta^a_b. \quad (5.21)$$

Now, the triad is chosen such that the metric represents GW background in flat spacetime. Using [195], we represent triads as

$$e_1^a = \left(\sqrt{(1+h_+(t,z))}, 0, 0\right), \tag{5.22a}$$

$$e_2^a = \left(0, \sqrt{(1-h_+(t,z))}, 0\right), \tag{5.22b}$$

$$e_3^a = (0,0,1)\,. \tag{5.22c}$$

Considering a binomial expansion of fractional powers and restricting only to first-order terms, the triads will be in the linear order of h_+. Using this and keeping the only terms in linear order in h_+ and $\tilde{A}_i^a$, one can write the gauge field as

$$A_i^a = U(t)\delta_i^a + \frac{1}{2}h_i^a U + \tilde{A}_i^a. \tag{5.23}$$

Comparing with Eq. (5.16), we get a solution for fluctuations with the GW part is

$$\tilde{A'}_i^a = \frac{1}{2}h_i^a U + \tilde{A}_i^a. \tag{5.24}$$

One can easily check that the above gauge field satisfied the Eq. (5.17) by removing all GW-dependent terms leaving with a differential equation for fluctuations without GW. In terms of Ψ_α and Ψ'_α, we get

$$\Psi'_\alpha = \Psi_\alpha + \frac{1}{4}Q_{ik}^\alpha h_{ik} U. \tag{5.25}$$

with explicit forms given by

$$\Psi'_1 = \Psi_1 + \frac{1}{2}h_+ U; \qquad \Psi'_2 = \Psi_2. \tag{5.26}$$

From the above solutions, one can see that the transverse modes can be generated from the interaction of GW with condensate even when they were zero at $t = 0$.

5.2.2 Higher order corrections

We extended the analysis to include the higher-order terms in transverse traceless modes, which means to include the interaction between different modes as well. Considering only the symmetric transverse traceless modes (Ψ_α), the Eqs. (5.12 & 5.13) changed to

$$\Box\Psi_1 - 2g_{ym}U\partial_z\Psi_2 - g_{ym}^2(\Psi_1^3 + \Psi_1\Psi_2^2) = 0, \tag{5.27}$$

$$\Box\Psi_2 + 2g_{ym}U\partial_z\Psi_1 - g_{ym}^2(\Psi_2^3 + \Psi_1^2\Psi_2) = 0. \tag{5.28}$$

The equations were solved numerically and plots are shown in Figs. (5.6(a) & 5.6(b)). Similarly, in the case of GW, the Eqs. (5.18 & 5.19) changes to

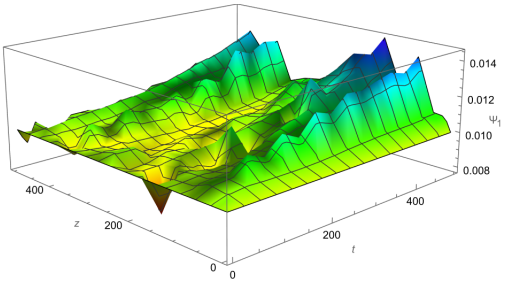

((a)) $\Psi_1(t,z)$

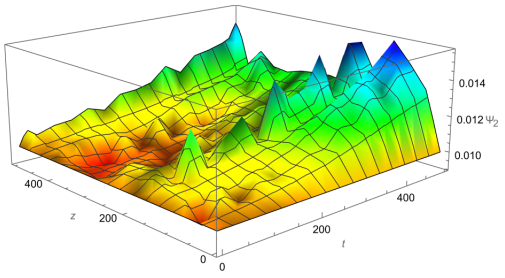

((b)) $\Psi_2(t,z)$

Figure 5.6: Figures showing $\Psi_1(t,z)$ and $\Psi_2(t,z)$ in the presence of condensate to all orders in the self-interactions in transverse-traceless modes. We choose $g_{ym} = 0.5$, $c_1 = c_2 = 1$, $\Psi_1(0,z) = \Psi_1(t,0) = \Psi_2(0,z) = \Psi_2(t,0) = 0.01$ and $\partial_z\Psi_1(t,0) = \partial_z\Psi_2(t,0) = 0$.

$$\Box\Psi_1' - 2g_{ym}U\partial_z\Psi_2' - g_{ym}^2({\Psi_1'}^3 + \Psi_1'{\Psi_2'}^2) = A_+(g_{ym}^2U^3\cos(\omega_g(t-z)) + \partial_0UA_+\omega_g\sin(\omega_g(t-z)), \tag{5.29}$$

$$\Box\Psi_2' + 2g_{ym}U\partial_z\Psi_1' - g_{ym}^2({\Psi_2'}^3 + {\Psi_1'}^2\Psi_2') = -A_+g_{ym}\omega_gU^2\sin(\omega_g(t-z)). \tag{5.30}$$

We solved these equations numerically using the same techniques which are shown in

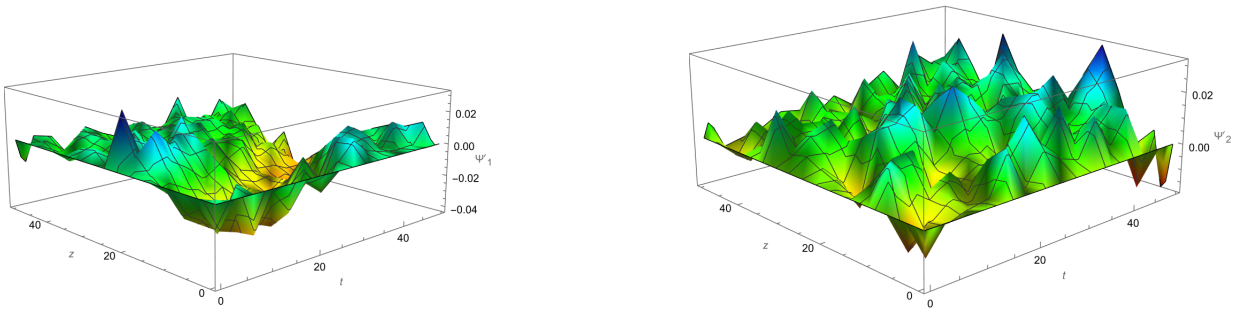

((a)) $\Psi_1'(t,z)$ ((b)) $\Psi_2'(t,z)$

Figure 5.7: Figures showing $\Psi_1'(t,z)$ and $\Psi_2'(t,z)$ in the presence of a gravitational wave and condensate to all orders in the self-interactions in transverse-traceless modes. We choose $g_{ym} = 0.5, c_1 = c_2 = 1, A_+ = 0.0001, \omega_g = 50, \Psi_1'(0,z) = \Psi_1'(t,0) = \Psi_2'(0,z) = \Psi_2'(t,0) = 0$ and $\partial_z\Psi_1'(t,0) = \partial_z\Psi_2'(t,0) = 0$.

Figs. (5.7(a) & 5.7(b)). It is very hard to find the analytical solutions as opposed to the previous section due to the presence of nonlinear terms. From the Figs. (5.6 & 5.7), we can see that there is a clear difference by including higher-order corrections. One can find that the magnitude of modes is higher at later times due to the interactions between the fluctuation modes even though the GW amplitude is low.

5.2.3 Summary

So far, we have considered only the transverse traceless modes and their interaction with GW. Authors in [38] found that there is a net energy swap effect from condensate to the wave modes. We found that the transverse modes can be generated due to the interaction between condensate and GW even if they were zero initially. This illustrates that the GW can induce the condensate to decay into transverse modes. And then due to interactions between condensate and modes, there will be a net energy transfer effect from condensate to fluctuations. However, the splitting of the gauge field as in [38] shows that the GW does not interact with longitudinal modes. To include the longitudinal modes in the discussion, we consider a different ansatz by splitting the gauge field into transverse and longitudinal vector modes (and not tensor) using a different decomposition in the next section.

5.3 Condensate + Fluctuations (Vector Decomposition)

As discussed at the end of the previous section, we consider a different decomposition of the YM gauge field other than what is used in [38]. We consider the vector decomposition of fluctuations around the condensate. In this way, we can avoid the use of triads which are useful in defining gauge invariant fluctuations, but not so much in identifying the longitudinal and transverse modes. Thus, we use the following form of ansatz in Hamilton's gauge:

$$A_i^a(t,\mathbf{x}) = U(t)\delta_i^a + n_i\Phi^a(t,\mathbf{x}) + \varepsilon_{ijk}n_j s_k^\sigma \chi_\sigma^a(t,\mathbf{x}). \tag{5.31}$$

In the above ansatz, Φ^a are the longitudinal modes for a wave propagating in the n_i direction. Since a can be $1,2,3$, we have three Φ^a 'plasmon' fields. The χ_σ^a modes represent the transverse modes to $\mathbf{n}$. As there are two transverse directions to $\mathbf{n}$ which are obtained using two arbitrary vectors $\mathbf{s}^\sigma$ such that the $\mathbf{n}\times\mathbf{s}^\sigma$ always form a vector perpendicular to $\mathbf{n}$. At an initial glance the number of degrees of freedom, we find there are 10: $U(t)\to 1, \Phi^a \to 3, \chi_\sigma^a \to 6$. However, the condensate cannot be identified as a longitudinal or transverse mode component. It is isolated as the trace of the gauge field, $A_i^i = 3U(t)$. One has to impose constraints on longitudinal and transverse modes such these modes will not give a contribution to the trace of the gauge field (and therefore are independent of $U(t)$). In other words the condensate is a non-propagating mode (no space dependence), and therefore we don't categorize it as a longitudinal or transverse mode.

$$\mathbf{n}\cdot\mathbf{\Phi} = 0, \tag{5.32}$$

$$(\mathbf{n}\times\mathbf{s}^\sigma)\cdot\boldsymbol{\chi}_\sigma = 0. \tag{5.33}$$

The above constraints reduce two degrees of freedom, one for Φ^a and one for χ_σ^a. Also, to remove the transverse modes along the propagating direction $\mathbf{n}$, we impose another constraint as

$$\mathbf{n}\cdot\boldsymbol{\chi}_\sigma = 0. \tag{5.34}$$

Since $\sigma = 1,2$, this constraint reduces another 2 degrees of freedom. With that, the total degrees of freedom of the gauge field becomes 6: $U(t) \to 1, \Phi^a \to 2, \chi^a_\sigma \to 3$. Thus, requiring an isotropic independent condensate reduces the number of degrees of freedom of the YM gauge field to 6. The constraints $\mathbf{n}\cdot\mathbf{\Phi} = 0$ and $\mathbf{n}\cdot\chi_\sigma = 0$ are required to decouple the kinetic terms for wave fluctuations.

Next, considering the YM wave propagates in the z-direction i.e. $\mathbf{n} = (0,0,1)$; $\mathbf{s}^1 = (1,0,0)$, $\mathbf{s}^2 = (0,1,0)$ and taking $\chi^2_1 = \chi^1_2 = 0$ (this is a specific solution choice), we derived the equations of motion for $U(t)$, $\Phi^1 = \Phi_1, \Phi^2 = \Phi_2$, $\chi^1_1 = \chi_1$ and $\chi^2_2 = \chi_2$.

$$\partial_0^2 U - \frac{2g_{ym}}{3} U \partial_z(\chi_1+\chi_2) + g_{ym}^2\Big[2U^3 + \frac{1}{3}U(\Phi_1^2+\Phi_2^2) + \frac{1}{3}U(\chi_1+\chi_2)^2 - \frac{1}{3}(\chi_1-\chi_2)\Phi_1\Phi_2\Big] = 0, \tag{5.35}$$

$$\partial_0^2\Phi_1 + g_{ym}^2\Big[U^2\Phi_1 - U(\chi_1-\chi_2)\Phi_2 + \Phi_1\chi_2^2\Big] = 0, \tag{5.36}$$

$$\partial_0^2\Phi_2 + g_{ym}^2\Big[U^2\Phi_2 - U(\chi_1-\chi_2)\Phi_1 + \Phi_2\chi_1^2\Big] = 0, \tag{5.37}$$

$$\Box\chi_1 + g_{ym}^2\Big[U\Phi_1\Phi_2 - U^2(\chi_1+\chi_2) - \chi_1\chi_2^2 - \Phi_2^2\chi_1\Big] = 0, \tag{5.38}$$

$$\Box\chi_2 - g_{ym}^2\Big[U\Phi_1\Phi_2 + U^2(\chi_1+\chi_2) + \chi_1^2\chi_2 + \Phi_1^2\chi_2\Big] = 0. \tag{5.39}$$

The details regarding the derivation of equations of motion from Lagrangian using the above ansatz are given in Appendix D.4. Note that the Gauss constraint is automatically satisfied with the solutions from the above equations. As there are no space derivatives for Φ_1 and Φ_2, we can set them to be functions of time only without losing any dynamical information. All the space-dependent dynamics is present in transverse modes. As a first approximation, we consider all the modes to be functions of time only. This allows us to study the exchange of energy between condensate and wave modes to all order in a clean way.

We solved the above equations by considering modes to be functions of time, numerically using Mathematica, and are shown in Fig. (5.8). At zero-order, we already found the solution to be $U(t) = c_1\,\mathrm{sn}(g_{ym}c_1(t+c_2),-1)$ in Eq. (5.5). The time period of this

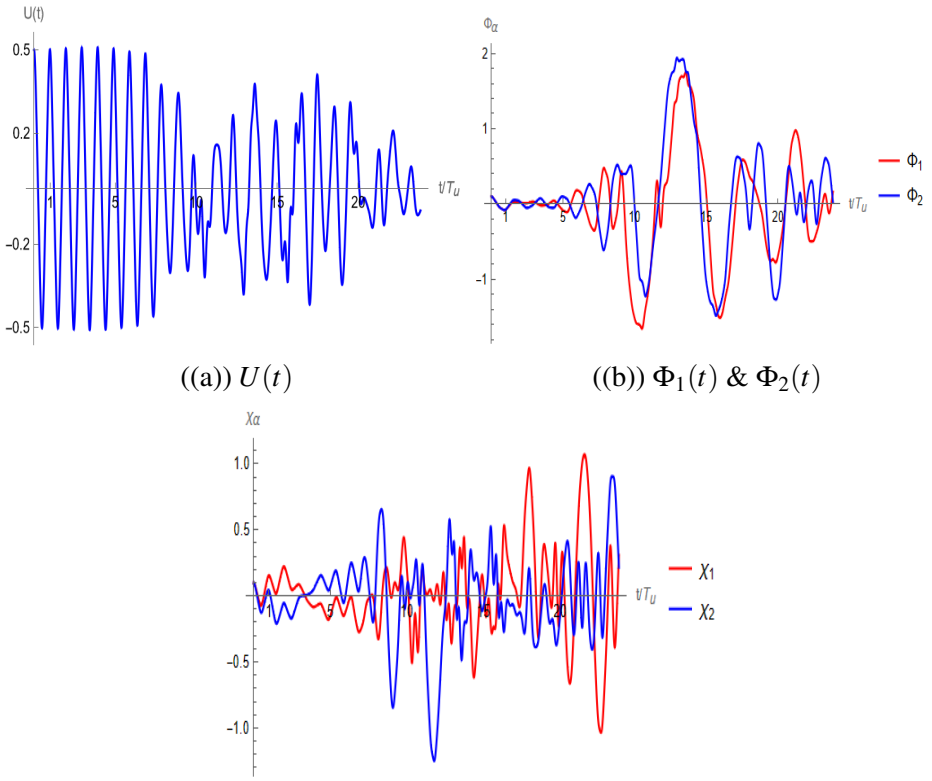

((a)) $U(t)$ ((b)) $\Phi_1(t)$ & $\Phi_2(t)$

((c)) $\chi_1(t)$ & $\chi_2(t)$

Figure 5.8: Figures showing U, Φ_1, Φ_2, χ_1 and χ_2 as a function of time. We choose $g_{ym} = 0.5$, $U(0) = 0.5$, $\Phi_1(0) = 0.1$, $\Phi_2(0) = 0.1$, $\chi_1(0) = 0.1$, $\chi_2(0) = 0.1$, $\dot{U}(0) = 0$, $\dot{\Phi}_1(0) = 0$, $\dot{\Phi}_2(0) = 0$, $\dot{\chi}_1(0) = 0$ and $\dot{\chi}_2(0) = 0$, where $\dot{} \equiv d/dt$.

unperturbed solution is given by $T_u = (4K(-1))/(g_{ym}U(0))$, where $K(-1)$ is the Complete elliptic integral of first kind. To keep all the information of the Jacobi function in c_1, we choose the initial conditions such that $U(0) = c_1$ and $U'(0) = 0$ which gives the $c_2 = K(-1)/(g_{ym}c_1)$. Then, the time period of unperturbed condensate solution is $T_u = (4K(-1))/(g_{ym}U(0))$. The plots are given in terms of this time period, t/T_u. From Fig. (5.8(a)), it is found that the amplitude of condensate starts decreasing only after a certain amount of time, and then it increases again. In the quantum scenario, this late decay of condensate is related to the stability of the vacuum expectation value of the condensate [196]. From now on, we call the time at which the condensate decay starts as delay decay time (T_0). This delay decay time is around 10 in terms of T_u. As T_u depends on g_{ym} and c_1, the delay decay time always happens at the same time even for different initial conditions.

One can see from the Eqs. (5.36) & (5.37) that the Φ_1 and Φ_2 have the same functional behaviour which is also shown in Fig. (5.8(b)). The only difference in those differential equations (Eqs.(5.36 & 5.37)) is different dependence on transverse modes. One can see from Eqs. (5.38 & 5.39) that the transverse modes' differential equations differ from one another with signs that result in complementary behaviour of these functions as shown in Fig. (5.8(c)). From comparing the plots of longitudinal and transverse modes (Fig. 5.8), we see that the longitudinal modes reach higher magnitudes much quicker than the transverse modes. This is due to the quadratic nature of the potential terms.

Since the Eqs. (5.38 & 5.39) are coupled, it is clear that either one of the transverse modes will be generated even if the other mode is zero initially. Also, from Eqs. (5.38 & 5.39), there is a term devoid of transverse mode, $g_{ym}^2 U\Phi_1\Phi_2$ which generates transverse modes even if they were zero as long as the condensate and longitudinal modes are nonzero. From Eqs. (5.36 & 5.37), it can be found that the longitudinal modes can also be generated by condensate alone which is due to the self-interaction of YM fields.

Dependence on other factors

By changing the initial condensate value ($U(t=0)$) or YM coupling constant (g_{ym}), it is found that the delay decay time is also changing. To see this, we change the time axis from t/T_u to time (t), and the plots are shown in Fig. (5.9). One can see the dependence of the initial condensate value and coupling constant from the time period expression of unperturbed condensate value ($T_u = (4K(-1))/(g_{ym}U(0))$). If we keep increasing the initial value of condensate while keeping the coupling constant the same, the delay decay time decreases. If we keep the initial value of condensate to be constant while increasing the coupling constant, then also the delay decay time decreases.

Energy analysis

To discuss the energy exchange, we construct the Hamiltonian density ($\mathcal{H}$) of $SU(2)$ YM system as the sum of individual contributions from the condensate ($\mathcal{H}_u$), particles/

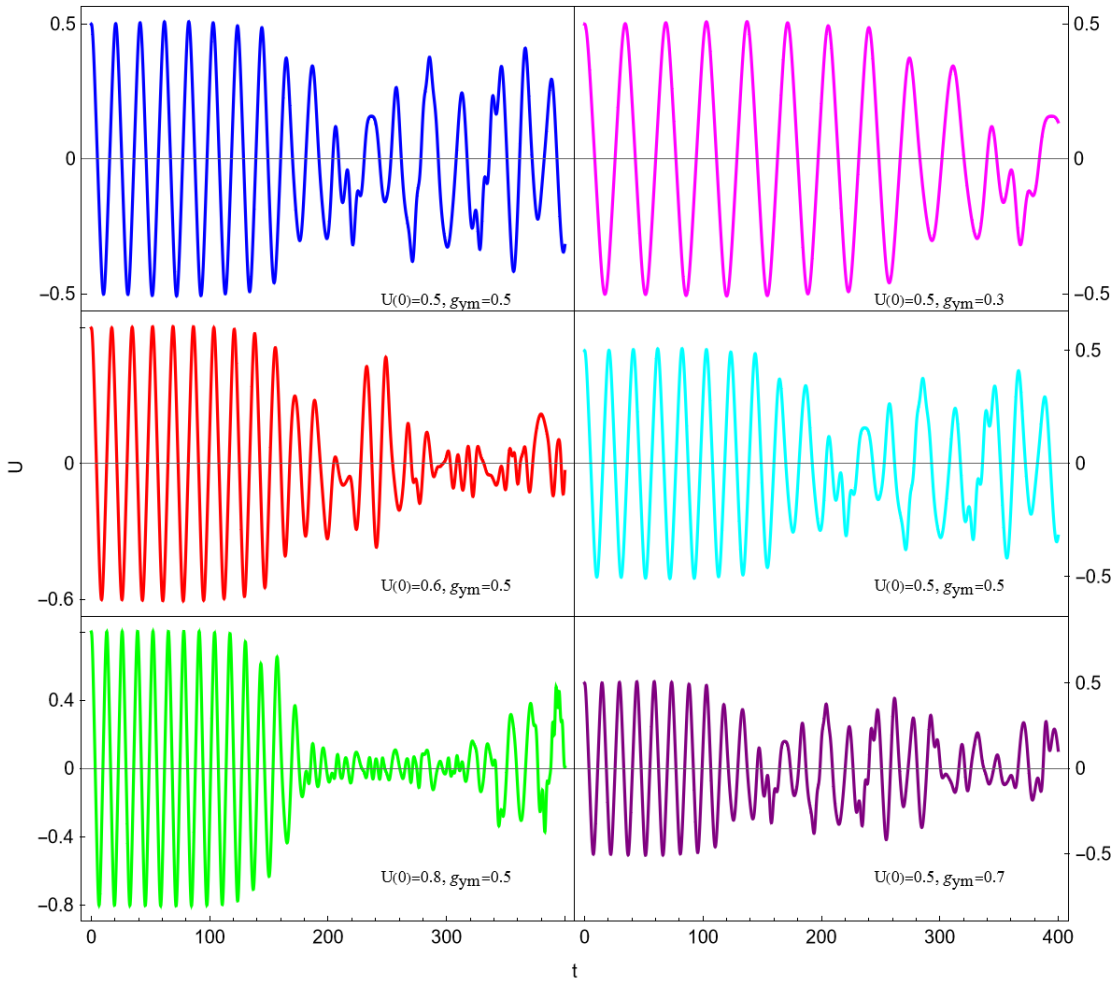

Figure 5.9: U for different initial conditions and different coupling constants. We choose $\Phi_1(0) = 0.1$, $\Phi_2(0) = 0.1$,$\chi_1(0) = 0.1$, $\chi_2(0) = 0.1$, $\dot{\Phi}_1(0) = 0$, $\dot{\Phi}_2(0) = 0$, $\dot{U}(0) = 0$, $\dot{\chi}_1(0) = 0$ and $\dot{\chi}_2(0) = 0$.

modes ($\mathcal{H}_p$), and the interaction term ($\mathcal{H}_{int}$) as follows:

$$\mathcal{H} = \mathcal{H}_u + \mathcal{H}_p + \mathcal{H}_{int}, \tag{5.40}$$

where

$$\mathcal{H}_u = \frac{3}{2}(\partial_t U \partial_t U + g_{ym}^2 U^4), \tag{5.41}$$

$$\mathcal{H}_p = \frac{1}{2}\left((\partial_t \Phi_1)^2 + (\partial_t \Phi_2)^2 + (\partial_t \chi_1)^2 + (\partial_t \chi_2)^2 + g_{ym}^2 \chi_1^2 \chi_2^2\right), \tag{5.42}$$

$$\mathcal{H}_{int} = \frac{1}{2} g_{ym}^2 \left[U^2\left(\Phi_1^2 + \Phi_2^2 + \chi_1^2 + \chi_2^2\right) + \Phi_1^2 \chi_2^2 + \Phi_2^2 \chi_1^2 + 2U^2 \chi_1 \chi_2 - 2U \Phi_1 \Phi_2 (\chi_1 - \chi_2)\right]. \tag{5.43}$$

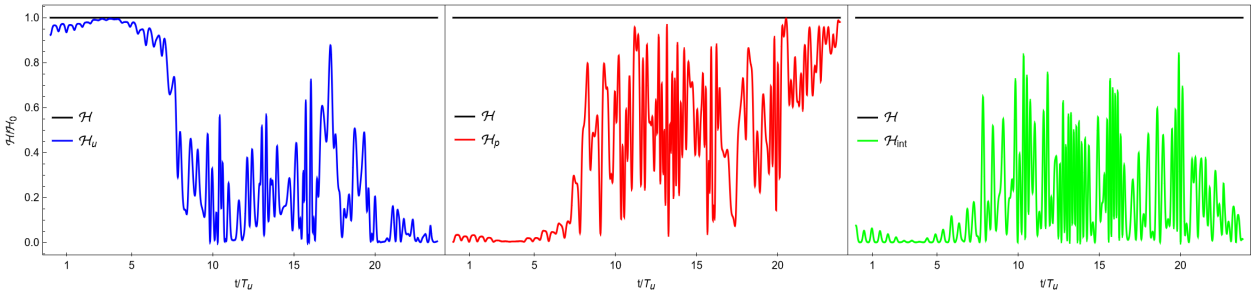

Figure 5.10: Figure showing the contributions of the condensate $\mathcal{H}_u(t)$, YM wave modes $\mathcal{H}_p(t)$ and interaction terms $\mathcal{H}_{int}(t)$ to the total energy $\mathcal{H}(t)$. We use the same initial conditions as in Fig. (5.8).

From the Figs. (5.10), it is clear that there was an exchange of energy between condensate and particles during early times. The energy swap was initially predicted in [38] and was found to be delayed by delay decay time (T_0) in our case as shown in Fig. (5.10). We also found that the total energy of the system seems to increase after a certain time as shown in Fig. (5.11). This could be due to numerical artefact and is still under investigation [44].

The vector decomposition that we did is different than that in [38] as they did the tensor decomposition of the gauge field into symmetric and antisymmetric components. In our vector decomposition, this split into symmetric and anti-symmetric components is not there.

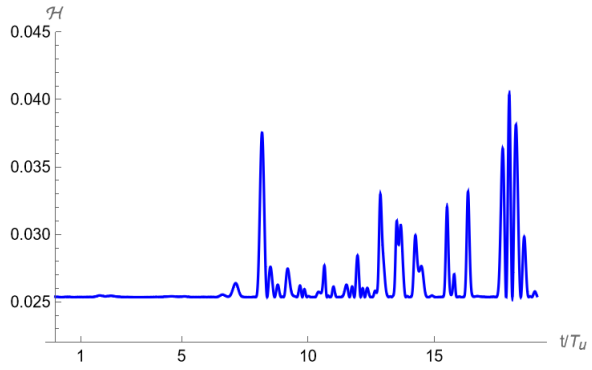

Figure 5.11: Figure showing the total energy $\mathcal{H}(t)$ as a function of time.

We have simply the identification of the vector longitudinal and transverse modes. One of the advantages of our decomposition is that it identifies the relevant longitudinal and transverse modes very easily. As the energy density is gauge invariant, our analysis using vector decomposition is valid for the energy analysis.

5.3.1 In the presence of Gravitational Waves

Now, we will study the above-discussed system in the background of GWs. Consider a $+$- polarised GW propagating in the z-direction, then the flat spacetime metric is changed to

$$g_{\mu\nu} = \eta_{\mu\nu} + h_{\mu\nu}, \tag{5.44}$$

where $\eta_{\mu\nu}$ is the flat spacetime metric and the only nonzero components for $h_{\mu\nu}$ are $h_{11} = h_+ = A_+\cos(\omega_g(t-z))$, and $h_{22} = -h_+$. Consider the same ansatz as in the previous section as

$$A^a_i(t,\mathbf{x}) = U(t)\delta^a_i + n_i\Phi^a(t,\mathbf{x}) + \varepsilon_{ijk}n_j s^\sigma_k \chi^a_\sigma(t,\mathbf{x}). \tag{5.45}$$

Using the GW perturbed metric and above ansatz (Eq. 5.45) in the Lagrangian and then varying the Lagrangian, we get the equations of motion as follows:

$$\partial_0^2 U - \frac{2g_{ym}}{3}U(\partial_z(\chi_1+\chi_2) + h_+\partial_z(\chi_1-\chi_2)) + g_{ym}^2\Big[2U^3 + \frac{1}{3}U(\Phi_1^2+\Phi_2^2) + \frac{1}{3}U(\chi_1+\chi_2)^2 - \frac{1}{3}(\chi_1-\chi_2)\Phi_1\Phi_2\Big] - \frac{g_{ym}^2 h_+}{3}\left[U\left(\chi_2^2-\chi_1^2+\Phi_2^2-\Phi_1^2\right)\right.$$

$$+\Phi_1\Phi_2(\chi_1+\chi_2)]=0, \quad (5.46)$$

$$\partial_0^2\Phi_1+g_{ym}^2\Big[U^2\Phi_1-U(\chi_1-\chi_2)\Phi_2+\Phi_1\chi_2^2\Big]-g_{ym}^2h_+\left[\chi_2^2\Phi_1-U^2\Phi_1+\Phi_2(\chi_1+\chi_2)U\right]=0, \quad (5.47)$$

$$\partial_0^2\Phi_2+g_{ym}^2\Big[U^2\Phi_2-U(\chi_1-\chi_2)\Phi_1+\Phi_2\chi_1^2\Big]-g_{ym}^2h_+\left[-\chi_1^2\Phi_2+U^2\Phi_2+\Phi_1(\chi_1+\chi_2)U\right]=0, \quad (5.48)$$

$$\Box\chi_1+h_+\Box\chi_1-\partial_th_+\partial_t\chi_1+\partial_zh_+\partial_z\chi_1-g_{ym}U^2\partial_zh_++g_{ym}^2\Big[U\Phi_1\Phi_2-U^2(\chi_1+\chi_2) -\chi_1\chi_2^2+\Phi_2^2\chi_1\Big]+g_{ym}^2h_+\left[-\chi_1\Phi_2^2-U^2\chi_1+\Phi_1\Phi_2U\right]=0, \quad (5.49)$$

$$\Box\chi_2-h_+\Box\chi_2+\partial_th_+\partial_t\chi_2-\partial_zh_+\partial_z\chi_2+g_{ym}U^2\partial_zh_+-g_{ym}^2\Big[U\Phi_1\Phi_2+U^2(\chi_1+\chi_2) +\chi_1^2\chi_2+\Phi_1^2\chi_2\Big]+g_{ym}^2h_+\left[\chi_2\Phi_1^2+U^2\chi_2+\Phi_1\Phi_2U\right]=0. \quad (5.50)$$

The details regarding the derivation of equations of motion is given in Appendix D.4. As a first approximation and to compare the solutions with those of the previous section, we set $z=0$ and solve the above equations numerically using Mathematica by considering the modes as functions of time only (Fig. (5.12)). To show the dependence of GWs, we plotted $U(t)$ with and without GWs in Fig. (5.13(a)). There is a change in the solutions of $U(t)$ in the presence of a GW. To show the impact of the strength of GWs on solutions, we plotted $U(t)$ for two different A_+ values of GW in Fig. (5.13(b)). For GW amplitudes of magnitude much smaller than the condensate (and fluctuation's) magnitude, the solutions approach the condensate solution (Blue plot in Fig. (5.13(b))) in the absence of GW. We also find that the GW makes the solutions stable for longer times delaying the condensate decay. This is observed in Fig. (5.13(b)) where the Blue plot approaches the free condensate solution (see Sec: 5.1).

There are terms like $g_{ym}U^2\partial_zh_+$ that do not depend on any other modes, giving rise to

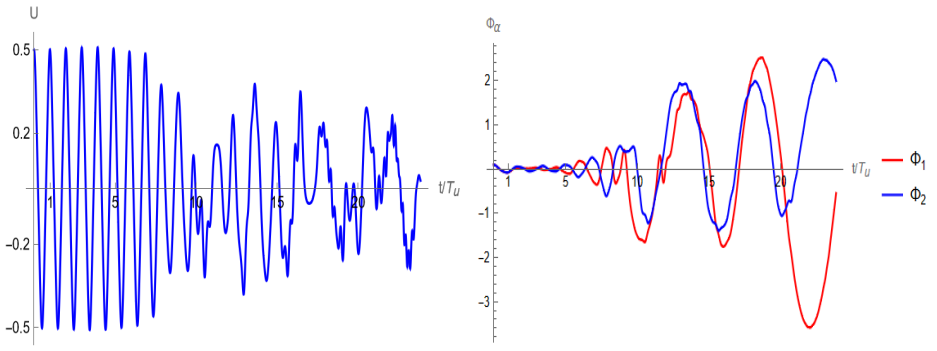

((a)) $U(t)$ ((b)) $\Phi_1(t)$ & $\Phi_2(t)$

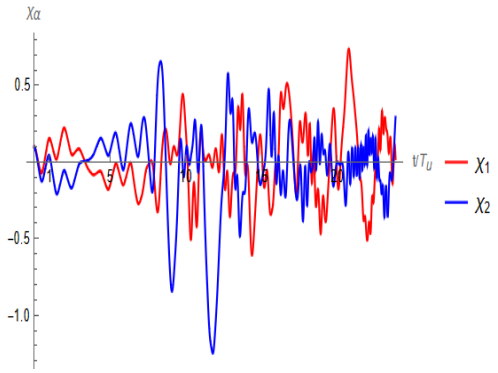

((c)) $\chi_1(t)$ & $\chi_2(t)$

Figure 5.12: Figures showing U, Φ_1, Φ_2, χ_1, and χ_2 as a function of time in the presence of a gravitational wave. We choose $g_{ym} = 0.5$, $A_+ = 0.01$, $\omega_g = 100$, $U(0) = 0.5$, $\Phi_1(0) = 0.1$, $\Phi_2(0) = 0.1$, $\chi_1(0) = 0.1$, $\chi_2(0) = 0.1$, $\dot{U}(0) = 0$, $\dot{\Phi}_1(0) = 0$, $\dot{\Phi}_2(0) = 0$, $\dot{\chi}_1(0) = 0$ and $\dot{\chi}_2(0) = 0$.

the generation of transverse wave modes just from the interaction between condensate and GW. We conclude that the GW initiates the decay of the condensate into fluctuations. From the generated transverse modes, longitudinal modes will be produced due to the non-linear interactions between them. This conclusion was the same as in the previous section.

Energy analysis

To study the energy exchange between the condensate and particles, we construct the Hamiltonian density ($\mathcal{H}_{GW}$) in the presence of GWs as follows

$$\mathcal{H}_{GW} = \mathcal{H}_{uGW} + \mathcal{H}_{pGW} + \mathcal{H}_{intGW}, \text{ where} \tag{5.51}$$

$$\mathcal{H}_{uGW} = \frac{3}{2}(\partial_t U \partial_t U + g_{ym}^2 U^4), \tag{5.52}$$

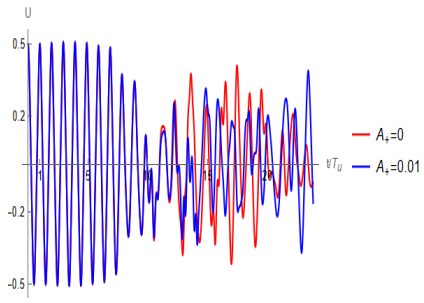

((a)) $U(t)$ without and with GW case

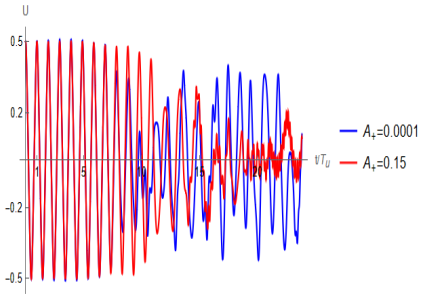

((b)) $U(t)$ with different GW amplitudes

Figure 5.13: Condensate $U(t)$ in different scenarios. We choose the other initial conditions as same as in Fig. (5.12).

$$\mathcal{H}_{pGW} = \frac{1}{2}\left((\partial_t\Phi_1)^2+(\partial_t\Phi_2)^2+(\partial_t\chi_1)^2+(\partial_t\chi_2)^2+g_{ym}^2\chi_1^2\chi_2^2\right), \tag{5.53}$$

$$\begin{aligned}\mathcal{H}_{intGW} = \frac{1}{2}g_{ym}^2\big[&U^2\left(\Phi_1^2+\Phi_2^2+\chi_1^2+\chi_2^2\right)+h_+\left(\Phi_1^2-\Phi_2^2+\chi_1^2-\chi_2^2\right)\\ &+(1-h_+)\Phi_1^2\chi_2^2+(1+h_+)\Phi_2^2\chi_1^2+2U^2\chi_1\chi_2\\ &-2U\Phi_1\Phi_2((1+h_+)\chi_1-(1-h_+)\chi_2)\big]+\frac{1}{2}h_+\left((\partial_t\chi_1)^2-(\partial_t\chi_2)^2\right).\end{aligned} \tag{5.54}$$

where $\mathcal{H}_{uGW}$,$\mathcal{H}_{pGW}$, and $\mathcal{H}_{intGW}$ are the contributions from the condensate, particles, and interaction terms, respectively. We obtained the same energy swap effect as in the previous section (Fig. (5.14)). Since the GW's amplitude is very tiny, the effect of GWs on modes energy is also small. But if we take the GW's amplitude to be high or comparable to that of modes or condensate, then GW stabilizes the condensate and the energy swap effect happens at a later time (Fig. (5.15)). For the blue plot in Fig. 5.15(a), the condensate decay is happening just after $10T_u$ as for the red plot, it is happening at around $15T_u$. This can be understood in the following way: The interaction potential energy changes in the presence of GWs. We included the interaction potential energy plot with and without the GWs in Fig. (5.16). Around the origin, the potential shows almost parabolic behaviour without the GWs. However, that behaviour changes in the presence of GW. As the χ fields take higher values, the potential shows almost the same behaviour as that without GW.

A. Solving in t and z (Linearized Approximation)

As of now, we studied the entire system by suppressing the z-dependence of the GW.

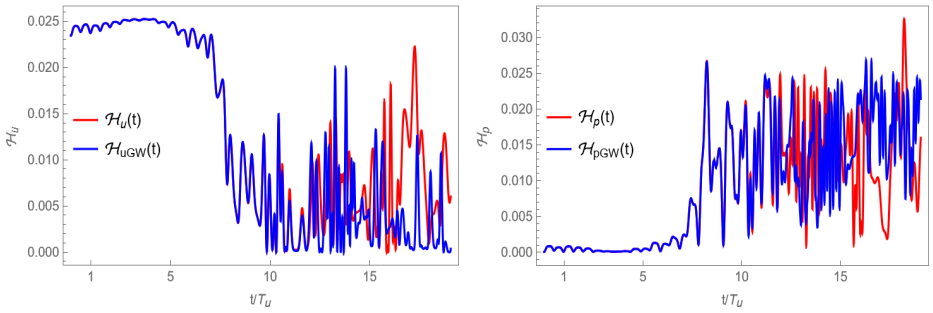

Figure 5.14: Figure showing energy density of condensate ($\mathcal{H}_u$) and particles/modes ($\mathcal{H}_p$) with and without GW cases. We choose $A_+ = 0.01$, $\omega_g = 10$ and same initial conditions as used in Fig. (5.12).

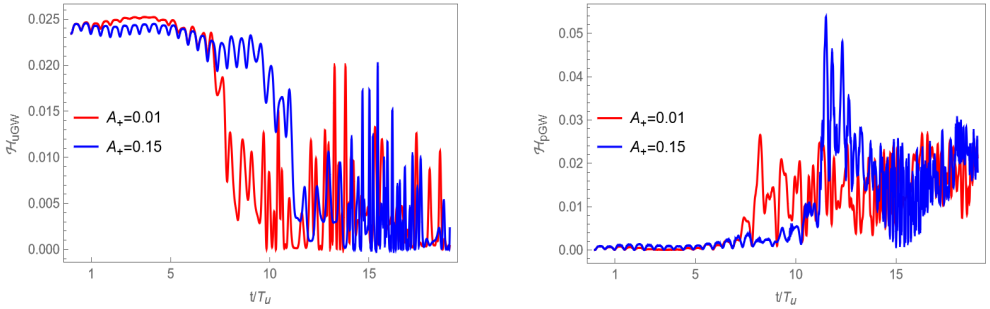

((a)) Energy density of condensate ($\mathcal{H}_{uGW}$) ((b)) Energy density of the particles $\mathcal{H}_{pGW}$

Figure 5.15: Figures showing the impact of high magnitude and high-frequency GWs on condensate decay. We choose the same initial conditions as in Fig. (5.12).

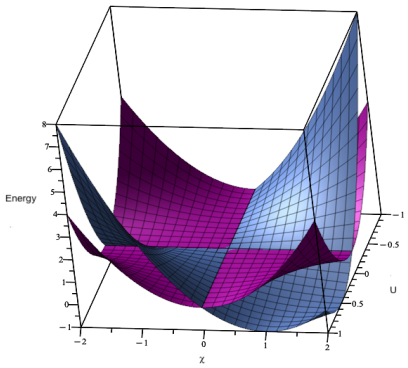

Figure 5.16: Schematic plot of interaction potential without GW (maroon) and potential with GW (azure), $A_+ = 0.0001$. In here the potential without GW is $U^2\chi^2$, where $\chi = \chi_1 + \chi_2$, and with the GW it is of the form $U^2\chi^2 - 2(0.0001)U\chi$. Note we have plotted only the terms that have U, χ in them.

To study the system with z-dependence, we first consider the reduced system (U,χ_1,χ_2) by assuming no longitudinal modes ($\Phi_1=\Phi_2=0$). Note that if we assume this reduced system without GW, we find that there is an interaction between condensate and fluctuations, but not an energy swap effect from condensate to modes. This tells us that the energy swap effect happens only in the presence of longitudinal modes.

Coming back to our reduced system and consider a perturbation in these modes as follows

$$U(t)\to U(t)+\tilde{U}(t,z), \tag{5.55}$$

$$\chi_1(t)\to\chi_1(t)+\tilde{\chi}_1(t,z), \tag{5.56}$$

$$\chi_2(t)\to\chi_2(t)+\tilde{\chi}_2(t,z), \tag{5.57}$$

where terms with $\tilde{}$ correspond to perturbation functions and the bare terms correspond to solutions of Eqs. (5.35, 5.38, 5.39) without longitudinal modes (Φ_1,Φ_2). When the condensate fluctuates to a propagating mode, it can be interpreted as longitudinal. In the linear-order approximation in h_+ and perturbations, the equations of motion become

$$\begin{aligned}-3\partial_t^2\tilde{U}+2\partial_z^2\tilde{U}+3g_{ym}U(\partial_z\tilde{\chi}_1+\partial_z\tilde{\chi}_2)+g_{ym}^2\Big[\tilde{U}(-18U^2-\chi_1^2-\chi_2^2)-2\tilde{U}\chi_1\chi_2\\ -2U(\chi_1+\chi_2)(\tilde{\chi}_1+\tilde{\chi}_2)\Big]-g_{ym}U(\chi_1-\chi_2)\partial_z h_+-g^2h_+U(\chi_2^2-\chi_1^2)=0,\end{aligned} \tag{5.58}$$

$$\begin{aligned}\Box\tilde{\chi}_1-3g_{ym}U\partial_z\tilde{U}-g_{ym}^2\Big[U^2(\tilde{\chi}_1+\tilde{\chi}_2)+2U\tilde{U}(\chi_1+\chi_2)+\tilde{\chi}_1\chi_2^2+2\chi_1\chi_2\tilde{\chi}_2\Big]\\ -\partial_t\chi_1\partial_t h_+-h_+\partial_t^2\chi_1-g_{ym}U^2\partial_z h_+-g_{ym}^2h_+U^2\chi_1=0,\end{aligned} \tag{5.59}$$

$$\begin{aligned}\Box\tilde{\chi}_2-3g_{ym}U\partial_z\tilde{U}-g_{ym}^2\Big[U^2(\tilde{\chi}_1+\tilde{\chi}_2)+2U\tilde{U}(\chi_1+\chi_2)+\tilde{\chi}_2\chi_1^2+2\chi_1\chi_2\tilde{\chi}_1\Big]\\ +\partial_t\chi_2\partial_t h_++h_+\partial_t^2\chi_2+g_{ym}U^2\partial_z h_++g_{ym}^2h_+U^2\chi_2=0.\end{aligned} \tag{5.60}$$

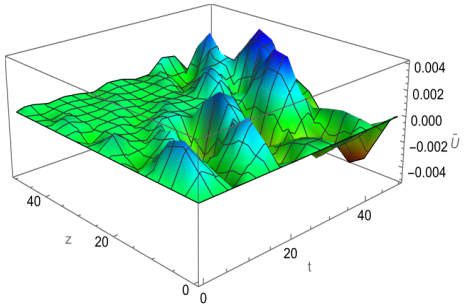

((a)) $\tilde{U}(t,z)$

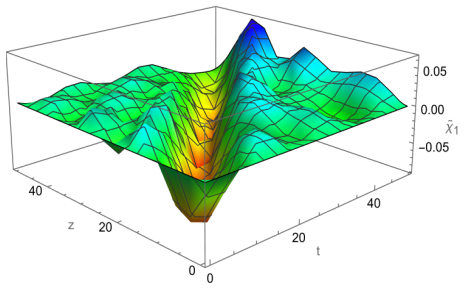

((b)) $\tilde{\chi}_1(t,z)$

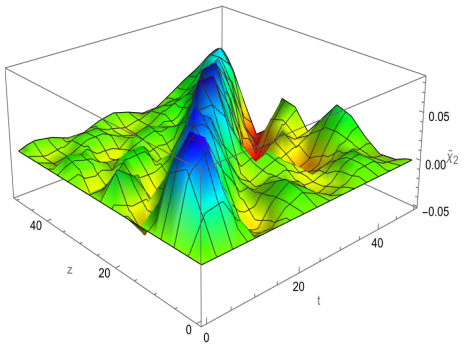

((c)) $\tilde{\chi}_2(t,z)$

Figure 5.17: Figures showing $\tilde{U}(t,z)$, $\tilde{\chi}_1(t,z)$ and $\tilde{\chi}_2(t,z)$ as a function of time and space in the presence of a gravitational wave. We choose $g_{ym} = 0.5$, $A_+ = 0.1$, $\omega_g = 100$, $U(0) = 1$, $\chi_1(0) = 0.1$, $\chi_2(0) = 0.2$, $\chi_1'(0) = 0$, $\chi_2'(0) = 0$, $\tilde{U}(t,0) = \tilde{U}(0,z) = 0$, $\tilde{\chi}_1(t,0) = \tilde{\chi}_1(0,z) = 0$, $\tilde{\chi}_2(t,0) = \tilde{\chi}_2(0,z) = 0$, $\partial_t\tilde{U}(0,z) = \partial_z\tilde{U}(t,0) = 0$, $\partial_t\tilde{\chi}_1(0,z) = \partial_z\tilde{\chi}_1(t,0) = 0$ and $\partial_t\tilde{\chi}_2(0,z) = \partial_z\tilde{\chi}_2(t,0) = 0$.

We solved the above equations numerically and the plots are shown in Fig. (5.17). From Fig. (5.17(a)), we can see that the perturbation in U is very small during early times as agreeable with the exact solution (Fig. 5.13). One can see that the magnitude of unperturbed condensate ($O(1)$) is much greater than the magnitude of perturbed condensate solution ($O(10^{-3})$). We also find that the condensate loses its homogeneity and isotropic nature and gets perturbed due to GW.

(i) Energy Analysis

To study the energy exchange, we construct the Hamiltonian density ($\mathcal{H}$), up to second-order terms, as follows:

$$\mathcal{H} = \mathcal{H}' + \mathcal{H}'' + \mathcal{H}''', \text{ where} \tag{5.61}$$

$$\mathcal{H}' = \frac{3}{2}\left[(\partial_t U)^2 + g_{ym}^2 U^4\right] + \frac{1}{2}\left[(\partial_t \chi_1)^2 + (\partial_t \chi_2)^2 + g_{ym}^2 \chi_1^2 \chi_2^2\right] + \frac{1}{2} g_{ym}^2 U^2 (\chi_1 + \chi_2)^2, \tag{5.62}$$

$$\begin{aligned}\mathcal{H}'' = {} & 3\partial_t U \partial_t \tilde{U} + \partial_t \chi_1 \partial_t \tilde{\chi}_1 + \partial_t \chi_2 \partial_t \tilde{\chi}_2 + g_{ym}\left[2U\partial_z \tilde{U}(\chi_1 + \chi_2) - 2U^2(\partial_z \tilde{\chi}_1 + \partial_z \tilde{\chi}_2)\right] \\ & + g_{ym}^2\left[6U^3\tilde{U} + U^2(\chi_1 + \chi_2)(\tilde{\chi}_1 + \tilde{\chi}_2) + U\tilde{U}(\chi_1 + \chi_2)^2 + \chi_1 \chi_2^2 \tilde{\chi}_1\right] \\ & + \frac{1}{2} h_+ ((\partial_t \chi_1)^2 - (\partial_t \chi_2)^2) + \frac{1}{2} g_{ym}^2 h_+ U^2 (\chi_1^2 - \chi_2^2),\end{aligned} \tag{5.63}$$

$$\begin{aligned}\mathcal{H}''' = {} & \frac{3}{2}(\partial_t \tilde{U})^2 + (\partial_z \tilde{U})^2 + \frac{1}{2}\left[(\partial_t \tilde{\chi}_1)^2 + (\partial_z \tilde{\chi}_1)^2 + (\partial_t \tilde{\chi}_2)^2 + (\partial_z \tilde{\chi}_2)^2\right] + g_{ym}\left[\tilde{U}\partial_z \tilde{U}(\chi_1 + \chi_2)\right. \\ & \left. + U\partial_z \tilde{U}(\tilde{\chi}_1 + \tilde{\chi}_2) - 4U\tilde{U}(\partial_z \tilde{\chi}_1 + \partial_z \tilde{\chi}_2)\right] + \frac{1}{2} g_{ym}^2 \left[18U^2\tilde{U}^2 + \tilde{U}^2(\chi_1 + \chi_2)^2\right. \\ & \left. + 4U\tilde{U}(\chi_1 + \chi_2)(\tilde{\chi}_1 + \tilde{\chi}_2) + U^2(\tilde{\chi}_1 + \tilde{\chi}_2)^2 + \chi_1^2 \tilde{\chi}_2^2 + \chi_2^2 \tilde{\chi}_1^2 + 4\chi_1 \chi_2 \tilde{\chi}_1 \tilde{\chi}_2\right] \\ & + h_+\left[\partial_t \chi_1 \partial_t \tilde{\chi}_1 + \partial_t \chi_1 \partial_t \tilde{\chi}_2\right] + g_{ym} h_+ \left(U\partial_z \tilde{U}(\chi_1 + \chi_2) - 2U^2(\partial_z \tilde{\chi}_1 - \partial_z \tilde{\chi}_2)\right) \\ & + \frac{1}{2} g_{ym}^2 h_+ \left(2U\tilde{U}(\chi_1^2 - \chi_2^2) + 2U^2(\chi_1 \tilde{\chi}_1 - \chi_2 \tilde{\chi}_2)\right).\end{aligned} \tag{5.64}$$

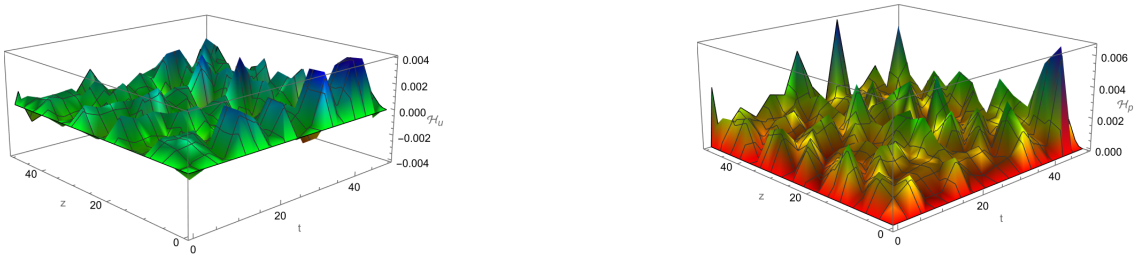

Figure 5.18: Figures showing perturbed energy density contribution of condensate (left) and wave modes (right) as a function of time and space in the presence of a gravitational wave. We choose the parameters same as in Fig. (5.17).

The perturbed energy plots are given in Figs. (5.18 & 5.19) as contributions from condensate and wave modes. As these are first-order contributions over the zero-order ones, they can be negative as shown in Fig. (5.19). From plots, one can see that there is an energy exchange between condensate and modes, but still oscillatory. If we still keep the assumption that the condensate is homogeneous and isotropic, then the equation of motion for condensate will act as a constraint on the perturbation functions $(\tilde{\chi}_1, \tilde{\chi}_2)$. Thus, we relax the isotropy assumption and consider a z-dependent perturbation.

(ii). Comparison between Linearized and exact solutions

Figure 5.19: Figures showing perturbed energy density contribution of condensate (Red plot) and wave modes (Blue plot) as a function of time (left) and space (right) separately in the presence of a gravitational wave. We choose the parameters same as in Fig. (5.17).

To verify the perturbation theory, we compare the solutions obtained perturbatively with those of exact solutions. For this, again consider the reduced system (U,χ_1,χ_2) and with only time dependence of modes. What we will be doing is as follows: Compare the solutions ($U_{GW}(t)$, $\chi_{1GW}(t)$ and $\chi_{2GW}(t)$) of Eqs. (5.46, 5.49, 5.50) without Φ^1 and Φ^2 with solutions $(U(t)+\tilde{U}(t,z),\ \chi_1(t)+\tilde{\chi}_1(t,z),\ \chi_2(t)+\tilde{\chi}_2(t,z).)$ where $(U(t),\chi_1(t),\chi_2(t))$ are solutions of Eqs. (5.35, 5.38, 5.39) without Φ^1 and Φ^2 and $(\tilde{U}(t),\tilde{\chi}_1(t),\tilde{\chi}_2(t))$ are the solutions of Eqs. (5.58, 5.59, 5.60). If we write all the equations explicitly, they are as follows:

$$\partial_0^2 U + g_{ym}^2\left[2U^3+\frac{1}{3}U(\chi_1+\chi_2)^2\right]=0, \tag{5.65}$$

$$-\partial_0^2\chi_1 + g_{ym}^2\left[-U^2(\chi_1+\chi_2)-\chi_1\chi_2^2\right]=0, \tag{5.66}$$

$$-\partial_0^2\chi_2 - g_{ym}^2\left[U^2(\chi_1+\chi_2)+\chi_1^2\chi_2\right]=0, \tag{5.67}$$

$$-3\partial_t^2\tilde{U}+g_{ym}^2\left[\tilde{U}(-18U^2-\chi_1^2-\chi_2^2)-2\tilde{U}\chi_1\chi_2-2U(\chi_1+\chi_2)(\tilde{\chi}_1+\tilde{\chi}_2)\right] -g^2h_+U(\chi_2^2-\chi_1^2)=0, \tag{5.68}$$

$$-\partial_0^2\tilde{\chi}_1-g_{ym}^2\left[U^2(\tilde{\chi}_1+\tilde{\chi}_2)+2U\tilde{U}(\chi_1+\chi_2)+\tilde{\chi}_1\chi_2^2+2\chi_1\chi_2\tilde{\chi}_2\right]-\partial_t\chi_1\partial_t h_+ - h_+\partial_t^2\chi_1 -g_{ym}^2h_+U^2\chi_1=0, \tag{5.69}$$

$$-\partial_0^2\tilde{\chi}_2-g_{ym}^2\left[U^2(\tilde{\chi}_1+\tilde{\chi}_2)+2U\tilde{U}(\chi_1+\chi_2)+\tilde{\chi}_2\chi_1^2+2\chi_1\chi_2\tilde{\chi}_1\right]+\partial_t\chi_2\partial_t h_+ + h_+\partial_t^2\chi_2$$

$$+g_{ym}^2 h_+ U^2 \chi_2 = 0, \tag{5.70}$$

$$\partial_0^2 U_{GW} + g_{ym}^2 \left[2U_{GW}^3 + \frac{1}{3} U_{GW} (\chi_{1GW} + \chi_{2GW})^2 \right] - \frac{g_{ym}^2 h_+}{3} \left[U_{GW} \left(\chi_{2GW}^2 - \chi_{1GW}^2 \right) \right] = 0, \tag{5.71}$$

$$-\partial_0^2 \chi_{1GW} - h_+ \partial_0^2 \chi_{1GW} - \partial_t h_+ \partial_t \chi_{1GW} + g_{ym}^2 \left[-U_{GW}^2 (\chi_{1GW} + \chi_{2GW}) - \chi_{1GW} \chi_{2GW}^2 \right] + g_{ym}^2 h_+ \left[-U_{GW}^2 \chi_{1GW} \right] = 0, \tag{5.72}$$

$$-\partial_0^2 \chi_{2GW} + h_+ \partial_0^2 \chi_{2GW} + \partial_t h_+ \partial_t \chi_{2GW} - g_{ym}^2 \left[U_{GW}^2 (\chi_{1GW} + \chi_{2GW}) + \chi_{1GW}^2 \chi_{2GW} \right] + g_{ym}^2 h_+ \left[U_{GW}^2 \chi_{2GW} \right] = 0. \tag{5.73}$$

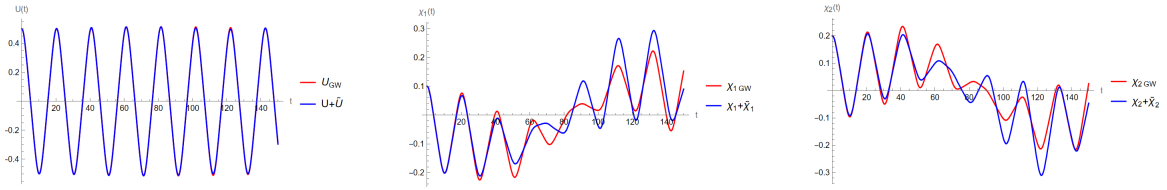

((a)) $U(t)$ ((b)) $\chi_1(t)$ ((c)) $\chi_2(t)$

Figure 5.20: Figures showing $U(t)$, $\chi_1(t)$ and $\chi_2(t)$ as a function of time in the presence of a gravitational wave. We choose the parameters same as in Fig. (5.17).

We solved the above equations and the plots are shown in Fig (5.20). From Fig. (5.20(a)), it is clear that the condensate solution is exactly aligned which agrees with the tiny magnitude of perturbation in U in Fig. (5.17(a)). From other Figs. (5.20(b) & 5.20(c)) as well, the perturbation solutions almost match with the exact solution. We can restore the longitudinal modes as well as z-dependence, but the question which we are interested in regarding the system has already been obtained here. Thus, restoring the modes does not give any more surprises.

5.3.2 Summary

In this section, we considered a different way of decomposition of the gauge field than in [38]. We find that there is an energy exchange between condensate and fluctuations for a long time and then later there is an energy swap effect from the condensate to the wave modes. We also find that the GW can induce the decay of the condensate into particles, but it also delays the decay effect even further by stabilizing the condensate.

5.4 Condensates in higher gauge groups

In previous sections, we deal with the condensate configuration in $SU(2)$ YM theory. As $SU(2)$ is a subgroup for any higher non-abelian gauge groups, it is expected that the higher groups also contain some YM condensates based on their different subgroups. For example, $SU(4)$ gauge group containing two unmixing $SU(2)$ subgroups can have two corresponding YM condensates. In [38], authors studied $SU(4)$ gauge group using two $SU(2)$ YM condensates along with the fluctuations. They found the same energy swap effect found in $SU(2)$ gauge theory. However, it is not that simple for a gauge group with mixing $SU(2)$ subgroups such as for $SU(3)$. Even though $SU(3)$ has three overlapping $SU(2)$ subgroups, one cannot take three $SU(2)$ YM condensates as suggested in [42]. A $SU(3)$ gauge field with three condensates (one for each subgroup) will not generate three independent equations of motion from YM equations. There will be some cross-terms that make equations not split. Thus, one has to be more careful in applying the simple $SU(2)$ condensate model to higher gauge groups. This line of work needs further investigation [197].

5.5 Conclusion

In this chapter, we studied the $SU(2)$ condensate model introduced in [38] in the presence of GWs. We reanalyzed the results of the net energy transfer from condensate to the plasmons/fluctuations. The authors in [38] studied the dynamics of fluctuations in the pres-

ence of condensate. They decomposed the fluctuations using tensor decomposition into transverse and longitudinal modes. They found that there is a net energy transfer from the condensate/plasma to fluctuations/plasmons. In our work, we aimed to study the condensate + fluctuations model in the presence of GWs. Using the tensor decomposition of fluctuations as done in [38], we found that only symmetric transverse-traceless modes interact with GWs. This is due to the transverse-traceless modes having the same structure as GWs. Using the transverse-traceless modes for fluctuations, we studied the condensate + fluctuations system in the presence of GWs. We found analytical solutions in terms of unperturbed transverse-traceless modes.

To investigate the role of longitudinal modes, we introduced a different mode decomposition, vector decomposition, where we split the gauge field into condensate, longitudinal, and transverse modes. We reanalyzed the energy exchange in this new condensate + fluctuations model. We found that the condensate dissipates into particles or plasmons but this energy exchange effect highly depends on the YM coupling constant (g_{ym}) and condensate initial conditions. We also find that the time taken for the condensate to decay is delayed compared to the time observed in [38]. The condensate does not decay all its energy monotonically, but the condensate and plasmons exchange energy in an oscillatory way eventually transferring all its energy to plasmons. This energy transfer happens only when all the modes have to be non-zero initially.

We studied the effect of GWs on the dynamics of fluctuations around the condensate. We found that the GW interacts with the condensate and leads the condensate to decay into plasmons, though at a delayed time. It means GWs can induce plasma oscillations and lead to the generation of plasmons. As opposed to the case in [38], we found that the longitudinal modes also interact with GWs. We also found that the GW tries to stabilize the condensate and causes the condensate decay to delay further. This stabilization of energy transfer of plasma-plasmon fields plays a vital role in the study of fluid properties of QGP like fluid density, viscosity, etc. There have been studies that the unusually low viscosity of

the QGP can be attributed to the gravitons [198] and our model can be used to study that hypothesis.

Chapter 6

Dynamics of Fermions in the presence of Condensates in a GW background

> ”Nobody ever figures out what life is all about, and it doesn’t matter. Explore the world. Nearly everything is really interesting if you go into it deeply enough.”
>
> *Richard P. Feynman*

QGP, a deconfined phase of quarks and gluons, forms at very high temperatures that existed in the early universe and is also being created in heavy ion colliders. The quarks in QGP are fermions, thus one has to study the combined dynamics of quarks and gluons to understand QGP. The gluons being modelled as $SU(2)$ YM condensate [38], we try to study the dynamics of quarks in the background of YM condensate.

A large amount of work in this area happened in the 1970s when there was a great interest in classical gauge theory. There are many interesting effects associated with the behaviour of fermions in the background fields of topological objects [50, 199–202]. One such phenomenon is the fractionalisation of fermion number and electric charge when fermions interact with solitons [199]. Due to the interest in grand unified theories, many have studied the behaviour of fermions in the background of monopoles and strings. These studies are also important for the experimental search for these objects and also help in understanding their role in the Early universe. A two-dimensional theory of massless fermions interact-

ing with abelian gauge fields results in a phenomenon of fermion level crossing and the corresponding non-conservation of fermion quantum numbers. In the case of non-abelian gauge theories having gauge field configurations with a nontrivial topological charge, can cause explicit violation of conservation laws [200]. This leads to a violation of chirality in QCD and conservation of baryon and lepton numbers in the Electroweak theory [201]. Under usual conditions of low temperatures and densities, the probabilities of these processes with non-conservation of baryon number are negligible because of suppression due to instantons. However, at sufficiently high temperatures, this suppressing picture will change [202] and these kinds of studies were also important for cosmology. Some of the studies focused on massless fermions [45]. Some were on the production and backreaction of massive fermions in spontaneously broken gauge theory [46, 47] and as well as during axion inflation [48, 49]. Most of the work in this area is done by studying fermions in the background of solitons, kinks, monopoles and strings. In this chapter, we analyse the dynamics of fermions in the background of a spatially homogeneous and isotropic condensate.

In many cases, the interaction of fermions with gauge fields can be analyzed in the following way: Assume that the gauge fields are external fields and study the Dirac equation in these background fields. Generally, such kind of description is only approximate, since the introduction of fermions changes the configuration of gauge fields. Mostly, this effect is small and usually neglected. However, there are some cases of where this backreaction of fermions cannot be neglected. Thus, we studied the backreaction of fermions on the condensate.

This chapter closely follows our work in papers [44, 52]. We will start with the dynamics of fermions in the presence of YM Condensate in Sec: 6.1 and followed by the backreaction of fermions on the gauge field in Sec: 6.1.1. In the later section (Sec: 6.2), we studied the fermions + condensate system in the presence of GWs.

6.1 Dynamics of Fermions in the presence of Condensate

We consider the $SU(2)$ YM condensate discussed in the previous chapter: 5.

$$A_0^a = 0,\ A_i^a = \delta_i^a U(t),\ i = 1,2,3, \tag{6.1}$$

where $U(t)$ is the spatially homogeneous and isotropic condensate. The solution for the YM equation with the above ansatz is given by Jacobi elliptic functions as

$$U(t) = c_1 \mathrm{sn}(g_{ym} c_1 (t + c_2), -1). \tag{6.2}$$

where g_{ym} is the YM coupling constant, c_1 and c_2 are the integration constants. We fix the background field to be this condensate and solve the Dirac equation in this background field as

$$i\gamma^\mu \partial_\mu \psi_\alpha + g_{ym}\gamma^\mu A_\mu^a T^a_{\alpha\beta}\psi_\beta = 0, \tag{6.3}$$

where A_μ^a is the $SU(2)$ gauge field with generators,$T^a = \sigma^a/2, \sigma^a$= Pauli matrices, γ^μ are the gamma matrices obeying Clifford algebra ($\{\gamma^\mu, \gamma^\nu\} = 2\eta^{\mu\nu}$) and Ψ_α is the $SU(2)$ fermion doublet and α, β are the fermion doublet index with $\alpha, \beta = 1, 2$. The fermion doublet is represented as ($\Psi = (\Psi_1 \Psi_2)^T$), and the Dirac equation becomes

$$i\gamma^\mu \partial_\mu \psi_1 + \frac{g_{ym}}{2} U(t) \left[\left(\gamma^1 - i\gamma^2\right) \psi_2 + \gamma^3 \psi_1 \right] = 0, \tag{6.4}$$

$$i\gamma^\mu \partial_\mu \psi_2 + \frac{g_{ym}}{2} U(t) \left[\left(\gamma^1 + i\gamma^2\right) \psi_1 - \gamma^3 \psi_2 \right] = 0. \tag{6.5}$$

Using the chiral (Weyl) representation of gamma matrices, one can represent the Dirac spinor in terms of left-handed and right-handed two-component Weyl spinors $\psi_1 = (\psi_{1L}\ \psi_{1R})^T$, $\psi_2 = (\psi_{2L}\ \psi_{2R})^T$. Usually in the Standard Model of Particle Physics, the left-handed spinors act as doublets, and the right-handed ones act as singlets. Here, we assume both as

doublets and the equations can be written as

$$i(\partial_0 - \sigma^i\partial_i)\psi_{1L} - \frac{g_{ym}}{2}U(t)[(\sigma^1 - i\sigma^2)\psi_{2L} + \sigma^3\psi_{1L}] = 0, \tag{6.6}$$

$$i(\partial_0 + \sigma^i\partial_i)\psi_{1R} + \frac{g_{ym}}{2}U(t)[(\sigma^1 - i\sigma^2)\psi_{2R} + \sigma^3\psi_{1R}] = 0, \tag{6.7}$$

$$i(\partial_0 - \sigma^i\partial_i)\psi_{2L} - \frac{g_{ym}}{2}U(t)[(\sigma^1 + i\sigma^2)\psi_{1L} - \sigma^3\psi_{2L}] = 0, \tag{6.8}$$

$$i(\partial_0 + \sigma^i\partial_i)\psi_{2R} + \frac{g_{ym}}{2}U(t)[(\sigma^1 + i\sigma^2)\psi_{1R} - \sigma^3\psi_{2R}] = 0. \tag{6.9}$$

As we can see the left and right-handed Weyl spinors got decoupled. Now, let the right-handed Weyl fermions set to zero and represent the two-component left-handed Weyl fermions as $\psi_{1L} = (\psi_{1L1} \quad \psi_{1L2})^T$, $\psi_{2L} = (\psi_{2L1} \quad \psi_{2L2})^T$. Assuming the fields depend only on time, the final equations are given by

$$i\partial_0\psi_{IL1} - \frac{g_{ym}}{2}U(t)\psi_{IL1} = 0, \tag{6.10}$$

$$i\partial_0\psi_{1L2} - g_{ym}U(t)\psi_{2L1} + \frac{g_{ym}}{2}U(t)\psi_{1L2} = 0, \tag{6.11}$$

$$i\partial_0\psi_{2L1} - g_{ym}U(t)\psi_{1L2} + \frac{g_{ym}}{2}U(t)\psi_{2L1} = 0, \tag{6.12}$$

$$i\partial_0\psi_{2L2} - \frac{g_{ym}}{2}U(t)\psi_{2L2} = 0. \tag{6.13}$$

As we can see from the equations, the Ψ_{1L1} and Ψ_{2L2} are decoupled from each other and can be solved separately. But, the equations for Ψ_{1L2} and Ψ_{2L1} are coupled together and have to be solved simultaneously. Taking the general solution for the YM condensate as $U(t) = c_1\,\mathrm{sn}(g_{ym}c_1(t+c_2), -1)$, the solutions for fermion fields are given by

$$\psi_{1L1}(t) = A_1\Lambda^{-1/2}, \tag{6.14}$$

$$\psi_{2L2}(t) = A_2\Lambda^{-1/2}, \tag{6.15}$$

$$\psi_{1L2}(t) = c_3\Lambda^{3/2} + c_4\Lambda^{-1/2}, \tag{6.16}$$

$$\psi_{2L1}(t) = -c_3\Lambda^{3/2} + c_4\Lambda^{-1/2}, \tag{6.17}$$

where $\Lambda = (\mathrm{dn}(g_{ym}c_1(t+c_2),-1) - i\,\mathrm{cn}(g_{ym}c_1(t+c_2),-1))$, A_1, A_2, c_3 and c_4 are integration constants, and dn and cn are Jacobi elliptic functions (See Appendix: D.1). Out of all constants, only c_1 and c_2 are real while others are complex constants. Since the fermions are not classical objects, it makes only sense to study the bilinears built from fermion fields. The quantity $\psi_1^\dagger\psi_1$ describes the probability that the system contains the fermion ψ_1. Similarly, $\psi_2^\dagger\psi_2$ describes the probability that the system contains the fermion ψ_2. Even though the condensate seems to couple two different components (ψ_{1L2}, ψ_{2L1}), the densities generated by these two types of fermions do not mix each other. This indicates that one can always find the system in favour of one flavour only. This is shown in Fig. (6.1).

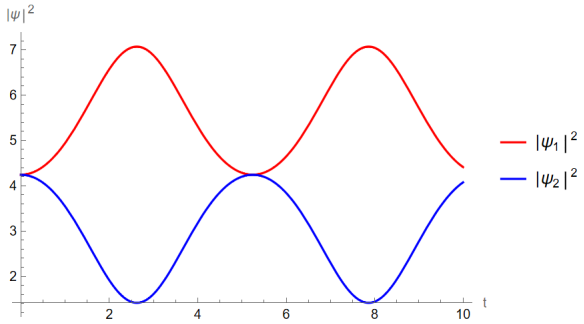

Figure 6.1: Figure showing the probability densities for ψ_1 and ψ_2. We use $A_1 = c_1 = c_3 = c_4 = 1$, $c_2 = 0$ and $g_{ym} = 0.5$.

As the components Ψ_{1L1} and Ψ_{2L2} decoupled, we can set the constants $A_1 = A_2 = 0$ without losing any generality. Now to understand the effect of fermions, we need to calculate the current densities generated by these fermionic fields. That can be done with the following formula:

$$(j^\nu)^a = \overline{\psi}_\alpha\, \gamma^\nu\, T^a_{\alpha\beta}\, \psi_\beta. \tag{6.18}$$

Then, we get the following non-zero components for current density:

$$(j^0)^3 = \frac{1}{2}\left(|\psi_{1L2}|^2 - |\psi_{2L1}|^2\right), \tag{6.19}$$

$$(j^1)^1 = -\frac{1}{2}\left(\psi^*_{1L2}\psi_{2L1} + \psi^*_{2L1}\psi_{1L2}\right), \tag{6.20}$$

$$(j^1)^2 = \frac{i}{2}\left(\psi^*_{1L2}\psi_{2L1} - \psi^*_{2L1}\psi_{1L2}\right), \tag{6.21}$$

$$(j^2)^1 = -\frac{i}{2}\left(\psi^*_{1L2}\psi_{2L1} - \psi^*_{2L1}\psi_{1L2}\right), \tag{6.22}$$

$$(j^2)^2 = -\frac{1}{2}\left(\psi^*_{1L2}\psi_{2L1} + \psi^*_{2L1}\psi_{1L2}\right), \tag{6.23}$$

$$(j^3)^3 = \frac{1}{2}\left(|\psi_{1L2}|^2 + |\psi_{2L1}|^2\right). \tag{6.24}$$

These nonzero current densities will act as a source for the YM fields. This is the general scenario in QGP, where the matter fields like the quark fields act as a source for the force fields like gluons.

6.1.1 Backreaction of Fermions on Condensate

As we discussed, the backreaction of fermions on gauge fields is negligible in most cases. But, there have been cases where this backreaction is important. For example, there have been studies on the production and backreaction of massive fermions during axion inflation with non-abelian gauge fields [48, 49]. In this section, we study the backreaction of fermions on the YM condensate. The current densities that we find at the end of the previous section act as a source for the generation of fluctuations around the condensate. We start with the YM equations with nonzero source terms as follows

$$\nabla_\mu F^{a\mu\nu} + g_{ym}\,\varepsilon^{abc}\,A^b_\mu\,F^{c\mu\nu} = -(j^\nu)^a, \tag{6.25}$$

where $F^a_{\mu\nu} = \partial_\mu A^a_\nu - \partial_\nu A^a_\mu + g_{ym}\varepsilon^{abc}A^b_\mu A^c_\nu$ is the anti-symmetric field strength tensor of gauge field A^a_μ, ε^{abc} are the structure constants, g_{ym} is the YM coupling constant and $(j^\nu)^a$ is fermion current density which is given in Eqs. (6.19) - (6.24).

In Hamilton's gauge ($A^a_0 = 0$), the YM equations are given by

$$g_{ym}\varepsilon^{abc}A^b_j\partial_0 A^{cj} = -(j^0)^a, \tag{6.26}$$

$$-\partial_0^2 A^a_i + g^2_{ym}(A^a_j A^b_j A^b_i - (A^b_j A^b_j)A^a_i) = -(j_i)^a,\ \ i = 1,2,3, \tag{6.27}$$

where the first and second equations are obtained by taking $\nu = 0$ and $\nu = i$ in the YM

equation, respectively. Consider the gauge field ansatz to be of the following form

$$A_i^a = U(t)\delta_i^a + \tilde{A}_i^a(t), \tag{6.28}$$

where the first term is the usual unperturbed condensate and the second term is the perturbed function. Now, we will focus on the solutions arising from the nonzero current densities. If we see the zeroth component ($\nu = 0$) of the current, only the 3rd component ($a = 3$) is nonzero. Inserting the above ansatz in Eq. (6.26), we get

$$(\partial_0\tilde{A}_1^2 - \partial_0\tilde{A}_2^1)U + (\tilde{A}_2^1 - \tilde{A}_1^2)\partial_0 U = -\frac{1}{g_{ym}}(j^0)^3. \tag{6.29}$$

By setting $Z(t) = \tilde{A}_1^2 - \tilde{A}_2^1$, we get a simple differential equation as follows

$$\partial_t Z(t) - \frac{\partial_t U}{U}Z(t) = -\frac{1}{g_{ym}}\frac{(j^0)^3}{U}. \tag{6.30}$$

For j^0, we take $c_2 = 0, c_3 = c_4 = 1$. Then, the solution obtained as

$$Z(t) = \left(-\frac{2\sqrt{2}}{g_{ym}c_1}t + c_5\right)\mathrm{sn}(g_{ym}c_1 t, -1), \tag{6.31}$$

where c_5 is the integration constant. Next, we solve for other components with nonzero current densities. Their equations are given as

$$-\partial_0^2\tilde{A}_1^2 + g_{ym}^2\, U^2(\tilde{A}_2^1 - \tilde{A}_1^2) = -(j^1)^2, \tag{6.32}$$

$$-\partial_0^2\tilde{A}_2^1 + g_{ym}^2\, U^2(\tilde{A}_1^2 - \tilde{A}_2^1) = -(j^2)^1, \tag{6.33}$$

$$-\partial_0^2\tilde{A}_1^1 - 2g_{ym}^2 U^2\tilde{A}_b^b = -(j^1)^1, \tag{6.34}$$

$$-\partial_0^2\tilde{A}_2^2 - 2g_{ym}^2 U^2\tilde{A}_b^b = -(j^2)^2, \tag{6.35}$$

$$-\partial_0^2\tilde{A}_3^3 - 2g_{ym}^2 U^2\tilde{A}_b^b = -(j^3)^3, \tag{6.36}$$

where $(j^2)^1 = (j^1)^2 = 2\sqrt{2}\,\mathrm{dn}(c_1 g_{ym}t, -1)\mathrm{cn}(c_1 g_{ym}t, -1)$, $(j^1)^1 = (j^2)^2 = 3/\sqrt{2}$ and $(j^3)^3 =$

$5/\sqrt{2}$. Since $Z(t) = \tilde{A}_1^2 - \tilde{A}_2^1$, we can easily solve the equations (6.32 & 6.33) for the components $\tilde{A}_2^1$ and $\tilde{A}_1^2$. Using Eq. (6.32) and $Z(t)$, we get

$$\partial_0^2 \tilde{A}_2^1 - g_{ym}^2 U^2 \, Z(t) - 2\sqrt{2} \, g_{ym} \, \mathrm{dn}(c_1 g_{ym} t, -1)\mathrm{cn}(c_1 g_{ym} t, -1) = 0, \tag{6.37}$$

and the solution obtained as

$$\tilde{A}_2^1 = c_6 + c_7 t - \frac{1}{2} Z(t). \tag{6.38}$$

With this, we find the $\tilde{A}_1^2$ as $\tilde{A}_1^2 = c_6 + c_7 t + \frac{1}{2} Z(t)$, where c_6 and c_7 are the integration constants. We can combine the remaining three equations (Eqs. (6.34, 6.35, 6.36)) into one equation for the trace of the gauge field ($\tilde{A}_a^a$) as

$$\partial_0^2 \tilde{A}_b^b + 6 g_{ym}^2 \, U^2 \tilde{A}_b^b = (j_b^b), \tag{6.39}$$

and the trace of fermion current densities is found to be a constant, $j_b^b = 11/\sqrt{2}$. Then, the above equation becomes

$$\partial_0^2 \tilde{A}_b^b(t) + 6 g_{ym}^2 \, c_1^2 \mathrm{sn}^2(c_1 g_{ym} t, -1) \tilde{A}_b^b(t) = \frac{11}{\sqrt{2}}. \tag{6.40}$$

To solve this, one has to remove the Jacobi functions from the differential equation. To do this, we change the variable $t \to x$ such that $x = \mathrm{am}(c_1 g_{ym} t, -1)$, where $\mathrm{am}(u, m)$ is the Jacobi Amplitude with modulus m. With this, the equation becomes

$$(1 + \sin^2(x)) \, \partial_x^2 \tilde{A}_b^b(x) + \frac{1}{2} \sin(2x) \, \partial_x \tilde{A}_b^b(x) + 6 \sin^2(x) \tilde{A}_b^b(x) = \frac{11}{\sqrt{2} g_{ym}^2 c_1^2}. \tag{6.41}$$

We found the analytical solution for the above differential equation. Again converting $x \to t$, we get the final solution to be

$$\tilde{A}_a^a(t) = \frac{\mathrm{cn}(g_{ym} c_1 t, -1)\mathrm{sn}^{1/2}(g_{ym} c_1 t, -1)(2 - \mathrm{cn}^2(g_{ym} c_1 t, -1))^{3/4}}{(2 - 3 \, \mathrm{cn}^2(g_{ym} c_1 t, -1) + \mathrm{cn}^4(g_{ym} c_1 t, -1))^{1/4}} \left[k_1 + \frac{k_2}{4} \left(\frac{-2}{\mathrm{cn}(g_{ym} c_1 t, -1)} \right. \right.$$

$$\sqrt{\frac{\mathrm{cn}^2(g_{ym}c_1t,-1)-1}{\mathrm{cn}^2(g_{ym}c_1t,-1)-2}}+\sqrt{2}\,F(\sin^{-1}\mathrm{cn}(g_{ym}c_1t,-1),\frac{1}{2})\Bigg)\Bigg]+\frac{11}{2\sqrt{2}g_{ym}^2c_1^2}\mathrm{sn}^2(g_{ym}c_1t,-1), \tag{6.42}$$

where k_1, k_2 are integration constants and $F(x,m)$ is the incomplete elliptic integral of first kind. Since the above expression is a function of Jacobi elliptic functions, it is very hard to solve for the diagonal components $(\tilde{A}_1^1,\ \tilde{A}_2^2,\ \tilde{A}_3^3)$ individually. Thus, we found the numerical solutions for $(\tilde{A}_1^1,\ \tilde{A}_2^2,\ \tilde{A}_3^3)$ which are given in Figs. (6.2).

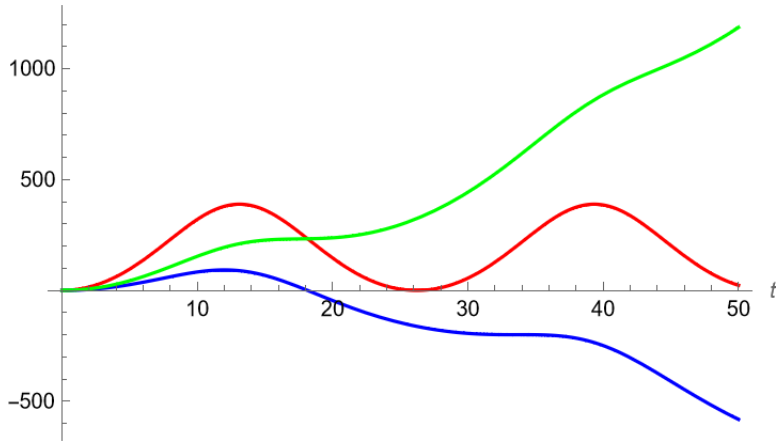

Figure 6.2: Figure showing the numerical solutions for diagonal components of the gauge field. The red, blue and green plots corresponds to $\tilde{A}_a^a$, $\tilde{A}_1^1=\tilde{A}_2^2$ and $\tilde{A}_3^3$, respectively. We choose $g_{ym}=0.1$ and $c_1=1$.

As one can see the $j_1^1=j_2^2$, thus $\tilde{A}_1^1$ and $\tilde{A}_2^2$ functional behaviour also remains the same. The trace function behaves like the square of the sine Jacobi function. The diagonal components $\tilde{A}_1^1=\tilde{A}_2^2$ shows complementary behaviour to $\tilde{A}_3^3$. All three functions show oscillatory behaviour. With the presence of nonzero components $\tilde{A}_2^1$, $\tilde{A}_1^2$, the isotropy of condensate solutions clearly gets broken. Thus, one cannot simply take a homogeneous and isotropic type of configuration for describing QGP.

The other components with zero current densities or zero source terms are $\tilde{A}_3^1, \tilde{A}_3^2, \tilde{A}_1^3$ and $\tilde{A}_2^3$. These components do not depend on current densities as well as the above other components, thus we can set them to zero without any inconsistency with the above analysis. Then, the components of sector $a=1,2$ & $i=1,2$ behave differently than the components

of sector a or $i = 3$. We can also try and stretch the idea further by keeping the a or $i = 3$ components separate from the system of $a = 1,2$ & $i = 1,2$ components. Thus, one can write the gluon ansatz in the presence of fermions as

$$A_i^a = U(t)\delta_i^a + \tilde{A}_i^a, \text{ where } i,a = 1,2, \tag{6.43}$$

$$A_3^3 = V(t). \tag{6.44}$$

As the above form of solution gives a correct description of gauge fields in the presence of fermions, we explore this idea further and investigate the thermodynamic properties of QGP with the above background in Chapter: 7.

6.2 Dynamics of Fermions in the presence of Condensate in a GW background

We will go back to the case where the gauge field is just the homogeneous and isotropic condensate. In this section, we will study the dynamics of fermions in the presence of condensates in the GW background. The Dirac equation in curved background is given by

$$i\bar{\gamma}^\mu(\partial_\mu + \Gamma_\mu)\psi_\alpha + g_{ym}\bar{\gamma}^\mu A_\mu^a T_{\alpha\beta}^a \psi_\beta = 0, \tag{6.45}$$

where $\bar{\gamma}^\mu$ are the spacetime-dependent gamma matrices, Γ_μ is the spinor affine connection and the remaining terms are the same as in the previous section. Consider a $+$-polarized GW propagating in z-direction as the curved background. The details regarding the Dirac equation in the curved spacetime are given in Appendix B. Following those details, we will end up with the following equations:

$$i\,(\partial_0 + \partial_3)\psi_{2L2} + \frac{g_{ym}}{2}h_+ U\psi_{1L1} - \frac{g_{ym}}{2}U\psi_{2L2} = 0, \tag{6.46}$$

$$i\,\partial_0\psi_{1L2} - g_{ym}U\psi_{2L1} + \frac{g_{ym}}{2}U\psi_{1L2} = 0, \tag{6.47}$$

$$i\,\partial_0\psi_{2L1} - g_{ym}U\psi_{1L2} + \frac{g_{ym}}{2}U\psi_{2L1} = 0, \tag{6.48}$$

$$i\,(\partial_0 - \partial_3)\psi_{1L1} + \frac{g_{ym}}{2}h_+U\psi_{2L2} - \frac{g_{ym}}{2}U\psi_{1L1} = 0. \tag{6.49}$$

From the above equations, one can see that the two modes ψ_{1L1}, ψ_{2L1} which were once decoupled (Eqs. 6.10 & 6.13) are now interacting due to the GW. The GW connects the two fermions from the different components of $SU(2)$ doublet. The fermion densities generated from the two components ψ_{1L1}, ψ_{2L2} of fermion $SU(2)$ doublet in the presence of GW are shown in Figs. (6.3) and (6.4) for two different GW frequencies. It is clear from plots that the fermion densities fluctuate and mix in time due to the GW. As GW couples these otherwise independent modes, there should be a flavour transition induced by the GW. The flavour transitions induced by a graviton have been studied in [203]. The evidence for the flavour transitions due to GWs has relevance for QGP since the QGP during the early universe exists in the Primordial GW background.

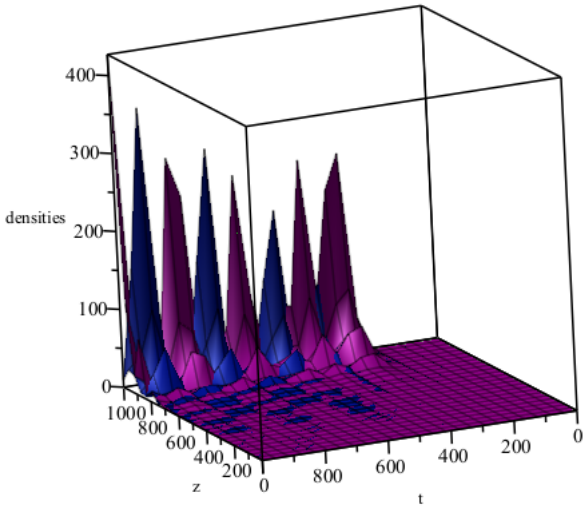

Figure 6.3: Fermion densities of two flavours in the presence of GW at $\omega_g = 10^{-4}, A_+ = 1$. $|\psi_{1L}|^2$ is plotted in blue color, and the $|\psi_{2L}|^2$ in maroon. In the above, we choose $c_1 = 1, c_2 = 1/2, g_{ym} = \sqrt{2}, \psi_{1L}(t,0) = 10^{-2}U(t) = \psi_{2L}(t,0), \psi_{1L} = (0,z) = \psi_{2L}(0,z) = 0$.

To show the flavour flip behaviour happens in the presence of GWs, we plotted the

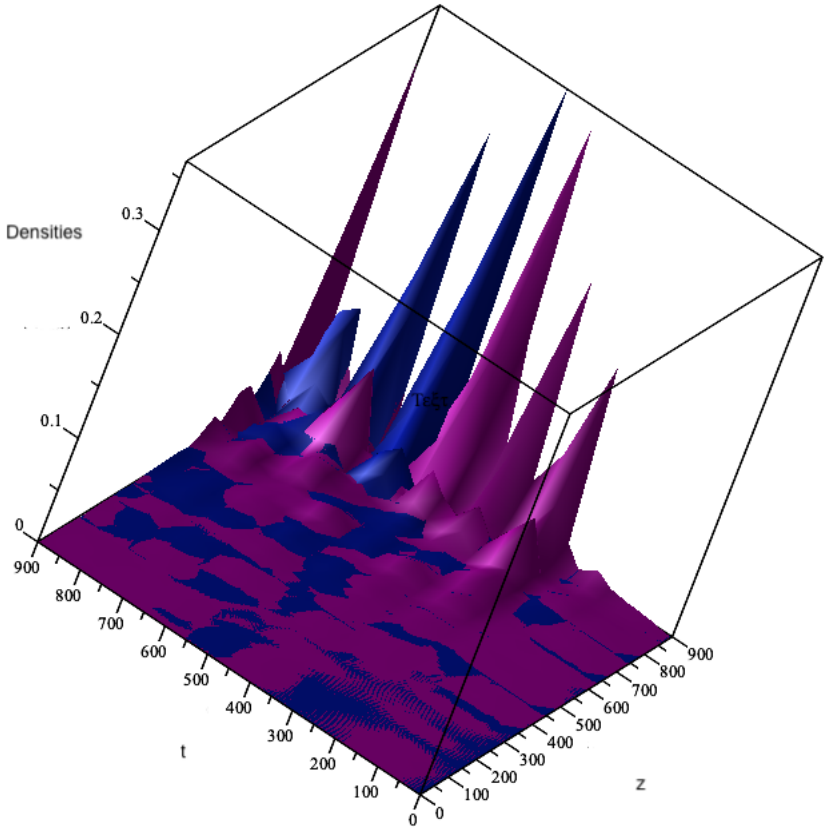

Figure 6.4: Fermion densities of two different flavours in the presence of GW at $\omega_g = 10$ and $A_+ = 1$. $|\psi_{1L}|^2$ is plotted in blue color, and the $|\psi_{2L}|^2$ in maroon. We choose $c_1 = 1, c_2 = 1/2, g_{ym} = \sqrt{2}, \psi_{1L}(t,0) = 10^{-2}U(t) = \psi_{2L}(t,0), \psi_{1L} = (0,z) = \psi_{2L}(0,z) = 0$.

fermion densities for two flavours without and with GW in Fig. (6.5) and Fig. (6.6), respectively. From Fig. (6.5(b)), one can see that the two flavour densities behave differently, one of them increases while the other one decreases. With the GW case, as in Fig. (6.6(b)), the densities show that there is a coupling effect of the flavours. One can see similar behaviour for the plots as functions of time in Figs. (6.5(a) & 6.6(a)). In the above analysis, we have taken the amplitude of GW to be the same as that of condensate. This is to solve for the combined effect of GW and condensate on fermions.

If we try to consider the effect of a weak GW, then one has to take the fermion wave

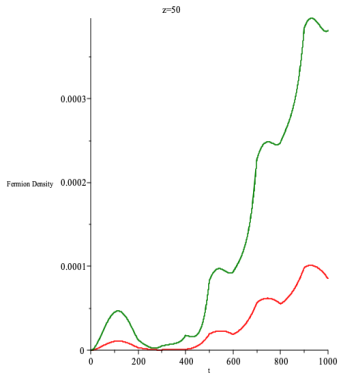

((a)) $|\psi_{1L}|^2$ in green and $|\psi_{2L}|^2$ in red without GW as a function of time.

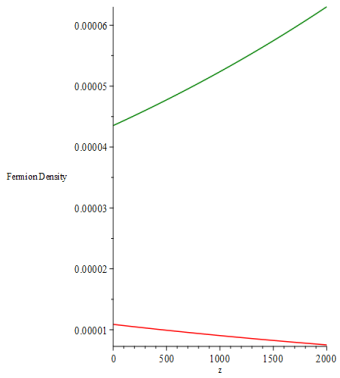

((b)) $|\psi_{1L}|^2$ in green and $|\psi_{2L}|^2$ in red without GW as a function of space.

Figure 6.5: Fermion densities plotted without a GW; We choose $c_1 = 1, c_2 = 1/2, g_{ym} = \sqrt{2}, \psi_{1L}(t,0) = 10^{-2}U(t) = \psi_{2L}(t,0)$, $\psi_{1L} = (0,z) = \psi_{2L}(0,z) = 0$.

functions as

$$\psi_{1L1} \to \psi_{1L1} + \tilde{\psi}_{1L1}, \;\; \psi_{2L1} \to \psi_{2L2} + \tilde{\psi}_{2L2},$$

where ψ_{1L1}, ψ_{2L2} are the solutions of Eqs. (6.10) & Eq. (6.13), respectively and $\tilde{\psi}_{1L1}, \tilde{\psi}_{2L2}$ are the perturbation functions due to GW.

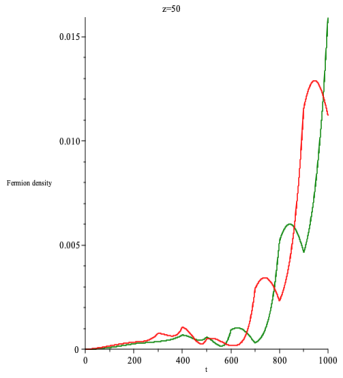

((a)) $|\psi_{1L}|^2$ in green and $|\psi_{2L}|^2$ in red with GW as a function of time.

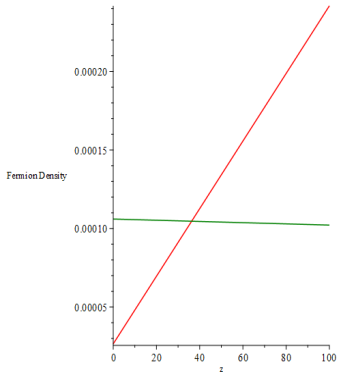

((b)) $|\psi_{1L}|^2$ in green and $|\psi_{2L}|^2$ in red with GW as a function of space.

Figure 6.6: Figures showing Fermion density with GW as a function of time and space separately. We choose $\omega_g = 10^{-4}, A_+ = 1, c_1 = 1, c_2 = 1/2, g_{ym} = \sqrt{2}, \psi_{1L}(t,0) = 10^{-2}U(t) = \psi_{2L}(t,0)$, $\psi_{1L} = (0,z) = \psi_{2L}(0,z) = 0$.

Using the linearized approximation in h_+ and perturbed functions, the Eqs. (6.46 &

6.49) transforms to

$$i\,(\partial_0+\partial_3)\tilde{\psi}_{2L2}-\frac{g_{ym}}{2}U\tilde{\psi}_{2L2} = -\frac{g_{ym}}{2}h_+U\psi_{1L1}, \tag{6.50}$$

$$i\,(\partial_0-\partial_3)\tilde{\psi}_{1L1}-\frac{g_{ym}}{2}U\tilde{\psi}_{1L1} = -\frac{g_{ym}}{2}h_+U\psi_{2L2}. \tag{6.51}$$

One can see that in the linear order, the equations for the perturbations get decoupled, but still coupled to the other flavour of zeroth order. We obtained the numerical solutions for the above equations which are shown in Figs. (6.7 & 6.8).

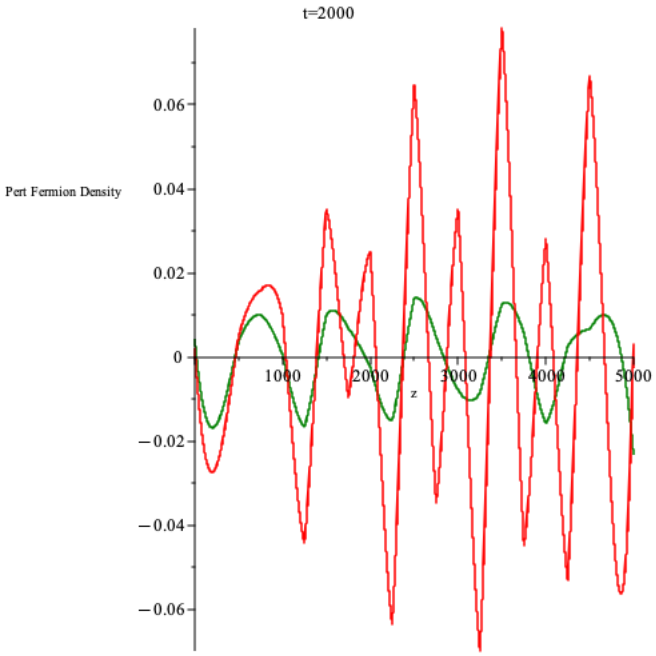

Figure 6.7: $\mathrm{Re}(\psi_{1L1}\tilde{\psi}^*_{1L1})$ in green and $\mathrm{Re}(\psi_{2L2}\tilde{\psi}^*_{2L2})$ in red plotted in z with $A_+ = 10^{-2}$ and $\omega_g = 1000$. We choose $c_1 = 1, c_2 = 1/2, g_{ym} = \sqrt{2}, \psi_{1L}(t,0)/2 = 10^{-2}U(t) = \psi_{2L}(t,0)$, $\psi_{1L} = (0,z) = \psi_{2L}(0,z) = 0$.

The fermion densities which have a form $\psi^*_{1L1}\tilde{\psi}_{1L1}+\tilde{\psi}^*_{1L1}\psi_{1L1}$ and $\psi^*_{2L2}\tilde{\psi}_{2L2}+\tilde{\psi}^*_{2L2}\psi_{2L2}$, flip at regular intervals both in space and time. In simple words, let us consider u and d quarks as a fermion doublet. If we have u quarks, then the interaction with a GW can change the flavour densities and increase the d quark probability density. This is due to the mixing of u and d quarks due to the presence of GW. This is clearly shown in Figs. (6.7 & 6.8). Note that in the above pictures, the fermion densities are allowed to be negative

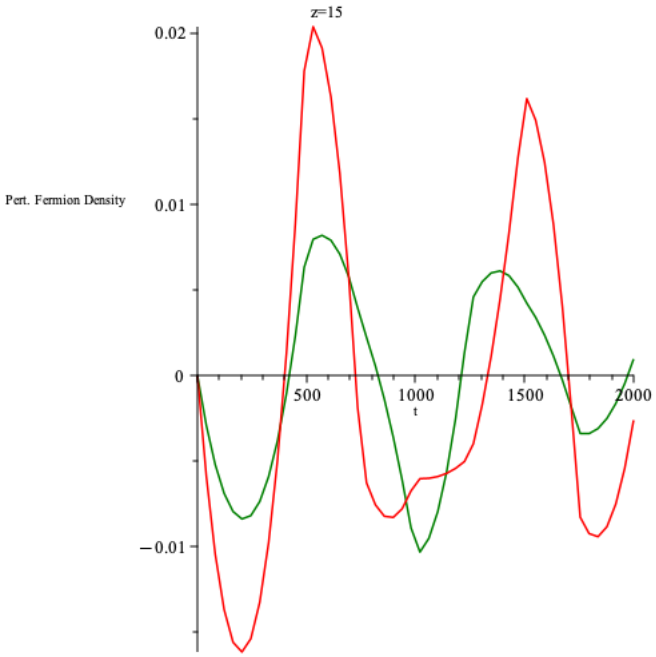

Figure 6.8: $\mathrm{Re}(\psi_{1L1}\tilde{\psi}^*_{1L1})$ in green and $\mathrm{Re}(\psi_{2L2}\tilde{\psi}^*_{2L2})$ in red as a function of time with $A_+ = 10^{-2}$ and $\omega_g = 1000$. We choose $c_1 = 1, c_2 = 1/2, g_{ym} = \sqrt{2}, \psi_{1L}(t,0)/2 = 10^{-2}U(t) = \psi_{2L}(t,0)$, $\psi_{1L} = (0,z) = \psi_{2L}(0,z) = 0$.

since they are over the zeroth order fermion densities. We have separated fluctuations in the flavour densities induced by GW since the GW is weaker in magnitude than the condensate. If we consider the condensate in a $SU(3)$ QGP system, then the GW will induce a transition of quarks which are coupled by the GW in a $SU(2)$ sub-group. This is an interesting result and has experimental consequences in relevance to both particle physics and GW physics.

6.3 Conclusion

In this chapter, we studied the dynamics of fermions in the presence of $SU(2)$ condensate in a flat background as well as in a GW background. At first, we studied the behaviour in Minkowski spacetime. We find there is a mixing of two different flavour fermion components. We found that the ψ_{1L1} & ψ_{2L2} (fermion with flavour 1, Left chirality, component 1; and fermion with flavour 2, left chirality and component 2) are decoupled and have separate evolution equations (Eqs. (6.10 & 6.13)), but, ψ_{1L2} & ψ_{2L1} (fermion with flavour 1, Left chirality, component 2; and fermion with flavour 2, left chirality and component 1) are

coupled to each other described by two coupled partial differential equations (Eqs. (6.11 & 6.12)). Even though there is a coupling of different types of fermions in the equations, their probability densities do not mix each other. This indicates if we start with a system with fermion 1 density greater than fermion 2 density, then at any later time, one can always find the system with fermion 1 density greater than fermion 2 density.

Next, we studied the backreaction of fermions on the condensate. We found that the isotropy of the condensate solutions gets broken with the introduction of fermions. We also found that the $a = 1,2$ & $i = 1,2$ components behave differently than the a or $i = 3$ components. It was expected that the gauge field configuration in the presence of fermions (like in QGP) is different than without fermions. It leads us to propose a new ansatz for the gluon field in QGP as $A^a_i = U(t)\delta^a_i + \tilde{A}^a_i,\ a,i = 1,2,\ \& A^3_3 = V(t)$. This kind of ansatz is relevant when studying the thermodynamics of QGP (chapter 7).

After this, we studied the dynamics of fermions in the presence of $SU(2)$ YM condensate in a GW background. We found no change in equations for ψ_{1L2} & ψ_{2L1}, which are still described by Eqs. (6.11 & 6.12). But, the ψ_{1L1} & ψ_{2L2} now become coupled with the interaction of GW as shown in Eqs. (6.46 & 6.49). We found that the fermion densities fluctuate in time exhibiting flavour transitions due to the GWs. It means that if we have two fermions of the same doublet, the fermion densities of those components flip at regular intervals. One can also interpret this as a transition of quarks transforming in the same $SU(2)$ subgroup in a $SU(3)$ plasma induced by GWs. Our calculations show the enhancement of one flavour over the other in the GW-induced interactions with a fermion doublet. But this enhancement is still oscillatory, thus one has to find the long term effects of this flavour flipping for any observable effects. The fermion doublets can also be lepton doublets or isospin doublets. In the case of QGP, the isospin doublets can be of (u,d) quarks or (c,s) quarks. This sort of flip in flavour fluxes can be used to generate strangeness observed in the QGP. Thus, this study of flavour flipping is very much relevant for QGP. These types of interaction vertices have been used to find the heavy flavour generation from the light quarks

in quantum field theories. In [204], it was studied that the form factors for $q\overline{q} \rightarrow s\bar{s}$ and $gg \rightarrow s\bar{s}$ were used to show the enhancement of strangeness. The GW-induced flavour transitions in our calculations represent the interaction vertices which have the same structure as three particle vertices used in [205]. We therefore expect the contribution of the above calculations to the strangeness generation to be a simple extension. Our calculations will definitely change the enhancement factors discussed in [204] for a QGP formed in heavy ion colliders. These classical field calculations have importance for deconfined YM fields and provide the basis for thermodynamic aspects of QGP found at high temperatures. We will be studying the thermodynamical description of QGP in the next chapter 7.

Part II

Thermodynamics of QGP

Chapter 7

Early Universe and Quark-Gluon Plasma

> "Physicists are made of atoms. A physicist is an attempt by an atom to understand itself."
>
> *Michio Kaku*

In the present state of the universe, the quarks and gluons cannot exist outside the hadrons since the temperatures are very low. The only places where we can have deconfined quarks and gluons are heavy ion colliders, the early universe, and quark stars (hypothetical stars with quarks inside). During the heavy ion collisions, the two heavy nuclei collide into each other, creating a mixture of quarks and gluons known as QGP, which exists for a very short amount of time. After that, the quarks and gluons combine to form hadrons through a process known as QCD Phase Transition. On the other hand, during the universe's evolution, the universe has passed through many stages, where one of the stages has the right conditions for the QGP to exist. We therefore expect the QGP to exist in the early Universe, and the hadrons were formed as the cosmos cooled down. In this chapter, we will study the thermodynamics of QGP and the QCD Phase Transition. To keep the content complete, we will start with a brief introduction to the history of the Universe.

In cosmology, we study the evolution of the universe based on cosmological models constructed on certain physics principles. With the inputs from the astrophysical and particle physics measurements, we improve the models. Out of many cosmological models,

we have converged to the standard model of Cosmology, the Big Bang Model. It states that the universe started expanding from an extremely dense and hot state, and continues to expand. However astrophysical observations suggest that the universe is made up of two unknown forms of energy and matter (apart from visible matter): Dark Matter and Dark Energy [206]. Now, the standard model of cosmology includes these two substances, along with visible matter, and is called the Lambda Cold Dark Matter (ΛCDM) model [207]. To understand further the early stage of the universe when it was very hot and dense, one needs to understand the particle interaction at high energy scales. As the universe expanded and cooled, the universe underwent many different cosmological phenomena. Here, we briefly explain the important phenomena that happened during the evolution (Table: 7.1) [15].

Table 7.1: Some of the important events during the evolution of the universe adapted from [15]

Events	Energy (GeV)	Time (s/yrs)	Temperature (K)
Big Bang	∞	0	∞
Planck scale	10^{19}	10^{-44}s	10^{32}
Grand Unification	10^{15}	10^{-37}s	10^{28}
Inflation, Lepton number violation			
EW symmetry breaking	10^{2}	10^{-10}s	10^{15}
QGP & QCD phase transition	10^{-1}	10^{-5}s	10^{12}
Neutrino decoupling	10^{-3}	1s	10^{10}
Big Bang Nucleosynthesis	10^{-4}	100s	10^{9}
Recombination (CMB)	2×10^{-10}	3×10^{5} yr	3000
Formation of large scale structure	10^{-12}	10^{9} yr	15
Present Universe	2.3×10^{-13}	13.7×10^{9}yr	2.73

The universe started with a big bang at all points in space and every point moved away from each other uniformly. When the universe cooled down to a temperature corresponding to the Planck's energy scale ($M_{Pl} \sim 10^{19}$GeV), the fundamental forces of nature which were unified before began to separate as gravity becomes weak. Before this time, the universe's evolution is determined by quantum gravity. As of now, we do not have a concrete theory of quantum gravity so we cannot extrapolate the results to the time before the Planck time. So, we usually discuss the processes that happened after Planck time.

As the universe expands and cools down further, it goes through many phase transitions. These phase transitions correspond to the some gauge symmetry breaking of the underlying theories. We will learn more about the phase transitions in the coming sections (Sec: 7.2). The first phase transition was related to the Grand Unified theory. In this epoch, the three fundamental forces (strong and weak nuclear forces, electromagnetic forces) were combined into a single unified force.

As the universe cooled down and reached an energy scale of 10^{10} GeV, many different phenomena happened. The main one was inflation, where the universe underwent a phase of exponential expansion. During the same time around, several phase transitions have taken place, such as left-right symmetry breaking, spontaneous parity violation, and supersymmetry breaking in the hidden sector. Another important phenomenon that happened is the lepton number violation, which generated a small asymmetry in the number density of matter and antimatter.

The next major event in cosmic evolution was the Electroweak phase transition, which happened around 100 GeV when the electroweak force got separated into electromagnetic and weak nuclear forces. The forces of the standard model started operating in their low-temperature form: the weak force carried by the massive W^+, W^-, and Z bosons, the electromagnetic force carried by the massless photons. Since the Higgs field acquired a nonzero expectation value, fermions acquired mass through a process known as spontaneous symmetry breaking. As the energy was still too high, the universe was filled with a mixture of familiar elementary particles, such as quarks and gluons, forming QGP.

After this, the universe underwent another phase transition, the QCD Phase transition at around $100-300$ MeV or around 10^{12} K, where the quarks and gluons combined to form hadrons (baryons and mesons). The QCD Phase transition also involved in symmetry breaking (Chiral symmetry breaking and $Z(3)$ center symmetry beraking), which we will discuss more in the coming sections (Sec: 7.2). As the weak gauge bosons become massive, the strength of weak interaction starts decreasing. At energies around 1 MeV, the neutrino's

interaction rate became smaller than the expansion rate, so the neutrinos became decoupled and formed a cosmic neutrino background.

The next major event in the evolution of the universe was the Big Bang Nucleosynthesis, which happened around the $\sim$ MeV scale. This is the process where light baryons – protons and neutrons – are bound into primordial atomic nuclei: hydrogen and helium. For a long time, the universe's temperature was too high to form atoms and the universe consisted of plasma of nuclei, electrons, and photons. During the recombination era, which happened around $18 - 370$ kyrs, the electrons and atomic nuclei bound to form neutral atoms. Due to the formation of atoms, the photons were no longer in thermal equilibrium with matter, and for the first time universe became transparent. As this era continued, the universe became more and more transparent, and the radiation decoupled from matter and formed a background. This radiation is the CMB radiation that we see today. These early universe phases set the stage for the further evolution of the universe into what we observe today, with galaxies, stars, and planets.

As we mentioned at the beginning of this chapter, we will mainly focus on the QGP and QCD phase transition. We will briefly introduce QGP and QCD Phase Transition in Sec. 7.1. Followed by a semi-classical analysis of Phase transitions in the Early Universe, in particular, QCD Phase Transition in Sec. 7.2. Later, we will study the QCD Phase transition in the presence of GWs using semi-classical analysis in Sec. 7.3. After that, we study the thermodynamics of QGP via full quantum analysis by finding the thermodynamic potential using finite temperature field theory in Sec. 7.4. Finally, we implement the thermodynamic potential for different backgrounds in Sec. 7.5, which includes the GW background.

7.1 Quark Gluon Plasma and QCD Phase Transition

Quarks and gluons are the building blocks of protons and neutrons, which in turn combine to form atomic nuclei. As far as we know, we cannot see the isolated quarks and gluons in the present low-energy scales. Quarks are the fermionic components and the gluons are

the force carriers mediating the interactions between the quarks. The gluons are the force carriers of the strong nuclear force. It is much stronger than the other three forces: gravity, weak nuclear, and electromagnetic forces. Since the strong nuclear force is very powerful, it makes it very difficult to separate quarks and gluons. In technical terms, we always see bound states of quarks and gluons due to a property called confinement. This is quite similar to decomposing the magnet into two in trying to isolate the north and south poles which does not happen.

The only place we can see the deconfined quarks and gluons is the QGP. In QGP, the temperature and energies are so high that the protons and neutrons become deconfined generating quarks and gluons. This mixture of quarks and gluons occupied the entire universe during the initial moments of the universe around 10^{-5} s. Now, scientists study this QGP at special facilities called heavy ion colliders, such as the LHC at CERN, and the RHIC at BNL. In the year 2000, CERN announced the circumstantial evidence for the existence of a new state of matter in Pb + Pb Collisions [208]. The actual discovery of the QGP happened in 2005 when four international collaborators investigated the Au + Au collisions at RHIC at BNL [209, 210]. To the surprise, the properties of this new matter varied differently from the predictions made over the years before the discovery. It was thought that the QGP should behave like a gas of free quarks and gluons, due to asymptotic freedom, at very high temperatures. However, the matter found at RHIC is found to be a highly interacting liquid [211, 212].

In general, the plasma is a state of matter consisting of charged particles and they interact via long-range gauge fields. The main difference one can find between plasmas and ideal gases is that the inter-particle distance between the particles is very low in plasmas [212]. The parameter that is needed to distinguish solids, liquids, and gases with plasmas is called the Plasma parameter (Γ), which is the ratio of interaction energy to kinetic energy [213]. In principle, a plasma is considered strongly interacting if $\Gamma > 1$. For the electromagnetic case, even though the $\Gamma > 1$ for certain materials, they are not exotic objects at all.

For example, table salt can be considered as a strong crystalline plasma made up of Na^+ and Cl^- ions. For QGP, it was found that $\Gamma_{QGP} = 1.5 - 6$ making it a strongly interacting one [214]. These are also characterized by their correlated behaviour, which measures the deviation from the usual ideal gas behaviour [215]. There is another parameter called shear viscosity-to-entropy density ratio (η/s), which characterizes how close the fluid is to perfect fluid [216]. It was found that the η/s is very small for QGP, smaller than any substance on Earth. The studies at LHC and RHIC show that the QGP behaves like a liquid with very small specific bulk and shear viscosity [217].

As the temperature drops down, the deconfined quarks and gluons combine to a bound state, called hadrons. The phase transition of QGP to hadronic matter is related to the symmetry breaking of the non-abelian gauge theory of strong interactions, which is QCD. Phase transition in QCD is related to two symmetry-breaking phenomena: one is the spontaneous symmetry breaking of the chiral symmetry of QCD [218] and the other one is the symmetry breaking of center symmetry [219, 220]. Even though QGP forms at very high temperatures, there is also a possibility of the existence of other exotic forms by increasing the degrees of freedom such as chemical potential (μ) and magnetic fields [221]. By considering μ, we will get a conjectured QCD Phase diagram in terms of temperature and quark chemical potential, as shown in Fig. (7.1) (suppressing magnetic fields). The quark chemical potential is a measure of the number of quark elements, and the higher the chemical potential, the higher the density of quarks.

As one can see from the picture in addition to QGP, there exist several phases of QCD matter [223, 224]. Ordinary atomic matter such as atomic nuclei exists as a low-temperature phase with high chemical potential. If we keep on increasing the quark density, then we reach a phase with more compressed nuclear matter such as in neutron stars. At ultra-high densities, it was conjectured that we would find the color-flavor-locked phase of color-superconducting quark matter [225]. Color superconductivity is analogous to conventional superconductors, instead, here the matter carries a color charge without loss. This kind of

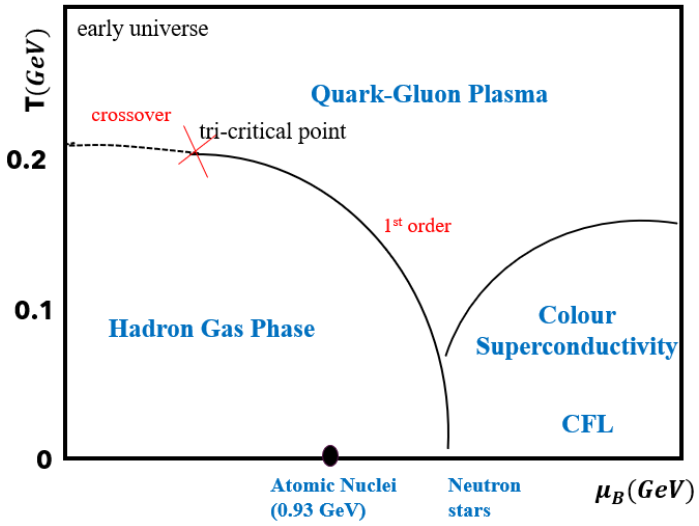

Figure 7.1: QCD phase diagram in terms of temperature (T) and baryon chemical potential (μ_B) adapted from [222]

phase is predicted to exist at ultra-high densities (above that of atomic matter and neutron stars) and low temperatures. The colour superconducting quark matter comes in many varieties because the quarks come in many species, i.e. each quark comes in three colours and there are 6 different quarks (usually 3 abundant ones). That gives various possible pairing patterns and is very hard to predict which ones are naturally favourable. In the limit of very high densities, the favoured phase in three-flavour quark matter is the color-flavour-locked phase [226–228]. It is a phase where quarks form Cooper pairs, whose flavour properties are correlated with their color properties in a one-to-one correspondence between three flavour pairs and three color pairs.

Now, consider moving along the temperature axis in the phase diagram. Consider a system with negligible chemical potential (with an equal amount of quarks and anti-quarks) and start heating the system, then the system moves vertically along the T axis in the phase diagram. Then, at about $T_{QCD} \sim 150 - 200$ MeV, the hadrons become deconfined giving rise to QGP. This kind of scenario probably happened in the early universe, where the universe began with almost negligible chemical potential (there was a slight preference for quarks over anti-quarks). In the figure, we also stated the current investigation results of the order

of phase transition. The approximate position of the critical point is also indicated in the figure.

For a complete description of the phase diagram, one needs to have a complete understanding of the strongly interacting gluonic and quark matter using the underlying theory, QCD. That requires the understanding of QCD in the non-perturbative regime, which is being investigated using sophisticated techniques like lattice gauge theory.

7.2 Study of phase transitions in Early Universe

Since we are about to discuss phase transitions, we will define what a phase transition is and how to classify the different types of phase transitions. A Phase transition is a transformation of a thermodynamic system from one state of matter or phase to another. The phase transition occurs due to external conditions such as temperature, pressure, magnetic fields, etc. During the phase transition, thermodynamic properties like free energy, of the medium change either smoothly or discontinuously, as a result of the change in external conditions. An order parameter is observable which is useful to distinguish between two phases. The order parameter varies from system to system. In most cases, the free energy is an order parameter. Depending on the behaviour of thermodynamic free energy [229], the phase transitions are classified into the following types:

- A **first order** phase transition is characterized by the discontinuity in the first derivative of thermodynamic free energy with respect to a thermodynamic variable like temperature. These phase transitions involve latent heat and the system either absorbs or releases a fixed amount of energy per volume. During the process, the temperature of the system remains constant and at the phase boundary, the system will be in a mixed-phase regime which means some parts of the system are in phase I while the other parts are in phase II. The familiar examples are the melting of ice or boiling of water.

- In the case of **second order** phase transitions, the free energy and its first derivative are continuous while the second derivative becomes discontinuous or diverges at critical temperature (T_c). In this case, a new phase grows continuously out of the previous phase. They are characterized by a divergent susceptibility, an infinite correlation length, and usually obey power law behaviour of form $(1-\frac{T}{T_c})^{\alpha}$, where α is critical exponent, at T_c. Examples are ferromagnetic transition, superconducting transition, and the superfluid transition.

- There is also a type of phase transition known as **Analytical Crossover**, where the free energy and all its derivatives are continuous at T_c. In this case, the system transforms smoothly from one phase to another.

As we discussed before, the QCD phase transition corresponds to two symmetry-breaking phenomena: Chiral symmetry breaking [230, 231] and $Z(3)$ Center symmetry breaking [219]. In the case of chiral symmetry breaking, we get chiral phase transition, while in the case of center symmetry breaking, we get confinement-deconfinement phase transition. The order parameter in the case of confinement-deconfinement transition is the Polyakov loop. The order parameter in the case of chiral phase transition is the chiral condensate, $<\overline{\psi}\psi>$. To be exact, the QCD system has $Z(3)$ symmetry only in the limit of infinitely heavy quarks or pure gauge sector, so the Polyakov loop will be an exact order parameter in the pure gauge sector. Similarly, the QCD has chiral symmetry in the chiral limit (zero mass quark limit), so the chiral condensate will be an exact order parameter only in the chiral limit. We describe the Polyakov loop in Sec. 3.1. The chiral condensate is the vacuum expectation of quark bilinear ($<\overline{\psi}\psi>$, ψ is the quark quantum field). In the case of the pure gauge sector of QCD where the Polyakov loop is the order parameter, it is found that the transition temperature is $\simeq 270$ MeV and the phase transition is of first order through lattice gauge theory calculations [232, 233]. In the case of the chiral limit of QCD where chiral condensate is the order parameter, it was found that the QCD phase transition follows the second order. The above two cases are limits of the physical scenario which

is the QCD system with small nonzero quark masses. In this case, the $Z(3)$ symmetry is explicitly broken by the presence of quarks and the chiral symmetry is explicitly broken by the nonzero quark masses [231]. It was found that in a system of dynamical quarks with physical masses, the QCD phase transition is an analytical crossover [234] with a transition temperature that is greater than that in the chiral limit and lower than that in the pure gauge limit [235, 236]. Even though the QCD Phase transition involves two symmetry-breaking phenomena, it was found that both occur at around the same temperature from the lattice gauge calculations.

The results discussed so far considered zero chemical potential. As we mentioned before, there are also other external parameters that affect the phase transition such as chemical potential, magnetic fields [221], etc. In the change of those external conditions, the order of phase transition also changes. There have been attempts to study the QCD phase diagram at finite chemical potential using lattice gauge calculations [237, 238]. Apart from non-perturbative techniques, there also have been studies using chiral effective models to investigate the unexplored regions of the phase diagram [239]. In Cosmology, the baryon asymmetry is very small $\eta_B = n_B/s \sim 10^{-9}$, with n_B as net baryon density and s as entropy density, as found out from the later stages in the evolution of the universe. Therefore, even in the early universe, it seems the QCD phase transition follows a smooth crossover. From the chiral effective models of QCD, it was found that at finite baryon densities, a first-order phase transition is possible for QCD phase transition [240]. There are also some scenarios where QCD phase transition can be of the first order in the early universe such as large baryon chemical potential [241], and lepton asymmetry [242]. In the case of the Early universe, there are also other parameters that affect the order of phase transition, such as the expansion of the universe, time scales, and gravitational waves.

The cosmological QCD phase transition has so much importance. Firstly, the QCD phase transition sets the initial conditions for one of the main phenomena in the early universe, the BBN. Depending on what type of phase transition happens, there will be a change

in the abundance of the first elements. For example, inhomogeneous BBN results in a higher abundance of certain elements when compared with homogeneous BBN [243]. Secondly, there will be after-effects of the QCD phase transition that can still be observable today [244]. Most of the relics are only formed if the QCD phase transition is of first order. Some of the relics include Strange Quark nuggets [244], QCD balls, black holes [245], small cold dark matter lumps [246] and gravitational waves [244]. The first-order phase transition happens via bubble nucleation [247, 248] with small supercooling [243, 244]. The bubbles were shown to grow mostly by weak deflagration [249, 250]. In the first-order phase transition, towards the end of phase transition during the coexistence of the QGP and hadron gas phases, the quark droplets that are shrinking remain intact. These quark droplets are called quark nuggets/ strangelets [244] which are thought to be candidates for dark matter. There is also a possibility of the generation of magnetic fields [251] and gravitational waves [244] in violent processes like bubble collisions. And, the most interesting aspect is the formation of planetary mass black holes during QCD phase transition.

The discussion in this section and the next one is based on assumption that the QCD phase transition follows a first-order phase transition [252, 253]. In a first-order QCD transition, the QGP supercools before the first bubbles of hadron gas forms. Under the consideration that the universe is homogeneous, the bubbles nucleate owing to the thermal fluctuations. This QCD phase transition can be explained using the homogeneous bubble nucleation theory as shown in Fig. (7.2). In our case, the high temperature to be of QGP phase and low temperature phase to be of hadronic phase. Above the critical temperature, only the QGP phase exists in the entire universe. After some amount of supercooling, the first hadronic bubbles/ droplets start forming at some time t_1 due to the statistical/thermal fluctuations. If the size of the droplet is too small to compensate for large surface free energy, then the droplet will evaporate owing to the positive total free energy. If the droplet size is large, then the surface free energy is irrelevant and the droplet will increase in size by accreting more hadrons. A bubble of critical size is metastable balancing between evapora-

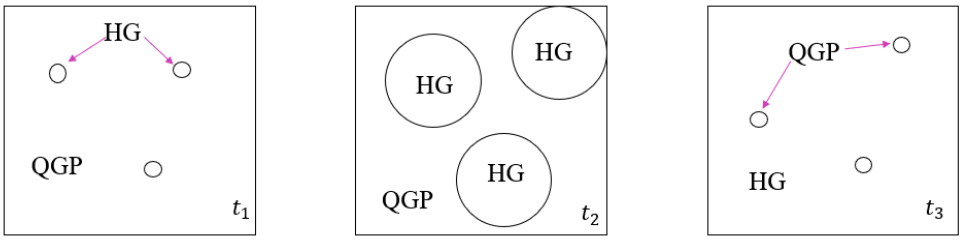

Figure 7.2: Process of QCD phase transition via homogeneous bubble nucleation adapted from [254]

tion and accretion. After some time $t_2 > t_1$, these hadronic bubbles slowly grow and release latent heat large enough to stop the formation of new hadronic bubbles. The processes such as supercooling, bubble formation and quenching take only 1% of the total transition time. During the remaining time, the bubbles slowly grow following the adiabatic expansion of the universe. Finally, the frame at t_3 shows the time almost at the end of the transition where the universe is covered almost entirely with the hadron gas phase.

One of the main parameters that have been calculated in the nucleation theory is the nucleation rate [252, 255]. The nucleation rate is the probability that a bubble of the second phase forms in the system filled with the first phase near the critical temperature (T_c). Consider the creation of a spherical bubble of radius R. The probability of forming a bubble by thermal fluctuation is proportional to $e^{\Delta F/T}$, where ΔF is the change in free energy for the creation of the bubble. The probability of an event occurring is proportional to the exponential of minus the free energy cost of the event over the thermal energy T. The change in free energy in creating the bubble is

$$\Delta F = \frac{4\pi}{3}(P_{QGP} - P_{HG})R^3 + 4\,\pi\,\sigma\,R^2. \tag{7.1}$$

where σ is the surface tension, P_{HG} is the pressure of the nucleating bubble/ hadronic bubble and P_{QGP} is the pressure of the QGP phase. As we discussed before, smaller bubbles disappear while large bubbles with a radius greater than the critical radius (R_c) can grow. The critical bubble radius is determined from the minimum value of the change in free

energy (ΔF) and is given by

$$R_c = \frac{2\sigma}{P_{HG} - P_{QGP}}. \tag{7.2}$$

One can recognize the above equation as Young-Laplace equation. Then, the free energy corresponding to the critical bubble radius is given by

$$\Delta F_c = \frac{4\pi}{3}\sigma\, R_c^2. \tag{7.3}$$

Finally, the nucleation rate or the probability of forming a hadronic bubble with a critical radius per unit time per unit volume is given by

$$I = I_0\, e^{-\Delta F_c/T}, \tag{7.4}$$

where I_0 is the prefactor calculated by various methods such as using the MIT bag model and coarse-grained effective field theory [253]. It depends on various factors such as the intrinsic properties of the liquid, the number of nucleation sites, the rate at which the molecules attach to the nucleus, and the probability that a critical-sized bubble will form a new phase rather than dissolve.

In the coexisting phase, the universe's temperature is almost constant at T_c. It is because the cooling due to expansion is compensated by the latent heat generated by the hadronic bubbles. Then, the equation of the state of fluid is given by

$$P \sim V^{-1}, \tag{7.5}$$

where P is the pressure of hadronic bubble i.e. $P \equiv P_{HG}$ and V is the volume of the hadronic bubble. If one considers a curved background instead of a flat background, the volume of the bubble changes. Using this idea, we are going to study the effect of GWs on the volume which in turn affects nucleation rate.

7.3 Gravitational Wave influence on QCD phase transition

As discussed in the previous section, the phase transition of matter from one phase to another is driven by the nucleation and subsequent growth of bubbles/ droplets in the case of first-order phase transition. In the early universe, this kind of phase change might have happened when the temperature was low enough to initiate the phase change from the primordial QGP to the hadron gas phase. The main gravitational effect that causes this phase change is the radiation-dominated expansion of the universe which makes the pressure and energy density fall below and initiate the bubble nucleation process. As the inflationary theory predicts the existence of the PGWs [106, 107], they exist and interact with all kinds of cosmological phenomena happening in the early universe.

We are interested in the influence of PGWs in the QCD phase transition which happened around $t \sim 10^{-5}$s after the Big Bang at an energy scale of around $T \sim 200$ MeV. We consider the effect of GW in the radiation-dominated universe on a homogeneous fluid of primordial QGP. For simplicity, we consider a single mode of a $+$-polarized GW propagating in the z-direction in this radiation-dominated universe. For this, the metric is given by

$$g_{\mu\nu} = a^2(\tau)(\eta_{\mu\nu} + h_{\mu\nu}), \tag{7.6}$$

where $\eta = \text{diag}(-1,1,1,1)$ is the Minkowski metric and the $h_{\mu\nu} = \text{diag}(0, h_+(\tau,z), -h_+(\tau,z), 0)$ where the h_+ is given in Chapter 2 as follows $h_+(\tau,z) = h(k,\tau)e^{ikz}$ where

$$h(k,\tau) = \frac{a(\tau_1)}{a(\tau)}\left[\alpha(k,\tau_1)e^{-ik(\tau-\tau_1)} + \beta(k,\tau_1)e^{ik(\tau-\tau_1)}\right], \tag{7.7}$$

where τ_1 is the de Sitter - radiation equality conformal time, and α and β are given by

$$\alpha(k,\tau_1) = 1 + \frac{i}{k\tau_1} - \frac{1}{2k^2\tau_1^2}, \tag{7.8}$$

$$\beta(k,\tau_1) = \frac{1}{2k^2\tau_1^2}. \tag{7.9}$$

From the above expressions, one can find the real part of h_+ as

$$Re(h_+(\tau,z)) = A(k,\tau_1)\cos(kz) + B(k,\tau_1)\sin(kz), \tag{7.10}$$

where

$$A(k,\tau_1) = \frac{a(\tau_1)}{a(\tau)}\left(\cos(k(\tau-\tau_1)) + \frac{1}{k\tau_1}\sin(k(\tau-\tau_1))\right),$$
$$B(k,\tau_1) = \frac{a(\tau_1)}{a(\tau)}\left(\frac{1}{k\tau_1}\cos(k(\tau-\tau_1)) + \left(1-\frac{1}{k^2\tau_1^2}\right)\sin(k(\tau-\tau_1))\right).$$

Now, we consider a box-like region with lengths L_x, L_y and L_z. Then, the volume of such a region is given by

$$V(\tau) = \int \sqrt{-g}\, dV = \int_0^{L_x}\int_0^{L_y}\int_0^{L_z} \sqrt{-g}\, dx\, dy\, dz, \tag{7.11}$$

where g is the determinant of the metric, which has a value $g = a^8(\tau)(1-h_+^2)$, Then, using the binomial expansion of the determinant term, the volume can be evaluated as

$$V(\tau) \approx a(\tau)^4 \int_0^{L_x}\int_0^{L_y}\int_0^{L_z}(1-\frac{1}{2}Re(h_+)^2)dxdydz, \tag{7.12}$$
$$\approx a(\tau)^4 L_x L_y L_z \left[1-\frac{1}{4}(A^2+B^2)\right], \tag{7.13}$$

where we considered only the terms up to the first order (neglecting terms with k dependence) and the term $L_xL_yL_z$ is identified with volume in flat spacetime. If we consider a spherical volume, we also get the same kind of expression up to a first-order. The volume correction is given by

$$V_{GW} = a(\tau)^4 V_M \left[1-\frac{1}{4}(A^2+B^2),\right] \tag{7.14}$$

where V_M is the volume in the absence of a GW. We are considering only the effect of GW

in modulating the volume occupied by the fluid. Then, the pressure modulation is given by

$$P_{GW} = \frac{P_M}{a(\tau)^4(1-(A^2+B^2)/4)}, \tag{7.15}$$

where $P_M \approx V_M^{-1}$ is the pressure of the bubble without GW. P_{GW} gives the pressure inside the hadronic bubble in the presence of a GW. As discussed before, the change in free energy for the formation of a hadronic bubble of radius R is

$$\Delta F_{GW} = \frac{4\pi}{3}(P_{QGP} - P_{GW})R^3 + 4\pi\,\sigma\,R^2. \tag{7.16}$$

Then, the free energy of a critical-sized bubble is

$$\Delta F_{c,GW} = \frac{4\pi}{3}\sigma R_{c,GW}^2, \text{with } R_{c,GW} = \frac{2\sigma}{P_{GW} - P_{QGP}}, \tag{7.17}$$

and the nucleation rate is

$$I_{GW} \propto e^{-\Delta F_{c,GW}/T}. \tag{7.18}$$

Comparing the probability of the formation of a critically sized bubble in the presence of GW to their absence, we get

$$\frac{I_{GW}}{I_M} = \exp[(\Delta F_{c,M} - \Delta F_{c,GW})/T], \tag{7.19}$$

$$= \exp\left[\frac{1}{T}\frac{4\pi}{3}\sigma(R_{c,M}^2 - R_{c,GW}^2)\right], \tag{7.20}$$

where $R_{c,M} = \frac{2\sigma}{P_M - P_{QGP}}$ and $R_{c,GW}$ is given by Eq (7.17). From the expression for volume, it is clear that $A^2 + B^2 > 0$. From this, we also get $P_{GW} > P_M$ and $R_{c,GW} < R_{c,M}$ and finally, we get $I_{GW} > I_M$.

This shows that the nucleation rate will be higher in the presence of GW. It means the probability of the formation of a hadronic bubble in the presence of GWs is higher than in their absence. The number of bubbles nucleated per time will be greater, causing the phase

change to occur sooner.

Our analysis was similar to the laboratory-based bubble chamber experiments. When high-energy particles interact with atomic nuclei in a fluid, a localized rise in temperature happens, which starts the bubble formation process in bubble chamber experiments. In our case, we are considering volume modulations due to GWs driving the nucleation rates. In the regions of the lowered volume, the energy barrier for the bubble nucleation is lowered along with the critical bubble size, which causes the nucleation rates to increase, allowing the phase transition to occur earlier.

This kind of effect of GWs is different from that studied in the interferometers. Also, the above analysis is based on some poorly understood parameters of QGP like the surface tension of QGP (σ), and the equilibrium pressure of QGP (P_{QGP}). The equilibrium pressure of the QGP is temperature dependent as well as on the other fluid parameters of the QGP. To understand more about the thermodynamic properties of the QGP, we studied the entire system using finite temperature field theory in the coming sections.

7.4 Thermodynamics of Quark Gluon Plasma

Finite temperature field theory

QFT is a theoretical framework that is used in many areas of physics such as particle physics, condensed matter physics, and combines classical field theory, quantum mechanics, and special relativity [30]. The usual quantum field theory describes the quantum fields and their interaction via gauge fields at absolute zero temperature ($T = 0$) and negligible system densities. Using zero temperature QFT, many predictions have been made and were verified experimentally which indicates the $T = 0$ QFT is mostly sufficient. It was not surprising given that the finite temperature effects become significant only when the thermal energy of the system ($k_B T$) is of the order of the magnitude of the masses of the fields. For example, for electrons, the finite temperature effects are important at a temperature of order $T \sim 10^{10} K$. Similarly, for protons, it is at order $T \sim 10^{13} K$. These kinds of tempera-

tures are usually beyond the regions of accessibility in daily life. However, there are some exceptions like the heavy ion colliders such as LHC at CERN and RHIC at BNL, where relativistic experiments have been carried out to study the QGP and the resulting matter. In those cases, one needs to consider the finite temperature effects to understand the QGP [256].

Apart from particle and nuclear physics, the finite temperature effects are important for astrophysical and cosmological phenomena. As we discussed in the previous sections, during the early universe, when the temperatures were going down, the universe had to undergo several phase transitions such as EW phase transition, and QCD phase transition, in different epochs. In the case of astrophysics, for neutron stars, the finite density and finite temperature effects play a vital role in understanding the dynamics of the system.

The principal idea of the finite temperature QFT is to combine the ideas of statistical mechanics with the quantum field theory. As we can see later, there are some similarities between the statistical mechanics and QFT. To incorporate finite temperature effects, one needs to find a way to include the temperature in QFT. There are many ways to do that such as imaginary time formalism [257], real time formalism [257, 258], and thermo-field dynamics [259]. In our case, we will be dealing with imaginary time formalism.

Partition function

We will start with deriving the most important quantity when dealing with many body systems and thermodynamic systems which is the partition function, $Z = \mathrm{Tr}\, e^{-\beta \mathrm{H}}$ where $\beta = 1/k_B T$ is a function of temperature T and Boltzmann's constant k_B, H is the Hamiltonian of the system, and the trace is over all the states of the system. The complete dynamics and thermodynamic behaviour of the system such as pressure, energy density, specific heat capacitance, etc, can be determined from the partition function Z by differentiating Z by variables such as volume, temperature, etc. The methods discussing the field theory at finite temperature in this subsection follow those of [260].

Consider a general field $\phi(\vec{x},t)$ in the Heisenberg picture and along with its conjugate momentum field $\pi(\vec{x},t)$ and the Hamiltonian density $\mathcal{H}(\pi,\phi)$. The general field can be of any type such as scalar, vector, and spinor. The transition amplitude from the initial state $\langle\phi_0|$ at initial time $t=0$ to the final state $\langle\phi_1|$ at final time $t=t_1$ is given in terms of Feynman functional as

$$\langle\phi_1|e^{-iHt_1}|\phi_0\rangle = N\int \mathcal{D}\pi\ \mathcal{D}\phi\ \exp\Big\{i\int_{t_0}^{t_1} dt\int d^3x\,[\pi\,\partial_t\phi - \mathcal{H}(\pi,\phi)]\Big\}, \tag{7.21}$$

where $\langle\phi_0|$, $\langle\phi_1|$ are the eigenstates of the Schrodinger field function $\phi(\vec{x},0)$, the integral over the momentum fields $\int\mathcal{D}\pi$ is unrestricted while the integral over the classical fields $\int\mathcal{D}\phi$ is restricted to the fields with the following configurations:

$$\phi_0(\vec{x}) \text{ at } t=0, \text{ and } \phi_1(\vec{x}) \text{ at } t=t_1, \tag{7.22}$$

and N is a normalisation constant. To incorporate finite temperature effects, one performs a change of variable

$$t = -i\,\tau, \tag{7.23}$$

and sets the time period in imaginary time as $it_1=\beta$, where $\beta=1/T$, T is the temperature (We set $k_B=1$). This variable change is well known as Wick rotation which converts the theory from Minkowski spacetime to Euclidean spacetime. Then, the transition amplitude becomes

$$\langle\phi_1|e^{-\beta H}|\phi_0\rangle = N\int \mathcal{D}\pi\ \mathcal{D}\phi\ \exp\Big\{i\int_0^{\beta} d\tau\int d^3x\,[i\,\pi\,\partial_\tau\phi - \mathcal{H}(\pi,\phi)]\Big\}. \tag{7.24}$$

Now, considering the field integration $\int\mathcal{D}\phi$ only over those periodic fields in time intervals, i.e. $\phi(\vec{x},0)=\phi(\vec{x},\beta)$, the partition function then becomes

$$\text{Tr}\ e^{-\beta H} = \sum_{\phi}\langle\phi|e^{-\beta H}|\phi\rangle \tag{7.25}$$

$$= N \int \mathcal{D}\pi \int_{\text{periodic}} \mathcal{D}\phi \, \exp\Big\{ i \int_0^\beta d\tau \int d^3x \, [i \, \pi \, \partial_\tau \phi - \mathcal{H}(\pi, \phi)] \Big\}. \tag{7.26}$$

In most cases, it is more advantageous to deal with Lagrangian density than the Hamiltonian density. To convert from Hamiltonian to effective Lagrangian formalism, one needs to perform the π integration in the partition function, Z. After doing the integrations, the partition function becomes

$$Z = N'(\beta) \int_{\text{periodic}} \mathcal{D}\phi \, \exp\Big\{ \int_0^\beta d\tau \int d^3x \, \mathcal{L} \Big\}, \tag{7.27}$$

where $\mathcal{L}$ is the effective Lagrangian and the $N'(\beta)$ is the new normalization constant dependent on temperature coming from the π integration. Usually, this normalization constant N' is infinite which has the same behaviour as the occurrences of infinite normalization constants in zero-temperature QFT.

Review on Functional methods

Before discussing the evaluation of the thermodynamic potential/ partition function, we will cover some basics of the functional methods [30, 261]. Effective action in QFT is the generating functional which contains all the information about the quantum system. For a system with classical action $S[\phi]$, the general generating functional is defined as

$$Z[J] = e^{-W[J]} = \int \mathcal{D}\phi \, e^{-S[\phi] - \int d^4x \, \phi(x) J(x)}. \tag{7.28}$$

The above functional is used to obtain different correlation functions thus called the generating functional and $W[J]$ is the generating functional for the connected green functions. The lowest correlation function is the mean-field/ classical field ϕ_{cl}, given by

$$\phi_{cl}(x) \equiv \langle \phi(x) \rangle = \frac{\delta W}{\delta J(x)}. \tag{7.29}$$

In analogy with thermodynamics, one can define the Legendre transform of $W[J]$:

$$\Gamma[\phi_{cl}] \equiv W[J] - \int d^4x\, \phi_{cl}(x) J(x). \tag{7.30}$$

The above quantity $\Gamma[\phi_{cl}]$ is called the effective action and is used to generate the quantum equations of motion,

$$\frac{\delta\Gamma[\phi_{cl}]}{\delta\phi_{cl}(x)} = -J(x). \tag{7.31}$$

The above equations are quantum generalizations of the classical field, classical action, and classical equations of motion. With this redefinition, we can rewrite the generating functional as

$$e^{-\Gamma[\phi_{cl}]} = \int \mathcal{D}\phi\ \exp\left\{ -S[\phi] + \int d^4x\, (\phi(x) - \phi_{cl}(x)) \frac{\delta\Gamma[\phi_{cl}]}{\delta\phi_{cl}(x)} \right\}, \tag{7.32}$$

to get a integro-differential equation for $\Gamma[\phi_{cl}]$. The semi-classical expansion of the effective action is obtained by the saddle point approximation of the integral at $\phi = \phi_{cl}$,

$$\Gamma[\phi_{cl}] = S[\phi_{cl}] + \Gamma_{1-loop}[\phi_{cl}] + \Gamma_{2-loop}[\phi_{cl}] + ..., \tag{7.33}$$

where the first term corresponds to the classical action and the next terms correspond to the quantum corrections to the classical action. The first quantum correction reads as the functional determinant of an operator (F) of the second functional derivative of the classical action given by

$$\Gamma_{1-loop} = \frac{1}{2} \ln\det F = \frac{1}{2} \mathrm{Tr}\ \ln F, \tag{7.34}$$

$$F\delta(x,y) = \frac{\delta^2 S}{\delta\phi(x)\ \delta\phi(y)}, \tag{7.35}$$

and the second quantum contribution is given by

$$\Gamma_{2-loop} = \frac{1}{8}\int dx_1 dx_2 dx_3 dx_4 G(x_1,x_2)\frac{\delta^4 S[\phi]}{\delta\phi(x_1)\,\delta\phi(x_2)\,\delta\phi(x_3)\,\delta\phi(x_4)}G(x_3,x_4)$$
$$+\frac{1}{12}\int dx_1 dx_2 dx_3 dy_1 dy_2 dy_3 \frac{\delta^3 S[\phi]}{\delta\phi(x_1)\,\delta\phi(x_2)\,\delta\phi(x_3)}G(x_1,y_1)G(x_2,y_2)G(x_3,y_3)\frac{\delta^3 S[\phi]}{\delta\phi(y_1)\,\delta\phi(y_2)\,\delta\phi(y_3)}, \tag{7.36}$$

where $G(x,y)$ is the Green's function of F,

$$F\ G(x,y) = -\delta(x,y). \tag{7.37}$$

Graphically, the quantum corrections correspond to the following 1-loop and 2-loop Feynman diagrams.

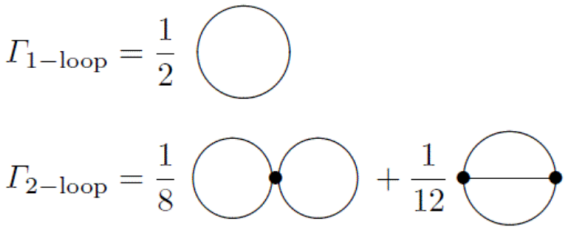

Figure 7.3: Feynman diagrams for Γ_{1-loop} and Γ_{2-loop}

Thus, by finding the effective action, we can find all the other correlation functions of the system. The functional differentiation of $\Gamma[\phi_{cl}]$ with respect to ϕ_{cl} gives the effective equations of motion and all necessary correlation functions on its background. As one can see, the 1-loop effective action is given by the functional determinants of an operator.

Generating functional for QCD

To evaluate this, we first need to know the true generating functional for the QCD. As QCD is a gauge theory, extra care has to be taken in dealing with the gauge field configurations. Since the gauge theories have gauge symmetry, the gauge fields will have some configurations that make the functional integral badly defined. To explain how to deal with gauge theories, we go back to the zero-temperature QFT. We will give an overview on dealing with gauge theories following [30].

To make the analysis simple, we deal with the pure non-Abelian Yang-Mills theory in Minkowski spacetime. Consider the following functional integral,

$$Z = \int \mathcal{D}A \; e^{i\,S[A]}, \quad S[A] = \int d^4x \left(-\frac{1}{4g_{ym}^2} F^{a\mu\nu} F^a_{\mu\nu} \right), \tag{7.38}$$

with $F^a_{\mu\nu} = \partial_\mu A^a_\nu - \partial_\nu A^a_\mu + f^{abc} A^b_\mu A^c_\nu$, where A^a_μ is the gauge field and f^{abc} are the structure constants. As we mentioned before, due to the gauge invariance, there will be several cases of physically equivalent field configurations. The Lagrangian is invariant under the gauge transformations of form,

$$A^a_\mu \to A'^a_\mu = A^a_\mu + \frac{1}{g_{ym}} \partial_\mu \alpha^a + f^{abc} A^b_\mu \alpha^c, \tag{7.39}$$

$$= A^a_\mu + \frac{1}{g_{ym}} \hat{\nabla}_\mu \alpha^a, \tag{7.40}$$

where $\hat{\nabla}_\mu$ is the gauge covariant derivative in the adjoint representation. It means $A^a_\mu(x)$ and $A'^a_\mu(x)$ are physically equivalent. The field modes of which $A^a_\mu = \frac{1}{g_{ym}} \hat{\nabla}_\mu \alpha^a(x)$ are gauge equivalent to the fields $A^a_\mu = 0$. Because of the integration of these modes, the functional integral becomes badly defined. To fix the problem, one has to choose the gauge that makes it possible to count each physical configuration only once. This is possible with the help of a trick done by Faddeev and Popov [262]. According to this, we constrain the gauge directions by applying a gauge-fixing condition, $G(A) = 0$. To impose this constraint, we introduce the following identity into the functional integral

$$1 = \int \mathcal{D}\alpha \; \delta(G(A^\alpha)) \det \left(\frac{\delta G(A^\alpha)}{\delta \alpha} \right), \tag{7.41}$$

where A^α is the gauge field A transformed as in 7.39. With this, the functional integral becomes

$$Z = \int \mathcal{D}\alpha \int \mathcal{D}A \; e^{iS[A]} \delta(G(A^\alpha)) \det \left(\frac{\delta G(A^\alpha)}{\delta \alpha} \right). \tag{7.42}$$

We choose a generalized Lorentz gauge condition:

$$G(A) = \partial^\mu A^a_\mu(x) - w^a(x), \tag{7.43}$$

where $w^a(x)$ are arbitrary scalar functions. Then, the determinant is given by

$$\det\left(\frac{\delta G(A^\alpha)}{\delta\alpha}\right) = \det\left(\frac{1}{g_{ym}}\partial^\mu\hat{\nabla}_\mu\right). \tag{7.44}$$

One can also represent the determinant as a functional integral over a new set of anti-commuting fields as

$$\det\left(\frac{1}{g_{ym}}\partial^\mu\hat{\nabla}_\mu\right) = \int \mathcal{D}c\mathcal{D}\bar{c}\; e^{i\int d^4x\bar{c}(-\partial^\mu\hat{\nabla}_\mu)c}. \tag{7.45}$$

where the factor of $1/g_{ym}$ is absorbed into normalization of the fields c and $\bar{c}$. With this, one gets a new term in $\mathcal{L}$ as ghost Lagrangian:

$$\mathcal{L}_{ghost} = \bar{c}(-\partial^\mu\hat{\nabla}_\mu)c, \tag{7.46}$$

Then, the functional integral becomes

$$Z = \int \mathcal{D}\alpha \int \mathcal{D}A\; \mathcal{D}c\mathcal{D}\bar{c}\; e^{iS[A]}e^{i\int d^4x\bar{c}(-\partial^\mu\hat{\nabla}_\mu)c}\delta(G(A^\alpha)). \tag{7.47}$$

One can see from the functional integral that there is still a free parameter function $w^a(x)$. Finally, we will integrate overall $w^a(x)$ with a Gaussian weight centered on $w^a = 0$ to get

$$Z = \int \mathcal{D}\alpha \int \mathcal{D}A\; \mathcal{D}c\mathcal{D}\bar{c}\; e^{iS[A]}e^{i\int d^4x\bar{c}(-\partial^\mu\hat{\nabla}_\mu)c}e^{-i\int d^4x\frac{1}{2\xi g_{ym}^2}(\partial^\mu A^a_\mu)^2}. \tag{7.48}$$

This is the final form of the generating functional. Now including the fermions, the final

Lagrangian for the QCD is given by

$$\mathcal{L}_{QCD} = -\frac{1}{4g_{ym}^2} F^{a\mu\nu}F^a_{\mu\nu} - \frac{1}{2\xi g_{ym}^2}(\partial^\mu A^a_\mu)^2 + \bar{c}(-\partial^\mu \hat{\nabla}_\mu)c + \overline{\psi}(i\gamma^\mu \nabla_\mu - m)\psi. \tag{7.49}$$

where ∇_μ is the gauge covariant derivative in fundamental representation.

7.4.1 Derivation of 1-loop effective action

Now, that we know the exact Lagrangian of the QCD, we will derive the 1-loop effective action. To do that, we use a technique called the Background Field Method () [51, 263]. It is a technique for quantizing gauge field theories without losing explicit gauge invariance. This method makes the gauge theories' computations much easier and easily understandable. We start with the bare Lagrangian of QCD in Euclidean spacetime [264]

$$\mathcal{L}_{QCD} = -\frac{1}{4g_0^2} F^{a\mu\nu}F^a_{\mu\nu} + \overline{\psi}(i\gamma^\mu \nabla_\mu - m)\psi, \tag{7.50}$$

with

$$F^{a\mu\nu} = \partial_\mu A^a_\nu - \partial_\nu A^a_\mu + f^{abc}A^b_\mu A^c_\nu, \tag{7.51}$$

$$\nabla_\mu = \partial_\mu + A_\mu = \partial_\mu + T^a A^a_\mu, \tag{7.52}$$

where $g_0 \equiv g_{ym}$ is the bare YM coupling constant, ∇_μ is the gauge covariant derivative in fundamental representation and T^a are the generators of the Lie group. In the BFM, we split the gauge field into a classical background field and a fluctuating quantum field:

$$A^a_\mu \to A^a_\mu + \tilde{A}^a_\mu. \tag{7.53}$$

Here, we will treat the classical field A^a_μ as a fixed field configuration and the fluctuating quantum part $\tilde{A}^a_\mu$ as an integration variable of the functional integral. With this, the Yang-

Mills field strength becomes as

$$\begin{aligned} F^a_{\mu\nu} \rightarrow & \partial_\mu A^a_\nu - \partial_\nu A^a_\mu + f^{abc} A^b_\mu A^c_\nu + \partial_\mu \tilde{A}^a_\nu - \partial_\nu \tilde{A}^a_\mu + f^{abc} \tilde{A}^b_\mu \tilde{A}^c_\nu + f^{abc}(A^b_\mu \tilde{A}^c_\nu - A^b_\nu \tilde{A}^c_\mu) \\ = & F^a_{\mu\nu} + \hat{\nabla}_\mu \tilde{A}^a_\nu - \hat{\nabla}_\nu \tilde{A}^a_\mu + f^{abc} \tilde{A}^b_\mu \tilde{A}^c_\nu, \end{aligned} \tag{7.54}$$

where $F^a_{\mu\nu}$ is the field strength of classical field A^a_μ and $\hat{\nabla}_\mu$ is the gauge covariant derivative in adjoint representation given as

$$\hat{\nabla}_\mu \tilde{A}^a_\nu \equiv \nabla^{ab}_\mu \tilde{A}^b_\nu, \text{ where } \nabla^{ab}_\mu = \delta^{ab}\partial_\mu + f^{acb} A^c_\mu. \tag{7.55}$$

Then, the fermionic part of Lagrangian will also change to

$$\overline{\psi}\, \gamma^\mu\, \nabla_\mu\, \psi \rightarrow \overline{\psi}\, \gamma^\mu\, \nabla_\mu\, \psi + \overline{\psi}\, \gamma^\mu\, \tilde{A}_\mu\, \psi. \tag{7.56}$$

Now the covariant derivatives are with respect to the fixed classical background field A^a_μ. If the classical field is fixed, then the Lagrangian has a local gauge symmetry according to the following transformations on $\tilde{A}^a_\mu$:

$$\tilde{A}^a_\mu \rightarrow \tilde{A}^a_\mu + \hat{\nabla}_\mu \alpha^a + f^{abc} \tilde{A}^b_\mu \alpha^c. \tag{7.57}$$

As we mentioned, one needs to fix the gauge to define the functional integral. For that, we use the Faddeev-Popov procedure. We choose a gauge-fixing condition which is covariant with respect to the background field:

$$G^a(A) = \hat{\nabla}^\mu \tilde{A}^a_\mu - w^a. \tag{7.58}$$

We use the same tricks as before to get the Faddeev-Popov determinant which generates an additional term in the Lagrangian as

$$\mathcal{L}_{FP} = \overline{c}^a(-\hat{\nabla}^2)^{ab}c^b, \tag{7.59}$$

where $(\hat{\nabla}^2)^{ab} \equiv (\hat{\nabla}^\mu\hat{\nabla}_\mu)^{ab} = \hat{\nabla}^{\mu ac}\hat{\nabla}_\mu^{cb}$. As we discussed before, we also have an additional gauge-fixing term in the Lagrangian with respect to the chosen gauge-fixing condition. The gauge fixing term in the Lagrangian is given by

$$\mathcal{L}_{GF} = -\frac{1}{2\xi g_0^2}(\hat{\nabla}^\mu\tilde{A}_\mu^a)^2. \tag{7.60}$$

where ξ is the gauge parameter. For the rest of our calculations, we choose $\xi = 1$ which is the Feynman-t' Hooft gauge. Then, the gauge-fixed QCD Lagrangian is

$$\mathcal{L} = \mathcal{L}_{YM} + \mathcal{L}_{FP} + \mathcal{L}_{GF} + \mathcal{L}_F, \tag{7.61}$$

where

$$\mathcal{L}_{YM} = -\frac{1}{4g_0^2}\left(F_{\mu\nu}^a + \hat{\nabla}_\mu\tilde{A}_\nu^a - \hat{\nabla}_\nu\tilde{A}_\mu^a + f^{abc}\tilde{A}_\mu^b\tilde{A}_\nu^c\right)^2, \tag{7.62}$$

$$\mathcal{L}_{FP} = \overline{c}^a(-\hat{\nabla}^2)^{ab}c^b, \tag{7.63}$$

$$\mathcal{L}_{GF} = -\frac{1}{2g_0^2}(\hat{\nabla}^\mu\tilde{A}_\mu^a)^2, \tag{7.64}$$

$$\mathcal{L}_F = \overline{\psi}\,\gamma^\mu\,\nabla_\mu\,\psi + \overline{\psi}\,\gamma^\mu\,\tilde{A}_\mu\,\psi. \tag{7.65}$$

Now come to the calculation of effective action to one-loop order. First, we will write the generating functional as

$$Z[A, j, \eta, \overline{\eta}] = \int \mathcal{D}a\;\mathcal{D}\psi\;\mathcal{D}\overline{\psi}\;\mathcal{D}c\;\mathcal{D}\overline{c}\;e^{\int d^4x(\mathcal{L} + j_\mu^a a_\mu^a + \overline{\psi}\eta + \psi\overline{\eta})}, \tag{7.66}$$

where $\mathcal{L}$ is given in 7.61. We keep only the terms quadratic in fluctuations because the terms linear in the fluctuating field $\tilde{A}^a_\mu$ become zero due to the equations of motion of background gauge field A^a_μ . The quadratic terms in $\tilde{A}^a_\mu$ coming from the Yang-Mills Lagrangian combined with the gauge fixing term are

$$\mathcal{L}^{(2)}_g = \frac{1}{2g_0^2} a^a_\mu \left(\delta_{\mu\nu} (\nabla^2)^{ab} + 2 f^{acb} F^c_{\mu\nu} \right) a^b_\nu = \frac{1}{2g_0^2} a_\mu \left(\delta_{\mu\nu} \hat{\nabla}^2 + 2\hat{F}_{\mu\nu} \right) a_\nu, \tag{7.67}$$

where we write in the shorthand notation by suppressing color indices. The ghost field Lagrangian is already quadratic in fluctuations as

$$\mathcal{L}^{(2)}_{FP} = \overline{c}^a (\nabla^2)^{ab} c^b = \overline{c} \hat{\nabla}^2 c, \tag{7.68}$$

Finally, the quadratic terms in fermion Lagrangian are

$$\mathcal{L}^{(2)}_q = \sum_{i=1}^{N_f} \overline{\psi}_i (\gamma^\mu \nabla_\mu) \psi_i. \tag{7.69}$$

Then, after doing all Gaussian integrations (E.2), we end up with the following generating functional:

$$Z[A] = e^{-\frac{1}{4g_0^2} \int d^4x \, F^a_{\mu\nu} F^a_{\mu\nu}} \left[\mathrm{Det}(-\hat{\nabla}^2 \delta_{\mu\nu} - 2\hat{F}_{\mu\nu}) \right]^{-1/2} \left[\mathrm{Det}(-\hat{\nabla}^2) \right] \prod_{i=1}^{N_f} \mathrm{Det} \left[\gamma_\mu \nabla_\mu \right]. \tag{7.70}$$

By defining Euclidean Effective action as $Z = e^{-\Gamma_E}$, we get the 1-loop effective action as

$$\Gamma_E = -\frac{1}{4g_0^2} \int d^4x \, F^a_{\mu\nu} F^a_{\mu\nu} + \Gamma_g + \Gamma_q = -\frac{1}{4g_0^2} \int d^4x \, F^a_{\mu\nu} F^a_{\mu\nu} + \int d^4x \, \mathcal{L}_g + \int d^4x \, \mathcal{L}_q, \tag{7.71}$$

where

$$\Gamma_g = \frac{1}{2} \mathrm{Tr} \ln \left(-\hat{\nabla}^2 \delta_{\mu\nu} - 2\hat{F}_{\mu\nu} \right) - \mathrm{Tr} \ln(-\hat{\nabla}^2), \tag{7.72}$$

$$\Gamma_q = -N_f \mathrm{Tr} \ln(\gamma_\mu \nabla_\mu). \tag{7.73}$$

As one can see now, the problem of finding the 1-loop effective action becomes the problem of evaluating functional determinants. An efficient tool to evaluate the functional determinants is the Schwinger proper time method or Heat Kernel method [265–268]. The details regarding the heat kernel method are given in Appendix E.1. According to this method, the trace of an operator is calculated from the coincidence limit of the operator matrix [269]. Consider an operator of form $K = -\nabla^2 + V$, then the trace of $\ln \mathrm{K}$ is given by

$$\mathrm{Tr} \ln \mathrm{K} = -\int_0^\infty \frac{d\tau}{\tau} \frac{1}{(4\pi\tau)^{d/2}} H(x,x;\tau), \tag{7.74}$$

where $H(x,x;\tau) = \int d^d x \ \sum_{n=0}^{\infty} \tau^n \ \mathrm{tr} b_n$ is the Heat kernel corresponding to the operator K and b_n are the Seeley-deWitt coefficients at zero temperature [267]. Here, d is the number of dimensions, and $\mathrm{tr} := \mathrm{tr_c} \ \mathrm{tr_d} \ \mathrm{tr_l}$ denotes the traces over color, Dirac, and Lorentz indices. To evaluate thermodynamic potential, one has to find the Seeley-deWitt coefficients at finite temperatures. At finite temperatures, the expression for $H(x,x;\tau)$ gets an overall factor term [270]. Later, it is found that the expression is incomplete and this incompleteness is due to the A_0 term behaving differently at finite temperature [271]. The heat kernel expansion at finite temperature is given by [272]

$$\mathrm{Tr} \ln \mathrm{K} = -\int_0^\infty \frac{d\tau}{\tau} \frac{1}{(4\pi\tau)^{d/2}} \int d^d x \sum_{n=0}^{\infty} \tau^n b_n^T(x), \tag{7.75}$$

where the Seeley-deWitt coefficients at finite temperature (up to mass dimension 4) are given in terms of coefficients at zero temperature as follows

$$b_0^T(x) = \mathrm{tr}(\varphi_0 b_0) = \mathrm{tr}(\varphi_0), \tag{7.76}$$

$$b_1^T(x) = \mathrm{tr}(\varphi_0 b_1) = \mathrm{tr}(-\varphi_0 V), \tag{7.77}$$

$$b_2^T(x) = \mathrm{tr}\left(\varphi_0 b_2 - \frac{1}{6}\overline{\varphi}_2 E_i^2\right) = \mathrm{tr}\left(\frac{1}{2}\varphi_0 V^2 - \frac{1}{3}\varphi_0 E_i^2 + \frac{1}{12}\varphi_0 F_{ij}^2\right), \tag{7.78}$$

where b_0, b_1, b_2 are Seeley-deWitt coefficients at zero temperature, $E_i^2 = E_i^a E^{ai}$, $\overline{\varphi}_2 = \varphi_0 +$

$2\varphi_2$, $E_i^a = F_{0i}^a$ and

$$\varphi_n^{\pm}(L) = (4\pi\tau)^{1/2}\frac{1}{\beta}\sum_{p_0^{\pm}}\tau^{n/2}R^n e^{\tau R^2},\ R = ip_0^{\pm} - \frac{1}{\beta}\ln(L),\ \beta = \frac{1}{T}, \tag{7.79}$$

$$p_0^+ = \frac{2\pi k}{\beta}\ (\text{for bosons}),\ p_0^- = \frac{2\pi}{\beta}\left(k+\frac{1}{2}\right)\ (\text{for fermions}), k \in \mathbb{Z}, \tag{7.80}$$

with L being the untraced Polyakov loop given by

$$L = T\exp\left[-\int_{x_0}^{x_0+\beta} A_0(x_0', x)dx_0'\right]. \tag{7.81}$$

where T refers to temporal ordering and $A_0 = A_0^a T^a$, where T^a are the generators of the Lie group. Notice that L is a matrix in color space.

Now we presented the general formalism for finding the 1-loop effective action. We are considering the classical background field to be of form:

$$A_0^a = 0,\ A_i^a \neq 0. \tag{7.82}$$

With the above ansatz, one can see that the $A_0 = 0 \implies L = I$ (Identity in color space). With this choice, we are considering the system in the deconfined QGP phase.

Now we will evaluate the contributions of gluons (Eq. 7.72) and fermions (7.73) to effective action separately.

Gluon Contribution

In this subsection, we will see gluons' contribution to the one-loop effective action. It is given as

$$\Gamma_g = \frac{1}{2}\mathrm{Tr}\ln\left(-\hat{\nabla}^2\delta_{\mu\nu} - 2\hat{F}_{\mu\nu}\right) - \mathrm{Tr}\ln(-\hat{\nabla}^2). \tag{7.83}$$

Applying the Heat kernel expansion procedure (7.75), we get

$$\Gamma_g = -\frac{1}{2}\Lambda^{2\varepsilon}\int_0^\infty \frac{d\tau}{\tau}\frac{1}{(4\pi\tau)^{d/2}}\int d^dx \sum_{n=0}^{\infty}\tau^n b^T_{n,g}(x) := \int d^dx \mathcal{L}_g, \tag{7.84}$$

where

$$\mathcal{L}_g = -\frac{1}{2}\Lambda^{2\varepsilon}\int_0^\infty \frac{d\tau}{\tau}\frac{1}{(4\pi\tau)^{d/2}}\sum_{n=0}^{\infty}\tau^n b^T_{n,g}(x), \tag{7.85}$$

with $b^T_{n,g} = b^T_{n,gl} - 2b^T_{n,gh}$ are Seeley-deWitt coefficients, the first one ($b^T_{n,gl}$) corresponds to the gluon operator (1^{st} term in Eq.(7.72)) and the second one ($b^T_{n,gh}$) corresponds to the ghost operator (2^{nd} term in Eq. (7.72)). We use dimensional regularization to regulate ultraviolet divergences by choosing the convention $d = 4-2\varepsilon$ and introducing a mass renormalization scale $\Lambda^{2\varepsilon}$.

The explicit expressions for the coefficients are given by [272]

$$b^T_{0,g} = (d-2)\,\mathrm{tr_c}(\varphi_0^+), \tag{7.86}$$

$$b^T_{1,g} = 0, \tag{7.87}$$

$$b^T_{2,g} = \left(-2+\frac{d-2}{12}\right)\mathrm{tr_c}(\varphi_0^+\,\hat{F}^2_{\mu\nu}) - \frac{d-2}{6}\mathrm{tr_c}(\overline{\varphi}_2^+\,\hat{E}_i^2), \tag{7.88}$$

In the above, $\varphi_n^+(L)$ corresponds to bosonic versions and all the terms are in the adjoint representation. tr_c is trace over color indices.

Let us rewrite the gluon effective Lagrangian as follows

$$\mathcal{L}_g = \mathcal{L}_{0,g} + \mathcal{L}_{1,g} + \mathcal{L}_{2,g} + ..., \tag{7.89}$$

where $\mathcal{L}_{0,g}, \mathcal{L}_{1,g}, \mathcal{L}_{2,g}, ...$ corresponds to $b^T_{0,g}, b^T_{1,g}, b^T_{2,g}, ..$, respectively. While evaluating the functional determinants, we encounter the following type of integrals

$$I^+_{n,\alpha} = \int_0^\infty d\tau\,\tau^\varepsilon\,\tau^{\alpha-1}\varphi_n^+. \tag{7.90}$$

These integrals can be done in a closed form (See Appendix E.2) and is given by

$$I^{+}_{n,\alpha} = 4\pi^{1/2} i^n \frac{1}{\beta}\left(\frac{\beta}{2\pi}\right)^{2\varepsilon}\left(\frac{\beta}{2\pi}\right)^{2\alpha+1}\Gamma\left(\alpha+\varepsilon+\frac{n}{2}+\frac{1}{2}\right)\zeta(2\alpha+2\varepsilon+1), \tag{7.91}$$

where $\Gamma(z)$ is the Gamma function and $\zeta(s)$ is the Riemann Zeta function. Now, we will find each term's contribution to the effective Lagrangian. The zeroth order term requires only one integral $I^{+}_{0,-2}$.

$$\begin{aligned}
\mathcal{L}_{0,g} &= -\frac{1}{2}\Lambda^{2\varepsilon}\int_0^\infty \frac{d\tau}{\tau}\frac{1}{(4\pi\tau)^{d/2}} b^T_{0,g} && (7.92)\\
&= -\frac{1}{(4\pi)^2}(N^2-1)(4\pi\Lambda^2)^{\varepsilon}\int_0^\infty d\tau\tau^{\varepsilon-3}\varphi^{+}_0 && (7.93)\\
&= -\frac{1}{(4\pi)^2}(N^2-1)(4\pi\Lambda^2)^{\varepsilon} I^{+}_{0,-2} && (7.94)\\
&= -\frac{2}{\beta}^4 \pi^{3/2}(N^2-1)(4\pi\Lambda^2)^{\varepsilon}\left(\frac{\beta}{2\pi}\right)^{2\varepsilon}\Gamma\left(\varepsilon-\frac{3}{2}\right)\zeta(2\varepsilon-3) && (7.95)\\
&= -\frac{\pi^2}{45}T^4(N^2-1), && (7.96)
\end{aligned}$$

where we used the following expansions in the last expression as $\varepsilon \to 0$:

$$\Gamma(\varepsilon-\frac{3}{2}) \approx \frac{4}{3}\sqrt{\pi} + O(\varepsilon), \tag{7.97}$$

$$\zeta(2\varepsilon-3) \approx \frac{1}{120} + O(\varepsilon). \tag{7.98}$$

The above zero-order term corresponds to the free gluons' contribution. The first-order term is zero because $b^T_{1,g} = 0$. Similarly, we can find the second-order term's contribution as follows

$$\mathcal{L}_{2,g} = -\frac{1}{2}\Lambda^{2\varepsilon}\int_0^\infty \frac{d\tau}{\tau}\frac{1}{(4\pi\tau)^{d/2}}\tau^2 b^T_{2,g}. \tag{7.99}$$

Using the $b^T_{2,g}$ and integrals notation ($I^{+}_{n,\alpha}$), we can evaluate as follows

$$\mathcal{L}_{2,g} = \frac{1}{(4\pi)^2}\frac{11}{12}(4\pi\Lambda^2)^{\varepsilon} I^{+}_{0,0}\mathrm{tr_c}(\hat{F}^2_{\mu\nu}) + \frac{1}{(4\pi)^2}\frac{1}{6}(4\pi\Lambda^2)^{\varepsilon}(I^{+}_{0,0}+2I^{+}_{2,0})\mathrm{tr_c}(\hat{E}^2_i) \tag{7.100}$$

$$= \frac{1}{(4\pi)^2}\frac{11}{12}2\pi^{-1/2}\left[(4\pi\Lambda^2)^{\varepsilon}\left(\frac{\beta}{2\pi}\right)^{2\varepsilon}\Gamma\left(\varepsilon+\frac{1}{2}\right)\zeta(2\varepsilon+1)\right]\mathrm{tr_c}(\hat{F}_{\mu\nu}^2)$$
$$+\frac{1}{(4\pi)^2}\frac{1}{6}2\pi^{-1/2}\left[(4\pi\Lambda^2)^{\varepsilon}\left(\frac{\beta}{2\pi}\right)^{2\varepsilon}\zeta(2\varepsilon+1)\left(\Gamma\left(\varepsilon+\frac{1}{2}\right)-2\Gamma\left(\varepsilon+\frac{3}{2}\right)\right)\right]\mathrm{tr_c}(\hat{E}_i^2) \tag{7.101}$$

$$= \frac{1}{(4\pi)^2}\frac{11}{12}\left[\frac{1}{\varepsilon}+\gamma_E+\ln(4\pi)\right]\mathrm{tr_c}(\hat{F}_{\mu\nu}^2)+\frac{11}{6}\frac{1}{(4\pi)^2}\ln\left(\frac{\Lambda}{4\pi T}\right)\mathrm{tr_c}(\hat{F}_{\mu\nu}^2)-\frac{1}{3}\frac{1}{(4\pi)^2}\mathrm{tr_c}(\hat{E}_i^2). \tag{7.102}$$

where we used the following expansions in the last expression as $\varepsilon \to 0$:

$$\Gamma(\varepsilon+\frac{1}{2}) \approx \sqrt{\pi}+\sqrt{\pi}\,\psi\left(\frac{1}{2}\right)\varepsilon+O(\varepsilon^2), \tag{7.103}$$

$$\zeta(2\varepsilon+1) \approx \frac{1}{2\varepsilon}+\gamma_E+O(\varepsilon), \tag{7.104}$$

$$\Gamma(\varepsilon+\frac{3}{2}) \approx \frac{\sqrt{\pi}}{2}+\frac{\sqrt{\pi}}{2}\,\psi\left(\frac{3}{2}\right)\varepsilon+O(\varepsilon^2), \tag{7.105}$$

where $\psi(z)$ is the Digamma function and γ_E is the Euler's constant.

One can see that the first term has a pole at $\varepsilon = 0$ and the divergent terms can be removed by adopting the $\overline{MS}$ scheme. We will discuss this method in the next section along with quarks.

Finally, combining all terms up to mass dimension 4, we get

$$\mathcal{L}_g = \mathcal{L}_{0,g}+\mathcal{L}_{1,g}+\mathcal{L}_{2,g} \tag{7.106}$$
$$= -\frac{\pi^2}{45}T^4(N^2-1)+\frac{1}{(4\pi)^2}\frac{11}{12}\left[\frac{1}{\varepsilon}+\gamma_E+\ln(4\pi)\right]\mathrm{tr_c}(\hat{F}_{\mu\nu}^2)+\frac{11}{6}\frac{1}{(4\pi)^2}\ln\left(\frac{\Lambda}{4\pi T}\right)\mathrm{tr_c}(\hat{F}_{\mu\nu}^2)$$
$$-\frac{1}{3}\frac{1}{(4\pi)^2}\mathrm{tr_c}(\hat{E}_i^2). \tag{7.107}$$

Quark Contribution

Here, we will study the contribution of quarks to the one-loop effective action. It is given by

$$\Gamma_q = -N_f \mathrm{Tr}\ln(\gamma^\mu \nabla_\mu), \tag{7.108}$$

To apply the heat kernel procedure, we need to find the Klein-Gordon operator related to the above one. One can use the following manipulations:

$$\mathrm{Tr}\ln(\gamma^\mu\nabla_\mu) = \frac{1}{2}\mathrm{Tr}\ln(-(\gamma^\mu\nabla_\mu)^2),\ \ -(\gamma^\mu\nabla_\mu)^2 = -\nabla^2 - \frac{1}{2}\sigma^{\mu\nu}F_{\mu\nu},\ \ \sigma^{\mu\nu} = \frac{1}{2}[\gamma^\mu,\gamma^\nu], \tag{7.109}$$

which makes the quark effective action as

$$\Gamma_q = -\frac{N_f}{2}\mathrm{Tr}\ln\left(-\nabla^2 - \frac{1}{2}\sigma^{\mu\nu}F_{\mu\nu}\right). \tag{7.110}$$

Now, again using Heat kernel expansion (7.75), we get

$$\Gamma_q = \frac{N_f}{2}\Lambda^{2\varepsilon}\int_0^\infty \frac{d\tau}{\tau}\frac{1}{(4\pi\tau)^{d/2}}\int d^dx \sum_{n=0}^{\infty}\tau^n b^T_{n,q}(x) := \int d^dx \mathcal{L}_q, \tag{7.111}$$

where

$$\mathcal{L}_q = \frac{N_f}{2}\Lambda^{2\varepsilon}\int_0^\infty \frac{d\tau}{\tau}\frac{1}{(4\pi\tau)^{d/2}}\sum_{n=0}^{\infty}\tau^n b^T_{n,q}(x) \tag{7.112}$$

with $b^T_{n,q}$ being the Seeley-deWitt coefficients which are given by

$$b^T_{0,q} = 4\ \mathrm{tr_c}(\varphi_0^-), \tag{7.113}$$

$$b^T_{1,q} = 0, \tag{7.114}$$

$$b^T_{2,q} = -\frac{2}{3}\mathrm{tr_c}(\varphi_0^- F^2_{\mu\nu}) - \frac{2}{3}\mathrm{tr_c}(\overline{\varphi}_2^- E_i^2), \tag{7.115}$$

where $\varphi_n^-(L)$ is the fermionic version and all the terms are in fundamental representation. Similarly, let us rewrite the quark-effective Lagrangian as

$$\mathcal{L}_q = \mathcal{L}_{0,q} + \mathcal{L}_{1,q} + \mathcal{L}_{2,q} + ..., \tag{7.116}$$

where $\mathcal{L}_{0,q}, \mathcal{L}_{1,q}, \mathcal{L}_{2,q}, ...$ corresponds to the coefficients $b_{0,q}^T, b_{1,q}^T, b_{2,q}^T, ..$, respectively. We can proceed to evaluate the terms individually. We note that we encounter the same type of integrals as in the gluon case [See Appendix E.2]:

$$I_{n,\alpha}^- = \int_0^\infty d\tau\, \tau^\varepsilon\, \tau^{\alpha-1} \varphi_n^- = 4\pi^{1/2} i^n \frac{1}{\beta} \left(\frac{\beta}{2\pi}\right)^{2\varepsilon} \left(\frac{\beta}{2\pi}\right)^{2\alpha+1} \Gamma\left(\alpha+\varepsilon+\frac{n}{2}+\frac{1}{2}\right) \zeta\left(2\alpha+2\varepsilon+1, \frac{1}{2}\right), \tag{7.117}$$

where $\zeta(a,z) = \Sigma_{n=0}^\infty (n+z)^{-a}$ is the generalized Riemann-zeta function. Now, the zeroth order term of quark effective Lagrangian is

$$\begin{aligned}
\mathcal{L}_{0,q} &= \frac{N_f}{2} \Lambda^{2\varepsilon} \int_0^\infty \frac{d\tau}{\tau} \frac{1}{(4\pi\tau)^{d/2}} b_{0,q}^T(x) && (7.118)\\
&= 2NN_f \Lambda^{2\varepsilon} \int_0^\infty \frac{d\tau}{\tau} \frac{1}{(4\pi\tau)^{d/2}} \varphi_0^- && (7.119)\\
&= \frac{2}{(4\pi)^2} NN_f (4\pi\Lambda^2)^\varepsilon I_{0,-2}^- && (7.120)\\
&= 4NN_f T^4 \pi^{3/2} (4\pi\Lambda^2)^\varepsilon \left(\frac{\beta}{2\pi}\right)^{2\varepsilon} \Gamma\left(\varepsilon - \frac{3}{2}\right) \zeta\left(2\varepsilon - 3, \frac{1}{2}\right) && (7.121)\\
&= -\frac{7\pi^2}{180} NN_f T^4, && (7.122)
\end{aligned}$$

where we used the following expansions of Gamma and generalized Riemann zeta functions as $\varepsilon \to 0$:

$$\begin{aligned}
\Gamma(\varepsilon - \frac{3}{2}) &\approx \frac{4}{3}\sqrt{\pi} + O(\varepsilon), && (7.123)\\
\zeta(2\varepsilon - 3, \frac{1}{2}) &\approx -\frac{7}{960} + O(\varepsilon). && (7.124)
\end{aligned}$$

The above zero-order term corresponds to the free quarks' contribution. The first-order term is zero because $b_{1,q}^T = 0$. Similarly, we can find the second order's contribution as follows

$$\mathcal{L}_{2,q} = \frac{N_f}{2}\Lambda^{2\varepsilon}\int_0^\infty \frac{d\tau}{\tau}\frac{1}{(4\pi\tau)^{d/2}}\tau^2 b_{2,q}^T \tag{7.125}$$

$$= -\frac{1}{(4\pi)^2}\frac{N_f}{3}(4\pi\Lambda^2)^\varepsilon I_{0,0}^- \mathrm{tr_c}(F_{\mu\nu}^2) - \frac{1}{(4\pi)^2}\frac{N_f}{3}(4\pi\Lambda^2)^\varepsilon (I_{0,0}^- + 2I_{2,0}^-)\mathrm{tr_c}(E_i^2) \tag{7.126}$$

$$= -\frac{1}{(4\pi)^2}\frac{N_f}{3}2\pi^{-1/2}\left[(4\pi\Lambda^2)^\varepsilon\left(\frac{\beta}{2\pi}\right)^{2\varepsilon}\Gamma\left(\varepsilon+\frac{1}{2}\right)\zeta\left(2\varepsilon+1,\frac{1}{2}\right)\right]\mathrm{tr_c}(F_{\mu\nu}^2)$$

$$-\frac{1}{(4\pi)^2}\frac{N_f}{3}2\pi^{-1/2}\left[(4\pi\Lambda^2)^\varepsilon\left(\frac{\beta}{2\pi}\right)^{2\varepsilon}\zeta\left(2\varepsilon+1,\frac{1}{2}\right)\left(\Gamma\left(\varepsilon+\frac{1}{2}\right)-2\Gamma\left(\varepsilon+\frac{3}{2}\right)\right)\right]\mathrm{tr_c}(E_i^2) \tag{7.127}$$

$$= -\frac{1}{(4\pi)^2}\frac{N_f}{3}\left[\frac{1}{\varepsilon}+\gamma_E+\ln(4\pi)\right]\mathrm{tr_c}(F_{\mu\nu}^2) - \frac{N_f}{3}\frac{1}{(4\pi)^2}\left[2\ln\left(\frac{\Lambda}{4\pi T}\right)+2\ln 4\right]\mathrm{tr_c}(F_{\mu\nu}^2)$$

$$+\frac{1}{(4\pi)^2}\frac{2}{3}N_f\mathrm{tr_c}(E_i^2). \tag{7.128}$$

where we used the following expansions in the last expression as $\varepsilon \to 0$:

$$\Gamma(\varepsilon+\frac{1}{2}) \approx \sqrt{\pi}+\sqrt{\pi}\,\psi\left(\frac{1}{2}\right)\varepsilon + O(\varepsilon^2), \tag{7.129}$$

$$\zeta(2\varepsilon+1,\frac{1}{2}) \approx \frac{1}{2\varepsilon}+\gamma_E+2\ln 2+O(\varepsilon), \tag{7.130}$$

$$\Gamma(\varepsilon+\frac{3}{2}) \approx \frac{\sqrt{\pi}}{2}+\frac{\sqrt{\pi}}{2}\,\psi\left(\frac{3}{2}\right)\varepsilon + O(\varepsilon^2), \tag{7.131}$$

where $\psi(z)$ is the Digamma function and γ_E is the Euler's constant.

Here also, we can see that the first term has a pole as $\varepsilon = 0$. Combining all the terms in quark contribution (up to mass dimension 4), we get as in [272]

$$\mathcal{L}_q = -\frac{7\pi^2}{180}NN_fT^4 - \frac{1}{(4\pi)^2}\frac{N_f}{3}\left[\frac{1}{\varepsilon}+\gamma_E+\ln(4\pi)\right]\mathrm{tr_c}(F_{\mu\nu}^2) - \frac{N_f}{3}\frac{1}{(4\pi)^2}\left[2\ln\left(\frac{\Lambda}{4\pi T}\right)+2\ln 4\right]$$
$$\mathrm{tr_c}(F_{\mu\nu}^2) + \frac{1}{(4\pi)^2}\frac{2}{3}N_f\mathrm{tr_c}(E_i^2). \tag{7.132}$$

Renormalized Lagrangian

Finally, we will see how to deal with divergent terms in both gluon and quark effective actions. Consider the divergent terms in quark and gluon along with the tree Lagrangian:

$$\mathcal{L}_0+\mathcal{L}_g^{div}+\mathcal{L}_q^{div}=-\frac{1}{4g_0^2}F^{a\mu\nu}F^a_{\mu\nu}+\frac{1}{(4\pi)^2}\frac{11}{12}\left[\frac{1}{\varepsilon}+\gamma_E+\ln(4\pi)\right]\mathrm{tr_c}(\hat{F}^2_{\mu\nu}) \\ -\frac{1}{(4\pi)^2}\frac{N_f}{3}\left[\frac{1}{\varepsilon}+\gamma_E+\ln(4\pi)\right]\mathrm{tr_c}(F^2_{\mu\nu}). \quad (7.133)$$

Using the trace properties of SU(N) matrices ($\mathrm{tr_c}(\hat{F}^2_{\mu\nu})=N\,\mathrm{tr_c}(F^2_{\mu\nu})=\frac{N}{2}F^{a\mu\nu}F^a_{\mu\nu}$), we get

$$\mathcal{L}_0+\mathcal{L}_g^{div}+\mathcal{L}_q^{div}=-\frac{1}{4g^2(\Lambda)}F^{a\mu\nu}F^a_{\mu\nu}, \quad (7.134)$$

with the standard one-loop beta function using $\overline{MS}$ scheme [30, 272],

$$\frac{1}{g^2(\Lambda)}=\frac{1}{g_0^2}-\beta_0\left(\frac{1}{\varepsilon}+\ln(4\pi)+\gamma_E\right),\quad \beta_0=\frac{1}{(4\pi)^2}\left(\frac{11}{3}N-\frac{2}{3}N_f\right). \quad (7.135)$$

Finally, putting together all the terms (both gluon and quark) up to mass dimension 4, we find the renormalized Lagrangian to be

$$\mathcal{L}=-\frac{\pi^2}{45}T^4(N^2-1)-\frac{7\pi^2}{180}NN_fT^4+\left[-\frac{1}{4g^2(\Lambda)}+\frac{1}{2}\beta_0\ln\left(\frac{\Lambda}{4\pi T}\right)-\frac{1}{(4\pi)^2}\frac{N_f}{3}\ln 4\right]F^{a\mu\nu}F^a_{\mu\nu} \\ +\frac{1}{3}\frac{1}{(4\pi)^2}(N_f-N)E^{ai}E^a_i. \quad (7.136)$$

7.4.2 Thermodynamic Potential of QGP

With the known partition function, one can find the thermodynamic potential as

$$\Omega(T)=-\frac{T}{V}\ln Z(T), \quad (7.137)$$

If we know the thermodynamic potential, we can derive other thermodynamic quantities such as pressure P, entropy density S, energy density ε, trace anomaly Θ^μ_μ and speed of

sound c_s^2 using the following expressions:

$$P = -\Omega, \quad S = -\frac{\partial \Omega}{\partial T}, \quad \varepsilon = -P + TS, \tag{7.138}$$

$$\Theta^{\mu}_{\mu} = \varepsilon - 3P, \quad c_s^2 \equiv \frac{\partial P}{\partial \varepsilon}. \tag{7.139}$$

Using the renormalized Lagrangian, we get the thermodynamic potential to be

$$\Omega(T) = -\frac{\pi^2}{45}T^4(N^2-1) - \frac{7\pi^2}{180}NN_fT^4 + \frac{T}{V}\left[-\frac{1}{4g^2(\Lambda)} + \frac{1}{2}\beta_0 \ln\left(\frac{\Lambda}{4\pi T}\right) - \frac{1}{(4\pi)^2}\frac{N_f}{3}\ln 4\right] \left[\int d^4x F^{a\mu\nu}F^a_{\mu\nu}\right] + \frac{T}{3V}\frac{1}{(4\pi)^2}(N_f - N)\left[\int d^4x E^{ai}E^a_i\right]. \tag{7.140}$$

Before discussing specific cases, we consider the one-loop running coupling constant. By rewriting the coupling constant at some energy scale as [253, 273]

$$\alpha_s(\Lambda) \equiv \frac{g^2(\Lambda)}{4\,\pi} = \frac{1}{4\,\pi\,\beta_0\,\ln(\Lambda^2/\Lambda^2_{\overline{MS}})}. \tag{7.141}$$

One can fix the scale $\Lambda^2_{\overline{MS}}$ which is the QCD energy scale, by knowing the running coupling constant value at some energy scale. These kinds of measurements are usually obtained from Lattice calculations. In particular, by setting $\alpha_s(1.5\text{GeV}) = 0.326$ [274], we can fix the $\Lambda^2_{\overline{MS}} = 176\text{MeV}$ for one-loop running coupling constant. We choose the renormalization scales to be $\Lambda = 2\pi T$. With these in mind, we evaluated the thermodynamic quantities for different configurations in the next section.

In the plots, we normalized the quantities with respect to the ideal gas limits which are given as [275]

$$P_{id} = \frac{\pi^2}{45}T^4(N^2-1) + \frac{7\pi^2}{180}T^4NN_f, \tag{7.142}$$

$$\varepsilon_{id} = \frac{\pi^2}{15}T^4(N^2-1) + \frac{7\pi^2}{60}T^4NN_f, \tag{7.143}$$

$$S_{id} = \frac{4\pi^2}{45}T^3(N^2-1) + \frac{7\pi^2}{45}T^3NN_f. \tag{7.144}$$

7.5 Thermodynamic properties of QGP with different background fields

The main quantity in describing the thermodynamic properties is the thermodynamic potential obtained in the previous section (Eq. 7.140). This section follows the work we did in [52]. In this section, we consider different backgrounds obtained in the previous chapters. We first consider a spatially homogeneous and isotropic condensate (Sec: 7.5.1), followed by a modified condensate (with the introduction of quarks) (Sec: 7.5.2), and conclude with a GW-modified condensate (Sec: 7.5.3).

7.5.1 Condensate Model

In this case, we consider a spatially homogeneous and isotropic condensate which is well studied in the previous chapters (5 & 6) :

$$A_0^a = 0,\ \ A_i^a = \delta_i^a U(t), \tag{7.145}$$

where $a, i = 1,2,3$ for $SU(2)$ and $U(t)$ is the solution of YM equations in Euclidean space-time given as

$$U(t) = c_1 \mathrm{sn}[c_1(-it + c_2), -1]. \tag{7.146}$$

With this classical condensate as a background field, we found thermodynamic potential to be

$$\begin{aligned}\Omega = &-\frac{\pi^2}{45}T^4(N^2-1) - \frac{7\pi^2}{180}NN_fT^4 - 2\left[-\frac{1}{4g^2(\Lambda)} + \frac{1}{2}\beta_0 \ln\left(\frac{\Lambda}{4\pi T}\right) - \frac{1}{(4\pi)^2}\frac{N_f}{3}\ln 4\right] \\ &c_1^3\Bigg(c_1 - 2iT\,\mathrm{cn}(c_1c_2,-1)\mathrm{sn}(c_1c_2,-1)\mathrm{dn}(c_1c_2,-1) + 2iT\,\mathrm{cn}(c_1(c_2-\frac{i}{T}),-1)\mathrm{sn}(c_1(c_2-\frac{i}{T}),-1) \\ &\mathrm{dn}(c_1(c_2-\frac{i}{T}),-1)\Bigg) - \frac{1}{3}\frac{1}{(4\pi)^2}(N_f-N)c_1^3(2c_1 - iT\,\mathrm{cn}(c_1c_2,-1)\mathrm{sn}(c_1c_2,-1)\mathrm{dn}(c_1c_2,-1) \\ &+iT\,\mathrm{cn}(c_1(c_2-\frac{i}{T}),-1)\mathrm{sn}(c_1(c_2-\frac{i}{T}),-1)\mathrm{dn}(c_1(c_2-\frac{i}{T}),-1)\Bigg),\end{aligned} \tag{7.147}$$

where c_1 and c_2 are the initial conditions of the condensate. We considered the $SU(2)$ QCD

model with 2 fermion flavours which means $N = 2$ and $N_f = 2$.

If one considers the condensate a separate non-dynamical background field away from the thermodynamic equilibrium, we can treat the constants c_1 and c_2 as individual variables. Then, the thermodynamic potential will be a function of c_1, c_2 and T. For simplicity, we first consider the effect of only c_1 on Ω. We find that for a particular temperature, the thermodynamic potential shows a three-well potential in the parameter c_1. This is shown in Fig. 7.4. With the increasing temperature, the point of the false vacuum is moving away from the origin. If one considers the system starting at a high c_1 value, then the system tries to reach equilibrium by getting to the minimum. As one can see the system first reaches a false bottom/vacuum as it moves toward minima and then, finally reaches a true vacuum in which the thermodynamic potential is minimum. This view is the same as that of inflationary theory. The main difference is that one gets the inflationary type potential without introducing any scalar particle but with gauge fields alone. This line of study, using gauge fields to drive inflation has been researched by many authors [36]. However, here, we show that this kind of inflationary scenario can occur at any particular temperature as opposed to the traditional view of inflation, which is driven by the temperature. As we discussed earlier, all this happens when one treats the condensate as an independent background field.

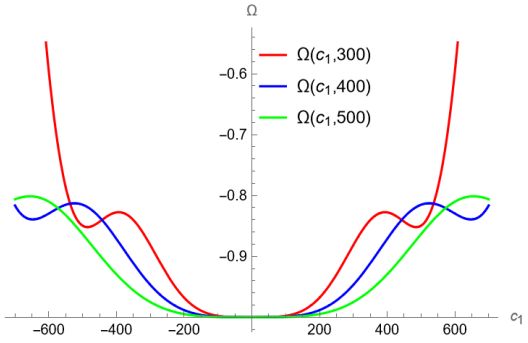

((a)) Ω as a function of c_1

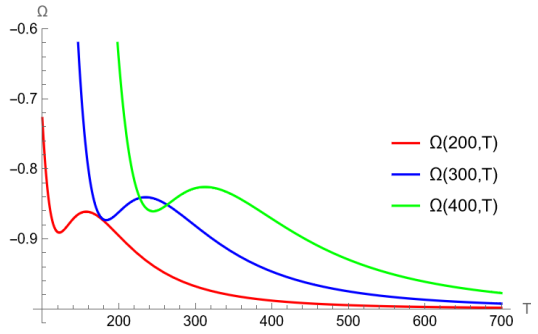

((b)) Ω as a function of T

Figure 7.4: Figures showing the thermodynamic potential Ω as a function of c_1 and T. For this, we set $\Lambda_{\overline{MS}} = 176$ MeV.

But, if we treat the condensate along with fluctuations in the thermodynamic equilib-

rium, then one has to modify the variables c_1 and c_2 to accommodate the temperature dependence. This is because to match with the Matsubara frequencies formalism (interpreting the period of fields in imaginary time as inverse temperature), we have to do one-to-one mapping of the period of Jacobi functions to temperature. We use the fact that the period of the above condensate solution is $4\,K(m)/c_1$. After interpreting this as an inverse temperature, we get $c_1 = 4iK(-1)T$, where $K(m)$ is the Complete Elliptic integral of the first kind while c_2 is still independent of temperature. Now, the thermodynamic potential (Ω) is a function of temperature T and c_2. After plugging c_1 in Eq. (7.147) and using periodic properties of Jacobi elliptic functions, we found that that the terms involving c_2 will get cancel each other leaving the thermodynamic potential to be a function of temperature T.

$$\Omega(T) = -\frac{\pi^2}{45}T^4(N^2-1) - \frac{7\pi^2}{180}NN_fT^4 - 2\left[-\frac{1}{4g^2(\Lambda)} + \frac{1}{2}\beta_0 \ln\left(\frac{\Lambda}{4\pi T}\right) - \frac{1}{(4\pi)^2}\frac{N_f}{3}\ln 4\right] (4iK(-1)T)^4 - \frac{1}{3}\frac{1}{(4\pi)^2}(N_f - N)2(4iK(-1)T)^4. \quad (7.148)$$

With this, we calculated the other thermodynamic quantities such as pressure, entropy density, and energy density, and plots were shown in Fig. 7.5.

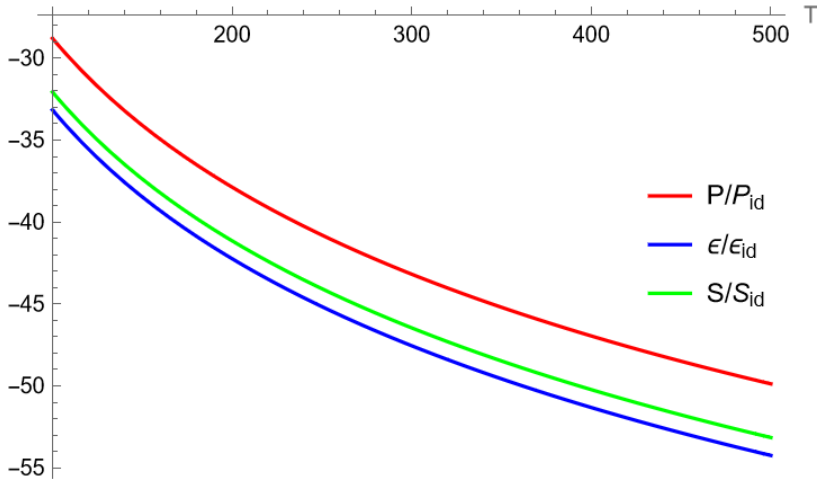

Figure 7.5: Figures showing the normalized pressure, entropy density, and energy density as a function of temperature T(MeV). For this, we set $N = 2$, $N_f = 2$ and $\Lambda_{\overline{MS}} = 176$ MeV.

From the plots, it is clear that we have a thermodynamic system with negative pressure, entropy density, and as well as energy density. This shows the system with condensate only does not exist at finite temperatures. The partition function calculations are based on grand canonical ensemble formalism which suggests the existence of a thermal bath at some temperature T that allows for the exchange of energy and particles. If we take the condensate to be at the same temperature as quantum fluctuations, then the condensate has to exchange energy with fluctuations via its fluctuation modes. If we still keep only condensate, then it allows for a negative energy density state.

There are investigations on the search for a non-trivial QCD ground state by analyzing the effective action that depends on the vacuum expectation value of the gauge field operator [264, 276, 277]. This non-trivial ground state is approximated using different types of condensates such as chromomagnetic and chromoelectric gluon condensates. It was found that the true vacuum state of Yang-Mills theory is described by a nonzero chromomagnetic gluon condensate having a negative energy density. Our work provides a finite temperature extension to the investigations on the existence and stability of condensates in the true vacuum of YM theory [276].

In the later section (Sec: 7.5.3), we will see that the condensate along with the fluctuations can exist at a finite temperature.

7.5.2 Modified Condensate Model

In this section, we consider the modified condensate ansatz which is a modification of the original ansatz due to its interaction with quarks (Sec: 6.1.1):

$$A_0^a = 0: \;\; A_i^a = \delta_i^a U(t) + \tilde{A}_i^a(t). \tag{7.149}$$

where $\tilde{A}_i^a$ are the fluctuations in condensate configuration generated due to the backreaction of quarks on condensate. The expressions for these fluctuations functions are obtained in Sec: 6.1.1. As these fluctuations are very small, these impacts are also very small.

The form of thermodynamic potential is the same as in the previous case Eq. (7.140). With the modification of ansatz, the expression of $F^{a\mu\nu}F^{a}_{\mu\nu}$ changes to

$$F^{a\mu\nu}F^{a}_{\mu\nu} = 2\Big[\big((\tilde{A}^1_2)^2+(\tilde{A}^2_1)^2+(\tilde{A}^2_2+U)^2\big)(\tilde{A}^3_3+U)^2+\big(\tilde{A}^1_2\tilde{A}^2_1-(\tilde{A}^1_1+U)(\tilde{A}^2_2+U)\big)^2 \\ +(\partial_t\tilde{A}^1_2)^2+(\partial_t\tilde{A}^2_1)^2+(\partial_t U+\partial_t\tilde{A}^1_1)^2+(\partial_t U+\partial_t\tilde{A}^2_2)^2+(\partial_t U+\partial_t\tilde{A}^3_3)^2\Big], \quad (7.150)$$

and $E^a_i E^{ai}$ changes to

$$E^a_i E^{ai} = (\partial_t\tilde{A}^1_2)^2+(\partial_t\tilde{A}^2_1)^2+(\partial_t\tilde{A}^1_1+\partial_t U)^2+(\partial_t\tilde{A}^2_2+\partial_t U)^2+(\partial_t\tilde{A}^3_3+\partial_t U)^2. \quad (7.151)$$

With these changes, we found the thermodynamic potential and other thermodynamic quantities. Since we are not able to find the analytical solutions for some of the perturbation functions $(\tilde{A}^1_1,\tilde{A}^2_2,\tilde{A}^3_3)$, we find the numerical solutions for the thermodynamic quantities. We found that all the thermodynamic quantities are the same as in the previous case. This is due to the very small magnitudes of the fluctuations. Thus, we did not explore this further. For comparison, we plotted the pressure when condensate is at a different temperature than quantum fluctuations in Fig. (7.6).

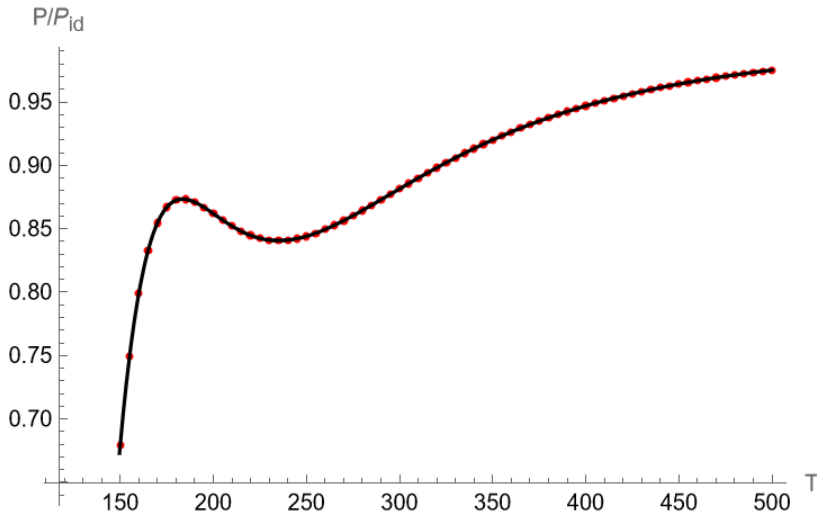

Figure 7.6: Comparison of pressure in two different cases. The black line corresponds to the condensate ansatz and the red dots correspond to the modified condensate ansatz. We choose $c_1 = 300$ and $c_2 = 0$.

7.5.3 Gravitational wave modified condensate model

In this section, we study the effect of a GW on the thermodynamics of QGP. For this, we consider the GW-dependent condensate configuration studied in Sec: 5.2. In that section, we studied the condensate + fluctuations model (in tensor decomposition) in the presence of GWs. We found that the transverse traceless modes can be generated from the interactions between condensate and GWs. We use this solution because of its simplicity and it is the only analytical solution we were able to found in case of condensates. The gauge field configuration in the presence of GW is given by

$$A_i^a = \delta_i^a U(t) + \delta^{aj}\tilde{A}_{ji} + \frac{1}{2}\delta^{aj}h_{ji}U(t), \tag{7.152}$$

where $U(t)$ is the spatially homogeneous and isotropic condensate, $\tilde{A}_{ji}$ are the fluctuations without GWs and h_{ji} is the $+$-polarised GW with $h_{11} = -h_{22} = h_+ = A_+\cos(\omega_g(t-z))$. Consider the fluctuations $\tilde{A}_{ji} = 0$, then the gauge field to be of form $A_i^a = \text{diag}\ (U + \frac{1}{2}h_+U, U - \frac{1}{2}h_+U, U)$.

The form of thermodynamic potential is the same as in the previous cases (Eq. 7.140). As the gauge field is different, $F^{a\mu\nu}F^a_{\mu\nu}$ and $E^a_iE^{ai}$ changes to

$$F^{a\mu\nu}F^a_{\mu\nu} = 6U'^2 + 6U^4 - 6h_+^2U^4 + \frac{9}{8}h_+^4U^4 - \frac{1}{8}h_+^6U^4 - 3h_+^2U'^2 - 2h_+UU'\partial_t h_+ + U^2\left[(\partial_z h_+)^2 + (\partial_t h_+)^2\right], \tag{7.153}$$

and

$$E^a_iE^{ai} = 3U'^2 - \frac{3}{2}h_+^2U'^2 - h_+UU'\partial_t h_+ + \frac{1}{2}U^2(\partial_t h_+)^2. \tag{7.154}$$

For simplicity, we consider only the time dependence in GW. When everything is in equilibrium, we have to fix the constants in expressions of condensate and GW. For condensate, we already found that the constant c_1 has a linear relationship with T ($c_1 = 4\ i\ K(-1)\ T$). Using the same analysis, we also found that the ω_g is related to T by the

relation: $\omega_g = 2\pi\, i\, T$. With that, we have a thermodynamic potential dependent on the temperature T, c_2 and A_+. By setting $c_2 = 0$ and considering small amplitudes for A_+, we recover the standard thermodynamic behaviour of QGP as obtained in Lattice QCD calculations or other perturbative QCD techniques such as three loop HTL theory [278]. The plots of Pressure, energy density, and entropy density normalized to the idealized quantities are shown in Fig. (7.7).

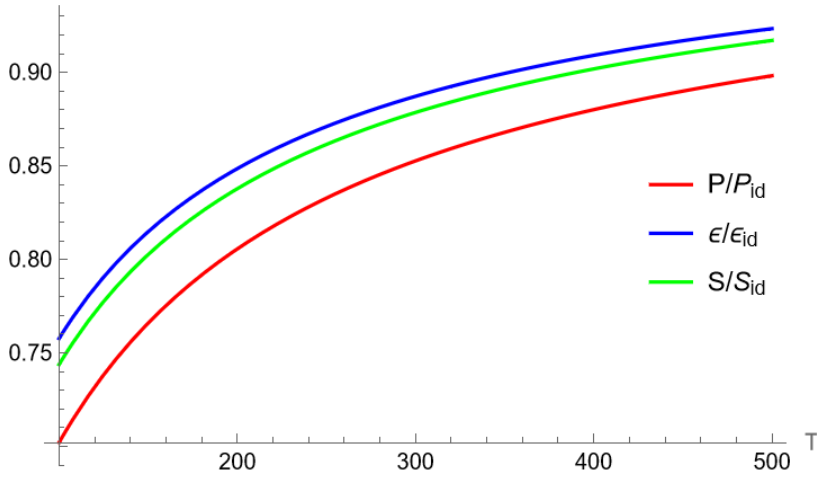

Figure 7.7: The plots of normalized pressure, entropy density, and energy density as a function of temperature T(MeV). We choose $A_+ = 0.001$, $c_2 = 0$, and $\Lambda_{\overline{MS}} = 176$ MeV.

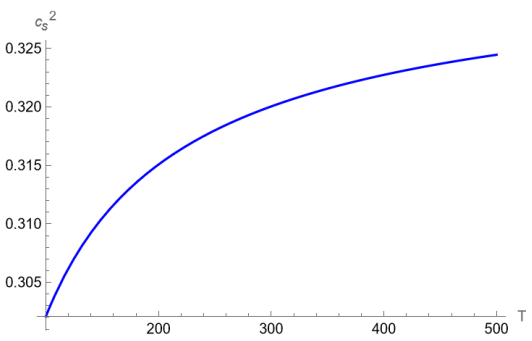

((a)) c_s^2 as a function of T

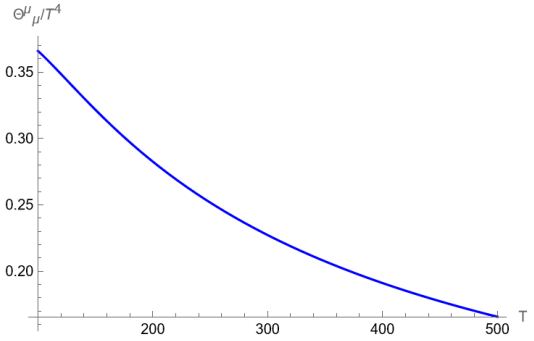

((b)) Θ^μ_μ as a function of T

Figure 7.8: Figures showing the speed of sound c_s^2 and trace anomaly Θ^μ_μ as a function of temperature T(MeV). We choose $A_+ = 0.001$, $c_2 = 0$, and $\Lambda_{\overline{MS}} = 176$ MeV.

Another important quantity that is conveniently calculated on the lattice is the trace anomaly or interaction measure ($\Theta^\mu_\mu = \varepsilon - 3P$) defined as the trace of the energy-momentum tensor. One can also discuss another quantity that is relevant for dealing with phase transi-

tion is the speed of sound (c_s^2) in the deconfined medium defined as the change of pressure with respect to energy density. It is also related to the specific heat, $C_v = d\varepsilon/dT$ as

$$c_s^2 = \frac{\partial P}{\partial \varepsilon} = \frac{S}{C_v}, \text{ where } C_v = \frac{d\varepsilon}{dT}. \tag{7.155}$$

But, in our case, we are dealing with a deconfined phase, then the speed of sound is not that much relevant. The plots for these quantities are given in Fig. (7.8).

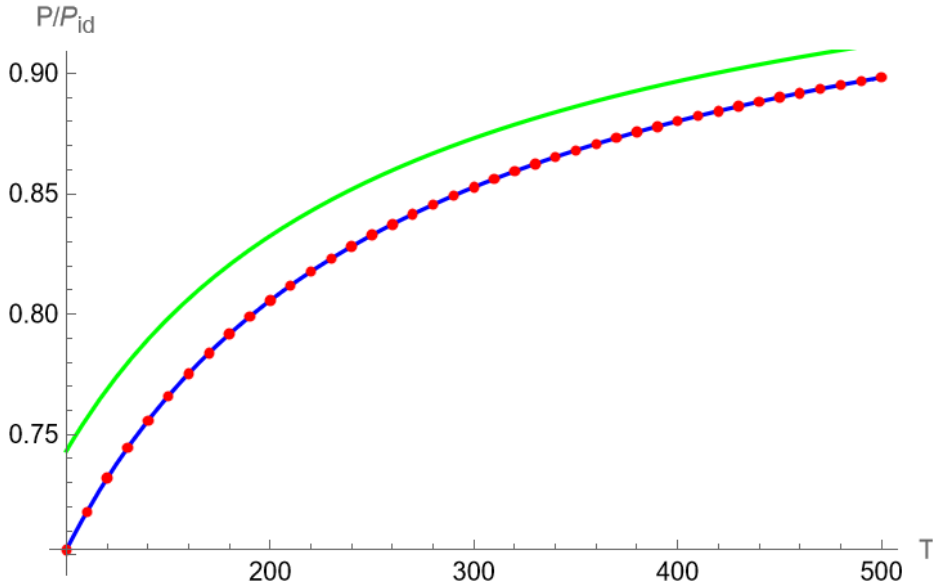

Figure 7.9: Figure showing normalized pressure in the presence of GWs for different A_+. The blue line, red dots, and green line correspond to $A_+ = 0.0001$, 0.01, and 1.1, respectively. We choose $c_2 = 0$ and $\Lambda_{\overline{MS}} = 176$ MeV.

As we can see we have freedom of choosing A_+ and c_2. Keeping $c_2 = 0$, let us investigate the dependence of A_+ on thermodynamic quantities. We plotted the normalized pressure for different A_+ in Fig. (7.9). We found that for any small magnitude $A_+ \ll 1$, the quantities are constant. This can be observed from the blue line and red dots in Fig. (7.9). Whereas for any higher magnitudes ($A_+ > 1$), the quantities change drastically.

To check the dependency of c_2, we plotted the normalized pressure for different values on c_2 while keeping A_+ fixed. The plots are shown in Fig. (7.10). We found that the thermodynamic quantities do not depend on c_2. This observation is the same as in the case

of condensate. Ultimately, the thermodynamic quantities are functions of temperature T and GW amplitude, A_+.

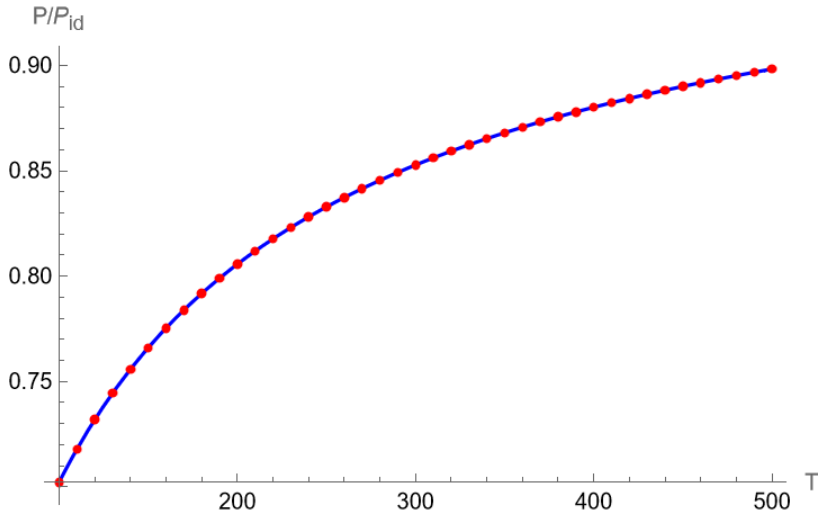

Figure 7.10: Normalized pressure for different c_2 values. The blue line and red dots correspond to $c_2 = 0$ and 100, respectively. We choose $A_+ = 0.01$ and $\Lambda_{\overline{MS}} = 176$ MeV.

As GW enters the calculations as a transverse and traceless mode with a sinusoidal type form, any fluctuation of the same form will do the job. Thus, for a condensate type of configuration to exist at finite temperatures, it has to include fluctuations (here, transverse and traceless modes) along with condensate.

To compare with the lattice QCD results, we have to move to $SU(3)$ with $N_f = 3$ fermion flavours. As our results work for any $SU(N)$ gauge theory, we can extend our results to $SU(3)$. This way of $SU(3)$ analysis is based on the assumption that the QCD system has three separate $SU(2)$ condensates which is not the case. Thus, to compare $SU(3)$ lattice results, one has to study the $SU(3)$ condensates before doing the thermodynamic analysis. This requires more investigation which is a case of future work.

7.6 Conclusion

In this chapter, we investigated many aspects of QGP and QCD phase transition and also the effect of GWs on these phenomena. We start by giving a review of early universe cosmology while going through different epochs. Then, we focussed on QGP and QCD

phase transition in Sec: 7.1. We explained the importance of QGP as it holds answers to many fundamental and interesting questions such as the formation of nuclei from quarks and gluons. The only places on earth to study the QGP are heavy-ion colliders such as LHC, and RHIC. The experimental studies at these colliders show that QGP does not behave as a gas of almost free quarks and gluons but as a strongly interacting fluid. Then, we explored the QCD phase diagram by including finite quark densities and non-zero magnetic fields. QGP is formed at high temperatures and high densities. There are several exotic phases in the QCD phase diagram (μ, T). One such phase is color superconductivity, where quarks form cooper pairs, analogous to conventional superconductivity, which forms at ultra-high densities (higher than nuclear density) and low temperatures. We also stated the current stages of experiments in exploring the finite density regime of the QCD phase diagram.

Then, we explored the phase transitions, particularly the QCD phase transition, that happened in the early universe. We started with the classification of phase transitions (1^{st} order or 2^{nd} order or Crossover) based on their free energy. Every phase transition is associated with symmetry-breaking phenomena. Similarly, for QCD phase transitions, it is associated with two symmetry-breaking phenomena: Chiral symmetry breaking and $Z(3)$ symmetry breaking. Depending on which symmetry breaking, there are two phase transitions: chiral phase transition and confinement-deconfinement phase transition. Both work at two different regimes: chiral symmetry (only for zero mass quarks (Chiral limit)) and $Z(3)$ symmetry (only for pure gauge sector). In the chiral limit, the QCD phase transition is a 1^{st} order phase transition while in the pure gauge limit, it is of 2^{nd} order phase transition. We are interested in the case where the QCD phase transition goes through 1^{st} order phase transition due to its relevance in cosmology explained in the latter part of the section.

Continuing, we explained the importance of a cosmological 1^{st} order QCD phase transition of the BBN. Then, we described the scenario of a QCD phase transition via homogeneous bubble nucleation. In a semi-classical analysis, a first-order phase transition such as a QCD phase transition can be explained using homogeneous bubble nucleation theory.

Thus, we explained the main aspects of the nucleation theory and gave a derivation of a parameter called nucleation rate. The nucleation rate is the probability that a bubble of the second phase is created in a first-phase-filled system near the critical temperature. Following the derivation of nucleation rate, we examined the effect of GWs on QCD phase transition. Here, we considered the effect of GWs on the volume of a bubble which correspondingly influences the nucleation rate. We found that the nucleation rate will be higher in the presence of a GW. It means the QCD phase transition happens sooner in the presence of a GW than without it.

Finally, we come to the main focus of the chapter: Thermodynamics of QGP using finite temperature QFT. We started with an introduction to finite temperature QFT and gave the derivation of the main quantity in finite QFT, the Partition function. After that, we gave a review of functional methods in QFT along with the derivation of effective action. Then, we turn to a crucial tool for studying QGP which is QCD. This is a non-abelian gauge theory which means extra care has to be taken when deriving physical observables. We gave the derivation of QCD generating functional by including the ghost fields present due to gauge freedom. Then, we gave the derivation of 1-loop effective action for QCD using a technique called Background Field Method. According to this method, the gauge field is split into a classical background and a quantum field. Using this method, we end up with a generating functional/effective action dependent on the classical background field. Now, the evaluation of effective action depends on evaluating functional determinants. We calculated these functional determinants using a technique called Heat kernel/Schwinger proper time method. We calculated the effective action for a general configuration in Hamilton's gauge ($A_0^a = 0$). From the effective action, we calculated the thermodynamic potential from which all other thermodynamic quantities can be derived. Then, we calculated the potential for different types of background fields. We first considered the usual spatially homogeneous and isotropic condensate configuration as the background field. We considered two cases: when condensate is at a different temperature than fluctuations and when condensate and

fluctuations are in thermal equilibrium. In the first case, we found that the system has an inflationary type of potential as a function of the c_1 parameter. In the second case, we found the thermodynamic system has a negative pressure (P), entropy density (S), and energy density (ε), but a positive $w = P/\varepsilon$. This indicates the presence of a new state of matter or it could be signifying the non-existence of condensate-only configuration at finite temperatures. However, with the introduction of GWs, we recover the standard behaviour with $P > 0,\ S > 0,\ \varepsilon > 0$ as predicted in lattice gauge theories. We introduced the GWs in such a way that it is presented in the form of a solution of extended condensate configuration obtained in Sec: 5.2. The work done by GWs can also be recovered with condensate + transverse-traceless sinusoidal mode fluctuations type of background. We conclude that at finite temperatures, the QGP condensate requires interaction with GW or induced transverse traceless plasmons to be a stable fluid with standard behavior.

Chapter 8

Conclusions

> ”The scientist does not study nature because it is useful to do so. He studies it because he takes pleasure in it, and he takes pleasure in it because it is beautiful. If nature were not beautiful it would not be worth knowing, and life would not be worth living.”
>
> *Henri Poincare*

Gravitational Waves, the ethereal whispers of the cosmos, ripple through the very fabric of spacetime, unveiling the majestic symphony of celestial events that shape our universe. With each pulse, they carry the echoes of cataclysmic collisions and cosmic dances, offering humanity a profound glimpse into the hidden realms of existence, where time and space intertwine in a magnificent cosmic ballet. It is one of the two waves that can travel across the cosmos bringing us information about the events that happen far away. The other is electromagnetic waves (including microwaves, radio waves, X-rays,..). EM waves consist of oscillating electric and magnetic fields that travel at light speed. When EM waves interact with a charged particle, those particles get excited and oscillate back and forth, while the information carried by waves gets imprinted in the particles. On the other hand, the GWs consist of oscillation of spacetime itself. The study of the cosmos with electromagnetic telescopes started by Galileo led to a separate branch known as Electromagnetic Astron-

omy. As the GWs can be produced by some of the strong objects in the entire cosmos and can travel without interacting through long distances, they provide information about these events such as the collision of binary black holes, and neutron stars, or the events in the very early universe. The discovery of the first GWs leads to the birth of a new branch of astronomy known as GW astronomy. As GWs hold information about the cosmos, one needs to understand the interaction of GWs with matter particles through which we can extract the information. In Chapter 2, we presented a review of the interaction of GWs with different matter fields such as scalar fields, fermionic fields, and electromagnetic waves.

Now, let us consider imagining a world where the very fabric of matter is stripped down to its most fundamental components. In the realm of QGP, this extraordinary state of matter emerges, akin to a cosmic furnace where quarks and gluons roam unbound, liberated from the confines of protons and neutrons. This ephemeral phase, believed to have existed within the first moments of the universe, holds the key to understanding the intricate framework of particle interactions and the birth of the cosmos itself. Exotic matter of this nature is currently being produced and studied in some of the largest experimental facilities on the planet, including the LHC at CERN and the RHIC at BNL. The underlying theory that is used to study the QGP and hadronization is QCD. QCD is a $SU(3)$ non-abelian gauge theory. In chapter 3, we described the basics of non-abelian gauge theory along with some of the classical solutions of the theory. In heavy-ion colliders, massive gauge bosons such as W and Z bosons were observed as opposed to the case of gluons. To investigate these bosons, we also described the theory of Electroweak symmetry breaking (see Sec: 3.3). For the entire thesis, we focused on dealing with $SU(2)$ gauge theory.

In our thesis, we planned to understand the interplay between the GWs and non-abelian gauge fields and their relation with the QGP. As QGP forms at very high temperatures, the quarks and gluons in it can propagate as waves. With this approximation, we investigated the interaction of GWs with non-abelian waves in Minkowski spacetime (see Sec:4.2) and deSitter spacetime (see Sec: 4.3). For simplicity, we considered only gluons. We derived

the linearized YM equations for the gauge field perturbations in the presence of GWs. We find that the interaction with the GWs causes perturbations in the gauge field configurations. Depending on the YM coupling constant (g_{ym}), we classified the YM waves into types: Type I and Type II. Type I waves are similar to electromagnetic waves as in this case, there will be no nonlinear terms in the YM equations of motion. We find the results of the interaction of GWs with type I waves are the same as those interaction with EM waves. We find no interaction between the waves when they are propagating in the parallel direction same as in the EM case. We found that perturbed waves show a beat pattern as expected. We also find that the nature of interaction also depends on the relative propagating direction between GW and YM waves. In Coleman type of waves, we found a new mode of frequency $\sqrt{\omega_g^2+\omega_y^2}$ when waves are propagating perpendicular to each other. For the type II waves, we found a nonzero interaction between the waves even in parallel directions. This is due to the presence of non-linear terms in the YM equations. Even in this case, we found an overall beat pattern for the perturbed waves. However, due to having a complicated frequency pattern for the unperturbed type II solutions, we found there are more frequency modes other than the usual two-beat frequencies.

In the later section 4.3, we analyze the interaction of GWs with $SU(2)$ YM waves in the background of de-Sitter spacetime. As GWs propagate in the expanding de-Sitter spacetime, the expressions for GWs also become complicated (see Sec:2.1.3). We found there is a non-zero interaction between the waves even when they are propagating in parallel directions because of having a complicated expression for GW. We found that both types of perturbed waves show an attenuation behaviour. Then, in section 4.4, we analyzed the interaction of GWs with massive gauge bosons (W and Z). For this, we used the type II wave configuration to represent W and Z bosons. We found that the GWs can perturb the W and Z bosons and increase their magnitudes to high values rapidly signifying the breakdown of linearized analysis. To fully understand the system, one has to investigate the system using non-perturbative methods. This will be a work of the future.

The heavy-ion collision experiments aimed to create the primordial soup found that the QGP created in heavy-ion colliders does not behave as a gas of almost free quarks and gluons but as a strongly interacting fluid. This is because the QGP created at colliders is around the critical temperature (T_c). Under these temperatures, QGP behaves like a strongly interacting fluid showing the features of an almost perfect fluid. In GR, the usage of perfect fluids is very well known. In our case, we can approximate the QGP as a condensate + fluctuations. Here, condensate resembles the fluid with perfect fluidity and the fluctuations are to capture the deviations from perfect fluid nature. With this, we studied the condensate + fluctuations model in two different ways depending on the fluctuations mode decomposition. In the first way, we did the fluctuations decomposition using tensor decomposition introduced in [38]. It was found that there is a net energy exchange from the condensate to fluctuations [38]. Then, we studied the system in the presence of a GW background. We found that only transverse-traceless modes interact with GWs. We also found that the transverse-traceless modes can be generated due to the interaction between GWs and condensate even if they were set to zero initially. Also, within this decomposition, GWs do not interact with longitudinal modes. To include the discussion of longitudinal modes, we considered a different decomposition: Vector decomposition. This way of decomposition clearly distinguishes the longitudinal from the transverse modes. With this decomposition, we studied the condensate + fluctuations (transverse + longitudinal modes) model (see Sec: 5.3). Even in this model, we found there is an energy exchange between the condensate and fluctuations for a long time and eventually to a net energy transfer from condensate to fluctuations. We found that the energy swap effect highly depends on the YM coupling constant and condensate initial conditions. The energy exchange happens in an oscillatory way instead of a monotonic decay. In this decomposition, the longitudinal modes were also interacting with GWs. Later, we studied the system in the presence of GW (see Sec: 5.3.1). We found that the GWs can induce plasmon oscillations. We also found that the GWs stabilize the gauge field ansatz (condensate + longitudinal modes + transverse modes)

by delaying the condensate decay. This analysis is crucial in understanding the QGP in the presence of GWs.

As quarks are an integral part of QGP, we investigated the dynamics of quarks in the background of condensate (see Sec: 6.1). For this, we solved the Dirac equation in the presence of $SU(2)$ YM condensate in the Minkowski background. Due to the presence of condensate, we found that there is a mixing of two fermion components from different flavours. However, the fermion probability densities for these different fermion flavour components remain unmixed. As the non-zero fermions fields create non-zero current densities, these current densities generate the gauge field fluctuations which ultimately results in a change of condensate configuration. The backreaction of fermions on the condensate is investigated in Sec. 6.1.1. We found that the condensate loses its isotropic and homogenetic nature with the introduction of fermions. Under certain initial conditions, we obtained a configuration such that a or $i = 1,2$ behaves in a different way than a or $i = 3$ components.

Then, we investigated the behaviour of fermions in the presence of condensate in the GW background (see Sec: 6.2). In this case, we found two fermion components from two different flavours become coupled due to the interaction among GW, condensate, and fermion flavour components. Here, the two coupled components are different from the ones without the GW case. We found that the fermion probability densities of the coupled components are still mixed signifying the fermion flavour transition. This fermion flavour transition is very relevant for the QGP as quarks and gluons continuously interact in QGP. Our calculations showed the enhancement of one flavour over the other in the presence of both GWs and condensate. We demonstrated the fermion flavour transition for a general fermion doublet. This can be of lepton doublets or isospin doublets such as (u,d) quarks or (c,s) quarks. In the case of an isospin doublet (u,d), if we start with a system with more up (u) quarks, then due to interactions with condensate and GWs, we end up with a system with more down (d) quarks than up (u) quarks. This flavour transition is also relevant for investigating the strangeness in QGP.

As QGP is a many-body system, one has to investigate the statistical aspects of the system. In the second part of the thesis, we started with a review of the thermodynamic aspects of QGP and QCD phase transition. We also explored the different aspects of the QCD phase diagram such as colour superconductivity apart from QGP. Then, we focused our attention on the first-order QCD phase transition due to its importance in setting the initial conditions for the Big Bang Nucleosynthesis. As the first-order phase transition goes through homogeneous bubble nucleation, we gave an overview of it including the derivation of nucleation rate. Then, we studied the effect of GWs on the QCD phase transition (see Sec: 7.3). We found that the nucleation rate in the presence of GW is higher than in the absence of GW. It means the QCD phase transition happens faster in the presence of a GW.

Then, we investigated the thermodynamics of QGP by calculating the thermodynamic potential of QGP in different background gauge fields using finite temperature QFT. The background gauge fields include the usual spatially homogeneous and isotropic condensate (see Sec: 5.1), a modified condensate ansatz (see Sec: 6.1.1) and the GW modified condensate configuration (see Sec: 5.2). For the condensate field, at thermal equilibrium, we find the system has negative pressure, energy and entropy densities. As the energy density is negative, this signifies a new form of matter or it is indicative of the non-existence of a condensate type of configuration at finite temperatures. However, we found that we can obtain the standard thermodynamic behaviour of QGP with the introduction of GWs. We also found a different approximation for the QGP as a condensate + GWs model or a condensate + fluctuations (transverse- traceless sinusoidal) model. This shows the importance of GWs in recovering the standard QGP behaviour.

8.1 Open Problems

As the QGP holds secrets to understanding the matter we are made of, it is vital to investigate it more deeply. Also, the GWs from the very early universe form a GW background across the entire universe. Thus, the QGP in the presence of GWs is needed to be under-

stood to understand the early universe. Thus, the following research extensions motivated by this work, are proposed.

1. Flavour transitions induced by gravity and Strangeness in QGP

Coupling gravity with matter has been ongoing since everyone tried to unify the four fundamental forces. In our work, using the Dirac equation in the presence of condensate and GW, we found there is a fermion flavour transition. This project will be a QFT version of it by examining the effect of GWs in these flavour-changing processes. This work can also explain the enhanced strangeness in QGP. This can be done by extending my work to $SU(3)$ with up (u), down (d) and strange (s) quarks which might able to extend the flavour transition process to the generation of strange quarks from the light quarks.

2. Transport Properties of QGP such as dissipation, viscosity, etc..

QGP produced in heavy-ion colliders is usually not in perfect thermal equilibrium. Collision experiments show non-zero transport properties such as bulk and shear viscosities, thermal conductivities and heat dissipation. Furthermore, its shear-viscosity observed in the experiment is lower than that of any substance on Earth. We plan to extend our condensate (and its modifications) models to investigate the transport properties.

3. Condensates in higher gauge groups $SU(N), N > 2$

In this work, we worked with $SU(2)$ condensates. We would like to extend that work to higher gauge groups such as $SU(N)$. The most important higher gauge group is that of QCD which is $SU(3)$. A generalisation of these studies to the $SU(3)$ theory appears to be conceptually straightforward but technically much more involved.

4. Generalising $SU(2)$ condensate model to curved spacetimes

While investigating the condensate + transverse-traceless modes in a GW background (see Sec: 5.2), we used the triads to find out the analytical solutions. Using the same triad formalism, we can extend the $SU(2)$ condensate analysis to curved spacetimes. Using the ADM formalism along with the triad formalism, one can extend the condensate + fluctuations model to more general spacetimes. We already found that a thermodynamic model of

QGP with only condensate as a background field cannot exist at finite temperatures. However, with the introduction of GWs, the QGP model shows a standard behaviour similar to the lattice gauge results. In this work, we will investigate the influence of background spacetimes on the stability of condensate. This work will help in a greater understanding of QGP during the very early universe.

8.2 Summary

This thesis has aimed to explore the "Interaction of Gravitational waves with non-abelian gauge fields and Quark-Gluon Plasma". This project is an interplay between Gravitational waves, non-abelian gauge fields and Quark-Gluon Plasma. It involves the combination of the two pillars of modern physics: General relativity and Quantum Physics. This work is relevant for both the Quantum Chromodynamics and gravitational physics communities. From our investigations, we conclude the following main observations:

1. GWs interact non-trivially with YM gauge fields. Some of the results include the interaction of GWs with massive YM fields like W and Z bosons. These non-trivial interactions might cause a change in the decay pattern of plasma that can be detected in heavy-ion colliders such as LHC, and RHIC.

2. The QGP with an almost perfect fluid nature is approximated with a Condensate (Plasma) + Fluctuations (plasmons) model. We found that there is an energy exchange between the condensate and fluctuations for a longer time than predicted in [38]. After that, there is an oscillatory net energy transfer effect from condensate to fluctuations.

3. With our model of QGP + GW, we found that GWs can induce plasmon oscillations and generate fluctuations. Then, these fluctuations exchange the energy with condensate. Apart from generating fluctuations, GWs also stabilize the condensate making the energy exchange take place for even longer times.

4. When fermions interacts in the background of condensate in the presence of GWs, we found there is an occurrence of a flavour transition of fermions. Even a small perturbation in spacetime (like GW) can lead to a transition of fermions from one flavour to another, like an u quark to a d quark.

5. Using finite temperature field theory, with the condensate model as background, we found that the only-condensate model cannot exist at finite temperatures. But, with GWs, we were able to recover the standard lattice gauge theory behaviour. Thus, GWs are required to stabilize/ permit the condensate to exist at finite temperatures.

These findings not only contribute to the theoretical understanding of QGP but also predict what can be detectable in particle physics experiments. Looking forward, the findings of this thesis not only illuminate the path ahead but also inspire a renewed commitment to advancing our understanding of interdisciplinary research between General Relativity and Quantum Physics.

Bibliography

[1] A. A. Penzias and R. W. Wilson, "A measurement of excess antenna temperature at 4080 Mc/s.", Astrophys. J. **142**, 419–421 (1965).

[2] C. L. Bennett et al., "Nine-year Wilkinson Microwave Anisotropy Probe (WMAP) observations: Final maps and results", Astrophys. J. **208**, 20, 20 (2013), arXiv:1212.5225 [astro-ph.CO].

[3] L. Amendola et al., "Cosmology and fundamental physics with the Euclid satellite", Living Rev. Rel **16**, 6, 6 (2013), arXiv:1206.1225 [astro-ph.CO].

[4] K. S. Dawson et al., "The Baryon Oscillation Spectroscopic survey of SDSS-III", Astrophys. J. **145**, 10, 10 (2013), arXiv:1208.0022 [astro-ph.CO].

[5] R. Adam et al., "Planck 2015 results. I. Overview of products and scientific results", Astron. Astrophys. **594**, A1 (2016), arXiv:1502.01582 [astro-ph.CO].

[6] V. F. Mukhanov and G. V. Chibisov, "Quantum fluctuations and a nonsingular universe", JETP Lett. **33**, 532–535 (1981).

[7] A. H. Guth, "Inflationary universe: a possible solution to the horizon and flatness problems", Phys. Rev. D **23**, 347–356 (1981).

[8] A. A. Starobinsky, "Spectrum of relic gravitational radiation and the early state of the universe", JETP Lett. **30**, edited by I. M. Khalatnikov and V. P. Mineev, 682–685 (1979).

[9] M. Kamionkowski, A. Kosowsky, and A. Stebbins, "Statistics of cosmic microwave background polarization", Phys. Rev. D **55**, 7368–7388 (1997), arXiv:astro-ph/9611125.

[10] B. P. Abbott et al., "Observation of gravitational waves from a Binary Black Hole merger", Phys. Rev. Lett. **116**, 061102 (2016).

[11] C. Caprini and D. G. Figueroa, "Cosmological backgrounds of gravitational waves", Class. Quant. Grav. **35**, 163001, 163001 (2018), arXiv:1801.04268 [astro-ph.CO].

[12] R. Allahverdi, R. Brandenberger, F. Y. Cyr-Racine, and A. Mazumdar, "Reheating in inflationary cosmology: Theory and applications", Ann. Rev. Nucl. Part. Sci. **60**, 27–51 (2010), arXiv:1001.2600 [hep-th].

[13] M. A. Amin, M. P. Hertzberg, D. I. Kaiser, and J. Karouby, "Nonperturbative dynamics of reheating after inflation: A review", Int. J. Mod. Phys. D **24**, 1530003 (2014), arXiv:1410.3808 [hep-ph].

[14] V. A. Rubakov and D. S. Gorbunov, *Introduction to the theory of the early universe: Hot Big Bang theory* (World Scientific Publishing, 2018).

[15] U. Sarkar, *Particle and astroparticle physics*, Series in high energy physics, cosmology, and gravitation (Taylor & Francis, New York, USA, 2008).

[16] U. Vojtěch, *Gravity, space-time, the theory of relativity - how the universe works*, Obtained permission from the author (Czechoslovak astronomical society, 1986).

[17] J. P. Blaizot and E. Iancu, "Non-abelian plane-waves in the quark-gluon plasma", Phys. Lett. B **326**, 138–144 (1994), arXiv:hep-ph/9401323 [hep-ph].

[18] E. P. Politis, C. E. Tsagkarakis, F. K. Diakonos, X. N. Maintas, and A. Tsapalis, "A non-abelian quasi-particle model for gluon plasma", Phys. Lett. B **763**, 139–144 (2016), arXiv:1501.01032 [hep-ph].

[19] S. S. Dave, S. Digal, and V. Mamale, "Parametric resonance in abelian and non-abelian gauge fields via spacetime oscillations", Phys. Rev. D. **109**, 076023, 076023 (2024), arXiv:2301.07456 [hep-ph].

[20] C. Barrabès and P. A. Hogan, "Interaction of gravitational waves with magnetic and electric fields", Phys. Rev. D **81**, 064024 (2010).

[21] F. I. Cooperstock, "The interaction between electromagnetic and gravitational waves", Annals Phys **47**, 173–181 (1968).

[22] D. M. Zipoy, "Light fluctuations due to an intergalactic flux of gravitational waves", Phys. Rev. **142**, 825–838 (1966).

[23] R. Fakir, "Gravitational wave detection: A nonmechanical effect", Astrophys. J. **418**, 202 (1993).

[24] S. Kopeikin, P. Korobkov, and A. Polnarev, "Propagation of light in the field of stationary and radiative gravitational multipoles", Class. Quant. Grav. **23**, 4299–4322 (2006), arXiv:gr-qc/0603064 [gr-qc].

[25] C. G. Tsagas, "Gravitoelectromagnetic resonances", Phys. Rev. D **84**, 043524 (2011).

[26] A. Patel and A. Dasgupta, "Interaction of Electromagnetic field with a Gravitational wave in Minkowski and de-Sitter space-time", arXiv e-prints:2108.01788 (2021), arXiv:2108.01788 [gr-qc].

[27] N. R. Gosala and A. Dasgupta, "Interaction of gravitational waves with Yang-Mills fields", Gen. Rel. Grav. **56**, 36, 36 (2024), arXiv:2212.02416 [gr-qc].

[28] C. H. Oh and R. Teh, "Nonabelian progressive waves", J. Math. Phys. **26**, 841–844 (1985), eprint: https://doi.org/10.1063/1.526576.

[29] M. Siddhartha and A. Dasgupta, "Scalar and fermion field interactions with a gravitational wave", Class. Quant. Grav. **37**, 105001 (2020), arXiv:1907.07531 [gr-qc].

[30] M. E. Peskin and D. V. Schroeder, *An Introduction to quantum field theory* (Addison-Wesley, Reading, USA, 1995).

[31] W. A. Zajc, "The fluid nature of quark-gluon plasma", Nucl. Phys. A **805**, 283–294 (2008), arXiv:0802.3552 [nucl-ex].

[32] V. V. Dyadichev, D. V. Gal'tsov, A. G. Zorin, and M. Y. Zotov, "Nonabelian Born-Infeld cosmology", Phys. Rev. D **65**, 084007 (2002), arXiv:hep-th/0111099.

[33] D. V. GalTsov and E. A. Davydov, "Yang-Mills Condensates in Cosmology", in International journal of modern physics conference series, Vol. 14, International Journal of Modern Physics Conference Series (July 2012), pp. 316–325, arXiv:1112.2943 [hep-th].

[34] D. V. Galtsov and M. S. Volkov, "Yang-Mills cosmology: Cold matter for a hot universe", Phys. Lett. B **256**, 17–21 (1991).

[35] J. Cembranos, A. Maroto, and S. N. Jareno, "Isotropy theorem for cosmological Yang-Mills theories", Phys. Rev. D **87**, 043523, 043523 (2013), arXiv:1212.3201 [astro-ph.CO].

[36] A. Maleknejad and M. M. Sheikh-Jabbari, "Gauge-flation: Inflation from non-abelian gauge fields", Phys. Lett. B **723**, 224–228 (2013), arXiv:1102.1513 [hep-ph].

[37] A. Maleknejad and M. M. Sheikh-Jabbari, "Non-abelian gauge field inflation", Phys. Rev. D **84**, 043515 (2011), arXiv:1102.1932 [hep-ph].

[38] G. Prokhorov, R. Pasechnik, and G. Vereshkov, "Dynamics of wave fluctuations in the homogeneous Yang-Mills condensate", JHEP **07**, 003 (2014), arXiv:1307.5695 [hep-th].

[39] V. M. Bannur, "Relativistic longitudinal non-abelian oscillations in quark-antiquark plasma", Pramana **59**, 671–677 (2002).

[40] J. P. Blaizot and E. Iancu, "Nonabelian plane waves in the quark - gluon plasma", Phys. Lett. B **326**, 138–144 (1994), arXiv:hep-ph/9401323.

[41] B. Schenke, "Collective phenomena in the non-equilibrium quark-gluon plasma", PhD thesis (Frankfurt U., 2008), arXiv:0810.4306 [hep-ph].

[42] G. Prokhorov, R. Pasechnik, and G. Vereshkov, "Wave fluctuations in the system with some Yang-Mills condensates", Phys. Atom. Nuclei **79**, 1502–1504 (2016).

[43] D. Fogaca and F. Navarra, "Gluon condensates in a cold quark–gluon plasma ", Phys. Lett. B **700**, 3, 236 (2011).

[44] N. R. Gosala and A. Dasgupta, "Effect of gravitational Waves on Yang-Mills condensates", arXiv e-prints :2401.12330, arXiv:2401.12330, 10.48550/arXiv.2401.12330 (2024), arXiv:2401.12330 [gr-qc].

[45] V. Domcke, Y. Ema, K. Mukaida, and R. Sato, "Chiral anomaly and Schwinger effect in non-abelian gauge theories", JHEP **2019**, 111, 111 (2019), arXiv:1812.08021 [hep-ph].

[46] L. Mirzagholi, A. Maleknejad, and K. D. Lozanov, "Production and backreaction of fermions from axion-SU(2) gauge fields during inflation", Phys. Rev. D. **101**, 083528, 083528 (2020), arXiv:1905.09258 [hep-th].

[47] E. Farhi, J. Goldstone, S. Gutmann, K. Rajagopal, and R. Singleton, "Fermion production in the background of Minkowski space classical solutions in spontaneously broken gauge theory", Phys. Rev. D **51**, 4561–4572 (1995).

[48] P. Adshead and E. I. Sfakianakis, "Fermion production during and after axion inflation", Journ. Cosmol. Astr. Phys. **2015**, 021–021 (2015), arXiv:1508.00891 [hep-ph].

[49] P. Adshead, L. Pearce, M. Peloso, M. A. Roberts, and L. Sorbo, "Phenomenology of fermion production during axion inflation", Journ. Cosmol. Astr. Phys. **2018**, 020, 020 (2018), arXiv:1803.04501 [astro-ph.CO].

[50] V. A. Rubakov, *Classical theory of gauge fields* (Princeton University Press, Princeton, New Jersey, May 2002).

[51] L. F. Abbott, "Introduction to the Background Field Method", Acta Phys. Polon. B **13**, 33 (1982).

[52] N. Gosala and A. Dasgupta, "Thermodynamics of Quark-Gluon Plasma using time-dependent condensates", in preparation (2024).

[53] M. P. Hobson, G. P. Efstathiou, and A. N. Lasenby, *General relativity: An introduction for physicists* (Cambridge University Press, 2006).

[54] A. Ali, C. Isham, T. Kibble, and Riazuddin, eds., *Selected papers of Abdus Salam: With commentary* (World Scientific Publishing, 1994).

[55] S. Weinberg, *Gravitation and Cosmology: Principles and applications of the General Theory of Relativity* (John Wiley and Sons, New York, 1972).

[56] C. Ma and E. Bertschinger, "Cosmological perturbation theory in the synchronous and conformal Newtonian gauges", Astrophys. J. **455**, 7–25 (1995), arXiv:astro-ph/9506072.

[57] H. Stephani, D. Kramer, M. A. H. MacCallum, C. Hoenselaers, and E. Herlt, *Exact solutions of Einstein's field equations*, Cambridge Monographs on Mathematical Physics (Cambridge Univ. Press, Cambridge, 2003).

[58] B. P. Abbott et al., "GW151226: Observation of gravitational waves from a 22-Solar-Mass Binary Black Hole coalescence", Phys. Rev. Lett. **116**, 241103 (2016).

[59] B. P. Abbott et al., "GW170104: Observation of a 50-Solar-Mass Binary Black Hole Coalescence at Redshift 0.2", Phys. Rev. Lett. **118**, 221101 (2017).

[60] B. P. Abbott et al., "GW170817: Observation of gravitational waves from a Binary Neutron Star Inspiral", Phys. Rev. Lett. **119**, 161101 (2017).

[61] B. P. Abbott et al., "Multi-messenger observations of a Binary Neutron star merger", Astrophys. J. Lett. **848**, L12, L12 (2017), arXiv:1710.05833 [astro-ph.HE].

[62] T. Baker, E. Bellini, P. G. Ferreira, M. Lagos, J. Noller, and I. Sawicki, "Strong constraints on cosmological gravity from GW170817 and GRB 170817A", Phys. Rev. Lett. **119**, 251301, 251301 (2017), arXiv:1710.06394 [astro-ph.CO].

[63] J. Sakstein and B. Jain, "Implications of the Neutron star merger GW170817 for cosmological scalar-tensor theories", Phys. Rev. Lett. **119**, 251303, 251303 (2017), arXiv:1710.05893 [astro-ph.CO].

[64] J. M. Ezquiaga and M. Zumalacárregui, "Dark energy after GW170817: Dead ends and the road ahead", Phys. Rev. Lett. **119**, 251304, 251304 (2017), arXiv:1710.05901 [astro-ph.CO].

[65] L. Lombriser and A. Taylor, "Breaking a dark degeneracy with gravitational waves", JCAP **2016**, 031, 031 (2016), arXiv:1509.08458 [astro-ph.CO].

[66] L. Lombriser and N. A. Lima, "Challenges to self-acceleration in modified gravity from gravitational waves and large-scale structure", Phys. Lett. B **765**, 382–385 (2017), arXiv:1602.07670 [astro-ph.CO].

[67] P. Creminelli and F. Vernizzi, "Dark energy after GW170817 and GRB170817A", Phys. Rev. Lett. **119**, 251302, 251302 (2017), arXiv:1710.05877 [astro-ph.CO].

[68] B. P. Abbott et al., "A gravitational-wave standard siren measurement of the Hubble constant", Nature **551**, 85–88 (2017), arXiv:1710.05835 [astro-ph.CO].

[69] M. Maggiore, "Gravitational wave experiments and early universe cosmology", Phys. Rept. **331**, 283–367 (2000), arXiv:gr-qc/9909001 [gr-qc].

[70] B. S. Sathyaprakash and B. F. Schutz, "Physics, Astrophysics and Cosmology with gravitational waves", Living Rev. Rel. **12**, 2, 2 (2009), arXiv:0903.0338 [gr-qc].

[71] O. D. Aguiar, "Past, present and future of the Resonant-Mass gravitational wave detectors", Res. Astron. Astrophys. **11**, 1 (2011).

[72] M. Gregory, "Second generation gravitational wave detectors", in *The twelfth marcel grossmann meeting* (World Scientific Publishing, 2012), pp. 628–644, eprint: https://www.worldscientific.com/doi/pdf/10.1142/9789814374552_0032.

[73] LIGO Scientific Collaboration, "Advanced LIGO", Class. Quant. Grav. **32**, 074001, 074001 (2015), arXiv:1411.4547 [gr-qc].

[74] H. Abe et al., "The current status and future prospects of KAGRA, the large-scale cryogenic gravitational wave telescope built in the Kamioka underground", Galaxies **10**, 10.3390/galaxies10030063 (2022).

[75] B. F. Schutz, "Networks of gravitational wave detectors and three figures of merit", Class. Quant. Grav. **28**, 125023, 125023 (2011), arXiv:1102.5421 [astro-ph.IM].

[76] M. Punturo, R. De Salvo, C. D. Ott, and K. Somiya, "The third generation of gravitational wave observatories and their science reach", Classical and Quantum Gravity **27**, Funding by European Commission Framework Programme 7 (FP7), Art. No. 084007 (2010).

[77] A. Freise et al., "Triple Michelson interferometer for a third-generation gravitational wave detector", Class. Quant. Grav. **26**, 085012, 085012 (2009), arXiv:0804.1036 [gr-qc].

[78] D. Reitze et al., "Cosmic explorer: The U.S. contribution to gravitational-wave astronomy beyond LIGO", in Bull. am. astron. soc. Vol. 51 (Sept. 2019), p. 35, arXiv:1907.04833 [astro-ph.IM].

[79] P. Amaro-Seoane et al., "Low-frequency gravitational-wave science with eLISA/NGO", Class. Quant. Grav. **29**, 124016, 124016 (2012), arXiv:1202.0839 [gr-qc].

[80] S. Kawamura et al., "The Japanese space gravitational wave antenna DECIGO", Class. Quant. Grav. **23**, edited by N. Mio, S125–S132 (2006).

[81] J. Luo et al., "TianQin: a space-borne gravitational wave detector", Class. Quant. Grav. **33**, 035010, 035010 (2016), arXiv:1512.02076 [astro-ph.IM].

[82] G. Hobbs et al., "The International Pulsar Timing Array project: using pulsars as a gravitational wave detector", Class. Quant. Grav. **27**, 084013, 084013 (2010), arXiv:0911.5206 [astro-ph.SR].

[83] M. Rini, "Researchers capture gravitational-wave background with Pulsar "Antennae"", APS Physics **16**, 118 (2023).

[84] R. Geiger, "Future gravitational wave detectors based on atom interferometry", in *An overview of gravitational waves: theory* (World Scientific Publishing, 2017), pp. 285–313.

[85] E. Flanagan and S. A. Hughes, "The basics of gravitational wave theory", New J. Phys. **7**, 204 (2005), arXiv:gr-qc/0501041 [astro-ph].

[86] J. M. Bardeen, "Gauge-invariant cosmological perturbations", Phys. Rev. D **22**, 1882–1905 (1980).

[87] E. Bertschinger, "Cosmological perturbation theory and structure formation", in Cosmology 2000 (Jan. 2001), pp. 1–25, arXiv:astro-ph/0101009.

[88] J. M. Stewart, "Perturbations of Friedmann-Robertson-Walker cosmological models", Class. Quant. Grav. **7**, 1169 (1990).

[89] E. Lifshitz, "Republication of: on the gravitational stability of the expanding universe", Gen. Rel. Grav. **49**, 10.1007/s10714-016-2165-8 (2017).

[90] J. Bladel, "On Helmholtz's theorem in finite regions", IRE Transactions on Antennas and Propagation **7**, 119–119 (1959).

[91] J. Stewart, *Advanced General Relativity*, Cambridge Monographs on Mathematical Physics (Cambridge University Press, 1991).

[92] Y. Watanabe and E. Komatsu, "Improved calculation of the primordial gravitational wave spectrum in the standard model", Phys. Rev. D **73**, 123515, 123515 (2006), arXiv:astro-ph/0604176 [astro-ph].

[93] S. Nakamura, N. Yoshino, and S. Kobayashi, "Background gravitational wave produced in inflationary universe", Prog. Theor. Phys. **88**, 1107–1118 (1992).

[94] A. Najmi and A. C. Ottewill, "Quantum states and the Hadamard form. I. Energy minimization for scalar fields", Phys. Rev. D **30**, 1733–1741 (1984).

[95] B. Allen, "Vacuum states in de Sitter space", Phys. Rev. D **32**, 3136–3149 (1985).

[96] A. Buonanno, "TASI lectures on gravitational waves from the early universe", in Theoretical Advanced Study Institute in Elementary Particle Physics (TASI 2002): Particle Physics and Cosmology: The Quest for Physics Beyond the Standard Model(s) (Mar. 2003), pp. 855–892, arXiv:gr-qc/0303085.

[97] B. Allen, "The Stochastic Gravity-wave background: Sources and detection", in Relativistic gravitation and gravitational radiation, edited by J.-A. Marck and J.-P. Lasota (Jan. 1997), p. 373, arXiv:gr-qc/9604033 [gr-qc].

[98] B. Allen, "Stochastic gravity-wave background in inflationary-universe models", Phys. Rev. D **37**, 2078–2085 (1988).

[99] T. S. Bunch, P. C. W. Davies, and R. Penrose, "Quantum field theory in de Sitter space: renormalization by point-splitting", Proc. Roy. Soc. Lond. A **360**, 117–134 (1978), eprint: https://royalsocietypublishing.org/doi/pdf/10.1098/rspa.1978.0060.

[100] L. F. Abbott and D. D. Harari, "Graviton production in inflationary cosmology", Nucl. Phys. B **264**, 487–492 (1986).

[101] Sources and types of gravitational waves, https://www.ligo.caltech.edu/page/gw-sources, LIGO Caltech.

[102] P. C. Peters, "Gravitational radiation and the motion of two point masses", Phys. Rev. **136**, B1224–B1232 (1964).

[103] P. D. Lasky, "Gravitational waves from Neutron stars: A Review", Publ. Astron. Soc. Austral. **32**, e034 (2015).

[104] A. H. Guth, "Inflationary universe: a possible solution to the horizon and flatness problems", Phys. Rev. D **23**, 347–356 (1981).

[105] A. D. Linde, "A new inflationary universe scenario: A possible solution of the horizon, flatness, homogeneity, isotropy and primordial monopole problems", Phys. Lett. B **108**, 389–393 (1982).

[106] V. A. Rubakov, M. V. Sazhin, and A. V. Veryaskin, "Graviton creation in the inflationary universe and the grand unification scale", Phys. Lett. B **115**, 189–192 (1982).

[107] A. A. Starobinsky, "Spectrum of relic gravitational radiation and the early state of the universe", JETP Lett. **30**, edited by I. M. Khalatnikov and V. P. Mineev, 682–685 (1979).

[108] L. P. Grishchuk, "Amplification of gravitational waves in an isotropic universe", Zh. Eksp. Teor. Fiz. **67**, 825–838 (1974).

[109] P. Cabella and M. Kamionkowski, "Theory of cosmic microwave background polarization", in International School of Gravitation and Cosmology: The Polarization of the Cosmic Microwave Background (Mar. 2004), arXiv:astro-ph/0403392.

[110] U. Seljak and M. Zaldarriaga, "Signature of gravity waves in the polarization of the Microwave background", Phys. Rev. Lett. **78**, 2054–2057 (1997), arXiv:astro-ph/9609169 [astro-ph].

[111] F. Finelli and A. Gruppuso, "Resonant amplification of gauge fields in expanding universe", Phys. Lett. B **502**, 216–222 (2001), arXiv:hep-ph/0001231 [hep-ph].

[112] M. Biagetti, M. Fasiello, and A. Riotto, "Enhancing inflationary tensor modes through spectator fields", Phys. Rev. D **88**, 103518, 103518 (2013), arXiv:1305.7241 [astro-ph.CO].

[113] A. D. Linde, *Particle physics and inflationary cosmology*, Vol. 5 (Taylor & Francis group, 1990), arXiv:hep-th/0503203.

[114] L. Kofman, A. Linde, and A. A. Starobinsky, "Reheating after inflation", Phys. Rev. Lett. **73**, 3195–3198 (1994), arXiv:hep-th/9405187 [hep-th].

[115] G. Felder, L. Kofman, and A. Linde, "Tachyonic instability and dynamics of spontaneous symmetry breaking", Phys. Rev. D **64**, 123517 (2001), arXiv:hep-th/0106179 [astro-ph].

[116] E. Witten, "Cosmic separation of phases", Phys. Rev. D **30**, 272–285 (1984).

[117] A. Kosowsky, M. S. Turner, and R. Watkins, "Gravitational radiation from colliding vacuum bubbles", Phys. Rev. D **45**, 4514–4535 (1992).

[118] M. Hindmarsh, S. J. Huber, K. Rummukainen, and D. J. Weir, "Numerical simulations of acoustically generated gravitational waves at a first order phase transition", Phys. Rev. D **92**, 123009, 123009 (2015), arXiv:1504.03291 [astro-ph.CO].

[119] C. Caprini, R. Durrer, and G. Servant, "The stochastic gravitational wave background from turbulence and magnetic fields generated by a first-order phase transition", JCAP **2009**, 024, 024 (2009), arXiv:0909.0622 [astro-ph.CO].

[120] A. Vilenkin and E. P. S. Shellard, *Cosmic strings and other topological defects* (Cambridge University Press, July 2000).

[121] M. B. Hindmarsh and T. W. B. Kibble, "Cosmic strings", Rept. Prog. Phys. **58**, 477–562 (1995), arXiv:hep-ph/9411342.

[122] T. W. B. Kibble, "Topology of cosmic domains and strings", J. Phys. A **9**, 1387–1398 (1976).

[123] D. G. Figueroa, M. Hindmarsh, and J. Urrestilla, "Exact scale-invariant background of gravitational waves from cosmic defects", Phys. Rev. Lett. **110**, 101302, 101302 (2013), arXiv:1212.5458 [astro-ph.CO].

[124] R. Onofrio, "Higgs-induced spectroscopic shifts near strong gravity sources", Phys. Rev. D **82**, 065008 (2010).

[125] G. A. Wegner and R. Onofrio, "Higgs shifts from electron-positron annihilations near neutron stars", Eur. Phys. J. C **75**, 307, 307 (2015), arXiv:1503.01738 [astro-ph.IM].

[126] M. A. Kurkov, "Emergent spontaneous symmetry breaking and emergent symmetry restoration in rippling gravitational background", Eur. Phys. J. C **76**, 329, 329 (2016), arXiv:1601.00622 [hep-th].

[127] P. Jones, P. McDougall, M. Ragsdale, and D. Singleton, "Scalar field vacuum expectation value induced by gravitational wave background", Phys. Lett. B **781**, 621–625 (2018).

[128] R. van Haasteren and T. Prokopec, "Scalar propagator for planar gravitational waves", arXiv e-prints (2022), arXiv:2204.12930 [gr-qc].

[129] V. M. Villalba, "Exact solution to the Dirac equation in the presence of an exact gravitational plane wave", Phys. Lett. A **136**, 197–199 (1989).

[130] H. Bondi, F. A. E. Pirani, and I. Robinson, "Gravitational waves in general relativity. 3. Exact plane waves", Proc. Roy. Soc. Lond. A **251**, 519–533 (1959).

[131] S. Gurtas Dogan and Y. Sucu, "Quasinormal modes of Dirac field in 2+1 dimensional gravitational wave background", Phys. Lett. B **797**, 134839 (2019).

[132] J. A. Lobo, "Effect of a weak plane GW on a light beam", Class. Quant. Grav. **9**, 1385 (1992).

[133] J. C. Lobato, I. S. Matos, L. T. Santana, R. R. R. Reis, and M. O. Calvão, "Influence of gravitational waves upon light. Part II. Electric field propagation and interference pattern in a gravitational wave detector", arXiv e-prints, arXiv:2103.02688, arXiv:2103.02688 (2021), arXiv:2103.02688 [gr-qc].

[134] M. Calura and E. Montanari, "Exact solution to the homogeneous Maxwell equations in the field of a gravitational wave in linearized theory", Class. Quant. Grav. **16**, 643 (1999).

[135] T. B. Mieling, P. T. Chruściel, and S. Palenta, "The electromagnetic field in gravitational wave interferometers", Class. Quant. Grav. **38**, 215004, 215004 (2021), arXiv:2107.07727 [gr-qc].

[136] A. M. Cruise, "An interaction between gravitational and electromagnetic waves", Mon.Not.Roy.Astron.Soc. **204**, 485–492 (1983).

[137] G. Brodin and M. Marklund, "Parametric excitation of plasma waves by gravitational radiation", Phys. Rev. Lett. **82**, 3012–3015 (1999).

[138] M. Servin, G. Brodin, M. Bradley, and M. Marklund, "Parametric excitation of alfvén waves by gravitational radiation", Phys. Rev. E **62**, 8493–8500 (2000).

[139] R. Bingham, R. A. Cairns, J. M. Dawson, R. O. Dendy, C. N. Lashmore-Davies, J. T. Mendonça, P. K. Shukla, L. O. Silva, and L. Stenflo, "Scattering of neutrinos and gravitational waves in supernovae", Phys. Scr. **1998**, 61 (1998).

[140] L. Di Lella and C. Rubbia, "The Discovery of the W and Z Particles", Adv. Ser. Direct. High Energy Phys. **23**, 137–163 (2015).

[141] P. Söding, "On the discovery of the gluon", Int. J. Mod. Phys. A **35**, 3–28 (2010).

[142] J. Ellis, "The discovery of the gluon", Intern. J. Mod. Phys. A **29**, 1430072, 1430072 (2014), arXiv:1409.4232 [hep-ph].

[143] T. Kobayashi, "Experimental verification of the standard model of particle physics", Proceed. Jap. Acad., Series B **97**, 211–235 (2021).

[144] E. Malec, "On classical solutions of nonabelian gauge theories. Part 1.", Acta Phys. Polon. B **18**, 1017 (1987).

[145] R. Jackiw, "Quantum meaning of classical field theory", Rev. Mod. Phys. **49**, 681–706 (1977).

[146] F. Gelis, E. Iancu, J. Jalilian-Marian, and R. Venugopalan, "The Color Glass Condensate", Ann. Rev. Nucl. Part. Sci. **60**, 463–489 (2010), arXiv:1002.0333 [hep-ph].

[147] E. Iancu, "QCD in heavy ion collisions", in 2011 European School of High-Energy Physics (2014), pp. 197–266, arXiv:1205.0579 [hep-ph].

[148] E. Iancu and R. Venugopalan, "The Color Glass Condensate and high energy scattering in QCD", in *Quark-gluon plasma 3. edited by hwa rudolph c & wang xin-nian. published by world scientific publishing co. pte. ltd* (World Scientific Publishing Co. Pte. Ltd, 2004), pp. 249–363.

[149] S. McDonald, S. Jeon, and C. Gale, "3 + 1 D initialization and evolution of the glasma", Phys. Rev. C **108**, 064910, 064910 (2023), arXiv:2306.04896 [hep-ph].

[150] X. G. Huang and J. Liao, "Glasma evolution and Bose-Einstein condensation with elastic and inelastic collisions", Phys. Rev. D **91**, 116012 (2015), arXiv:1303.7214 [nucl-th].

[151] D. Müller, "Simulations of the Glasma in 3+1D", arXiv e-prints, arXiv:1904.04267, arXiv:1904.04267 (2019), arXiv:1904.04267 [hep-ph].

[152] H. Georgi, *Lie algebras in particle physics*, 2nd ed., Vol. 54 (Perseus Books, Reading, MA, 1999).

[153] D. Tong, *Lectures on gauge theory* (John Wiley & Sons, 2011).

[154] J. A. Sanchez-Monroy and C. Quimbay, "Some classical properties of the non-abelian Yang-Mills theories", arXiv e-prints, hep-ph/0702173, hep–ph/0702173 (2007), arXiv:hep-ph/0702173 [hep-ph].

[155] K. G. Wilson, "Confinement of quarks", Phys. Rev. D **10**, 2445–2459 (1974).

[156] Y. Aharonov and D. Bohm, "Significance of electromagnetic potentials in the Quantum Theory", Phys. Rev. **115**, 485–491 (1959).

[157] G. 't Hooft, "On the phase transition towards permanent quark confinement", Nucl. Phys. B **138**, 1–25 (1978).

[158] A. Polyakov, "Compact gauge fields and the infrared catastrophe", Phys. Lett. B **59**, 82–84 (1975).

[159] M. Ikeda and Y. Miyachi, "On the static and spherically symmetric Solutions of the Yang-Mills field", Prog. Theor. Phys. **27**, 474–482 (1962).

[160] H. G. Loos, "The range of gauge fields", Nucl. Phys. **72**, 677–691 (1965).

[161] T. T. Wu and C. N. Yang, "Properties of matter under unusual conditions", Mark and S. Fernbach, eds., Interscience Publ., New York (1969).

[162] G. 't Hooft, "Magnetic monopoles in Unified Gauge Theories", Nucl. Phys. B **79**, edited by J. C. Taylor, 276–284 (1974).

[163] F. Melia and S. Lo, "Linear Plane Wave Solutions of the Yang-Mills Theory", Phys. Lett. B **77**, 71–72 (1978).

[164] A. Actor, "Classical solutions of SU(2) Yang-Mills theories", Rev. Mod. Phys. **51**, 461–525 (1979).

[165] M. K. Prasad, "Instantons and monopoles in Yang-Mills gauge field theories", Phys. D **1**, 167 (1980).

[166] G. Baseyan, S. Matinyan, and G. Savvidy, "Nonlinear plane waves in massless Yang-Mills theory", JETP **29**, 587–589 (1979).

[167] S. Coleman, "Non-abelian plane waves", Phys. Lett. B **70**, 59–60 (1977).

[168] W. Campbell and T. Morgan, "Non-abelian plane-fronted waves", Phys. Lett. B **84**, 87–88 (1979).

[169] A. Tsapalis, E. P. Politis, X. N. Maintas, and F. K. Diakonos, "Gauss' law and nonlinear plane waves for Yang-Mills theory", Phys. Rev. D **93**, 085003 (2016).

[170] G. Z. Baseian, S. G. Matinyan, and G. K. Savvidy, "Nonlinear plane waves in massless Yang-Mills theory", Pisma Zh. Eksp. Teor. Fiz. **29**, 641–644 (1979).

[171] S. Lo, P. Desmond, and E. Kovacs, "General self-dual non-abelian plane waves", Phys. Lett. B **90**, 419–421 (1980).

[172] M. Basler and A. Hädicke, "On non-abelian SU(2) plane waves", Phys. Lett. B **144**, 83–86 (1984).

[173] P. A. Raczka, "Colliding plane waves in non-abelian gauge theory", Phys. Lett. B **177**, 60–62 (1986).

[174] A. Rabinowitch, "Exact axially symmetric wave solutions of the Yang-Mills equations", Theor. Math. Phys. **148**, 1081–1085 (2006).

[175] A. Rabinowitch, "On non-abelian expanding waves", J. Phys. A: Math. Theor. **40**, 14575 (2007).

[176] A. Rabinowitch, "On a new class of non-abelian expanding waves", Phys. Lett. B **664**, 295–300 (2008).

[177] L. Weijun, "Wave solutions to the Yang-Mills equation", MA thesis (National University of Singapore, 2017).

[178] A. Pich, "The Standard Model of Electroweak Interactions", arXiv e-prints, arXiv:1201.0537, arXiv:1201.0537 (2012), arXiv:1201.0537 [hep-ph].

[179] L. R. Weih, M. Hanauske, and L. Rezzolla, "Postmerger gravitational-wave signatures of phase transitions in Binary Mergers", Phys. Rev. Lett. **124**, 171103 (2020).

[180] E. Zauderer, *Partial differential equations of applied mathematics* (John Wiley & Sons, 2011).

[181] M. Luzum and P. Romatschke, "Conformal relativistic viscous hydrodynamics: Applications to RHIC results at s_{NN}=200 GeV", Phys. Rev. C **78**, 034915, 034915 (2008), arXiv:0804.4015 [nucl-th].

[182] R. Pasechnik and M. Šumbera, "Phenomenological review on Quark–Gluon Plasma: Concepts vs. Observations", Universe **7**, 7, 64 (2017), arXiv:1611.01533 [hep-ph].

[183] J. P. Blaizot, J. Liao, and L. McLerran, "Gluon transport equation in the small angle approximation and the onset of Bose-Einstein condensation", Nucl. Phys. A **920**, 58–77 (2013), arXiv:1305.2119 [hep-ph].

[184] R. C. Hwa and X. N. Wiang, *Quark-gluon plasma 4* (World Scientific Publishing, 2010).

[185] A. Chodos, R. L. Jaffe, K. Johnson, C. B. Thorn, and V. F. Weisskopf, "New extended model of hadrons", Phys. Rev. D **9**, 3471–3495 (1974).

[186] S. P. Klevansky, "The Nambu-Jona-Lasinio model of quantum chromodynamics", Rev. Mod. Phys. **64**, 649–708 (1992).

[187] E. Elizalde, A. J. Lopez-Revelles, S. D. Odintsov, and S. Y. Vernov, "Cosmological models with Yang-Mills fields", Phys. Atom. Nucl. **76**, 996–1003 (2013), arXiv:1201.4302 [hep-th].

[188] D. V. Gal'tsov and E. A. Davydov, "Cosmological models with Yang-Mills fields", Proc. Steklov Inst. Math. **272**, 119–140 (2011), arXiv:1012.2861 [gr-qc].

[189] F. R. Urban and A. R. Zhitnitsky, "The QCD nature of Dark Energy", Nucl. Phys. B **835**, 135–173 (2010), arXiv:0909.2684 [astro-ph.CO].

[190] R. Pasechnik, V. Beylin, and G. Vereshkov, "Dark Energy from graviton-mediated interactions in the QCD vacuum", JCAP **06**, 011 (2013), arXiv:1302.6456 [gr-qc].

[191] R. Pasechnik, G. Prokhorov, and O. Teryaev, "Mirror QCD and Cosmological Constant", Universe **3**, 43, 43 (2017), arXiv:1609.09249 [hep-ph].

[192] W. Magnus and S. Winkler, *Hill's Equation. II: Transformations, Approximation, Examples* (Creative Media Partners, LLC, 2017).

[193] I. Kovacic, R. Rand, and S. Mohamed Sah, "Mathieu's Equation and its generalizations: Overview of stability charts and their features", App. Mech. Rev. **70**, 020802 (2018).

[194] I. Kovacic, L. Cveticanin, M. Zukovic, and Z. Rakaric, "Jacobi elliptic functions: A review of nonlinear oscillatory application problems", J. Sound Vib. **380**, 1–36 (2016).

[195] A. Dasgupta and J. Fajardo-Montenegro, "Aspects of Quantum Gravity Phenomenology and Astrophysics", Universe **9**, 128 (2023), arXiv:2303.05042 [gr-qc].

[196] R. Allahverdi and A. Mazumdar, "Affleck-Dine condensate, late thermalization, and the gravitino problem", Phys. Rev. D **78**, 043511, 043511 (2008), arXiv:0802.4430 [hep-ph].

[197] N. Gosala and A. Dasgupta, "Condensates in Higher gauge groups", in preparation (2024).

[198] Y. Kimura, "Viscosity of quark-gluon plasma and gravitons Bose-Einstein condensate", arXiv e-prints (2024), arXiv:2401.16436 [physics.gen-ph].

[199] R. Jackiw and C. Rebbi, "Solitons with fermion number ½", Phys. Rev. D **13**, 3398–3409 (1976).

[200] S. L. Adler, "Axial-Vector Vertex in Spinor Electrodynamics", Phys. Rev. **177**, 2426–2438 (1969).

[201] G. 't Hooft, "Computation of the quantum effects due to a four-dimensional pseudoparticle", Phys. Rev. D **14**, 3432–3450 (1976).

[202] V. Kuzmin, V. Rubakov, and M. Shaposhnikov, "On anomalous electroweak baryon-number non-conservation in the early universe", Phys. Lett. B **155**, 36–42 (1985).

[203] C. Corianò, L. D. Rose, E. Gabrielli, and L. Trentadue, "Fermion scattering in a gravitational background: electroweak corrections and flavour transitions", JHEP **2014**, 136, 136 (2014), arXiv:1312.7657 [hep-ph].

[204] J. Rafelski, "Discovery of Quark-Gluon Plasma: Strangeness Diaries", Eur. Phys. J. ST **229**, 1–140 (2020), arXiv:1911.00831 [hep-ph].

[205] B. L. Combridge, "Associated production of heavy flavor states in p p and anti-p p Interactions: Some QCD estimates", Nucl. Phys. B **151**, 429–456 (1979).

[206] P. J. Peebles and B. Ratra, "The cosmological constant and dark energy", Rev. Mod. Phys. **75**, 559–606 (2003), arXiv:astro-ph/0207347 [astro-ph].

[207] S. Dodelson, *Modern Cosmology* (Academic Press, Amsterdam, 2003).

[208] U. W. Heinz and M. Jacob, "Evidence for a new state of matter: An Assessment of the results from the CERN lead beam program", (2000), arXiv:nucl-th/0002042.

[209] J. Adams et al., "Experimental and theoretical challenges in the search for the quark–gluon plasma: The STAR Collaboration's critical assessment of the evidence from RHIC collisions", Nucl. Phys. A **757**, First Three Years of Operation of RHIC, 102–183 (2005).

[210] K. Adcox et al., "Formation of dense partonic matter in relativistic nucleus–nucleus collisions at RHIC: Experimental evaluation by the PHENIX Collaboration", Nucl. Phys. A **757**, First Three Years of Operation of RHIC, 184–283 (2005).

[211] M. Gyulassy and L. McLerran, "New forms of QCD matter discovered at RHIC", Nucl. Phys. A **750**, edited by D. Rischke and G. Levin, 30–63 (2005), arXiv:nucl-th/0405013.

[212] E. Shuryak, "Physics of Strongly coupled Quark-Gluon Plasma", Prog. Part. Nucl. Phys. **62**, 48–101 (2009), arXiv:0807.3033 [hep-ph].

[213] S. Ichimaru, "Strongly coupled plasmas: high-density classical plasmas and degenerate electron liquids", Rev. Mod. Phys. **54**, 1017–1059 (1982).

[214] M. H. Thoma, "The Quark-Gluon-Plasma Liquid", J. Phys. G **31**, [Erratum: J.Phys.G 31, 539 (2005)], L7 (2005), arXiv:hep-ph/0503154.

[215] M. Bonitz, C. Henning, and D. Block, "Complex plasmas: a laboratory for strong correlations", Rep. Prog. Phys. **73**, 066501 (2010).

[216] P. K. Kovtun, D. T. Son, and A. O. Starinets, "Viscosity in strongly interacting quantum field theories from black hole physics", Phys. Rev. Lett. **94**, 111601 (2005).

[217] T. Schafer and D. Teaney, "Nearly perfect fluidity: From cold atomic gases to hot Quark Gluon Plasma", Rept. Prog. Phys. **72**, 126001 (2009), arXiv:0904.3107 [hep-ph].

[218] Y. Nambu, "The confinement of quarks", Sci. Am. **235N5**, 48–70 (1976).

[219] A. M. Polyakov, "Thermal properties of gauge fields and quark liberation", Phys. Lett. B **72**, 477–480 (1978).

[220] L. Susskind, "Lattice models of quark confinement at high temperature", Phys. Rev. D **20**, 2610–2618 (1979).

[221] J. O. Andersen, W. R. Naylor, and A. Tranberg, "Phase diagram of QCD in a magnetic field", Rev. Mod. Phys. **88**, 025001 (2016).

[222] The CMS Collaboration et al., "CMS physics technical design report: Addendum on high density QCD with heavy ions", J. Phys. G **34**, 2307 (2007).

[223] P. Braun-Munzinger and J. Wambach, "The phase diagram of strongly-interacting matter", Rev. Mod. Phys. **81**, 1031–1050 (2009), arXiv:0801.4256 [hep-ph].

[224] K. Fukushima and T. Hatsuda, "The phase diagram of dense QCD", Rept. Prog. Phys. **74**, 014001 (2011), arXiv:1005.4814 [hep-ph].

[225] M. G. Alford, A. Schmitt, K. Rajagopal, and T. Schäfer, "Color superconductivity in dense quark matter", Rev. Mod. Phys. **80**, 1455–1515 (2008), arXiv:0709.4635 [hep-ph].

[226] M. G. Alford, K. Rajagopal, and F. Wilczek, "QCD at finite baryon density: Nucleon droplets and color superconductivity", Phys. Lett. B **422**, 247–256 (1998), arXiv:hep-ph/9711395.

[227] M. Buballa, J. Hosek, and M. Oertel, "Anisotropic admixture in color superconducting quark matter", Phys. Rev. Lett. **90**, 182002 (2003), arXiv:hep-ph/0204275.

[228] M. G. Alford, K. Rajagopal, and F. Wilczek, "Color flavor locking and chiral symmetry breaking in high density QCD", Nucl. Phys. B **537**, 443–458 (1999), arXiv:hep-ph/9804403.

[229] G. Jaeger, "The Ehrenfest Classification of Phase Transitions: Introduction and Evolution", Archive for History of Exact Sciences **53**, 51–81 (1998).

[230] Y. Nambu and G. Jona-Lasinio, "Dynamical model of elementary particles based on an analogy with superconductivity. I", Phys. Rev. **122**, 345–358 (1961).

[231] V. Koch, "Introduction to chiral symmetry", in 3rd TAPS Workshop on Electromagnetic and Mesonic Probes of Nuclear Matter (Dec. 1995), arXiv:nucl-th/9512029.

[232] C. Ratti, M. A. Thaler, and W. Weise, "Phases of QCD: Lattice thermodynamics and a field theoretical model", Phys. Rev. D **73**, 014019 (2006).

[233] O. Kaczmarek, F. Karsch, P. Petreczky, and F. Zantow, "Heavy quark-antiquark free energy and the renormalized Polyakov loop [rapid communication]", Phys. Lett. B **543**, 41–47 (2002), arXiv:hep-lat/0207002 [hep-lat].

[234] S. Borsanyi, Z. Fodor, C. Hoelbling, S. D. Katz, S. Krieg, C. Ratti, and K. K. Szabo, "Is there still any T_c mystery in lattice QCD? Results with physical masses in the continuum limit III", JHEP **09**, 073 (2010), arXiv:1005.3508 [hep-lat].

[235] A. Bazavov et al., "Chiral crossover in QCD at zero and non-zero chemical potentials", Phys. Lett. B **795**, 15–21 (2019), arXiv:1812.08235 [hep-lat].

[236] S. Borsanyi, Z. Fodor, J. N. Guenther, R. Kara, S. D. Katz, P. Parotto, A. Pasztor, C. Ratti, and K. K. Szabó, "QCD Crossover at finite chemical potential from Lattice simulations", Phys. Rev. Lett. **125**, 052001 (2020).

[237] Z. Fodor and S. D. Katz, "Critical point of QCD at finite T and μ, lattice results for physical quark masses", JHEP **04**, 050 (2004), arXiv:hep-lat/0402006.

[238] C. R. Allton, S. Ejiri, S. J. Hands, O. Kaczmarek, F. Karsch, E. Laermann, C. Schmidt, and L. Scorzato, "QCD thermal phase transition in the presence of a small chemical potential", Phys. Rev. D **66**, 074507 (2002).

[239] R. D. Pisarski and F. Wilczek, "Remarks on the chiral phase transition in chromodynamics", Phys. Rev. D **29**, 338–341 (1984).

[240] M. Stephanov, K. Rajagopal, and E. Shuryak, "Signatures of the Tricritical Point in QCD", Phys. Rev. Lett. **81**, 4816–4819 (1998).

[241] T. Boeckel and J. Schaffner-Bielich, "Little inflation at the cosmological QCD phase transition", Phys. Rev. D **85**, 103506, 103506 (2012), arXiv:1105.0832 [astro-ph.CO].

[242] D. J. Schwarz and M. Stuke, "Lepton asymmetry and the cosmic QCD transition", JCAP **11**, [Erratum: JCAP 10, E01 (2010)], 025 (2009), arXiv:0906.3434 [hep-ph].

[243] J. H. Applegate and C. J. Hogan, "Relics of cosmic quark condensation", Phys. Rev. D **31**, 3037–3045 (1985).

[244] E. Witten, "Cosmic separation of phases", Phys. Rev. D **30**, 272–285 (1984).

[245] M. Crawford and D. N. Schramm, "Spontaneous generation of density perturbations in the Early universe", Nature **298**, 538–540 (1982).

[246] C. Schmid, D. J. Schwarz, and P. Widerin, "Deviations from the Harrison-Zel'dovich spectrum due to the quark - gluon to hadron transition", Helv. Phys. Acta **69**, edited by N. Straumann, P. Jetzer, and G. V. Lavrelashvili, 198–201 (1996), arXiv:astro-ph/9611186.

[247] C. J. Hogan, "Nucleation of cosmological phase transitions", Phys. Lett. B **133**, 172–176 (1983).

[248] T. DeGrand and K. Kajantie, "Supercooling, entropy production, and bubble kinetics in the quark-hadron phase transition in the early universe", Phys. Lett. B **147**, 273–278 (1984).

[249] M. Gyulassy, K. Kajantie, H. Kurki-Suonio, and L. McLerran, "Deflagrations and detonations as a mechanism of hadron bubble growth in supercooled quark-gluon plasmas", Nucl. Phys. B **237**, 477–501 (1984).

[250] H. Kurki-Suonio, "Deflagration bubbles in the quark-hadron phase transition", Nucl. Phys. B **255**, 231–252 (1985).

[251] C. J. Hogan, "Magnetohydrodynamic effects of a first-order cosmological phase transition", Phys. Rev. Lett. **51**, 1488–1491 (1983).

[252] J. S. Langer, "Statistical theory of the decay of metastable states", Annals Phys. **54**, 258–275 (1969).

[253] L. P. Csernai and J. I. Kapusta, "Nucleation of relativistic first order phase transitions", Phys. Rev. D **46**, 1379–1390 (1992).

[254] D. J. Schwarz, "The first second of the Universe", Annal. Phys. **12**, 220–270 (2003), arXiv:astro-ph/0303574 [astro-ph].

[255] J. S. Langer and L. A. Turski, "Hydrodynamic model of the condensation of a vapor near its critical point", Phys. Rev. A **8**, 3230–3243 (1973).

[256] A. A. Rawlinson, "Calculations in gauge field theory at finite temperature", PhD thesis (Adelaide U., 1992).

[257] N. P. Landsman and C. G. van Weert, "Real- and imaginary-time field theory at finite temperature and density", phys. Rep. **145**, 141–249 (1987).

[258] L. Dolan and R. Jackiw, "Symmetry behavior at finite temperature", Phys. Rev. D **9**, 3320–3341 (1974).

[259] H. Umezawa, H. Matsumoto, and M. Tachiki, *Thermo field dynamics and condensed states* (North-Holland Publishing Company, 1982).

[260] C. W. Bernard, "Feynman rules for gauge theories at finite temperature", Phys. Rev. D **9**, 3312–3320 (1974).

[261] A. O. Barvinsky, "Heat kernel expansion in the background field formalism", Scholarpedia **10**, revision #186569, 31644 (2015).

[262] L. Faddeev and V. Popov, "Feynman diagrams for the Yang-Mills field", Phys. Lett. B **25**, 29–30 (1967).

[263] B. S. DeWitt, "Dynamical theory of groups and fields", Conf. Proc. C **630701**, edited by C. DeWitt and B. DeWitt, 585–820 (1964).

[264] D. Ebert, V. C. Zhukovsky, and A. S. Vshivtsev, "Thermodynamic potential with condensate fields in an SU(2) model of QCD", Int. J. Mod. Phys. A **13**, 1723–1742 (1998).

[265] J. Schwinger, "On gauge invariance and vacuum polarization", Phys. Rev. **82**, 664–679 (1951).

[266] I. G. Avramidi, *Heat kernel and quantum gravity*, Vol. 64 (Springer, New York, 2000).

[267] D. V. Vassilevich, "Heat kernel expansion: user's manual", Phys. Rep. **388**, 279–360 (2003).

[268] G. V. Dunne, "Functional determinants in quantum field theory", J. Phys. Math. Gen. **41**, 304006, 304006 (2008), arXiv:0711.1178 [hep-th].

[269] A. O. Barvinsky and G. A. Vilkovisky, "The Generalized Schwinger-Dewitt technique in gauge theories and quantum gravity", Phys. Rept. **119**, 1–74 (1985).

[270] H. Boschi-Filho, C. P. Natividade, and C. Farina, "Heat-kernel expansion at finite temperature", Phys. Rev. D **45**, 586–594 (1992).

[271] D. Diakonov and M. Oswald, "Covariant derivative expansion of the Yang-Mills effective action at high temperatures", Phys. Rev. D **68**, 025012, 025012 (2003), arXiv:hep-ph/0303129 [hep-ph].

[272] E. Megías, E. Ruiz Arriola, and L. L. Salcedo, "Thermal heat kernel expansion and the one-loop effective action of QCD at finite temperature", Phys. Rev. D **69**, 116003 (2004).

[273] J. C. Collins, *Renormalization*, Vol. 26, Cambridge Monographs on Mathematical Physics (Cambridge University Press, Cambridge, July 2023).

[274] A. Bazavov, N. Brambilla, X. Garcia i Tormo, P. Petreczky, J. Soto, and A. Vairo, "Determination of α_s from the QCD static energy", Phys. Rev. D **86**, 114031 (2012).

[275] J. I. Kapusta and C. Gale, *Finite-Temperature Field Theory : Principles and Applications, 2nd edition* (Cambridge University Press, 2007).

[276] G. Savvidy, "From Heisenberg–Euler Lagrangian to the discovery of Chromomagnetic Gluon Condensation", Eur. Phys. J. C **80**, 165, 165 (2020), arXiv:1910.00654 [hep-th].

[277] M. Ninomiya and N. Sakai, "Finite temperature behavior of a color ferromagnetic state in QCD", Nucl. Phys. B **190**, 316–324 (1981).

[278] N. Haque, A. Bandyopadhyay, J. O. Andersen, M. G. Mustafa, M. Strickland, and N. Su, "Three-loop HTLpt thermodynamics at finite temperature and chemical potential", JHEP **2014**, 27, 27 (2014), arXiv:1402.6907 [hep-ph].

[279] I. S. Gradshteyn and I. M. Ryzhik, *Table of integrals, series, and products*, Seventh, Translated from the Russian, Translation edited and with a preface by Alan Jeffrey and Daniel Zwillinger, With one CD-ROM (Windows, Macintosh and UNIX) (Elsevier/Academic Press, Amsterdam, 2007), pp. xlviii+1171.

[280] S. Hamdi, W. E. Schiesser, and G. W. Griffiths, "Method of lines", Scholarpedia **2**, revision #124335, 2859 (2007).

[281] A. O. Barvinsky, "Heat kernel expansion in the background field formalism", Scholarpedia **10**, revision #186569, 31644 (2015).

Appendix A

Linearized Gravity

In the linearized approximation, we can write the metric as

$$g_{\mu\nu}(x) = \eta_{\mu\nu} + h_{\mu\nu}(x),\ |h_{\mu\nu}(x)| \ll 1. \tag{A.1}$$

The condition $|h_{\mu\nu}(x)| \ll 1$ implies that (i) the gravitational field is very weak, and (ii) sets a restriction on coordinate systems. As we said before, the coordinates are arbitrary and one can create weak gravitational fields in any coordinate system. It means that if in one coordinate system, the condition holds, then we can find many other systems where this holds. Consider a general infinitesimal coordinate transformation

$$x'^{\mu} = x^{\mu} + \xi^{\mu}(x), \tag{A.2}$$

where $\xi^{\mu}(x)$ are four arbitrary infinitesimal functions of space and time. From the above equation, we can write the

$$\frac{\partial x'^{\mu}}{\partial x^{\nu}} = \delta^{\mu}_{\nu} + \partial_{\nu}\xi^{\mu}, \tag{A.3}$$

Using this and the inverse form of this, one can write the metric transforms as follows:

$$g'_{\mu\nu} = \eta_{\mu\nu} + h_{\mu\nu} - \partial_{\mu}\xi_{\nu} - \partial_{\nu}\xi_{\mu}, \tag{A.4}$$

Taking the $g'_{\mu\nu}$ is also of form Eq. A.1, we write the transformation of metric perturbation as

$$h'_{\mu\nu} = h_{\mu\nu} - \partial_{\mu}\xi_{\nu} - \partial_{\nu}\xi_{\mu}. \tag{A.5}$$

For the above transformation to be of the form Eq. A.1, we require that $|\partial_{\mu}\xi_{\nu}| \lesssim |h_{\mu\nu}|$. Then we say that the linearized gravity is invariant under slowly varying infinitesimal coordinate transformations. One can see that the above transformation is analogous to gauge transformation in gauge theories. In evaluating the linearized field equations, we make use of a new metric perturbation known as trace-reversed metric perturbation, $\overline{h}_{\mu\nu} \equiv h_{\mu\nu} - \frac{1}{2}\eta_{\mu\nu}h^{\alpha}_{\alpha}$. Under the infinitesimal coordinate transformations $x^{\mu} \to x^{\mu} + \xi^{\mu}$, the trace reversed metric perturbation ($\overline{h}_{\mu\nu}$) transforms as

$$\overline{h}'_{\mu\nu}(x') = \overline{h}_{\mu\nu}(x) + \eta_{\mu\nu}\partial_{\alpha}\xi^{\alpha} - \partial_{\mu}\xi_{\nu} - \partial_{\nu}\xi_{\mu}. \tag{A.6}$$

We consider the Lorenz gauge ($\partial^\mu \overline{h}_{\mu\nu}(x) = 0$) to simplify the field equations. We will now show that this type of gauge choice is always possible. Consider an arbitrary metric perturbation that does not satisfy the Lorenz gauge ($\partial^\mu \overline{h}_{\mu\nu}(x) \neq 0$). Using the above transformations, we can write the transformed Lorenz gauge as

$$\partial'^\mu \overline{h}'_{\mu\nu}(x') = \partial^\mu \overline{h}_{\mu\nu}(x) - \Box \xi_\nu, \tag{A.7}$$

We can see that even if $\partial^\mu \overline{h}_{\mu\nu}(x) \neq 0$, we can always make a transformation such that it satisfies Lorenz gauge as long as

$$\Box \xi_\nu = \partial^\mu \overline{h}_{\mu\nu}(x), \tag{A.8}$$

We can always find a solution to the above equation because the operator is invertible. Therefore, one can use the coordinate invariance to choose the Lorenz gauge.

By choosing the Lorenz gauge, one gets a simplified Einstein tensor (Eq. (2.13)). This is always possible as long as one restricts to the coordinate systems that satisfy the Lorenz gauge. But even after the Lorenz gauge is chosen, there is still some residual gauge freedom. This we can see from Eq. (A.7) that even if we choose $\partial^\mu \overline{h}_{\mu\nu}(x) = 0$, we can still have the freedom of choosing $\xi_\mu(x)$ such that it still satisfies Lorenz gauge. This residual gauge freedom amounts to choosing four functions ($\xi_\mu(x)$) which satisfied $\Box \xi_\nu = 0$ to remain in Lorenz gauge.

The Lorenz gauge imposes four constraints on the trace-reversed metric perturbation. As we see before, the residual gauge freedom is removed by choosing ξ_ν which amounts to another four constraints on $\overline{h}_{\mu\nu}$. In other words, out of 10, these constraints reduce the radiative degrees of freedom to $10 - 8 = 2$, thus, saying that gravity propagates at the speed of light.

Appendix B

Dirac Equation in general spacetimes

We start with the notations for different types of indices. $a, b, c, ...$ represents Lie algebra indices, $\mu, \nu, ...$ represents curved spacetime indices, $A, B, C, ...$ represents flat spacetime indices, and α, β represents spinor indices.

To connect flat and curved spacetime indices, we define tetrads. A Tetrad is a set of four linearly independent vectors that can be defined at each point in the curved spacetime. The following relations define the tetrads:

$$g_{\mu\nu} = e^A_\mu e^B_\nu \eta_{AB}, \qquad \eta_{AB} = e^\mu_A e^\nu_B g_{\mu\nu}, \tag{B.1}$$

$$e^A_\mu e^\nu_A = \delta^\nu_\mu, \qquad e^A_\mu e^\mu_B = \delta^A_B. \tag{B.2}$$

where η_{AB} is the flat spacetime metric, $g_{\mu\nu}$ is the curved spacetime metric, e^μ_A and e^A_μ are the vector and co-vector fields, respectively. As the gamma matrices are defined through anti-commutation relations in Clifford algebra involving spacetime metric, the gamma matrices will become spacetime-dependent in the curved background. These spacetime-dependent gamma matrices $\bar{\gamma}^\mu(x)$ are related to the gamma matrices in flat spacetime as

$$\bar{\gamma}^\mu(x) := e^\mu_A(x)\, \gamma^A, \tag{B.3}$$

where the constant gamma matrices satisfy the $\{\gamma^A, \gamma^B\} = 2\, \varepsilon\, \eta^{AB} I$ and the spacetime dependent gamma matrices satisfy $\{\bar{\gamma}^\mu(x), \bar{\gamma}^\nu(x)\} = 2\varepsilon g^{\mu\nu} I$ with $\varepsilon = \pm 1$ (depends on metric convention).

With the above definitions, the Dirac equation in curved spacetime is as follows

$$i\bar{\gamma}^\mu(\partial_\mu + \Gamma_\mu)\psi_\alpha + g_{ym}\bar{\gamma}^\mu A^a_\mu T^a_{\alpha\beta}\psi_\beta = 0, \tag{B.4}$$

where Γ_μ is the spinor affine connection given by

$$\Gamma_\mu = \frac{\varepsilon}{4} w_{AB\mu}\gamma^A\gamma^B, \tag{B.5}$$

where $w_{AB\mu}$ are the spin connection coefficients given in terms of tetrads as

$$w_{AB\mu} = \eta_{AC}\, e^C_\nu\, \nabla_\mu\, e^\nu_B. \tag{B.6}$$

In our case, we are dealing with $+$-polarized GW propagating in z-direction which is

given by the following metric:

$$ds^2 = -dt^2 + (1+h_+(t,z))dx^2 + (1-h_+(t,z))dy^2 + dz^2, \tag{B.7}$$

With our metric convention $((-,+,+,+))$, we have $\varepsilon = -1$. Using the above metric, the tetrads are obtained as

$$e^A_\mu = \begin{pmatrix} 1 & 0 & 0 & 0 \\ 0 & \sqrt{1+h_+} & 0 & 0 \\ 0 & 0 & \sqrt{1-h_+} & 0 \\ 0 & 0 & 0 & 1 \end{pmatrix}, \qquad e^\mu_A = \begin{pmatrix} 1 & 0 & 0 & 0 \\ 0 & \frac{1}{\sqrt{1+h_+}} & 0 & 0 \\ 0 & 0 & \frac{1}{\sqrt{1-h_+}} & 0 \\ 0 & 0 & 0 & 1 \end{pmatrix} \tag{B.8}$$

Using linear order approximation in h_+, we get $\sqrt{1+h_+} \approx 1 + \frac{1}{2}h_+$ and $1/\sqrt{1+h_+} \approx 1 - \frac{1}{2}h_+$. With this, we calculated the spin connection coefficients and corresponding spinor affine connection. We also considered the gauge field to be spatially homogeneous and isotropic as $A^a_0 = 0$, $A^a_i = \delta^a_i U(t)$. Now, plugging everything into the Dirac equation (B.4), we get

$$i\gamma^0\partial_0\psi_\alpha + i\gamma^3\partial_3\psi_\alpha + g_{ym}U\left[\gamma^1(1-\frac{1}{2}h_+)T^1_{\alpha\beta} + \gamma^2(1+\frac{1}{2}h_+)T^2_{\alpha\beta} + \gamma^3 T^3_{\alpha\beta}\right]\psi_\beta = 0 \tag{B.9}$$

Using the same assumptions for ψ_α as in without GW case (Sec: 6.1), we get equations for individual components as follows:

$$i(\partial_0+\partial_3)\psi_{2L2} + \frac{g_{ym}}{2}h_+U\psi_{1L1} - \frac{g_{ym}}{2}U\psi_{2L2} = 0, \tag{B.10}$$

$$i(\partial_0-\partial_3)\psi_{1L1} + \frac{g_{ym}}{2}h_+U\psi_{2L2} - \frac{g_{ym}}{2}U\psi_{1L1} = 0, \tag{B.11}$$

$$i(\partial_0+\partial_3)\psi_{1L2} - g_{ym}U(t)\psi_{2L1} + \frac{g_{ym}}{2}U(t)\psi_{1L2} = 0, \tag{B.12}$$

$$i(\partial_0-\partial_3)\psi_{2L1} - g_{ym}U(t)\psi_{1L2} + \frac{g_{ym}}{2}U(t)\psi_{2L1} = 0, \tag{B.13}$$

Appendix C

Lie Groups and Lie Algebras

A group is a set of abstract elements/objects under which a group operation ($\bullet$) is defined such that the group elements obey certain rules. Let the group be G with elements $\{A,B,C,...\}$. The group rules are given by

- Closure: The product of two group elements should also be in the group.
  $A \bullet B \subset G$
- Identity: There should be an element (I) in the group that satisfies
  $A \bullet I = I \bullet A = A$
- Inverse: For every element (A) in the group, there exists an element (A^{-1}) that satisfies
  $A \bullet A^{-1} = A^{-1} \bullet A = 1$
- Associativity: For any three group elements (A,B,C), it should satifies
  $A \bullet (B \bullet C) = (A \bullet B) \bullet C$

There are three types of groups classified as follows

- Discrete groups are groups when there are finite numbers of elements in a group. Example: The set $\{\pm 1, \pm i\}$ forms a finite group Z_4 with product group operation.
- Infinite discrete groups are the groups with denumerable infinite numbers of elements. Example: Additive group of integers – A set of integers with addition as a product operation.
- Continuous groups are the groups in which elements form a continuum. Example: an infinite set of matrices of form $\begin{pmatrix} \cos\theta & \sin\theta \\ -\sin\theta & \cos\theta \end{pmatrix}$ where θ vary from 0 to 2π continuously.

Groups can be formed by any kind of abstract elements. The most relevant ones for our study are the matric groups. Any set of $n \times n$ square nonsingular matrices (including identity matrix) with matrix multiplication as group operation forms a regular matrix group. Some of the important matrix groups are as follows

1. General Linear Group $GL(n,C)$ is a set of complex $n \times n$ matrices with a non-zero determinant. The group operation is the usual matrix multiplication. We get a subgroup $GL(n,R)$ if all the matrix elements are real.

2. Unitary groups $U(n)$ is a set of $n \times n$ unitary matrices such that $U^\dagger U = I$, I is the identity matrix.

3. Special Unitary group $SU(n)$ is a group of unitary matrices with determinant equal to 1.

4. Orthogonal group $O(n)$ is a group of real $n \times n$ orthogonal matrices such that $O^T O = I$.

5. Special Orthogonal Group $SO(n)$ is a subgroup of the Orthogonal group with determinant equal to 1.

For now, we focus on continuous matrix groups, these arguments also work for any arbitrary group. In a space of $n \times n$ matrices in a continuous matrix group, the notion of closeness/nearby is defined in a way that two matrices are said to be close if their elements are close by. The space of all $n \times n$ matrices with complex elements can be viewed as a real Euclidean space of dimension $2n^2$. Each matrix M will be a point in that space whose coordinates are $2n^2$ matrix elements Re M_{ij} and Im M_{ij}. Consider a set of matrices $M(\alpha)$, depending on a real parameter α, which forms a curve in R^{2n^2} Euclidean space. These matrix groups which also form a smooth manifold in R^{2n^2} space are called Lie groups. A simple example of a Lie group is the unitary group $U(1)$. It is a set of complex numbers with usual multiplication as group operation.

$$U(1) = \{z_1, z_2, z_3, ...\}, \tag{C.1}$$

where $z_i = x_i + i\ y_i$ is a complex number and in polar form (with magnitude 1), $z = e^{i\theta}$, where θ is the real parameter varies from 0 to 2π. In a complex plane, the group $U(1)$ forms a circle. The other groups which are Lie groups are $U(n)$, $SU(n)$, $O(n)$ and $SO(n)$.

Since each matrix forms a point of dimension r in $2n^2$ dimensional Euclidean space, we can define the tangent space of dimension r to the manifold at that point. For example, for $U(1)$, the vector space dimension is 1 as there is only one free parameter θ. This tangent space is a vector space of dimension r consisting of vectors tangent to the manifold at a given point. The tangent space for a Lie group at the identity element is the Lie algebra $\mathfrak{g}$ of that Lie group G.

Consider the infinitesimal transformation in the neighbourhood of identity element. Then, any element $g(\alpha)$ in the Lie group G can be represented near identity as

$$g(\alpha) = 1 + \alpha\, A + O(\alpha^2), \tag{C.2}$$

where α is group parameter and $A = (\partial g/\partial\alpha)_{\alpha=0}$ belongs to the Lie algebra of the group G. The above equation is viewed as the definition of Lie algebra $\mathfrak{g}$. Including the properties of vector space, the commutator also has to be defined to consider the vector space as a Lie algebra as if $A_1, A_2 \in \mathfrak{g}$, then $[A_1, A_2] = A_1A_2 - A_2A_1$ also belongs to $\mathfrak{g}$. Some examples of Lie algebras are

1. $\mathfrak{u}(n)$ algebra is the algebra of all anti-hermitian matrices

2. $\mathfrak{su}(n)$ algebra is the algebra of all anti-hermitian matrices with zero trace

3. $\mathfrak{so}(n)$ algebra is the algebra of all real matrices satisfying $A^T = -A$

Usually, in physics, we use hermitian matrices rather than anti-hermitian matrices. Since every anti-hermitian matrix can be written in the form iA, where A is a hermitian matrix, the group element $g(\alpha)$ near identity is also written as $g(\alpha) = 1 + iA\alpha + O(\alpha^2)$. Thus, for $\mathfrak{su}(n)$ can be defined as the algebra of hermitian matrices with zero trace.

The dimension of the vector space is the dimension of algebra which is equal to the dimension of the group manifold for the corresponding group. For example, for $\mathfrak{u}(1)$, the dimension is 1 as it has only one infinitesimal parameter θ. For $su(n)$, it is equal to $n^2 - 1$.

As in any vector space, one has to choose a basis for the Lie algebra. The elements of this basis are r matrices $T_a,\ a = 1, 2, .., r$ are called the generators of the Lie algebra and of the corresponding Lie group. The commutator of these generators is a linear combination of generators and the commutation relations are given by

$$[T^a, T^b] = if^{abc}T^c, \tag{C.3}$$

where f^{abc} are called structure constants of Lie algebra and its values depend on the choice of the basis.

C.1 Representations of Lie groups and Lie algebras

In a physical system, any transformation of a state vector to another state vector is associated with an operator. For example, in quantum mechanics, these correspond to unitary operators represented by matrices. A representation T of a group G in a linear vector space V is a mapping under which each element $g \in G$ is mapped to an invertible linear operator $R(g)$. A finite-dimensional unitary representation of the Lie algebra is a set of $d \times d$ Hermitian matrices T^a that satisfy the commutation relations (C.3), where d is the dimension of representation.

For a $SU(N)$ group, the basic fundamental representation is the N-dimensional complex vector. The dimension of this representation of group $SU(N)$ is N. Another important representation is the adjoint representation, where the representation matrices are given by structure constants: $(T^b_{adj})_{ac} = if^{abc}$. The dimension of the representation of the group $SU(n)$ is $n^2 - 1$. This adjoint representation is very useful in studying the gauge covariant derivative of the fields. To give the usage of these two representations, consider a $SU(N)$ gauge theory including fermions such as QCD. In such kind of a theory, the fermions transform under fundamental representation while the gluons/ gauge fields transform under adjoint representation.

For example, for $SU(2)$, the fundamental representation is the 2-dimensional spinor representation given in terms of Pauli matrices as $T^a_{fun} = \frac{1}{2}\sigma^a$, where

$$\sigma^a = \begin{pmatrix} 0 & 1 \\ 1 & 0 \end{pmatrix}, \sigma^2 = \begin{pmatrix} 0 & -i \\ i & 0 \end{pmatrix}, \sigma^3 = \begin{pmatrix} 1 & 0 \\ 0 & -1 \end{pmatrix}. \tag{C.4}$$

Then, the structure constants are given by commutation relations as

$$[T^a_{fun}, T^b_{fun}] = i\varepsilon^{abc}T^c_{fun}, \tag{C.5}$$

where ε^{abc} are the Levi-Civita tensor with values

$$\begin{aligned}\varepsilon^{abc} &= +1 \text{ if } (a,b,c) \text{ is even permutation, } (1,2,3),\ (2,3,1),\ (3,1,2)\\ &= -1 \text{ if } (a,b,c) \text{ is odd permutation, } (3,2,1),\ (1,3,2),\ (2,1,3)\\ &= 0 \text{ if any index is repeated, i.e. remaining terms}\end{aligned}$$

As the Pauli matrices are 2×2, they act on a 2-dimensional vector space giving the dimension of this representation as 2. As for the adjoint representation, the representation matrices are of the form

$$T^a_{adj} \equiv (T^a_{adj})_{bc} = i\varepsilon^{bac}.$$

Now, consider $SU(3)$, the fundamental representation is the 3-dimensional representation given in terms of Gell-mann matrices as $T^a = \frac{1}{2}\lambda^a$, $a = 1,2,..,8$, where

$$\lambda^1 = \begin{pmatrix}0&1&0\\1&0&0\\0&0&0\end{pmatrix}, \lambda^2 = \begin{pmatrix}0&-i&0\\i&0&0\\0&0&0\end{pmatrix}, \lambda^3 = \begin{pmatrix}1&0&0\\0&-1&0\\0&0&0\end{pmatrix} \tag{C.6}$$

$$\lambda^4 = \begin{pmatrix}0&0&1\\0&0&0\\1&0&0\end{pmatrix}, \lambda^5 = \begin{pmatrix}0&0&-i\\0&0&0\\i&0&0\end{pmatrix}, \tag{C.7}$$

$$\lambda^6 = \begin{pmatrix}0&0&0\\0&0&1\\0&1&0\end{pmatrix}, \lambda^7 = \begin{pmatrix}0&0&0\\0&0&-i\\0&i&0\end{pmatrix}, \lambda^8 = \frac{1}{\sqrt{3}}\begin{pmatrix}1&0&0\\0&1&0\\0&0&-2\end{pmatrix} \tag{C.8}$$

Using the above basis, the structure constants for $\mathfrak{su}(3)$ are obtained as

$$\begin{aligned}&f^{123} = 1\\ &f^{147} = -f^{156} = f^{246} = f^{257} = f^{345} = -f^{367} = \frac{1}{2}\\ &f^{458} = f^{678} = \frac{\sqrt{3}}{2}\end{aligned}$$

and the remaining values are zero.

Appendix D

Mathematical Techniques

D.1 Jacobi Elliptic Functions

Jacobi Elliptic functions are the standard forms of elliptic functions. We encounter these functions in the description of certain problems such as the motion of a pendulum and, the design of electronic elliptic filters. There are twelve Jacobi elliptic functions denoted by $pq(u,m)$ where p and q can be of letters c, s, d, and n (The repeated letter functions are zero). u is the argument and $m = k^2$ is parameter, where k is the elliptic modulus. The complements of k and m are defined as $m' = 1 - m$ and $k' = \sqrt{m'}$. The three main functions are denoted as $cn(u,m)$, $dn(u,m)$, and $sn(u,m)$. There are many definitions for these functions. One of the definitions is based on the inversion of the incomplete elliptic integral of the first kind F,

$$F(\varphi, m) = \int_0^{\varphi} \frac{d\theta}{\sqrt{1 - m\sin^2\theta}}, \tag{D.1}$$

The parameter φ that satisfies $u = F(\varphi, m)$ is called Jacobi amplitude: $\mathrm{am}(u,m) = \varphi$. From this, the three basic functions follow as

$$\mathrm{sn}(u,m) = \sin \mathrm{am}(u,m), \tag{D.2}$$

$$\mathrm{cn}(u,m) = \cos \mathrm{am}(u,m), \tag{D.3}$$

$$\mathrm{dn}(u,m) = \frac{d}{du}\mathrm{am} = \sqrt{1 - m\sin^2\varphi}, \tag{D.4}$$

Thus, the elliptic functions are given in terms of two variables, u and m. From these three, the remaining nine functions can be written in a compact way as

$$\mathrm{pq}(u,m) = \frac{\mathrm{pn}(u,m)}{\mathrm{qn}(u,m)}, \tag{D.5}$$

where p and q are any of the letters s, c, d.

The Jacobi elliptic functions are doubly periodic, with one period along the real axis and one along the imaginary axis. The periodicity of three standard Jacobi elliptic functions is given by

$$\mathrm{sn}(u + 2\,\alpha K + 2\,\beta i\,K', k) = (-1)^{\alpha}\mathrm{sn}(u,k), \tag{D.6}$$

$$\mathrm{cn}(u+2\,\alpha K+2\,\beta i\,K',k) = (-1)^{\alpha+\beta}\mathrm{cn}(u,k), \tag{D.7}$$

$$\mathrm{dn}(u+2\,\alpha K+2\,\beta i\,K',k) = (-1)^{\beta}\mathrm{dn}(u,k), \tag{D.8}$$

where $K(k)$ is the complete elliptic integral of the first kind and $K' = K(k')$.

The three basic Jacobi elliptic functions are also defined as solutions to the nonlinear ordinary differential equations as

$$\mathrm{sn}(x,m) \text{ solves } \frac{d^2y}{dx^2} + (1+m)y - 2my^3 = 0, \tag{D.9}$$

$$\mathrm{cn}(x,m) \text{ solves } \frac{d^2y}{dx^2} + (1-2m)y + 2my^3 = 0, \tag{D.10}$$

$$\mathrm{dn}(x,m) \text{ solves } \frac{d^2y}{dx^2} - (2-m)y + 2y^3 = 0, \tag{D.11}$$

$$\tag{D.12}$$

Some of the standard identities and formulae involving the Jacobi functions are

$$\mathrm{sn}^2(u,m) + \mathrm{cn}^2(u,m) = 1,\ \mathrm{dn}^2(u,m) + m\,\mathrm{sn}^2(u,m) = 1, \tag{D.13}$$

$$\frac{d}{du}\mathrm{sn}(u,m) = \mathrm{cn}(u,m)\mathrm{dn}(u,m),\ \frac{d}{du}\mathrm{cn}(u,m) = -\mathrm{sn}(u,m)\mathrm{dn}(u,m), \tag{D.14}$$

$$\frac{d}{du}\mathrm{dn}(u,m) = -m\mathrm{cn}(u,m)\mathrm{sn}(u,m), \tag{D.15}$$

We will get some properties for the functions by setting m to some specific values as follows: By setting $m = 0$ or 1, the Jacobi elliptic functions reduce to non-elliptic functions such as trigonometric and hyperbolic functions. There is another special value, by setting $m = -1$ for some Jacobi functions, we get Lemniscate elliptic functions:

$$\mathrm{sl}(u) = \mathrm{sn}(u,-1),\ \mathrm{cl}(u) = \mathrm{cd}(u,-1) = \frac{\mathrm{sn(u,-1)}}{\mathrm{dn}(u,-1)}. \tag{D.16}$$

The Lemniscate sine (sl) and Lemniscate cosine (cl) elliptic functions are elliptic functions analogous to usual sine and cosine trigonometric functions. These functions have some properties due to their resemblance to trigonometric functions. Some of them are

$$\mathrm{cl}(-u) = \mathrm{cl}(u),\ \mathrm{sl}(u) = -\mathrm{sl}(u), \tag{D.17}$$

$$\mathrm{cl}(\overline{u}) = \overline{\mathrm{cl}(u)},\ \mathrm{sl}(\overline{u}) = \overline{\mathrm{sl}(u)}, \tag{D.18}$$

$$\mathrm{cl}(i\,u) = \frac{1}{\mathrm{cl}(u)},\ \mathrm{sl}(i\,u) = i\mathrm{sl}(u) \tag{D.19}$$

D.2 Solving Inhomogeneous wave equations

Consider an inhomogeneous wave equation

$$\Box\psi(t,\mathbf{x}) = h(t,\mathbf{x}), \tag{D.20}$$

with the boundary conditions $\psi(0,\mathbf{x}) = 0$ and $\frac{\partial\psi(0,\mathbf{x})}{\partial t} = 0$. Then, the solution for the above equation is obtained using Duhamel's principle and Kirchhoff's theorem as

$$\psi(t,\mathbf{x}) = -\frac{1}{4\pi}\int_{\overline{B}(t,\mathbf{x})} \frac{h(t',\mathbf{x}')}{r} d^3\mathbf{x}', \tag{D.21}$$

where $r = ||\mathbf{x}-\mathbf{x}'|| = \sqrt{(x-x')^2+(y-y')^2+(z-z')^2}$, $t' = t-r$ and $\overline{B}(t,\mathbf{x})$ is the ball in $\mathbb{R}^3$ with center at $\mathbf{x}$ and radius t.

In the derivations of the solutions (Eqs. 4.49 - 4.51), we encounter the integrals of the form

$$\int \frac{\sin(\omega_g(t'-z'))\cos(\omega_y(t'+x'))}{r} d^3\mathbf{x}', \tag{D.22}$$

By converting them into their exponential forms, we end up with integrals of the form

$$I(\omega_y,\omega_g) = \int_{\overline{B}(t,\mathbf{x})} \frac{1}{r} e^{i\omega_g(t'-z')} e^{i\omega_y(t'+x')} d^3\mathbf{x}'. \tag{D.23}$$

Since the integration over the ball with center at $\mathbf{x}$, we can make a variable change to make the center as origin. Then, the transformation relations are $\mathbf{x}' = \mathbf{x}+\mathbf{r}$. In spherical coordinates, it can be written as

$$z' = z + r\cos\theta,\ \ x' = x + r\sin\theta\cos\phi, \tag{D.24}$$

With the above relations, $t' = t-r$ and converting integral to spherical coordinates ($d^3\mathbf{x}' = r^2\sin\theta d\phi d\theta dr$), we get

$$I(\omega_y,\omega_z) = e^{i\omega_g(t-z)}e^{i\omega_y(t+x)}\int_0^t e^{-i(\omega_y+\omega_g)r}\left(\int_0^\pi e^{-i\omega_g r\cos\theta}\left(\int_0^{2\pi} e^{i\omega_y r\sin\theta\cos\phi}d\phi\right)\right.$$
$$\left.\sin\theta d\theta\right) r\, dr. \tag{D.25}$$

Now, we can do the integrals one by one starting with the innermost one. Start with ϕ integral as

$$I_\phi = \int_0^{2\pi} e^{i\omega_y r\sin\theta\cos\phi} d\phi \tag{D.26}$$
$$= 2\pi\, J_0(\omega_y r\sin\theta), \tag{D.27}$$

where $J_n(x)$ is the Bessel function of the first kind. Then, the θ integral is given by

$$I_\theta = \int_0^\pi e^{-i\omega_g r\cos\theta}\left(\int_0^{2\pi} e^{i\omega_y r\sin\theta\cos\phi}d\phi\right)\sin\theta d\theta, \tag{D.28}$$
$$= \int_0^\pi e^{-i\omega_g r\cos\theta} I_\phi \sin\theta d\theta, \tag{D.29}$$
$$= 2\pi\int_0^\pi e^{-i\omega_g r\cos\theta} J_0(\omega_y r\sin\theta)\sin\theta d\theta, \tag{D.30}$$

$$=4\pi\frac{\sin(||\omega||r)}{||\omega||r},\ \text{where}\ ||\omega|| = \sqrt{\omega_y^2+\omega_g^2} \tag{D.31}$$

Finally, doing the r integral will give

$$I_r = \int_0^t e^{-i(\omega_y+\omega_g)r}\left(\int_0^\pi e^{-i\omega_g r\cos\theta}\left(\int_0^{2\pi} e^{i\omega_y r\sin\theta\cos\phi}d\phi\right)\sin\theta d\theta\right) r\,dr \tag{D.32}$$

$$= \int_0^t e^{-i(\omega_y+\omega_g)r} I_\theta r\,dr \tag{D.33}$$

$$= \frac{4\pi}{||\omega||}\int_0^t e^{-i(\omega_y+\omega_g)r}\sin(||\omega||r) \tag{D.34}$$

$$= \frac{2\pi}{\omega_y\omega_g}\left(-1+e^{-i(\omega_y+\omega_g)t}\left[\cos(||\omega||t)+i\frac{\omega_y+\omega_g}{||\omega||}\sin(||\omega||t)\right]\right). \tag{D.35}$$

Then, the total integral is

$$I(\omega_y,\omega_g) = e^{i\omega_g(t-z)}e^{i\omega_y(t+x)}I_r \tag{D.36}$$

$$= \frac{2\pi}{\omega_y\omega_g}e^{i\omega_g(t-z)}e^{i\omega_y(t+x)}\left(-1+e^{-i(\omega_y+\omega_g)t}\left[\cos(||\omega||t)+i\frac{\omega_y+\omega_g}{||\omega||}\sin(||\omega||t)\right]\right). \tag{D.37}$$

In evaluating the above integral, especially ϕ and θ integral, we used the formulas given in [279]. After evaluating all integrals in exponential form, we have taken the real part of the solution.

D.3 Method of Lines

Method of Lines is a technique used to solve partial differential equations (PDEs) by taking advantage of existing and more precise numerical solvers for ordinary differential equations (ODEs). The idea behind this technique is to replace the spatial derivatives in a PDE with algebraic approximations using finite difference methods. Then, the spatial derivatives will no longer be a function of spatial variables, but a function of time only. Thus, the PDE is approximated by the system of ODEs in time or a system of Differential Algebraic Equations (DAEs). The problem of solving a PDE is now reduced to an initial value problem of the system of ODEs or DAEs [280].

Consider a PDE

$$\partial_t^2 w(t,x) - \partial_x^2 w(t,x) = f(t,x). \tag{D.38}$$

The first step is to convert the spatial derivatives into their algebraic approximations. For this, one needs to form a grid (x_i) of N points, with a left end value of x to be $i=1$ and a right end value of x to be $i=N$, where i is the index designating a position along the grid. Then, for algebraic approximations, one can use finite difference formulas such as forward difference, backward difference, or center difference formulas. Using the center difference formula, we can approximate

$$\partial_x w \approx \frac{w_{i+1}-w_{i-1}}{2\Delta x}, \tag{D.39}$$

where Δx is the spacing in x along the grid. Similarly, using the second-order central difference formula, we approximate the second-order derivative as

$$\partial_x \partial_x w \approx \frac{w_{i+1} - 2w_i + w_{i-1}}{\Delta x^2}. \tag{D.40}$$

Then, the method of lines approximation of PDE is

$$\frac{d^2 w_i}{dt^2} = \frac{w_{i+1} - 2w_i + w_{i-1}}{\Delta x^2} + f(t, x_i),\ 1 \leq i \leq N. \tag{D.41}$$

To solve the above second-order PDE in t and x exactly, we need two initial conditions and two boundary conditions. Consider the following initial and boundary conidtions as we used in this thesis for solving Eqs. (5.36 & 5.37):

$$w(t=0,x) = 0, \qquad \frac{\partial w(t=0,x)}{\partial t} = 0, \tag{D.42}$$

$$w(t, x = x_1) = g(t), \qquad w(t, x = x_N) = h(t), \tag{D.43}$$

where $g(t)$ and $f(t)$ are functions of time. Since Eq. (D.41) contains N initial value second-order ODEs, $2N$ initial conditions are required. From Eq. (D.42), we have

$$w(t=0,x_i) = 0,\ \frac{\partial w(t=0,x_i)}{\partial t} = 0,\ 1 \leq i \leq N. \tag{D.44}$$

Using the boundary conditions (D.43), we get the values at grid endpoints

$$w_1(t) = w(t, x = x_1) = g(t), \text{and } w_N = w(t, x = x_N) = h(t). \tag{D.45}$$

Now for the intermediate points, we can use Eq. (D.41) which is

$$\frac{d^2 w_i}{dt^2} = \frac{w_{i+1} - 2w_i + w_{i-1}}{\Delta x^2} + f(t, x_i),\ i = 2, 3, ..., N. \tag{D.46}$$

The Eqs. (D.44), (D.45) and (D.46) make the Method of lines' approximation of the Eq. (D.38) subject to Eqs. (D.42) and (D.43). The solution of this ODE system gives N functions,

$$w_1(t), w_2(t), w_3(t), .., w_{N-1}(t), w_N(t)$$

as an approximation of $w(t,x)$ at grid points $i = 1, 2, .., N$.

The above ODE system was solved using Mathematica.

D.4 Deriving equations of motion in vector decomposition

The $SU(2)$ YM Lagrangian density is

$$\mathcal{L} = -\frac{1}{4} F^a_{\mu\nu} F^{a\mu\nu}. \tag{D.47}$$

In Hamilton's gauge ($A_0^a = 0$), $\mathcal{L}$ can be expanded as

$$\mathcal{L} = \frac{1}{2}\partial_0 A_i^a \partial_0 A_i^a - \frac{1}{2}\partial_i A_j^a \partial_i A_j^a + \frac{1}{2}\partial_i A_j^a \partial_j A_i^a + g_{ym}\varepsilon^{abc}\partial_i A_j^a A_i^b A_j^c - \frac{g_{ym}^2}{4}\left((A_i^a A_i^a)^2 - (A_i^a A_j^a)(A_i^b A_j^b)\right).$$

Then, we considered the vector decomposition of the gauge field as given in Eq:5.3 as

$$A_i^a = U(t)\delta_i^a + n_i \Phi^a + \varepsilon_{ilm} n_l s_m^\sigma \chi_\sigma^a. \tag{D.48}$$

where $a, i = 1,2,3$ and $\sigma = 1,2$. We use the following constraints for the corrected splitting of modes and also to keep the diagonal information of the gauge field in the condensate:

$$\mathbf{n}\cdot\Phi = 0, \tag{D.49}$$
$$\mathbf{n}\cdot\chi_\sigma = 0, \tag{D.50}$$
$$\varepsilon_{ilm} n_l s_m^\sigma \chi_\sigma^i = 0, \ . \tag{D.51}$$

We explained further using these constraints in the Sec 5.3. Using those constraints, we have a total of 6 degrees of freedom ($U \to 1$, $\Phi^a \to 2$ and $\chi_\sigma^a \to 3$). Using the gauge field and constraints in $\mathcal{L}$, we get

$$\begin{aligned}\mathcal{L} = {} & \frac{3}{2}(\partial_0 U)^2 + \frac{1}{2}n^2(\partial_0\Phi^a)(\partial_0\Phi^a) + \frac{1}{2}(\partial_0\Lambda_i^a)(\partial_0\Lambda_i^a) - \frac{1}{2}n^2(\partial_i\Phi^a)(\partial_i\Phi^a) \\ & - \frac{1}{2}(\partial_i\Lambda_j^a)(\partial_i\Lambda_j^a) + \frac{1}{2}n_i n_j \partial_i\Phi^a\partial_j\Phi^a + n_i\partial_j\Phi^a\partial_i\Lambda_j^a + \frac{1}{2}(\partial_i\Lambda_j^a)(\partial_j\Lambda_i^a) + g_{ym}\varepsilon^{abc}\Big[U^2 n_c\partial_b\Phi^a \\ & + Un^2\Phi^c\partial_b\Phi^a + Un_i n_c\Phi^b\partial_i\Phi^a + Un_c\Lambda_i^b\partial_i\Phi^a + n^2\Phi^c\Lambda_i^b\partial_i\Phi^a + U^2\partial_b\Lambda_c^a + U\Lambda_j^c\partial_b\Lambda_j^a \\ & + Un_i\Phi^b\partial_i\Lambda_c^a + n_i\Phi^b\Lambda_j^c\partial_i\Lambda_j^a + U\Lambda_i^b\partial_i\Lambda_c^a + \Lambda_i^b\Lambda_j^c\partial_i\Lambda_j^a\Big] - \frac{1}{4}g_{ym}^2\Big[6U^4 + 2n^2U^2(\Phi^a\Phi^a) \\ & + 2U^2(\Lambda_i^a\Lambda_i^a) - 4Un^2\Phi^a\Phi^i\Lambda_i^a - 2U^2\Lambda_j^i\Lambda_i^j - 4U\Lambda_j^i\Lambda_i^a\Lambda_j^a + (\Lambda_i^a\Lambda_i^a)^2 - (\Lambda_i^a\Lambda_j^a)(\Lambda_i^b\Lambda_j^b) \\ & + 2n^2(\Phi^a\Phi^a)(\Lambda_i^b\Lambda_i^b) - 2n^2(\Phi^a\Lambda_i^a)(\Phi^b\Lambda_i^b)\Big]. \end{aligned} \tag{D.52}$$

In the above expression, we used a shorthand notation $\Lambda_i^a = \varepsilon_{ilm} n_l s_m^\sigma \chi_\sigma^a$.

To find the equations of motion, one has to vary the above Lagrangian with respect to the modes. In our case, we choose the following vectors consistent with the above constraints:

$$n = (0,0,1), \ \ s^1 = (1,0,0), \quad s^2 = (0,1,0). \tag{D.53}$$

With the above choice, the constraints give

$$\Phi^3 = 0, \ \ \chi_\sigma^3 = 0, \ \ \chi_2^1 = \chi_1^2. \tag{D.54}$$

One can count the non-zero modes which add up to 6 which is consistent with the previous discussion below the constraints. The choice $\mathbf{n}$ gives us a wave propagating in the z-direction. Thus, the functions are functions of t and z. We also choose $\chi_1^2 = \chi_2^1 = 0$. This

is just a choice. Then, the Lagrangian becomes

$$\mathcal{L} = \frac{3}{2}(\partial_0 U)^2 + \frac{1}{2}(\partial_0\Phi_1)^2 + \frac{1}{2}(\partial_0\Phi_2)^2 + \frac{1}{2}[(\partial_0\chi_1)^2 - (\partial_3\chi_1)^2] + \frac{1}{2}[(\partial_0\chi_2)^2 - (\partial_3\chi_2)^2]$$
$$+ g_{ym}U^2\partial_z(\chi_1+\chi_2) - \frac{g_{ym}^2}{4}\left[6U^4 + 2U^2(\Phi_1^2+\Phi_2^2) - 4U(\chi_1-\chi_2)\Phi_1\Phi_2 + 2\Phi_1^2\chi_2^2\right.$$
$$\left. +2\Phi_2^2\chi_1^2 + 2U^2(\chi_1+\chi_2)^2 + 2\chi_1^2\chi_2^2\right], \quad \text{(D.55)}$$

where $\Phi^1 \equiv \Phi_1$, $\Phi^2 \equiv \Phi_2$, $\chi_1^1 \equiv \chi_1$ and $\chi_2^2 \equiv \chi_2$. We then use the above Lagrangian to find the equations of motion given in Eqs. (5.35)-(5.39).

D.4.1 With Gravitational wave

In the presence of GW, we can write the metric as $g^{\mu\nu} = \eta^{\mu\nu} - h^{\mu\nu}$. So, for the Lagrangian density, we will get an additional term proportional to GW fluctuation $h^{\mu\nu}$ along with the one obtained in the previous section. Those additional terms are given by

$$\mathcal{L}_1 = \frac{1}{4}F^a_{\mu\nu}\left(h^{\mu\lambda}\eta^{\nu\rho} + \eta^{\mu\lambda}h^{\nu\rho}\right)F^a_{\lambda\rho}. \quad \text{(D.56)}$$

Using Hamilton's gauge for the gauge field and TT-gauge for GW, with only h_+, the above term can be expanded as

$$\mathcal{L}_1 = -\frac{1}{2}h_+\left[\left((\partial_0 A_1^a)(\partial_0 A_1^a) - (\partial_0 A_2^a)(\partial_0 A_2^a)\right) + \eta^{ij}\left(\partial_i A_1^a \partial_j A_1^a - \partial_i A_2^a \partial_j A_2^a\right)\right]$$
$$+ \frac{g_{ym}^2 h_+}{4}\left[(A_1^a A_1^a - A_2^a A_2^a)A_i^b A_i^b - \eta^{ij}(A_1^a A_i^a)(A_1^b A_j^b) + \eta^{ij}(A_2^a A_i^a)(A_2^a A_j^a)\right]. \quad \text{(D.57)}$$

Using the same vector decomposition and constraints as before, one simply the above expression to

$$\mathcal{L}_1 = -\frac{1}{2}h_+\left[(\partial_0\chi_1)^2 - (\partial_0\chi_2)^2\right] + \frac{g_{ym}^2}{4}h_+\left[\chi_2^2\Phi_1^2 - \chi_1^2\Phi_2^2\right.$$
$$\left. + U^2(\chi_2^2 - \chi_1^2) + U^2(\Phi_2^2 - \Phi_1^2) + 2\Phi_1\Phi_2(\chi_1+\chi_2)U\right]. \quad \text{(D.58)}$$

Then, the total Lagrangian in a GW background is $\mathcal{L} + \mathcal{L}_1$. Using this total Lagrangian, we find the equations of motion given in Eqs. (5.46)-(5.50).

Appendix E

Techniques in finite temperature QFT

E.1 Heat Kernel Method

An efficient tool for the calculations of background field functionals is the Schwinger Proper time method or Heat Kernel method [281]. This method is based on the integral representation of the one-loop functional determinant of an operator K in terms of heat kernel. The heat kernel for an operator K is defined as $H(\tau) = e^{-\tau K}$. Then, the one-loop functional determinant is given by

$$\mathrm{Tr}\ln K = -\int_0^\infty \frac{d\tau}{\tau}\mathrm{Tr}\, H(\tau). \tag{E.1}$$

Usually, the operator K can be a matrix. For this, consider a multicomponent field $\psi = \psi^a(x)$, where a can be any index (spin, color), whose elements form a vector in the configuration space of the system. Then, the operator K will also acquire a matrix structure as $\hat{K} \equiv K^a_b$. Correspondingly, the heat kernel is also a matrix of form $\hat{H} \equiv H^a_b(\tau)$. The functional trace involves the integral over the spacetime and also trace over the matrix indices (spin, Dirac, color, Lorentz). Then, the trace of heat kernel given by

$$\mathrm{Tr}\, H(\tau) = \int dx\ \mathrm{tr}\, \hat{H}(\tau|x,x), \tag{E.2}$$

where tr is trace over all indices and $\hat{H}(\tau|x,x) \equiv \langle x|\, \hat{H}\, |x\rangle$ is defined as

$$\hat{H}(\tau|x,x) = \int dy\, \hat{H}(\tau|x,y)\ \delta(x,y). \tag{E.3}$$

and the untraced heat kernel $\hat{H}(\tau|x,y)$ satisfies the heat equation thus the name Heat kernel method.

$$\frac{\partial}{\partial\tau}\hat{H}(\tau|x,y) = \hat{K}\ \hat{H}(\tau|x,y),\ \ \hat{H}(0|x,y) = \hat{1}\ \delta(x,y). \tag{E.4}$$

This equation is the Euclidean version of the evolutionary Schrodinger-type equation, first given by Schwinger [265].

Finally, the functional determinant is

$$\ln\det K = \mathrm{Tr}\ln K = -\int_0^\infty \frac{d\tau}{\tau}\int dx\ \mathrm{tr}\ \langle x|\ e^{-\tau K}\ |x\rangle \tag{E.5}$$

In practice, the heat kernel is calculated through a method called heat kernel expansion.

This expansion terms contains various contributions from the background fields and their derivatives, classified by their mass scale dimension. This expansion is in the powers of proper time τ.

$$\ln\det K = -\int_0^\infty \frac{d\tau}{\tau}\int dx\ \frac{1}{(4\pi\tau)^{d/2}}\sum_n b_n\tau^n \tag{E.6}$$

where b_n are known as Seeley-De Witt or heat kernel coefficients which depends on local gauge invariant operators.

For an operator of form $K = -\nabla^\mu\nabla_\mu + V$, the first few Seeley-deWitt coefficients are given as

$$b_0 = \mathrm{tr}(I), \tag{E.7}$$
$$b_1 = \mathrm{tr}(-V), \tag{E.8}$$
$$b_2 = \mathrm{tr}(\frac{1}{2}V^2 - \frac{1}{6}V_{\mu\mu} + \frac{1}{12}F_{\mu\nu}^2), ... \tag{E.9}$$

where I is identity, $V_{\mu\mu} = \nabla^\mu\nabla_\mu V$, $F_{\mu\nu} = [\nabla_\mu, \nabla_\nu]$ and $F_{\mu\nu}^2 = F_{\mu\nu}F^{\mu\nu}$.

At finite temperatures, apart from the usual local operators, we also encounter a new operator known as Polyakov loop. The details regarding how the Polyakov loop enters the coefficients is given in [272].

E.2 Integrals in QFT

E.2.1 Common integrals in QFT

The most common integral in QFT is the functional Gaussian integral. Such integrals are

$$\int_\infty^\infty e^{-\frac{1}{2}x_iA_{ij}x_j}d^nx = \frac{(2\pi)^{n/2}}{(\det A)^{1/2}}, \tag{E.10}$$
$$\int_\infty^\infty e^{-\frac{1}{2}\theta_iA_{ij}\theta_j}d^n\theta = (\det A)^{1/2}, \tag{E.11}$$

where x is an ordinary variable and θ is a Grassmann variable (Example: fermion fields).

E.2.2 Integrals used in finite temperature QFT (Sec: 7.4.1)

The basic integrals are of the form

$$I^\pm_{n,\alpha} = \int_0^\infty d\tau\tau^\varepsilon\tau^{\alpha-1}\varphi_n^\pm(L), \tag{E.12}$$

where the function $\varphi_n^\pm(L)$ are defined by Eq. 7.79 and $\pm$ corresponds to bosonic and fermionic versions, respectively. For the bosonic version, the integrals are of form

$$I^+_{n,\alpha} = \int_0^\infty d\tau\tau^\varepsilon\tau^{\alpha-1}\varphi_n^+(L), \tag{E.13}$$

where $\varphi_n^+(L)$ is given by

$$\varphi_n^+(L) = (4\pi\tau)^{1/2}\frac{1}{\beta}\sum_{p_0^+}\tau^{n/2}R^n e^{\tau R^2},\ \ R = ip_0^+ - \frac{1}{\beta}\ln(L),\ \ p_0^+ = \frac{2\pi k}{\beta}. \tag{E.14}$$

Using the condensate ansatz ($A_0^a = 0, A_i^a = \delta_i^a U$), one can find the $\varphi_n^+(L)$ is

$$\varphi_n^+(L) = (4\pi\tau)^{1/2}\frac{1}{\beta}\left(\frac{2\pi i}{\beta}\right)^n\sum_{k\in\mathbb{Z}}\tau^{n/2}k^n e^{-\frac{4\pi^2k^2}{\beta^2}\tau}. \tag{E.15}$$

Using this, we evaluate the integral as

$$\begin{aligned}
I_{n,\alpha}^+ &= \int_0^\infty d\tau\tau^\varepsilon\tau^{\alpha-1}\varphi_n^+(L) && \text{(E.16)}\\
&= \int_0^\infty d\tau\tau^\varepsilon\tau^{\alpha-1}(4\pi\tau)^{1/2}\frac{1}{\beta}\left(\frac{2\pi i}{\beta}\right)^n\sum_{k\in\mathbb{Z}}\tau^{n/2}k^n e^{-\frac{4\pi^2k^2}{\beta^2}\tau} && \text{(E.17)}\\
&= \frac{1}{\beta}\left(\frac{2\pi i}{\beta}\right)^n\sqrt{4\pi}\sum_{k\in\mathbb{Z}}k^n\int_0^\infty d\tau\tau^{\alpha+\varepsilon+\frac{n}{2}+\frac{1}{2}-1}e^{-\frac{4\pi^2k^2}{\beta^2}\tau} && \text{(E.18)}\\
&= i^n\frac{\sqrt{4\pi}}{\beta}\left(\frac{\beta}{2\pi}\right)^{2\alpha+1+2\varepsilon}\Gamma\left(\alpha+\varepsilon+\frac{n}{2}+\frac{1}{2}\right)\sum_{k\in\mathbb{Z}}\frac{1}{k^{2\alpha+2\varepsilon+1}} && \text{(E.19)}\\
&= 2i^n\frac{\sqrt{4\pi}}{\beta}\left(\frac{\beta}{2\pi}\right)^{2\alpha+1+2\varepsilon}\Gamma\left(\alpha+\varepsilon+\frac{n}{2}+\frac{1}{2}\right)\zeta(2\alpha+2\varepsilon+1), && \text{(E.20)}
\end{aligned}$$

where we used the definitions of Gamma and Riemann zeta functions [279]:

$$\Gamma(z) = \int_0^\infty dt\ t^{z-1}e^{-t} \text{ and } \zeta(z) = \sum_{n=0}^\infty\frac{1}{n^z}.$$

For the fermionic version, the integrals are form

$$I_{n,\alpha}^- = \int_0^\infty d\tau\tau^\varepsilon\tau^{\alpha-1}\varphi_n^-(L) \tag{E.21}$$

where $\varphi_n^-(L)$ is given by

$$\varphi_n^-(L) = (4\pi\tau)^{1/2}\frac{1}{\beta}\sum_{p_0^-}\tau^{n/2}R^n e^{\tau R^2},\ \ R = ip_0^- - \frac{1}{\beta}\ln(L),\ \ p_0^- = \frac{2\pi}{\beta}(k+\frac{1}{2}), \tag{E.22}$$

As we can see the only difference from the bosonic versions is k is replaced by $k+\frac{1}{2}$. In the same way, one can evaluate the integral and the final expression is

$$I_{n,\alpha}^- = 2i^n\frac{\sqrt{4\pi}}{\beta}\left(\frac{\beta}{2\pi}\right)^{2\alpha+1+2\varepsilon}\Gamma\left(\alpha+\varepsilon+\frac{n}{2}+\frac{1}{2}\right)\zeta\left(2\alpha+2\varepsilon+1,\frac{1}{2}\right), \tag{E.23}$$

where we used the definition of the generalized Riemann zeta function [279]: $\zeta(z,a) = \sum_{n=0}^{\infty} 1/(n+a)^z$.